Publishing House ASV

begell house, inc. publishers

Scientific coordination is carried out by the Russian Academy of Architecture and Construction Sciences (RAACS)

Volume 20 • Issue 3 • 2024

ISSN 2588-0195 (Online)
ISSN 2587-9618 (Print) Continues ISSN 1524-5845

International Journal for

Computational Civil and Structural Engineering

Международный журнал по расчету гражданских и строительных конструкций

https://ijccse.iasv.ru/

DOI: 10.22337/2587-9618
GICID: 71.0000.1500.2830

EXECUTIVE EDITOR

Vladimir I. Travush,
Full Member of RAACS, Professor, Dr.Sc.,
Vice-President of the Russian Academy
of Architecture and Construction Sciences;
Urban Planning Institute
of Residential and Public Buildings;
24, Ulitsa Bolshaya Dmitrovka, 107031, Moscow, Russia

EDITOR-IN-CHIEF

Vladimir N. Sidorov,
Full Member of RAACS, Professor, Dr.Sc., National Research Moscow State University of Civil Engineering; Russian University of Transport (RUT – MIIT); Moscow Institute of Architecture (State Academy); Perm National Research Polytechnic University; 26, Yaroslavskoe Shosse, 129337, Moscow, Russia

EDITORIAL DIRECTOR

Valery I. Telichenko,
Full Member of RAACS, Professor, Dr.Sc.,
The First Vice-President of the Russian Academy
of Architecture and Construction Sciences;
Honorary President of National Research
Moscow State University of Civil Engineering;
24, Ulitsa Bolshaya Dmitrovka, 107031, Moscow, Russia

MANAGING EDITOR

Nadezhda S. Nikitina,
Professor, Ph.D.,
Director of ASV Publishing House;
National Research Moscow State University
of Civil Engineering;
26, Yaroslavskoe Shosse, 129337, Moscow, Russia

ASSOCIATE EDITORS

Pavel A. Akimov,
Full Member of RAACS, Professor, Dr.Sc.,
Acting Rector of National Research
Moscow State University of Civil Engineering;
Vice-President of the Russian Academy
of Architecture and Construction Sciences;
Tomsk State University of Architecture and Building;
Russian University of Friendship of Peoples;
26, Yaroslavskoe Shosse, 129337, Moscow, Russia

Alexander M. Belostotsky,
Full Member of RAACS, Professor, Dr.Sc.,
Research & Development Center "STADYO";
National Research Moscow State University of Civil Engineering; Russian University of Transport (RUT – MIIT); Russian University of Friendship of Peoples;
Perm National Research Polytechnic University;
Tomsk State University of Architecture and Building;
Irkutsk National Research Technical University;
8th Floor, 18, ul. Tretya Yamskogo Polya,
125040, Moscow, Russia

Mikhail Belyi, Professor, Dr.Sc.,
Dassault Systèmes Simulia;
1301 Atwood Ave Suite 101W
02919 Johnston, RI, United States

Vitaly Bulgakov, Professor, Dr.Sc.,
Micro Focus;
Newbury, United Kingdom

Nikolai P. Osmolovskii, Professor, Dr.Sc.,
Systems Research Institute, Polish Academy of Sciences;
Kazimierz Pulaski University
of Technology and Humanities in Radom;
29, ul. Malczewskiego, 26-600, Radom, Poland

Gregory P. Panasenko, Professor, Dr.Sc.,
Equipe d'Analise Numerique; NMR CNRS 5585
University Gean Mehnet;
23 rue. P.Michelon 42023, St.Etienne, France

Scientific coordination is carried out by the Russian Academy of Architecture and Construction Sciences (RAACS)

PUBLISHER

ASV Publishing House
(ООО «Издательство АСВ»)
19/1,12, Yaroslavskoe Shosse, 120338, Moscow, Russia
Tel. +7(925)084-74-24; E-mail: iasv@iasv.ru; Интернет-сайт: http://iasv.ru/

ADVISORY EDITORIAL BOARD

Mojtaba Aslami, Ph.D,
Fasa University; Daneshjou blvd,
Fasa, Fars Province, Iran

Klaus-Jurgen Bathe, Professor
Massachusetts Institute
of Technology;
Cambridge, MA 02139, USA

Alexander T. Bekker,
Academician of RAACS,
Professor, Dr.Sc.,
Far Eastern Federal University;
Russian Academy of Architecture
and Construction Sciences;
8, Sukhanova Street, Vladivostok,
690950, Russia

Tomas Bock, Professor, Dr.-Ing.,
Technical University of Munich,
Arcisstrasse 21, D-80333
Munich, Germany

Jan Buynak, Professor, Ph.D.,
University of Žilina;
1, Univerzitná, Žilina, 010 26,
Slovakia

Vladimir T. Erofeev,
Full Member of RAACS,
Professor, Dr.Sc.,
Ogarev Mordovia State University;
68, Bolshevistskaya Str., Saransk
430005, Republic of Mordovia,
Russia

Victor S. Fedorov,
Full Member of RAACS,
Professor, Dr.Sc.,
Russian University of Transport
(RUT – MIIT);
9b9 Obrazcova Street, Moscow,
127994, Russia

Sergey V. Fedosov,
Full Member of RAACS,
Professor, Dr.Sc.,
Russian Academy of Architecture
and Construction Sciences;
24, Ul. Bolshaya Dmitrovka, 107031,
Moscow, Russia

Sergiy Yu. Fialko,
Professor, Dr.Sc.,
Cracow University of Technology;
24, Warszawska Street, Kraków,
31-155, Poland

Vladimir G. Gagarin,
Corresponding Member
of RAACS, Professor, Dr.Sc.,
Research Institute of Building
Physics of Russian Academy
of Architecture and Construction
Sciences;
21, Lokomotivny Proezd,
Moscow, 127238, Russia

Vyatcheslav A. Ilyichev,
Full Member of RAACS,
Professor, Dr.Sc.,
Russian Academy of Architecture
and Construction Sciences;
Podzemproekt Ltd.;
24, Ulitsa Bolshaya Dmitrovka,
Moscow, 107031, Russia

Marek Iwański,
Professor, Dr.Sc.,
Kielce University of Technology;
7, al. Tysiąclecia Państwa Polskiego
Kielce, 25 – 314, Poland

Sergey Yu. Kalashnikov,
Advisor of RAACS,
Professor, Dr.Sc.,
Volgograd State Technical
University; 28, Lenin avenue,
Volgograd, 400005, Russia

Semen S. Kaprielov,
Academician of RAACS,
Professor, Dr.Sc.,
Research Center of Construction;
6, 2nd Institutskaya St., Moscow,
109428, Russia

Nikolay I. Karpenko,
Full Member of RAACS,
Professor, Dr.Sc.,
Research Institute of Building
Physics of Russian Academy
of Architecture and Construction
Sciences; Russian Academy of
Architecture and Construction
Sciences; 21, Lokomotivny Proezd,
Moscow, 127238, Russia

Vladimir V. Karpov,
Professor, Dr.Sc., Saint Petersburg
State University of Architecture and
Civil Engineering;
4, 2-nd Krasnoarmeiskaya Steet,
Saint Petersburg, 190005, Russia

Galina G. Kashevarova,
Corresponding Member
of RAACS, Professor, Dr.Sc.,
Perm National Research
Polytechnic University;
29 Komsomolsky pros., Perm,
Perm Krai, 614990, Russia

John T. Katsikadelis,
Professor, Dr.Eng, PhD, Dr.h.c.,
National Technical University of
Athens; Zografou Campus
9, Iroon Polytechniou str
15780 Zografou, Greece

Vitaly I. Kolchunov,
Full Member of RAACS,
Professor, Dr.Sc., Southwest State
University; Russian Academy of
Architecture and Construction
Sciences; 94, 50 let Oktyabrya,
Kursk, 305040, Russia

Dmitry V. Kozlov, Dr. Sc.
Engineering, Professor, Head of
the Department of Hydraulics and
Hydrotechnical Construction, NRU
MGSU,
26, Yaroslavskoe Shosse., 129337,
Moscow, Russia

Markus König, Professor
Ruhr-Universität Bochum;
150, Universitätsstraße, Bochum,
44801, Germany

Sergey B. Kositsin,
Advisor of RAACS,
Professor, Dr.Sc.,
Russian University of Transport
(RUT – MIIT); 9b9 Obrazcova
Street, Moscow, 127994, Russia

Sergey B. Krylov,
Corresponding Member
of RAACS, Professor, Dr.Sc.,
Research Center of Construction;
6, 2nd Institutskaya St., Moscow,
109428, Russia

Sergey V. Kuznetsov,
Professor, Dr.Sc.,
Ishlinsky Institute for Problems
in Mechanics of the Russian
Academy of Sciences;
101-1, Prosp. Vernadskogo,
Moscow, 119526, Russia

Vladimir V. Lalin,
Professor, Dr.Sc.,
Peter the Great Saint-Petersburg Polytechnic University;
29, Ul. Politechnicheskaya, Saint-Petersburg, 195251, Russia

Leonid S. Lyakhovich,
Full Member of RAACS, Professor, Dr.Sc., Tomsk State University of Architecture and Building; 2, Solyanaya Sq., Tomsk, 634003, Russia

Rashid A. Mangushev,
Corresponding Member of RAACS, Professor, Dr.Sc.,
Saint Petersburg State University of Architecture and Civil Engineering;
4, 2-nd Krasnoarmeiskaya Steet, Saint Petersburg, 190005, Russia

Ilizar T. Mirsayapov,
Advisor of RAACS,
Professor, Dr.Sc., Kazan State University of Architecture and Engineering; 1, Zelenaya Street, Kazan, 420043, Republic of Tatarstan, Russia

Vladimir L. Mondrus,
Corresponding Member of RAACS, Professor, Dr.Sc.,
National Research Moscow State University of Civil Engineering;
Yaroslavskoe Shosse 26, Moscow, 129337, Russia

Valery I. Morozov,
Corresponding Member of RAACS, Professor, Dr.Sc.,
Saint Petersburg State University of Architecture and Civil Engineering;
4, 2-nd Krasnoarmeiskaya Steet, Saint Petersburg, 190005, Russia

Anatoly V. Perelmuter,
Foreign Member of RAACS, Professor, Dr.Sc., SCAD Soft;
Office 1,2, 3a Osvity street, Kiev, 03037, Ukraine

Alexey N. Petrov,
Advisor of RAACS, Professor, Dr.Sc., Petrozavodsk State University; 33, Lenina Prospect, Petrozavodsk, 185910, Republic of Karelia, Russia

Vladilen V. Petrov,
Full Member of RAACS, Professor, Dr.Sc.,
Yuri Gagarin State Technical University of Saratov;
77 Politechnicheskaya Street, Saratov, 410054, Russia

Jerzy Z. Piotrowski,
Professor, Dr.Sc.,
Kielce University of Technology;
al. Tysiąclecia Państwa Polskiego 7, Kielce, 25 – 314, Poland

Chengzhi Qi, Professor, Dr.Sc.,
Beijing University of Civil Engineering and Architecture;
1, Zhanlanlu, Xicheng District, Beijing, China

Vladimir P. Selyaev,
Full Member of RAACS, Professor, Dr.Sc., Ogarev Mordovia State University;
68, Bolshevistskaya Str., Saransk 430005, Republic of Mordovia, Russia

Eun Chul Shin,
Professor, Ph.D.,
Incheon National University;
(Songdo-dong)119 Academy-ro, Yeonsu-gu, Incheon, Korea

D.V. Singh,
Professor, Ph.D,
University of Roorkee;
Roorkee, India, 247667

Wacław Szcześniak,
Foreign Member of RAACS, Professor, Dr.Sc.,
Lublin University of Technology;
Ul. Nadbystrzycka 40, 20-618 Lublin, Poland

Tadatsugu Tanaka,
Professor, Dr.Sc.,
Tokyo University; 7-3-1 Hongo, Bunkyo, Tokyo, 113-8654, Japan

Josef Vican,
Professor, Ph.D,
University of Žilina;
1, Univerzitná, Žilina, 010 26, Slovakia

Zbigniew Wojcicki,
Professor, Dr.Sc.,
Wroclaw University of Technology;
11 Grunwaldzki Sq., 50-377, Wrocław, Poland

Artur Zbiciak, Professor, Dr.Sc.,
Warsaw University of Technology;
Pl. Politechniki 1, 00-661 Warsaw, Poland

Segrey I. Zhavoronok, Ph.D.,
Institute of Applied Mechanics of Russian Academy of Sciences;
Moscow Aviation Institute (National Research University);
7, Leningradsky Prt., Moscow, 125040, Russia

Askar Zhussupbekov,
Professor, Dr.Sc.,
Eurasian National University;
5, Munaitpassov street, Astana, 010000, Kazakhstan

TECHNICAL EDITOR

Taymuraz B. Kaytukov,
Advisor of RAACS,
Associate Professor, Ph.D.,
Vice-Rector of National Research Moscow State University of Civil Engineering;
Yaroslavskoe Shosse 26, Moscow, 129337, Russia

EDITORIAL TEAM

Vadim K. Akhmetov, Professor, Dr.Sc., National Research Moscow State University of Civil Engineering; 26, Yaroslavskoe Shosse, 129337 Moscow, Russia

Pavel A. Akimov, Full Member of RAACS, Professor, Dr.Sc., Acting Rector of National Research Moscow State University of Civil Engineering; Vice-President of the Russian Academy of Architecture and Construction Sciences; Tomsk State University of Architecture and Building; Russian University of Friendship of Peoples; 26, Yaroslavskoe Shosse, 129337, Moscow, Russia

Alexander M. Belostotsky, Full Member of RAACS, Professor, Dr.Sc., Research & Development Center "STADYO"; National Research Moscow State University of Civil Engineering; Russian University of Transport (RUT – MIIT); Russian University of Friendship of Peoples; Perm National Research Polytechnic University; Tomsk State University of Architecture and Building; Irkutsk National Research Technical University; 8th Floor, 18, ul. Tretya Yamskogo Polya, 125040, Moscow, Russia

Mikhail Belyi, Professor, Dr.Sc., Dassault Systèmes Simulia; 1301 Atwood Ave Suite 101W 02919 Johnston, RI, United States

Vitaly Bulgakov, Professor, Dr.Sc., Micro Focus; Newbury, United Kingdom

Charles El Nouty, Professor, Dr.Sc., LAGA Paris-13 Sorbonne Paris Cite; 99 avenue J.B. Clément, 93430 Villetaneuse, France

Natalya N. Fedorova, Professor, Dr.Sc., Novosibirsk State University of Architecture and Civil Engineering (SIBSTRIN); 113 Leningradskaya Street, Novosibirsk, 630008, Russia

Darya Filatova, Professor, Dr.Sc., Probability, Assessment, Reasoning and Inference Studies Research Group, EPHE Laboratoire CHART (PARIS) 4-14, rue Ferrus, 75014 Paris

Vladimir Ya. Gecha, Professor, Dr.Sc., Research and Production Enterprise All-Russia Scientific-Research Institute of Electromechanics with Plant Named after A.G. Iosiphyan; 30, Volnaya Street, Moscow, 105187, Russia

Taymuraz B. Kaytukov, Advisor of RAACS, Associate Professor, Ph.D, Vice-Rector of National Research Moscow State University of Civil Engineering; 26, Yaroslavskoe Shosse, 129337, Moscow, Russia

Marina L. Mozgaleva, Professor, Dr.Sc., National Research Moscow State University of Civil Engineering; 26, Yaroslavskoe Shosse, 129337 Moscow, Russia

Nadezhda S. Nikitina, Professor, Ph.D., Director of ASV Publishing House; National Research Moscow State University of Civil Engineering; 26, Yaroslavskoe Shosse, 129337 Moscow, Russia

Nikolai P. Osmolovskii, Professor, Dr.Sc., Systems Research Institute Polish Academy of Sciences; Kazimierz Pulaski University of Technology and Humanities in Radom; 29, ul. Malczewskiego, 26-600, Radom, Poland

Gregory P. Panasenko, Professor, Dr.Sc., Equipe d'Analise Numerique NMR CNRS 5585 University Gean Mehnet; 23 rue. P.Michelon 42023, St.Etienne, France

Andreas Rauh, Prof. Dr.-Ing. habil. Carl von Ossietzky Universität Oldenburg, Germany School II - Department of Computing Science Group Distributed Control in Interconnected Systems D-26111 Oldenburg, Germany

Zhan Shi, Professor LPSM, Université Paris VI 4 place Jussieu, F-75252 Paris Cedex 05, France

Marina V. Shitikova, National Research Moscow State University of Civil Engineering, Advisor of RAACS, Professor, Dr.Sc., Voronezh State Technical University; 14, Moscow Avenue, Voronezh, 394026, Russia

Igor L. Shubin, Corresponding Member of RAACS, Professor, Dr.Sc., Research Institute of Building Physics of Russian Academy of Architecture and Construction Sciences; 21, Lokomotivny Proezd, Moscow, 127238, Russia

Vladimir N. Sidorov, Corresponding Member of RAACS, Professor, Dr.Sc., National Research Moscow State University of Civil Engineering; Russian University of Transport (RUT – MIIT); Moscow Institute of Architecture (State Academy); Perm National Research Polytechnic University; 26, Yaroslavskoe Shosse, 129337, Moscow, Russia

Valery I. Telichenko, Full Member of RAACS, Professor, Dr.Sc., The First Vice-President of the Russian Academy of Architecture and Construction Sciences; National Research Moscow State University of Civil Engineering; 24, Ulitsa Bolshaya Dmitrovka, 107031, Moscow, Russia

Vladimir I. Travush, Full Member of RAACS, Professor, Dr.Sc., Vice-President of the Russian Academy of Architecture and Construction Sciences; Urban Planning Institute of Residential and Public Buildings; 24, Ulitsa Bolshaya Dmitrovka, 107031, Moscow, Russia

INVITED REVIEWERS

Akimbek A. Abdikalikov, Professor, Dr.Sc.,
Kyrgyz State University of Construction, Transport and Architecture n.a. N. Isanov;
34 Maldybayeva Str., Bishkek, 720020, Biskek, Kyrgyzstan

Vladimir N. Alekhin, Advisor of RAACS, Professor, Dr.Sc.,
Ural Federal University named after the first President of Russia B.N. Yeltsin;
19 Mira Street, Ekaterinburg, 620002, Russia

Irina N. Afanasyeva, Ph.D., University of Florida; Gainesville, FL 32611, USA

Ján Čelko, Professor, PhD, Ing., University of Žilina; Univerzitná 1, 010 26, Žilina, Slovakia

Tatyana L. Dmitrieva, Professor, Dr.Sc.,
Irkutsk National Research Technical University; 83, Lermontov street, Irkutsk, 664074, Russia

Petr P. Gaidzhurov, Advisor of RAACS, Professor, Dr.Sc.,
Don State Technical University; 1, Gagarina Square, Rostov-on-Don, 344000, Russia

Jacek Grosel, Associate Professor, Dr inz.
Wroclaw University of Technology; 11 Grunwaldzki Sq., 50-377, Wrocław, Poland

Stanislaw Jemioło, Professor, Dr.Sc.,
Warsaw University of Technology; 1, Pl. Politechniki, 00-661, Warsaw, Poland

Konstantin I. Khenokh, M.Ing., M.Sc.,
General Dynamics C4 Systems; 8201 E McDowell Rd, Scottsdale, AZ 85257, USA

Christian Koch, Dr.-Ing., Ruhr-Universität Bochum;
Lehrstuhl für Informatik im Bauwesen, Gebäude IA, 44780, Bochum, Germany

Gaik A. Manuylov, Professor, Ph.D.,
Moscow State University of Railway Engineering; 9, Obraztsova Street, Moscow, 127994, Russia

Alexander S. Noskov, Professor, Dr.Sc.,
Ural Federal University named after the first President of Russia B.N. Yeltsin;
19 Mira Street, Ekaterinburg, 620002, Russia

Grzegorz Świt, Professor, Dr.hab. Inż.,
Kielce University of Technology; 7, al. Tysiąclecia Państwa Polskiego, Kielce, 25 – 314, Poland

AIMS AND SCOPE

The aim of the Journal is to advance the research and practice in structural engineering through the application of computational methods. The Journal will publish original papers and educational articles of general value to the field that will bridge the gap between high-performance construction materials, large-scale engineering systems and advanced methods of analysis.

The scope of the Journal includes papers on computer methods in the areas of structural engineering, civil engineering materials and problems concerned with multiple physical processes interacting at multiple spatial and temporal scales. The Journal is intended to be of interest and use to researches and practitioners in academic, governmental and industrial communities.

ОБЩАЯ ИНФОРМАЦИЯ О ЖУРНАЛЕ

International Journal for Computational Civil and Structural Engineering

(Международный журнал по расчету гражданских и строительных конструкций)

Международный научный журнал "International Journal for Computational Civil and Structural Engineering (Международный журнал по расчету гражданских и строительных конструкций)" (IJCCSE) является ведущим научным периодическим изданием по направлению «Инженерные и технические науки», издаваемым, начиная с 1999 года (ISSN 2588-0195 (Online); ISSN 2587-9618 (Print) Continues ISSN 1524-5845). В журнале на высоком научно-техническом уровне рассматриваются проблемы численного и компьютерного моделирования в строительстве, актуальные вопросы разработки, исследования, развития, верификации, апробации и приложений численных, численно-аналитических методов, программно-алгоритмического обеспечения и выполнения автоматизированного проектирования, мониторинга и комплексного наукоемкого расчетно-теоретического и экспериментального обоснования напряженно-деформированного (и иного) состояния, прочности, устойчивости, надежности и безопасности ответственных объектов гражданского и промышленного строительства, энергетики, машиностроения, транспорта, биотехнологий и других высокотехнологичных отраслей.

В редакционный совет журнала входят известные российские и зарубежные деятели науки и техники (в том числе академики, члены-корреспонденты, иностранные члены, почетные члены и советники Российской академии архитектуры и строительных наук). Основной критерий отбора статей для публикации в журнале − их высокий научный уровень, соответствие которому определяется в ходе высококвалифицированного рецензирования и объективной экспертизы, поступающих в редакцию материалов.

Журнал входит в Перечень ВАК РФ ведущих рецензируемых научных изданий, в которых должны быть опубликованы основные научные результаты диссертаций на соискание ученой степени кандидата наук, на соискание ученой степени доктора наук по научным специальностям и соответствующим им отраслям науки:

- 1.1.8 – Механика деформируемого твердого тела (технические науки),
- 1.2.2 – Математическое моделирование численные методы и комплексы программ (технические науки),
- 2.1.1 – Строительные конструкции, здания и сооружения (технические науки),
- 2.1.2 – Основания и фундаменты, подземные сооружения (технические науки),
- 2.1.5 – Строительные материалы и изделия (технические науки),
- 05.23.07 – Гидротехническое строительство (технические науки),
- 2.1.9 – Строительная механика (технические науки)

В Российской Федерации журнал индексируется Российским индексом научного цитирования (РИНЦ).

Журнал входит в базу данных Russian Science Citation Index (RSCI), полностью интегрированную с платформой Web of Science. Журнал имеет международный статус и высылается в ведущие библиотеки и научные организации мира.

Издатели журнала – *Издательство Ассоциации строительных высших учебных заведений /АСВ/* (Россия, г. Москва) и до 2017 года *Издательский дом Begell House Inc*. (США, г. Нью-Йорк). Официальными партнерами издания является *Российская академия архитектуры и строительных наук* (РААСН), осуществляющая научное курирование издания, и *Научно-исследовательский центр СтаДиО* (ЗАО НИЦ СтаДиО).

Цели журнала – демонстрировать в публикациях российскому и международному профессиональному сообществу новейшие достижения науки в области вычислительных методов

решения фундаментальных и прикладных технических задач, прежде всего в области строительства.

Задачи журнала:

• предоставление российским и зарубежным ученым и специалистам возможности публиковать результаты своих исследований;

• привлечение внимания к наиболее актуальным, перспективным, прорывным и интересным направлениям развития и приложений численных и численно-аналитических методов решения фундаментальных и прикладных технических задач, совершенствования технологий математического, компьютерного моделирования, разработки и верификации реализующего программно-алгоритмического обеспечения;

• обеспечение обмена мнениями между исследователями из разных регионов и государств.

Тематика журнала. К рассмотрению и публикации в журнале принимаются аналитические материалы, научные статьи, обзоры, рецензии и отзывы на научные публикации по фундаментальным и прикладным вопросам технических наук, прежде всего в области строительства. В журнале также публикуются информационные материалы, освещающие научные мероприятия и передовые достижения Российской академии архитектуры и строительных наук, научно-образовательных и проектно-конструкторских организаций.

Тематика статей, принимаемых к публикации в журнале, соответствует его названию и охватывает направления научных исследований в области разработки, исследования и приложений численных и численно-аналитических методов, программного обеспечения, технологий компьютерного моделирования в решении прикладных задач в области строительства, а также соответствующие профильные специальности, представленные в диссертационных советах профильных образовательных организациях высшего образования.

Редакционная политика. Политика редакционной коллегии журнала базируется на современных юридических требованиях в отношении авторского права, законности, плагиата и клеветы, изложенных в законодательстве Российской Федерации, и этических принципах, поддерживаемых сообществом ведущих издателей научной периодики.

За публикацию статей плата с авторов не взымается. Публикация статей в журнале бесплатная. На платной основе в журнале могут быть опубликованы материалы рекламного характера, имеющие прямое отношение к тематике журнала.

Журнал предоставляет непосредственный открытый доступ к своему контенту, исходя из следующего принципа: свободный открытый доступ к результатам исследований способствует увеличению глобального обмена знаниями.

Индексирование. Публикации в журнале входят в системы расчетов индексов цитирования авторов и журналов. «Индекс цитирования» – числовой показатель, характеризующий значимость данной статьи и вычисляющийся на основе последующих публикаций, ссылающихся на данную работу.

Авторам. Прежде чем направить статью в редакцию журнала, авторам следует ознакомиться со всеми материалами, размещенными в разделах сайта журнала (интернет-сайт Российской академии архитектуры и строительных наук (http://raasn.ru); подраздел «Издания РААСН» или интернет-сайт Издательства АСВ (http://iasv.ru); подраздел «Журнал IJCCSE»): с основной информацией о журнале, его целями и задачами, составом редакционной коллегии и редакционного совета, редакционной политикой, порядком рецензирования направляемых в журнал статей, сведениями о соблюдении редакционной этики, о политике авторского права и лицензирования, о представлении журнала в информационных системах (индексировании), информацией о подписке на журнал, контактными данными и пр. Журнал работает по лицензии Creative Commons типа cc by-nc-sa (Attribution Non-Commercial Share Alike) – Лицензия «С указанием авторства – Некоммерческая – Копилефт».

Рецензирование. Все научные статьи, поступившие в редакцию журнала, проходят обязательное двойное слепое рецензирование (рецензент не знает авторов рукописи, авторы рукописи не знают рецензентов).

Заимствования и плагиат. Редакционная коллегия журнала при рассмотрении статьи проводит проверку материала с помощью системы «Антиплагиат». В случае обнаружения многочисленных заимствований редакция действует в соответствии с правилами COPE.

Подписка. Журнал зарегистрирован в Федеральном агентстве по средствам массовой информации и охраны культурного наследия Российской Федерации. Индекс в общероссийском каталоге РОСПЕЧАТЬ − 18076.

По вопросам подписки на международный научный журнал “International Journal for Computational Civil and Structural Engineering (Международный журнал по расчету гражданских и строительных конструкций)” обращайтесь в Агентство «Роспечать» (Официальный сайт в сети Интернет: http://www.rosp.ru/) или в издательство Ассоциации строительных вузов (АСВ) в соответствии со следующими контактными данными:

ООО «Издательство АСВ»

Юридический адрес: 129337, Россия, г. Москва, Ярославское ш., д. 26, офис 705;

Фактический адрес: 129337, Россия, г. Москва, Ярославское ш., д. 19, корп. 1, 5 этаж, офис 12 (ТЦ Соле Молл);

Телефоны: +7 (925) 084-74-24;

Интернет-сайт: www.iasv.ru. Адрес электронной почты: iasv@iasv.ru.

Контактная информация. По всем вопросам работы редакции, рецензирования, согласования правки текстов и публикации статей следует обращаться к главному редактору журнала академику РААСН *Сидорову Владимиру Николаевичу* (адреса электронной почты: sidorov.vladimir@gmail.com, sidorov@iasv.ru, iasv@iasv.ru, sidorov@raasn.ru) или к техническому редактору журнала советнику РААСН *Кайтукову Таймуразу Батразовичу* (адреса электронной почты: tkaytukov@gmail.com; kaytukov@raasn.ru). Кроме того, по указанным вопросам, а также по вопросам размещения в журнале рекламных материалов можно обращаться к генеральному директору ООО «Издательство АСВ» *Никитиной Надежде Сергеевне* (адреса электронной почты: iasv@iasv.ru, nsnikitina@mail.ru, ijccse@iasv.ru).

Журнал становится технологичнее. Издательство АСВ с сентября 2016 года является членом Международной ассоциации издателей научной литературы (Publishers International Linking Association (PILA)), осуществляющей свою деятельность на платформе CrossRef. Оригинальным статьям, публикуемым в журнале, будут присваиваться уникальные номера (индексы DOI – Digital Object Identifier), что значительно облегчит поиск метаданных и местонахождение полнотекстового произведения. DOI – это система определения научного контента в сети Интернет.

С октября 2016 года стал возможен прием статей на рассмотрение и рецензирование через онлайн систему приема статей Open Journal Systems на сайте журнала (электронная редакция): https://ijccse.iasv.ru.

Автор имеет возможность следить за продвижением статьи в редакции журнала в личном кабинете Open Journal Systems и получать соответствующие уведомления по электронной почте.

В феврале 2018 года журнал был зарегистрирован в Directory of open access journals (DOAJ) (это один из самых известных поисковых сервисов в мире, который предоставляет открытый доступ к материалам и индексирует не только заголовки журналов, но и научные статьи), в сентябре 2018 года включен в продукты EBSCO Publishing.

В ноябре 2020 года журнал начал индексироваться в международной базе Scopus.

International Journal for
Computational Civil and Structural Engineering
(Международный журнал по расчету гражданских и строительных конструкций)
Volume 20, Issue 3 ***2024***

Scientific coordination is carried out by the Russian Academy of Architecture and Construction Sciences (RAACS)

CONTENTS

Deformation Modeling of Rod Structures Under Controlled Kinematic Action 14
Peter P. Gaydzhurov, Nadezhda G. Tsaritova

Contact Problem for a Spherical Shell Supported on Two Flat Surfaces 24
Alexey A. Kireenkov, Grigory V. Fedotenkov

Evaluate the Influence of Concrete Strength on the Level of Corrosion of Steel Reinforcement in Reinforced Concrete Beam Structures, Taking Into Account the Applied Load 35
Vo Van Nam, Nguyen Trong Tam

Numerical Solution of the Filtration-Deformation Problem in the Case of Phased Construction of a Storage Dam 45
Nikolay A. Aniskin, Stanislav A. Sergeev, Andrey V. Stupivtsev, Ilia A. Bokov

Nonlinear Dynamic Analysis of wind Actions on a Cable-Stayed Glass Façade System 56
Oleg S. Goryachevsky, Alexander M. Belostotsky

An Innovative Hybrid Machine Learning Techniques for Predicting Construction Cost Estimates 69
Kittisak Lathong, Kittipol Wisaeng

Diagnostics and Renovation Methods for Steel Pipelines 84
Vladimir A. Orlov , Sergey P. Zotkin, Dmitry V. Podolyan

Rational Design of Nonlinear-Deformable Structurally Heterogeneous Elements of Structures 97
Andrey V. Mishchenko, Maxim S. Veshkin, Vladimir L. Mondrus, Leonid Yu. Stupishin

Model of Cake Filtration in Porous Medium 116
Liudmila I. Kuzmina, Yuri V. Osipov

RC Buildings Response to Earthquakes: Nonlinear Static Analysis Considering Varying Soil Types and Seismic Codes 125
Amer Yassin, Rifat Resatoglu

The Problem of Normalizing the Parameters of the Second Group of Limits for High-Strength Reinforced Concrete Constructions **145**
Vladimir I. Kolchunov Sergei S. Fedorov

The Moisture Regime of Enclosing Structures in Different Construction Areas **159**
Kirill P. Zubarev

Nonlocal in Time Model of the Longitudinal Vibrations of the High-Damping Steel Rod Element **167**
Sergey I. Zhavoronok, Elena. S. Badina

Development of Computational Schemes of Group Target Constraints for Some Elastic Systems. Part 1: Theoretical Foundations **180**
Leonid S. Lyakhovich, Pavel A. Akimov, Zaur R. Galyautdinov, Andrey S. Plyaskin

Development of Computational Schemes of Group Target Constraints for Some Elastic Systems. Part 2: Samples of Analysis **186**
Leonid S. Lyakhovich, Pavel A. Akimov, Zaur R. Galyautdinov, Andrey S. Plyaskin

Consideration of the Seismic Impact's Wave Nature in the Design Justification of High-Rise Buildings' Seismic Resistance **198**
Dmitry S. Dmitriev, Pavel I. Novikov, Sergey O. Petryashev, Alexandr I. Nagibovich

Development of Methods for Designing Pile Foundations for Multi-Storey Civil Buildings Constructed on Macroporous Subsidence Soils **206**
Maxim B. Marinichev, Nadezhda S. Nikitina, Anatoly I. Polishchuk

International Journal for
Computational Civil and Structural Engineering
(Международный журнал по расчету гражданских и строительных конструкций)
Volume 20, Issue 3 ***2024***

Scientific coordination is carried out by the Russian Academy of Architecture and Construction Sciences (RAACS)

СОДЕРЖАНИЕ

Деформационное моделирование стержневых конструкций при управляемом кинематическом воздействии **14**
П.П. Гайджуров, Н.Г. Царитова

Контактная задача для сферической оболочки, опирающейся на две плоские поверхности **24**
А.А. Киреенков, Г.В. Федотенков

Оценка влияния прочности бетона на уровень коррозии стальной арматуры в железобетонных балочных конструкциях с учетом приложенной нагрузки **35**
Во Ван Нам, Нгуен Чонг Там

Численное решение фильтрационно-деформационной задачи при поэтапном возведении дамбы накопителя **45**
Н.А. Анискин, С.А. Сергеев, А.В. Ступивцев, И.А. Боков

Нелинейный динамический расчет вантового светопрозрачного фасада на ветровые воздействия **56**
О.С. Горячевский, А.М. Белостоцкий

Инновационные гибридные методы машинного обучения для прогнозирования стоимости строительства **69**
К. Латонг, К. Висенг

Диагностика стальных трубопроводов и методы их реновации **84**
Вл.А. Орлов, С.П. Зоткин, Д.В. Подолян

Рациональное проектирование нелинейно-деформируемых структурно-неоднородных элементов конструкций **97**
А.В. Мищенко, М.С. Вешкин, В.Л. Мондрус, Л.Ю. Ступишин

Модель поверхностной фильтрации в пористой среде **116**
Л.И. Кузьмина, Ю.В. Осипов

Отклик железобетонных каркасов зданий при землетрясениях: нелинейный статический анализ с учетом различных типов грунтов и сейсмических норм **125**
Амер Ясин, Рифат Ресатоглу

Проблема нормирования параметров предельных состояний второй группы для конструкций из высокопрочного железобетона **145**
Вл.И. Колчунов, С.С. Федоров

Влажностный режим ограждающих конструкций в различных районах строительства **159**
К.П. Зубарев

Нелокальная во времени модель продольных колебаний стержневого элемента, выполненного из стали со сверхвысоким демпфированием **167**
С.И. Жаворонок, Е.С. Бадьина

О формировании расчетных схем групповых прицельных связей для некоторых упругих систем. Часть 1: теоретические основы подхода **180**
Л.С. Ляхович, П.А. Акимов, З.Р. Галяутдинов, А.С. Пляскин

О формировании расчетных схем групповых прицельных связей для некоторых упругих систем. Часть 2: примеры расчетов **186**
Л.С. Ляхович, П.А. Акимов, З.Р. Галяутдинов, А.С. Пляскин

Учет волнового характера сейсмического воздействия при расчетном обосновании сейсмостойкости высотных зданий **198**
Д.С. Дмитриев, П.И. Новиков, С.О. Петряшев, А.И. Нагибович

Развитие методов проектирования свайных фундаментов на макропористых просадочных грунтах для многоэтажных гражданских зданий **206**
М.Б. Мариничев, Н.С. Никитина, А.И. Полищук

International Journal for Computational Civil and Structural Engineering, 20(3) 14–23 (2024)

DOI:10.22337/2587-9618-2024-20-3-14-23

DEFORMATION MODELING OF ROD STRUCTURES UNDER KINEMATIC CONTROLLED ACTION

Peter P. Gaydzhurov [1], Nadezhda G. Tsaritova [2]

[1] Don State Technical University, Rostov-on-Don, RUSSIA

[2] Platov South-Russian State Polytechnic University, Novocherkassk, RUSSIA

Abstract. Currently, transformable rod systems have found wide application in the designs of spacecraft panels and as various stents in medicine. It is of some theoretical interest to extent the idea of geometric variability to spatial rod systems of complex shape. The concept of kinematic shaping of a regular rod system from a flat to a domed position is proposed. The finite element method in combination with the modified Lagrange method was used for numerical implementation of this concept. To assess the level of deformed state of the rods of a modular lattice, an energy criterion is proposed that allows determining the most loaded rods considering genetic nonlinearity of the system.

Keywords: deformation modeling, rod system, finite element method, modified Lagrange method, genetic nonlinearity

ДЕФОРМАЦИОННОЕ МОДЕЛИРОВАНИЕ СТЕРЖНЕВЫХ КОНСТРУКЦИЙ ПРИ УПРАВЛЯЕМОМ КИНЕМАТИЧЕСКОМ ВОЗДЕЙСТВИИ

П.П. Гайджуров [1], Н.Г. Царитова [2]

[1] Донской государственный технический университет, г. Ростов-на-Дону, РОССИЯ

[2] «Южно-Российский государственный политехнический университет (НПИ) имени М.И. Платова», г. Новочеркасск, РОССИЯ

Аннотация. В настоящее время трансформируемые стержневые системы нашли широкое применение в конструкциях панелей космических аппаратов и медицине в виде различных стентов. Представляет определенный теоретический интерес развить идею геометрической изменяемости на пространственные стержневые системы сложной формы. Предлагается концепция кинематического формоизменения регулярной стержневой системы из плоского в куполообразное положение. Для численной реализации применен метод конечных элементов в сочетании модифицированным методом Лагранжа. Для оценки уровня деформированного состояния стержней регулярной решетки с учетом генетической нелинейности предложен энергетический критерий, позволяющий определить наиболее нагруженные стержни.

Ключевые слова: деформационное моделирование, стержневая система, метод конечных элементов, модифицированный метод Лагранжа, генетическая нелинейность

INTRODUCTION

Deformation modeling appeared as one of the directions of computer graphics, which allows to convert the kinematics of a physically observed object into virtual reality. The concept of a deformable model is usually considered from the point of view of mechanics of a deformable solid. In accordance with this concept, it is convenient to describe the deformation process of some continuum in Lagrangian coordinates. The paradigm of the deformable model is a “snake”, the shape and geometry of the “body” of which depends on the displacements of key points [1, 2, 3]. Formally, a “snake” is a contour defined parametrically, as a rule, by a cubic spline. The technology of approximation of the initial contour by a spline is based on the procedure of

minimization of the functional associated with the deformation energy of the contour within the boundaries of the area surrounding each key point (Fig. 1).

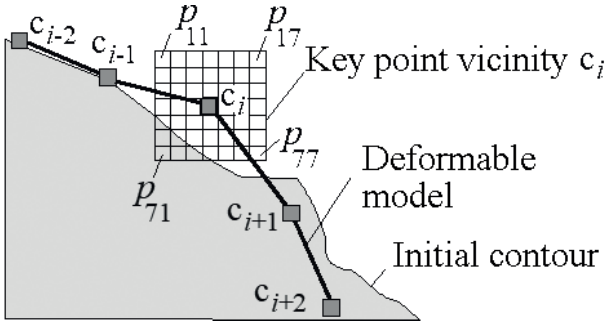


Figure 1. Deformable "snake" model

Approximation of the initial contour with a "snake"-type deformable model is widely used in biomedical research such as "computed tomography", as well as in applications of artificial intelligence to motion tracking and object identification tasks.

Another approach to the construction of a geometrically deformable model (GDM) is the concept based on the expansion of a virtual thin-walled balloon inside the boundaries of the scanned object (Fig. 2). The GDM technology uses the finite element method in the form of the displacement method as a mathematical apparatus. The balloon is modeled by momentless three-node plate finite elements. The geometry of the balloon at time t is represented in parametric form [4, 5]:

$$R(u,v,t)=\left[\psi_x(u,v,t),\psi_y(u,v,t),\psi_z(u,v,t)\right],$$

where ψ_x, ψ_y, ψ_z are approximating cubic spline functions along the axes x, y, z; u, v are dimensionless variables such that $u\in[0,1]$, $v\in[0,1]$. During the scanning of the internal cavity of the object under study, each node of the finite element model is attracted to a point of the bounding contour in the normal direction (Fig. 3). The current deformed state of the finite element is fully determined by the metric tensor [6, 7, 8]

$$g\left(R(u,v,t)\right)=\frac{\partial R}{\partial u}\frac{\partial R}{\partial v}.$$

The fundamental theorem of the mechanics of a deformable solid [9] stipulates that two bodies in Euclidean space will have the same instantaneous shape, i.e., differ only in displacement as a "rigid whole", if their metric tensors are identical at time t.



Figure 2. Visualization of GDM technology [6]

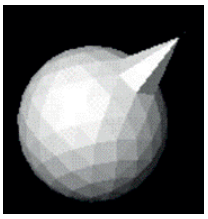


Figure 3. Balloon model deformed by a point force [7]

According to [6], the adaptation algorithm is constructed in such a way that the following condition is satisfied at each step in the nodes of the finite element mesh:

$$C(x,y,z)=\alpha_0 D(x,y,z)+\alpha_1 I(x,y,z)+\alpha_2 T(x,y,z)\geq 0, \quad (1)$$

where $C(x,y,z)$ is a target function associated with the current position of the model node point; $D(x,y,z)$ is the deformation potential (monotonically decreasing or increasing function); $I(x,y,z)$ is a constraint function "informing" a finite element mesh node that it can be in contact with a voxel (an element of the object image); $C(x,y,z)$ is the topological information function, preventing nodes of the finite element model from penetrating the object boundary; α_0, α_1, α_2 are weight factors. Condition (1)

causes the model to deform until all vertices reach the boundary of the scanned object.

Another direction of deformation modeling is the analysis of the behavior of spatial rod structures experiencing large linear and angular displacements at small deformations during operation. In this case, the numerical solution of the geometrically nonlinear problem is based on the Newton-Raphson iterative procedure and the method of "corrective arcs", the essence of which is the adaptive adjustment of the loading step value when approaching and after passing the bifurcation point [9,10]. It should be noted that the calculation of the rod system by the finite element method (FEM), taking into account large displacements, uses a tangent stiffness matrix. The construction of this matrix is based on the minimization of the strain energy potential [9]:

$$\frac{\partial^2 U}{\partial \mathbf{y}^2}\Delta\mathbf{y} + \frac{\partial U}{\partial \mathbf{y}} = \mathbf{P}^{(e)},$$

where $\mathbf{y}$, $\mathbf{P}^{(e)}$ are the vectors of displacements and generalized external forces. The potential energy of a finite element (FE) can be represented as

$$U = \frac{1}{2}\mathbf{y}^T \left[k\right]^{(e)} \mathbf{y},$$

where $\left[k\right]^{(e)}$ is the element stiffness matrix in global axes. The paper [11] proposes to consider the matrix elements $\left[k\right]^{(e)}$ to be constant for twice differentiation U.

As an illustration of the solution of such a problem in the geometrically nonlinear formulation, we have considered a test task from [9, 11]. A flexible curvilinear bar of rectangular cross-section of 1×1 m with arch radius of 100 m at central angle of 45^0 is rigidly fixed at the end (x = 0, y = 0, z = 0). It is subjected to bending out of the plane by a concentrated force F_z = 100 N. The coordinates of the free end of the rod in the initial position are [70,71; 70,71; 0] m. Mechanical constants of the rod material: modulus of elasticity E = 10 MPa; Poisson's ratio ν = 0. Fig. 4 shows the results of the analysis performed using the nonlinear solver of the ANSYS software [12]. The beam was divided into 16 spatial beam-type elements of BEAM4.

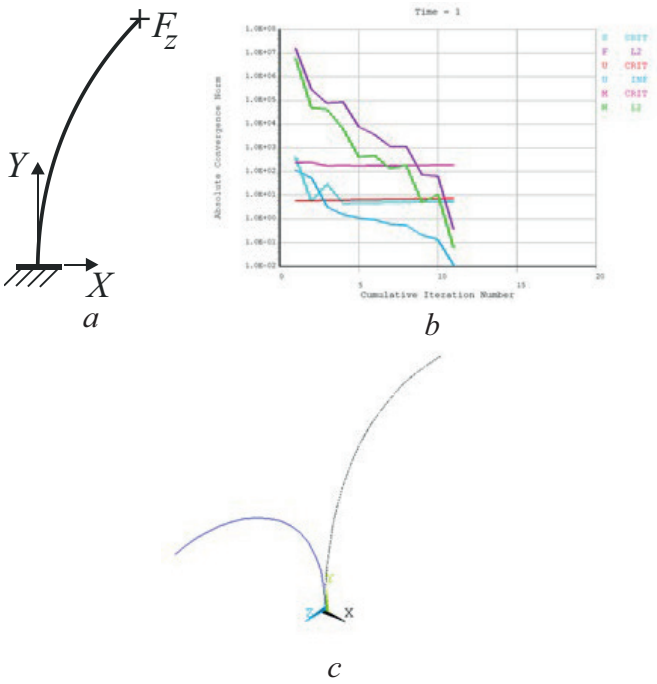


Figure 4. Results of analysis of a curved beam: a - initial state of the beam; b - parameters of ANSYS nonlinear solver; c - visualization of the beam deformation relative to the initial position

The displacement coordinates of the load application point were [46.84; 15.56; 53.66] m according to [9, 11] and [46.9; 15.6; 53.6] m according to the ANSYS solution. As can be seen, the given displacement values are quite close.

The above presented concepts of deformation modeling are highly specialized and cannot be extended to the problems of structural mechanics related to the study of kinematically transformed rod systems. In this regard, the development of a finite element modeling approach for rod structures considering the structural shape change of the initial geometry into some structural state is an urgent problem.

MATERIALS AND METHODS

Let us investigate the regular rod systems shown in the initial (undeformed) state in Fig. 5., tak-

ing into account the controlled displacement of contour nodes.

A distinctive feature of these computational schemes from the one presented in [13] is the presence of a nodal platform S modeled by rods with an elastic modulus exceeding the elastic modulus of the connecting rods by five orders of magnitude. From the structural point of view, the introduction of platforms S allows to conventionally account for the nodal connections of real rod systems. In the extracted fragments of Fig. 5, the letters L and B denote the lattices composed of hinged-rod (truss) and beam finite elements, respectively. In both cases, the nodal platforms S are modeled by almost non-deformable beam FE.

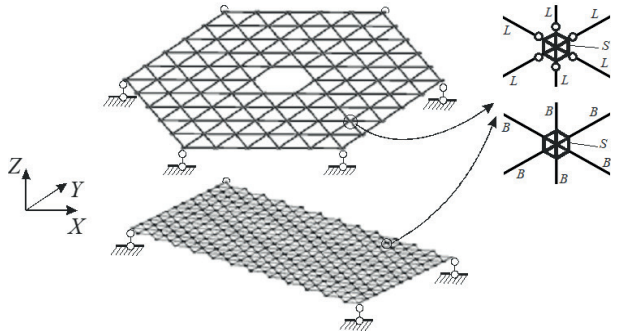


Figure 5. Rod model in the initial state

To investigate the process of change of a rod structure shape, we apply a modified Lagrange method [14], the essence of which consists in a discrete increment of displacements of contour nodes and reconstruction of the finite element mesh geometry in the current initial basis, taking into account the obtained nodal displacements. In the literature on structural mechanics, this type of nonlinearity is called genetic [15]. For program realization of this concept, we use the APDL programming language [12], embedded in the ANSYS Mechanical software package.

At kinematic quasi-static shape change, internal forces caused by gravitational influence and structural bonds will appear in the structure's rods. To assess the level of deformed state of the finite element model, we introduce an energy criterion, which for the adopted scheme of rod discretization can be indirectly represented in the form of longitudinal strain $\varepsilon = \Delta l / l$, where Δl is the changes in the rod length; l is the initial rod length.

RESEARCH RESULTS

First, as an object of study, consider a regular rod system that is hexagonal in plan (Fig. 6). The lengths of the rods forming the regular lattice of the structure are 0.4 m. The radius of the circumscribed circle of the platform S is 0.05 m. The mechanical constants of the rods (aluminum alloy) are $E = 7.2 \cdot 10^4$ MPa, $\nu = 0.32$, specific gravity = 2885 kg/m^3. The rods of the lattice and platforms S have a tubular cross-section with an outside diameter of 18 mm and a wall thickness of 1.5 mm.

Fig. 7 shows the visualization of the first mode of natural vibrations of the model for truss and beam FEs. As can be seen, the regular lattice modeled by truss FEs is kinematically variable, since it allows rotation of rigid platforms. Therefore, in the further study we will use only truss FEs.

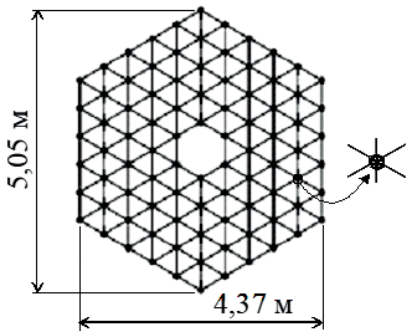
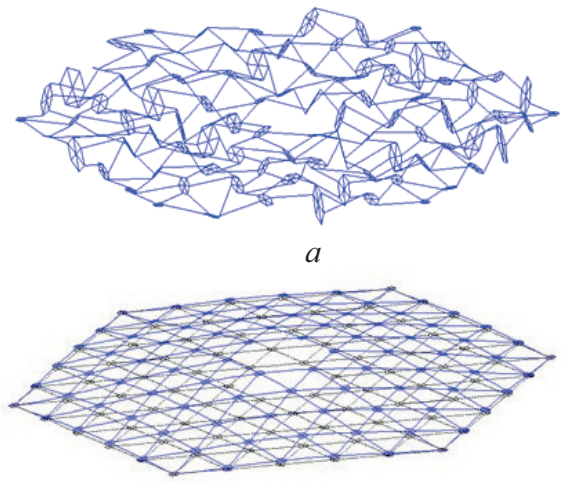


Figure 6. Initial dimensions of the rod structure with hexagonal plan

It should be noted that the transformation process will not lead to the expected lifting of the rod lattice from the position when the coordinates of all nodes $z_i = 0$. Thus, is necessary to "start" the transformation from a pre-prepared dome-shaped geometry (Fig. 8). Let's take the "starting" lifting height of $\Delta u_z = 0.1$ m.



a

b

Figure 7. The first eigenmode: a - truss FEs; b - bar FEs

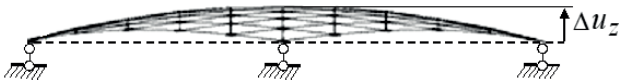


Figure 8. "Start" position of the rod structure

Let us analyze the kinematic change for the considered rod structure in the "starting" position, with discrete displacement of contour nodes in the direction of *X* and *Y* axes (Fig. 9). We assume that the displacement steps and are synchronous Δ_x and Δ_y equal to 0.01 m.

Figure 10 shows a visualization of the shape of the structure after 50 steps. The lift of the center point, when the transformation was completed, was of f_{max} = 0.92 m. Changes $\Delta l / l$ in the rods of the lattice at discrete displacements along the *X* and *Y* axes are plotted in Fig. 11.

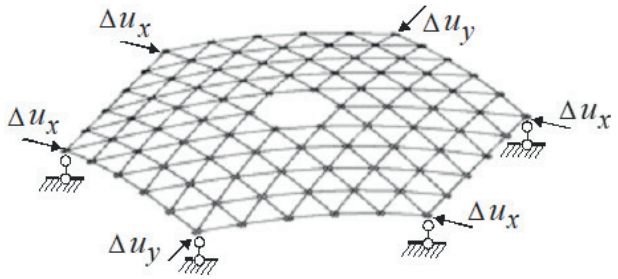


Figure 9. Discrete displacements along the X and Y axes

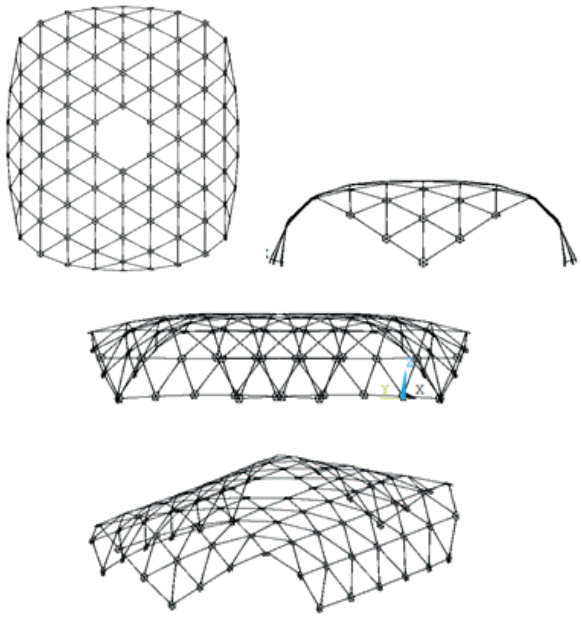


Figure 10. Visualization of a form change after 50 displacement steps along the X and Y axes

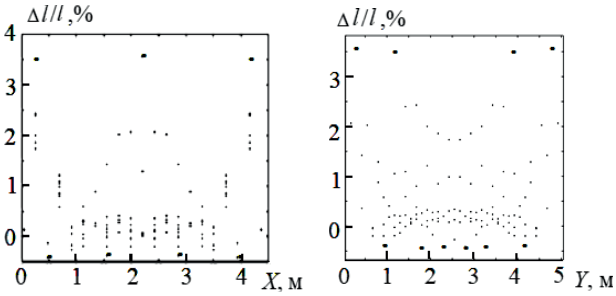


Figure 11. Changes $\Delta l / l$ in the rods at displacement of contour nodes along X and Y axes

Fig. 11 shows that the rods adjacent to the contour nodes will be the most stressed in this transformation scheme. In natural terms, the extreme value $\Delta l / l$ =3.5 % corresponds to the rod elongation Δl = 14 mm.

Fig. 12 shows the results of solving a similar problem using the nonlinear solver of ANSYS Mechanical. In this case, the "starting" position of the lattice was also used and kinematic boundary conditions in the form of displacements of contour nodes equal to 0.5 m were set. The simulation was performed taking into account large displacements (*Large Displacement Static*).

By comparing the patterns of the lattice in the deformed state shown in Figs. 10 and 12, we establish their qualitative agreement.

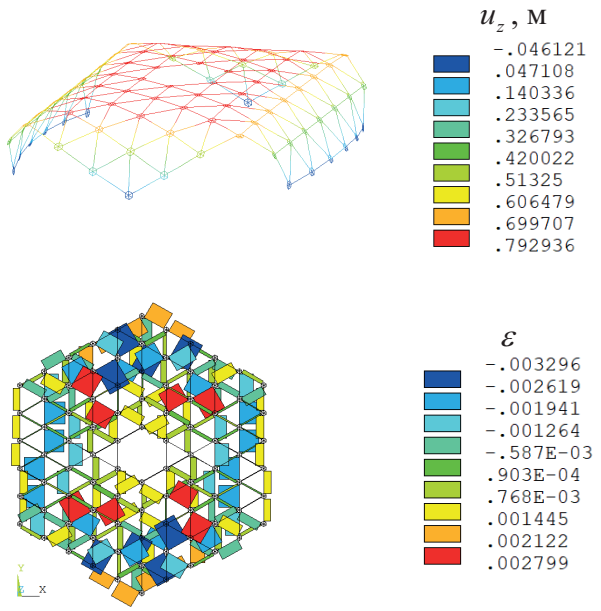


Figure 12. Results of the analysis using a non-linear solver: u_z - vertical displacements; ε – longitudinal strain

At the same time, the value of the maximum lift at one-step transformation is of f_{max} = 0.79 m, which is less than at discrete forming f_{max} = 0.92 m. There is also a significant qualitative and quantitative difference in the distribution patterns of longitudinal strains in the lattice rods. Moreover, at discrete shaping, the extreme value exceeds by more than an order of magnitude the similar value shown in Fig. 12. Thus, the proposed method of discrete shaping combined with step-by-step correction and reconstruction of the finite element mesh taking into account the obtained nodal displacements should be used when modeling the process of transformation of the geometry of a regular lattice system.

Let us consider the scheme of transformation of the rod structure at discrete displacements Δ_x = 0.01 mm along the X axis only (Fig. 13). Visualization of the lattice shape after 50 steps of transformation along X is shown in Fig. 14.

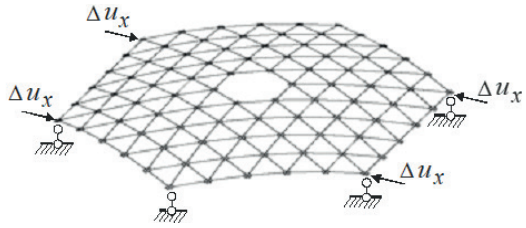


Figure 13. Discrete displacements along the X axis

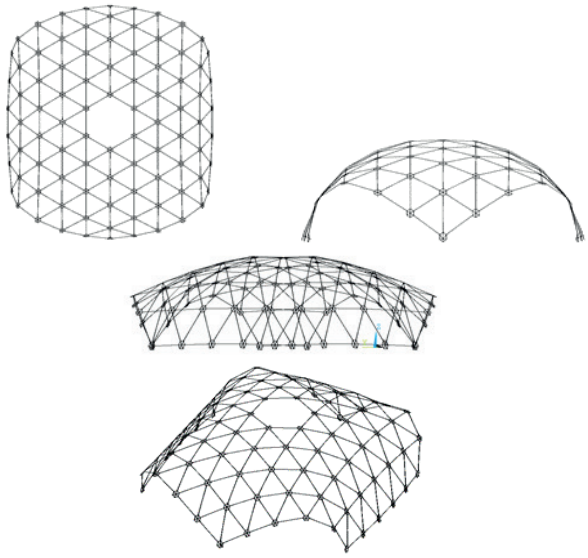


Figure 14. Visualization of the shape change after 50 displacement steps along the X-axis

In this case, the lift at the pole point, when the transformation was completed, was 1.3 m. The corresponding plots of longitudinal strain in the rods are shown in Fig. 15.

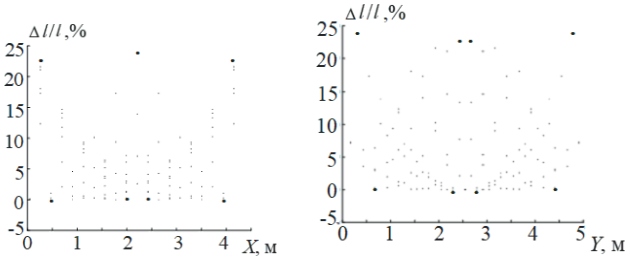


Figure 15. Change $\Delta l / l$ in rods when contour nodes are displaced along the X-axis

Comparing the dome shapes of the rod structure under uniform compression along the X and Y axes (Fig. 10) and compression only in the X

direction (Fig. 14), we conclude that in the second case there is a more pronounced roundness of the surface. At the same time, the maximum value of the ratio $\Delta l / l$ in Fig. 15 is almost seven times greater than the similar value presented in the plots of Fig. 11.

Finally, let us perform deformation modeling of a regular rod system with rectangular plan (Fig. 16). The design scheme for the transformation is shown in Fig. 17. The step Δ_x along the *X*-axis is assumed to be 0.05 m.

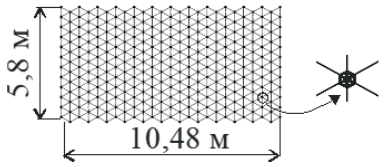


Figure 16. Initial dimensions of the rod rectangular structure

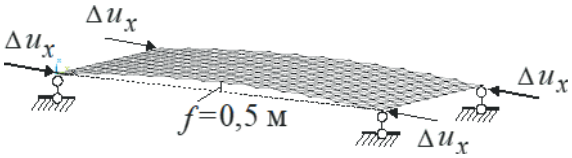


Figure 17. "Start" position of the rod structure

The visualization of the lattice patterns after 50 and 100 transformation steps are shown in Figures 18 and 19, respectively.

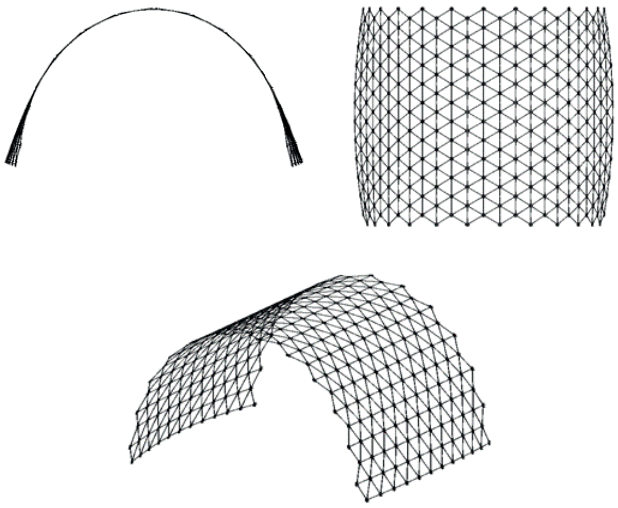


Figure 18. Visualization of the shape change after 50 displacement steps along the X-axis

The plots of changes $\Delta l / l$ in the rods of the lattice at 50 and 100 transformation steps are presented in Fig. 20. As can be seen from the plots in Figs. 11 and 20, the numerical values of extreme longitudinal strains in the rods of the considered hexagonal and rectangular regular lattices at 50 transformation steps practically coincide. In both schemes, the greatest longitudinal tensile strains are experienced by the contour nodes subjected to kinematic boundary conditions.

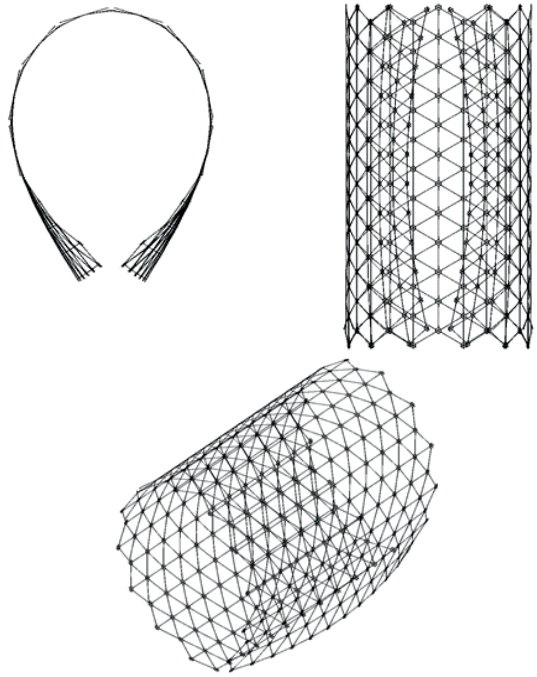


Figure 19. Visualization of the shape change after 100 displacement steps along the X-axis

It should be noted that the rectangular lattice (Fig. 19) has the greatest ability to change its shape; it practically rolls up into a "roll" at 100 transformation steps.

In order to investigate the influence of the scheme of kinematic boundary conditions on the transformation process of a rectangular lattice, we consider a two-sided scheme of discrete displacements at all nodes with coordinates $x = 0$ and $x = 10.48$ m. Visualization of the lattice pattern after 50 steps at $\Delta_x = 0.5$ m is shown in Fig. 21.

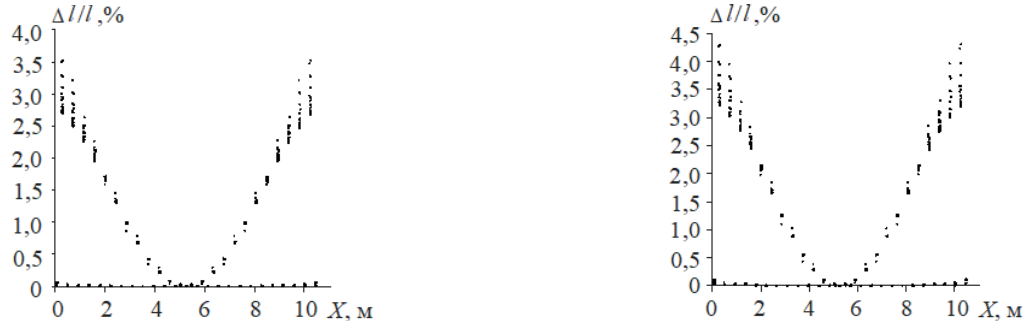


Figure 20. Plots of the change $\Delta l / l$ in the rods at displacement of contour nodes along the X axis: a - 50 steps; b - 100 steps

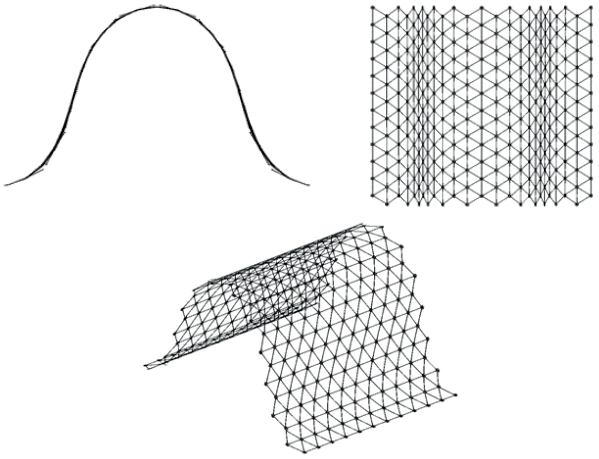


Figure 21. Visualization of lattice change after 50 displacement steps along the X-axis at two-sided discrete displacement

The plot of $\Delta l / l$ for a two-sided discrete displacement of the contour nodes is shown in Figure 22

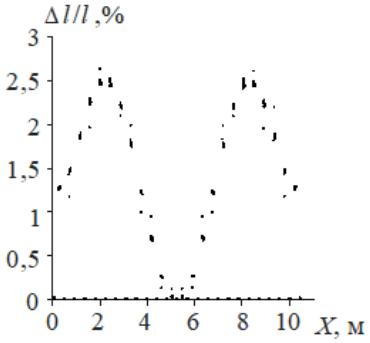


Figure 22. Plots of the change in the rods at a two-sided discrete displacement

It can be seen from the graph in Fig. 22 that the maximum tensile longitudinal strains at the two-sided discrete displacement of the contour nodes appear in the rods located in the kink areas.

CONCLUSIONS

1. A method of finite element modeling of transformation of a regular rod system from a flat to a dome-shaped state by discrete displacement of contour nodes of the lattice is proposed.
2. As a criterion limiting the process of the structure shape change, the values of longitudinal strains of the rods are proposed to be used.

REFERENCES

1. **D.P. Perrin and C.E. Smith**.(2001) Rethinking classical internal forces for active contour models, in 2013 IEEE Conference on Computer Vision and Pattern Recognition, vol.3, pp. 615. doi: 10.1109/CVPR.2001.991020.
2. **Kass M., Witkin A., Terzopoulos D. Snakes** (1988) Active contour models. Int J Comput Vision, vol.1, pp. 321–331.
3. **McInerney T, Terzopoulos D.** (1996) Deformable models in medical image analysis: a survey, Medical Image Analysis, vol. 1, no. 2, pp. 91-108. doi:10.1016/S1361-8415(96)80007-7.
4. **Terzopoulos D., Fleischer K.** (1988) Deformable models, The Visual Computer 4, pp. 306–331.

5. **Terzopoulos D., Platt J., Barr A., Fleischer K.** (1987). Elastically Deformable Models. ACM Siggraph Computer Graphics, vol.21.
6. **Miller J., Breen D., Lorensen W., O'Bara R., Wozny M.** (1991) Geometrically deformed models. ACM SIGGRAPH Computer Graphics, vol.25, pp. 217-226.
7. **McInerney, T., Terzopoulos, D.** (1995). A dynamic finite element surface model for segmentation and tracking in multidimensional medical images with application to cardiac 4D image analysis. Computerized medical imaging and graphics : the official journal of the Computerized Medical Imaging Society, vol.19 1, pp. 69-83.
8. **Terzopoulos D., Witkin A., Kass M.,** (1988). Constraints on Deformable Models: Recovering 3D Shape and Nonrigid Motion, Artificial Intelligence, vol.36, pp. 91-123.
9. **Popov V., Sorokin F.** (2017) Development of the final element of a flexible rod with separate storage of accumulated and additional rotations for modeling large movements of structural elements of aircraft. Proceedings of MAI, vol. 92, pp. 3. (in Russian).
10. **Battini J.M. (**2002) Co-rotational beam elements with warping effects in instability problems. Computer Methods in Applied Mechanics and Engineering, vol. 191, no. 17-18, P pp. 1755-1789.
11. **Nizametdinov F., Sorokin F.** (2018) Features of the application of the Euler vector to describe large turns in the modeling of structural elements of aircraft using the example of a rod finite element. Proceedings of MAI, vo.l 102, no. 1. (in Russian).
12. ANSYS Mechanical APDL Programmers Reference. Reference. Release 15.0ANSYS, Inc. http://www.ansys.com
13. **Gaydzhurov P., Tsaritova N., Kurbanov A., Kurbanova A., Iskhakova E.** (2022). Numerical simulation of the process of directed transformation of a regular hinge-rod system. International Journal for Computational Civil and Structural Engineering, vol. 18(3), pp.14–24. https://doi.org/10.22337/2587-9618-2022-18-3-14-24.
14. **Gaydzhurov P., Iskhakova E., Savelieva N., Tsaritova N.** (2020). Finite element modeling of the shaping process of a hinge-rod system under controlled kinematic action. News of higher educational institutions. The North Caucasus region. Technical sciences, vol.3 (207), pp. 5-12.
15. **Perelmuter A.V., Kabantsev O.V.** (2015). Analysis of structures with a changing calculation scheme. Moscow: SCUD SOFT Publishing House, DIA Publishing House,. 148 p.

СПИСОК ЛИТЕРАТУРЫ

1. **D.P. Perrin and C.E. Smith**.(2001) Rethinking classical internal forces for active contour models, in 2013 IEEE Conference on Computer Vision and Pattern Recognition, vol.3, pp. 615. doi: 10.1109/CVPR.2001.991020.
2. **Kass M., Witkin A., Terzopoulos D. Snakes** (1988) Active contour models. Int J Comput Vision, vol.1, pp. 321–331.
3. **McInerney T, Terzopoulos D.** (1996) Deformable models in medical image analysis: a survey, Medical Image Analysis, vol. 1, no. 2, pp. 91-108. doi:10.1016/S1361-8415(96)80007-7.
4. **Terzopoulos D., Fleischer K.** (1988) Deformable models, The Visual Computer 4, pp. 306–331.
5. **Terzopoulos D., Platt J., Barr A., Fleischer K.** (1987). Elastically Deformable Models. ACM Siggraph Computer Graphics, vol.21.
6. **Miller J., Breen D., Lorensen W., O'Bara R., Wozny M.** (1991) Geometrically deformed models. ACM SIGGRAPH Computer Graphics, vol.25, pp. 217-226.
7. **McInerney, T., Terzopoulos, D.** (1995). A dynamic finite element surface model for segmentation and tracking in multidimensional medical images with

application to cardiac 4D image analysis. Computerized medical imaging and graphics : the official journal of the Computerized Medical Imaging Society, vol.19 1, pp. 69-83.
8. **Terzopoulos D., Witkin A., Kass M.,** (1988). Constraints on Deformable Models: Recovering 3D Shape and Nonrigid Motion, Artificial Intelligence, vol.36, pp. 91-123.
9. **Попов В.В., Сорокин Ф.Д.** (2017) Разработка конечного элемента гибкого стержня с раздельным хранением накопленных и дополнительных вращений для моделирования больших перемещений конструктивных элементов летательных аппаратов. Труды МАИ, № 92, с. 3.
10. **Battini J.M. (**2002) Co-rotational beam elements with warping effects in instability problems. Computer Methods in Applied Mechanics and Engineering, vol. 191, no. 17-18, P pp. 1755-1789.
11. **Низаметдинов Ф.Р., Сорокин Ф.Д.** (2018). Особенности применения вектора эйлера для описания больших поворотов при моделировании элементов конструкций летательных аппаратов на примере стержневого конечного элемента. Труды МАИ, (102), с. 1.
12. ANSYS Mechanical APDL Programmers Reference. Reference. Release 15.0ANSYS, Inc. http://www.ansys.com
13. **Gaydzhurov P., Tsaritova N., Kurbanov A., Kurbanova A., Iskhakova E.** (2022). Numerical simulation of the process of directed transformation of a regular hinge-rod system. International Journal for Computational Civil and Structural Engineering, vol. 18(3), pp.14–24. https://doi.org/10.22337/2587-9618-2022-18-3-14-24.
14. **Гайджуров П.П., Исхакова Э.Р., Савельева Н.А., Царитова Н.Г.** (2020). Конечно-элементное моделирование процесса формоизменения шарнирно-стержневой системы при управляемом кинематическом воздействии. Известия высших учебных заведений. Северо-Кавказский регион. Технические науки, № 3 (207), с.5-12.
15. **Перельмутер А.В., Кабанцев О.В.** Анализ конструкций с изменяющейся расчетной схемой. М.: Издательство СКАД СОФТ, Издательский дом АСВ, 2015. 148 с.

Peter P. Gaydzhurov, PhD, DSc, Professor of the Department «Technical mechanics», Don State Technical University, Rostov-on-Don, Advisor to the Russian Academy of Architecture and Building Sciences
e-mail: gpp-161@yandex.ru

Nadezhda G. Tsaritova, PhD, Associate Professor of the Department «Urban development, designing of buildings and structures», Platov South-Russian State Polytechnic University, (NPI), Novocherkassk,
e-mail: ncaritova@yandex.ru

Гайджуров Петр Павлович, доктор технических наук, профессор кафедры «Техническая механика» Донского государственного технического университета, советник РААСН, г. Ростов-на-Дону, e-mail: gpp-161@yandex.ru

Царитова Надежда Геннадьевна, кандидат технических наук, доцент кафедры «Градостроительство, проектирование зданий и сооружений», Южно-Российского государственного политехнического университета им. М.И.Платова (НПИ), г. Новочеркасск. e-mail: ncaritova@yandex.ru

DOI:10.22337/2587-9618-2024-20-3-24-34

CONTACT PROBLEM FOR A SPHERICAL SHELL SUPPORTED ON TWO FLAT SURFACES

Alexey A. Kireenkov [1,2], Grigory V. Fedotenkov [3,4]

[1] Ishlinskiy Institute for Problems in Mechanics of the Russian Academy of Sciences, Moscow, RUSSIA
[2] Moscow Institute of Physics and Technology (National Investigation University), Dolgoprudny, Moscow Region, RUSSIA
[3] Research Institute of Mechanics Lomonosov Moscow State University, Moscow, RUSSIA,
[4] Moscow Aviation Institute (National Research University), Moscow, RUSSIA

Abstract: An effective numerical and analytical method is proposed for studying the force state inside the contact spots of elastic composite spherical shells resting on two flat surfaces inclined at an angle to each other. The method is based on constructing the influence function for the shell in an axisymmetric formulation, followed by its expansion into a Fourier series using the Legendre and Gegenbauer polynomials. A resolving system of equations for the corresponding coefficients is obtained. The developed methodology will allow for a more correct study of the dynamics of various robotic systems, the main controlled elements of which are elastic spherical shells that carry out complex kinematic movements on various surfaces. These systems, in particular, include a "butterfly robot", the main controlled element of which is a thin spherical shell, rolling with simultaneous spinning and sliding along two parallel plates, as if on rails.

Keywords: spherical composite shell; contact problem; theory of the multicomponent anisotropic dry friction

КОНТАКТНАЯ ЗАДАЧА ДЛЯ СФЕРИЧЕСКОЙ ОБОЛОЧКИ, ОПИРАЮЩЕЙСЯ НА ДВЕ ПЛОСКИЕ ПОВЕРХНОСТИ

А.А. Киреенков [1], Г.В. Федотенков [2,3]

[1] Институт проблем механики РАН им. А.Ю. Ишлинского, Московский физико-технический институт (национальный исследовательский университет), г. Москва, РОССИЯ
[2] НИИ механики МГУ имени М.В. Ломоносова, г. Москва, РОССИЯ
[3] Московский авиационный институт (национальный исследовательский университет), г. Москва, РОССИЯ

Резюме: Предложен эффективный численно-аналитический метод исследования силового состояния внутри пятен контакта упругих композитных сферических оболочек, опирающихся на две наклоненные под углом к друг другу плоские поверхности. Метод основан на построении функции влияния для оболочки в осесимметричной постановке, с последующим ее разложением в ряд Фурье по полиномам Лежандра и Гегенбауэра. Получена разрешающая система уравнений для соответствующих коэффициентов. Разработанная методика позволит провести более корректное исследования динамики различных робототехнических систем, основными управляемыми элементами которых являются упругие сферические оболочки, осуществляющие сложные кинематические движения по различным поверхностям. К числу этих систем, в частности, относится «робот-бабочка», основной управляемый элемент которого, тонкая сферическая оболочка, катящаяся с одновременным верчением и проскальзыванием по двум параллельным пластинам, как по рельсам.

Ключевые слова: сферическая композитная оболочка; контактная задача; теория многокомпонентного анизотропного сухого трения

INTRODUCTION

The main goal of the proposed research is to develop the effective numerical and analytical methods for studying the force state inside the contact spots of elastic composite spherical shells supported on two flat surfaces inclined at an angle to each other.

The contact problem for a spherical shell resting on two flat surfaces is generated by the need for

a detailed study of the dynamics of various robotic systems in order to construct more effective control laws. The main controlled elements of these systems are elastic spherical shells that carry out complex kinematical movements on various surfaces [1-29].

In the case of non-point contact of rubbing bodies, the dynamics of the shells are significantly influenced by the effects of combined dry friction [1-29]. These effects arise due to the nonlinear relationship of the parameters describing the force state inside the contact spot (components of force and moment of friction) with kinematics parameters. To determine this relationship and calculate the coefficients of the so-called multicomponent friction model, knowledge of the laws of distribution of normal and tangential stresses inside the contact patch is required, taking into account the nature of the movement of the objects under study.

The task becomes much more difficult if the shell moves, contacting two surfaces at the same time, as is the case with the so-called “butterfly robot”. The main controlled element of the “butterfly robot” is a thin spherical shell, rolling with simultaneous spinning and sliding along two parallel plates, as if on rails.

The first developed control algorithms neglected the effects of combined dry friction under conditions of complex kinematics, which leads to their ineffectiveness for certain combinations of kinematical parameters of shell motion. To improve them, approximate models of dry friction inside contact patches were developed, under the assumption that an elastic ball is used as a controlled element, which allows the use of classical Hertz laws of distribution of normal contact stresses. As a result, effective approaches to constructing friction models for such systems were developed, based on simple asymptotic representations for distribution functions inside contact patches.

The used methodology for constructing friction models and determining their coefficients was previously developed to study the complex dynamics of pneumatic tires of various structures. In accordance with this technique, the distribution of normal pressure inside the contact patch is approximated by a linear approximation of the Taylor series expansion in polar or Cartesian coordinates inside the contact patch. In this case, the zero term of the expansion, which makes the main contribution to the calculation of the coefficients of friction models, is a stationary distribution (state of rest). The effectiveness of this approach made it possible to apply it in the case where a composite, spherical shell acts as the main controlled element. At the same time, the calculation of the stationary normal pressure distribution was made under the assumption that the shell is on a horizontal plane.

The presence of contact along two symmetrically located, non-horizontal areas significantly distinguishes the problem under consideration from those studied in previous works [30]. The normal reaction vector is no longer oppositely directed to the gravity vector (the weight of the shell), which, in turn, can lead to a significant change in the shape of the distribution of normal contact stresses inside the contact spots.

STATEMENT OF THE PROBLEM AND THE MAIN RESOLVING INTEGRAL EQUATION

To It is considering the contact problem for a spherical shell of the Timoshenko type [34, 35], supported on two flat solid surfaces intersecting at an opening angle α (Fig. 1). Here R and h are radius and shell thickness. It is assumed that $h << R$.

Let’s assume that the contact occurs under free slip conditions.

During deformation, two contact surfaces Ω_1 и Ω_2 are formed. The dimensions and positions of their boundaries are unknown in advance and must be determined in the process of solving the problem. The purpose of the contact problem is to determine contact pressures p_1 and p_2,

distributed respectively over the surfaces Ω_1 and Ω_2.

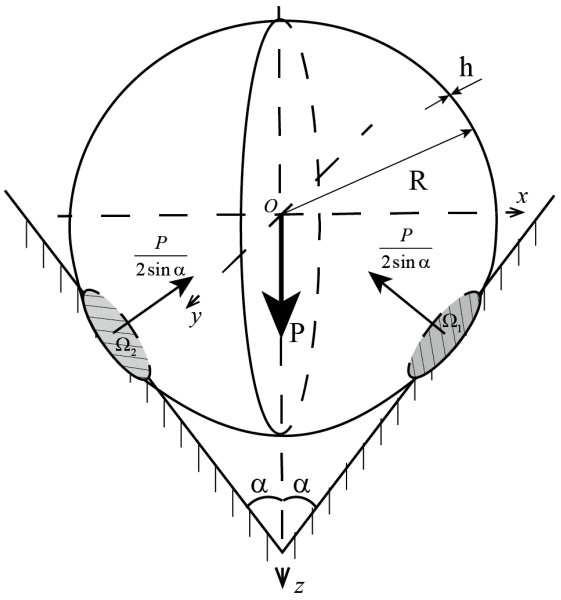


Figure 1. Contact problem

This problem is spatial but with two planes of symmetry: *Oxz* и *Oyz* (рис. 1). Consequently, $p_1 = p_2 = p$, as well as the size and geometry of the areas Ω_1 and Ω_2 are coincide. This fact makes it possible to reduce the dimension of the problem and present it as a superposition of two axisymmetric states with symmetry axes L_1 и L_2 (Fig. 2).

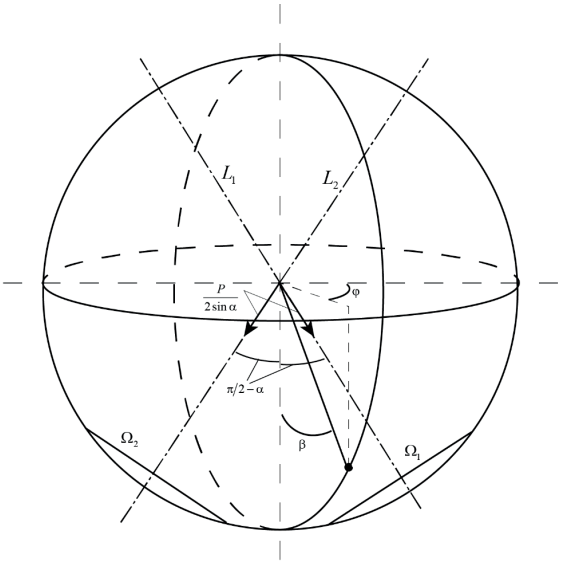


Figure 2. Superposition of axisymmetric states

Let's associate with the shell a spherical coordinate system with angles $\varphi \in [0, 2\pi)$ and $\beta \in [0, \pi]$ (Fig. 2). Further, when writing all equations and relationships, the following system of dimensionless quantities is used (if the quantities are written in the same way, they are indicated by the upper symbol «$*$», which is omitted in the subsequent presentation):

$$u^* = \frac{u}{R},\ w^* = \frac{w}{R}, p^* = \frac{p}{\lambda + 2\mu}\frac{R}{h},$$
$$\eta^2 = \frac{\mu}{\lambda + 2\mu},\ \gamma^2 = \frac{h^2}{12R^2},\ k^2 = \frac{5}{6} \qquad (1.1)$$

where u, w are the tangential and normal movements; χ is the angle of rotation of the normal to the median surface before the deformation of the fiber due to shear deformations; λ, μ are the Lame's elastic parameters of the shell material, p is the normal pressure. Under these assumptions, the dimensionless radius of the shell is 1.

Additionally, two local spherical coordinate systems are introduced. Their center coincide with the center of the shell, and the axes relative to which the meridional angles are counted coincide with the axes of symmetry L_1 and L_2. Point $M(\beta, \varphi)$ on the surface of a sphere with coordinates β, φ, specified in the main coordinate system is characterized by meridional angles β_1 and β_2 in additional coordinate systems. The same point belongs to the secant planes Π_1 and Π_2 with unit normal vectors $\mathbf{n}_1 = (\cos\alpha, 0, \sin\alpha)^T$ and $\mathbf{n}_2 = (-\cos\alpha, 0, \sin\alpha)^T$ given in rectangular Decaurt coordinates systems *Oxyz* (Fig. 3).

Then the connection of the angles $\beta_1 = \beta_1(\beta, \varphi)$ and $\beta_2 = \beta_2(\beta, \varphi)$ with coordinates β, φ are determined from the condition of intersection of the median surface of the shell with the planes Π_1 and Π_2:

$$\begin{aligned}&\left[\cos\left(\alpha-\beta_1\right)-\sin\beta\cos\varphi\right]\cos\alpha+\\&\left[\sin\left(\alpha-\beta_1\right)-\cos\beta\right]\sin\alpha=0,\ \beta_1>0;\\&\left[\cos\left(\alpha+\beta_2\right)-\sin\beta\cos\varphi\right]\cos\alpha+\\&\left[\sin\left(\alpha+\beta_2\right)-\cos\beta\right]\sin\alpha=0,\ \beta_2>0\end{aligned}\qquad(1.2)$$

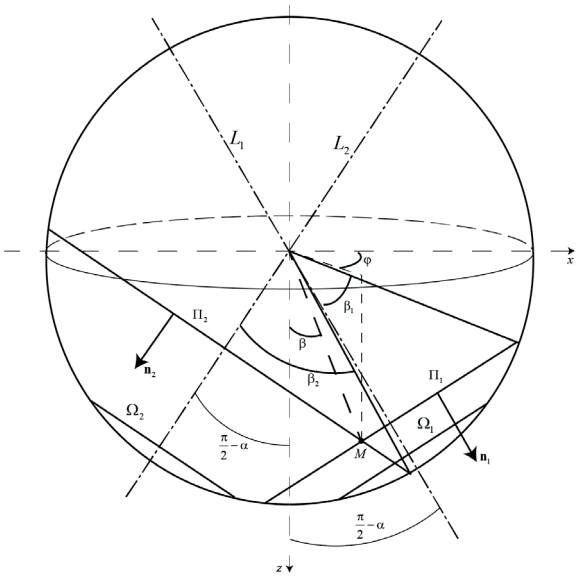


Figure 3. Relation of coordinates of a point on the shell surface

Thus, it is sufficient to construct a solution to the axisymmetric contact problem for a shell resting on a flat surface and being under the influence of a pressing force $Q=\dfrac{P}{2\sin\alpha}$. This solution depends only on the meridional angle β (in the local coordinate systems $\beta=\beta_1$ or $\beta=\beta_2$). Solving the original problem at an arbitrary point of the shell $M(\beta,\varphi)$ will represent a superposition of two solutions obtained from the solution of an axisymmetric problem in which the meridional angles β should be replaced by angles β_1 and β_2, connected with β and φ by formulas (1.2). In particular:

$$w(\beta,\varphi)=W\left[\beta_1(\beta,\varphi)\right]+W\left[\beta_2(\beta,\varphi)\right]\quad(1.3)$$

where $W(\beta)$ are the normal shell displacements obtained from the solution of the axisymmetric problem.

To solve the axisymmetric problem, we use a system of equations for the shell that takes into account the shear and rotational inertia of the cross sections according to the hypotheses of S.P. Tymoshenko [34, 35]:

$$\begin{aligned}&\mathbf{LW}+\mathbf{p}=0,\ \mathbf{L}=\left(L_{ij}\right)_{3\times3},\\&\mathbf{W}=\left(U,W,\mathrm{X}\right)^{\mathrm{T}},\ \mathbf{p}=\left(0,p,0\right)^{\mathrm{T}},\end{aligned}\qquad(1.4)$$

Coefficients in formulas (1.4) are determined by the following formulas:

$$L_{11}=\frac{\partial^2}{\partial\beta^2}+\operatorname{ctg}\beta\frac{\partial}{\partial\beta}+\eta^2\left(2-k^2\right)-\frac{1}{\sin^2\beta},$$

$$L_{12}=\left[2\left(1-\eta^2\right)+\eta^2k^2\right]\frac{\partial}{\partial\beta},$$

$$L_{13}=-\gamma^2\left(\frac{\partial^2}{\partial\beta^2}+\operatorname{ctg}\beta\frac{\partial}{\partial\beta}-\frac{1}{\sin^2\beta}\right)+\eta^2k^2,$$

$$L_{21}=-\left[2\left(1-\eta^2\right)+\eta^2k^2\right]\left(\frac{\partial}{\partial\beta}+\operatorname{ctg}\beta\right),$$

$$L_{22}=\eta^2k^2\left(\frac{\partial^2}{\partial\beta^2}+\operatorname{ctg}\beta\frac{\partial}{\partial\beta}\right)-4\left(1-\eta^2\right),$$

$$L_{23}=\eta^2k^2\left(\frac{\partial}{\partial\beta}+\operatorname{ctg}\beta\right),\ L_{31}=\gamma^{-2}L_{13},$$

$$L_{32}=-\eta^2k^2\gamma^{-2}\frac{\partial}{\partial\beta},\ L_{33}=-\gamma^{-2}L_{13}.$$

Based on the principle of superposition [5, 31-36], the following integral representation is valid for normal $W(\beta)$ displacements of the shell:

$$W(\beta)=2\pi\int_0^{\pi}G_w(\beta,\xi)\,p(\xi)\,d\xi\qquad(1.5)$$

where $G_w(\beta,\xi)$ is the influence function for the shell, which is the solution to the problem of

the effect of a single concentrated force on the shell [31-36]:

$$\mathbf{LG}+\mathbf{p}=0,$$
$$\mathbf{G}=\left(G_u,G_w,G_\chi\right)^{\mathrm{T}},\ \mathbf{p}=\left[0,\delta\left(\beta-\xi\right),0\right]^{\mathrm{T}} \quad (1.6)$$

Taking into account the symmetry properties of the problem, it is sufficient to determine the distribution of contact pressure over the Ω_1 domain, since in domain Ω_2 the distribution will be similar.

Using the influence function $G_w\left(\beta,\xi\right)$, integral representation (1.5) and formulas (1.2-1.3) it is possible to construct the main resolving integral equation of the contact problem:

$$2\pi\int_0^\pi G\left(\beta,\varphi,\xi\right)p\left(\xi\right)d\xi=w\left(\beta,\varphi\right),$$
$$G\left(\beta,\varphi,\xi\right)=G_w\left[\beta_1\left(\beta,\varphi\right),\xi\right]+ \quad (1.7)$$
$$+G_w\left[\beta_2\left(\beta,\varphi\right),\xi\right]$$

Displacement $w\left(\beta,\varphi\right)$ at the area of contact Ω_1 are determined by the distance (taking into account the sign) from the point $M\left(x_0,y_0,z_0\right)$ at the sphere surface with coorinates: $x_0=\sin\beta\cos\varphi$, $y_0=\sin\beta\sin\varphi$, $z_0=\cos\beta$ to plane Ω_1 (Fig.4): $x\cos\alpha+z\sin\alpha-1+w_0=0$

$$w\left(\beta,\varphi\right)=1-\sin\beta\cos\varphi\cos\alpha- \quad (1.8)$$
$$-\cos\beta\sin\alpha-w_0$$

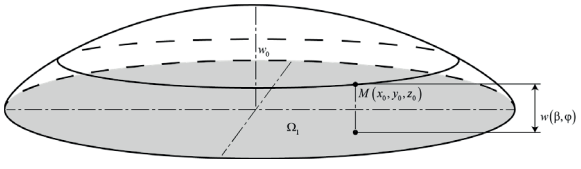


Figure 4. Determination of normal displacements in the contact area

Thus, the main resolving integral equation of the contact problem takes the form:

$$2\pi\int_0^\pi G\left(\beta,\varphi,\xi\right)p\left(\xi\right)d\xi=1-w_0-$$
$$-\sin\beta\cos\varphi\cos\alpha-\cos\beta\sin\alpha, \quad (1.9)$$
$$\left(\beta,\varphi\right):\ 1-\sin\beta\cos\varphi\cos\alpha-$$
$$-\cos\beta\sin\alpha-w_0\le 0$$

This equation is a one-dimensional integral equation with respect to the contact pressure distribution function $p\left(\xi\right)$. To solve it, we need to determine the kernel $G\left(\beta,\varphi,\xi\right)$ of this integral equation.

THE INFLUENCE FUNCTION FOR SHELL

The influence function $G_w\left(\beta,\xi\right)$ for the shell in the axisymmetric formulation is constructing using Fourier series expansions in Legendre $P_n\left(\cos\beta\right)$ and Gegenbauer $-\sin\beta C_{n-1}^{3/2}\left(\cos\beta\right)$ polynomials [34]:

$$\begin{Vmatrix}G_u\left(\beta,\xi\right)\\G_\chi\left(\beta,\xi\right)\end{Vmatrix}=-\sum_{n=1}^{\infty}\begin{Vmatrix}G_{un}\left(\xi\right)\\G_{\chi n}\left(\xi\right)\end{Vmatrix}C_{n-1}^{3/2}\left(\cos\beta\right)\times$$
$$\times-\sin\beta,$$
$$\begin{pmatrix}G_w\left(\beta,\xi\right)\\\delta(\beta-\xi)\end{pmatrix}=\sum_{n=0}^{\infty}\begin{pmatrix}G_{wn}\left(\xi\right)\\\delta_n\left(\xi\right)\end{pmatrix}P_n\left(\cos\beta\right), \quad (2.1)$$
$$\frac{2\delta_n(\xi)}{2n+1}=\int_0^\pi\delta\left(\beta-\xi\right)P_n\left(\cos\beta\right)\sin\beta d\beta=$$
$$=\frac{2n+1}{2}P_n\left(\cos\xi\right)\sin\xi.$$

Substituting (2.1) into (1.6) taking into account the known relations for Legendre and Gegenbauer polynomials [35] leads to a system of equations with respect to the coefficients of the series (2.1):

$$\begin{aligned}
&\mathbf{L}_n\mathbf{G}_n+\mathbf{p}_n=0,\ \mathbf{L}_n=\left(L_{nij}\right)_{3\times3},\\
&\mathbf{G}_n=\left(G_{un},G_{wn},G_{\varphi n}\right)^{\mathrm{T}},\\
&\mathbf{p}_n=\left[0,\delta_n(\xi),0\right]^{\mathrm{T}},\\
&L_{n11}=\eta^2\left(2-k^2\right)-n\left(n+1\right),\\
&L_{n12}=2\left(1-\eta^2\right)+\eta^2k^2,\\
&L_{n13}=\gamma^2n\left(n+1\right)+\eta^2k^2,\\
&L_{n21}=\left[2\left(1-\eta^2\right)+\eta^2k^2\right]n\left(n+1\right),\\
&L_{n22}=-\eta^2k^2n\left(n+1\right)-4\left(1-\eta^2\right),\\
&L_{n23}=-\eta^2k^2n\left(n+1\right),\ L_{n31}=\gamma^{-2}L_{n13},\\
&L_{n32}=-\eta^2k^2\gamma^{-2},\ L_{n33}=-\gamma^{-2}L_{n13}
\end{aligned}\qquad(2.2)$$

The coefficients of the series for the influence function are finding from the solution of system (2.2):

$$\begin{aligned}
&G_{wn}\left(\xi\right)=\frac{Q_{2n}}{Q_{3n}}\delta_n\left(\xi\right),\\
&Q_{2n}=Q_2\left[n\left(n+1\right)\right],\ Q_{3n}=Q_3\left[n\left(n+1\right)\right],\\
&Q_2\left(l\right)=\left(\eta^2k^2+\gamma^2l\right)\left[2\eta^2+l\left(\gamma^2-1\right)\right],\\
&Q_3\left(m\right)=k^2\eta^2l^3\gamma^2\left(\gamma^2-1\right)+2\gamma^2l^2\times\\
&\times\left[\eta^4\left(k^2+2\right)-2\eta^2\left(\gamma^2+1\right)+2\gamma^2\right]+\\
&+\eta^2l\left[k^2\eta^4-\left(\left(\gamma^2+1\right)k^2+2\gamma^2\right)4\eta^2+\right.\\
&\left.\left(4\gamma^2k^2+8\gamma^2\right)\right]+8\eta^4k^2\left(1-\eta^2\right)
\end{aligned}\qquad(2.3)$$

Thus, the desired influence function is a series (2.1) with coefficients determined by formula (2.3).

RESOLVING SYSTEM OF EQUATIONS

The expansion of contact pressure $p\left(\xi\right)$ in a series in terms of Legendre polynomials has the form:

$$p\left(\xi\right)=\sum_{m=0}^{\infty}p_mP_m\left(\cos\xi\right)\qquad(3.1)$$

Substituting representations (2.1), (2.2) and (2.3) into equation (1.9), taking into account the orthogonality property for Legendre polynomials [31, 34] leads to the equation:

$$\begin{aligned}
&2\pi\sum_{m=0}^{\infty}\frac{Q_{2m}}{Q_{3m}}p_m\left\{P_m\left[\cos\beta_1\left(\beta,\varphi\right)\right]+\right.\\
&\left.+P_m\left[\cos\beta_2\left(\beta,\varphi\right)\right]\right\}=1-w_0-\\
&-\sin\beta\cos\varphi\cos\alpha-\cos\beta\sin\alpha
\end{aligned}\qquad(3.2)$$

The solution to equation (3.2) can be obtained by reducing it to a system of algebraic equations for the coefficients p_m.

CONCLUSIONS

An effective numerical and analytical method is proposed for studying the force state inside the contact spots of elastic composite spherical shells supported on two flat surfaces inclined at an angle to each other.

The method is based on constructing the influence function for the shell in an axisymmetric formulation, followed by its expansion into a Fourier series using the Legendre and Gegenbauer polynomials. A resolving system of equations for the corresponding coefficients is obtained.

The developed methodology will allow for a more correct study of the dynamics of various robotic systems, the main controlled elements of which are elastic spherical shells that carry out complex kinematical movements on various surfaces. These systems, in particular, include a “butterfly robot”, the main controlled element of which is a thin spherical shell, rolling with simultaneous spinning and sliding along two parallel plates, as if on rails

ACKNOWLEDGEMENTS

A.A. Kireenkov was supported by the RSCF under the grant No. 23-29-00987, https://rscf.ru/project/23-29-00987.

REFERENCES

1. **Kireenkov A.A.**, AIP Conference Proceedings, Vol. 2611, p.100001 (2022)
2. **Kireenkov A.A.**, AIP Conference Proceedings, Vol. 2611, p.100002 (2022)
3. **Kireenkov A.A.**, AIP Conference Proceedings, Vol. 2343, p.120001 (2021)
4. **Kireenkov A.A.**, AIP Conference Proceedings, Vol. 2343, p.120002 (2021)
5. **Kireenkov A.A., Fedotenkov G.V., Shiriaev A.V., Zhavoronok S.I.**, International Journal for Computational Civil and Structural Engineering, Vol. 18(1), 14-26 (2022)
6. **Kireenkov A.**, Influence of the Combined Dry Friction on the Dynamics of the Rigid Ball Moving Along Two parallel Rails, in: 9th edition of the International Conference on Computational Methods for Coupled Problems in Science and Engineering (COUPLED PROBLEMS 2021). URL https://www.scipedia.com/public/Kireenkov_2021b.
7. **Kireenkov A., Zhavoronok S.** A Method of Parameters Identification for the Coupled Dry Friction Model for Pneumatic Tires, in: WCCM-ECCOMAS2020. URL https://www.scipedia.com/public/Kireenkov_Zhavoronok_2021a.
8. **Kireenkov A.A., Zhavoronok S.I.** Anisotropic combined dry friction in problems of pneumatics' dynamics // J. Vibration Engineering and Technology, Vol. 8, 365–372 (2020).
9. **Kireenkov A.A., Zhavoronok S.I.** Numeric-Analytical Methods of the Coefficients Definition of the Rolling Friction Model of the Pneumatic Aviation Tire, in: 8th International Conference on Coupled Problems in Science and Engineering, COUPLED PROBLEMS 2019 (2021), pp. 204-212.
10. **Kireenkov A.A., Ramodanov S.M.** Combined Dry Friction Models in the Case of Random Distribution of the Normal Contact Stresses Inside of Contact Patches, in: 8th International Conference on Coupled Problems in Science and Engineering, COUPLED PROBLEMS 2019 (2021), pp. 176-182.
11. **Kireenkov A.A., Zhavoronok S.I.** Implementation of analytical models of the anisotropic combined dry friction in problems of pneumatics' dynamics // MATEC Web of Conferences, Vol. 211 (2018), 08004
12. **Kireenkov A.A., Nushtaev D.V., Zhavoronok S.I.** A new approximate model of tyre accounting for both deformed state and dry friction forces in the contact spot on the background of the coupled model // MATEC Web of Conferences, Vol. 211 (2018), 08003.
13. **Kireenkov A.A.** Improved friction model of the aviation tyre contact with the landing strip // IFAC-PapersOnLine Vol. 51, No. 2, pp. 890-894.
14. **Kireenkov A.A., Zhavoronok S.I.** Coupled Dry Friction Models in Problems of Aviation Pneumatics' Dynamics // International Journal of Mechanical Sciences (2017), Vol. 127, pp. 198-203.
15. **Kireenkov A.A.** Improved theory of the combined dry friction in problems of aviation pneumatics' dynamics, in: Proceedings of the 7th International Conference on Coupled Problems in Science and Engineering, COUPLED PROBLEMS 2017 (2017), pp. 1293-1298.
16. **Zhavoronok S.I., Kireenkov A.A.** On the effect of the anisotropic dry friction and the deformed state of tires on the shimmy initiation, in: Proceedings of the 7th International Conference on Coupled Problems in Science and Engineering,

COUPLED PROBLEMS 2017 (2017), pp. 216-226.

17. **Ramodanov S.M., Kireenkov A.A.** Controllability of a rigid body in a perfect fluid in the presence of friction, in: Proceedings of the 7th International Conference on Coupled Problems in Science and Engineering, COUPLED PROBLEMS 2017 (2017), pp.179 – 184.
18. **Kireenkov A.A.** Further development of the theory of multicomponent dry friction, in: COUPLED PROBLEMS 2015 - Proceedings of the 6th International Conference on Coupled Problems in Science and Engineering (2015), pp. 203-209.
19. **Kireenkov A.A., Semendyaev S.V., Filatov V.V.** Experimental study of coupled two-dimensional models of sliding and spinning friction // Mechanics of Solids (2010), Vol. 45, No. 6, pp. 921–930.
20. **Kireenkov A.A.** Combined model of sliding and rolling friction in dynamics of bodies on a rough plane // Mechanics of Solids (2008), Vol. 43, No. 3, pp. 412-425.
21. **Kireenkov A.A.** Coupled models of sliding and rolling friction// Doklady Physics (2008), Vol. 53, No. 4, pp. 233-236
22. **Kireenkov A.A.** Modelling of the force state of contact of a ball rolling along the boundaries of two rails // AIP Conference Proceedings (2021), Vol. 2343,120002.
23. **Kireenkov A.** Influence of the Combined Dry Friction on the Dynamics of the Rigid Ball Moving Along Two parallel Rails, in: 9th edition of the International Conference on Computational Methods for Coupled Problems in Science and Engineering (COUPLED PROBLEMS 2021). URL https://www.scipedia.com/public/Kireenkov_2021b.
24. **Kireenkov A.** Dry Friction Model of a Contact of a Solid Ball Moving Along the Boundaries of Two Rails, in: WCCM-ECCOMAS2020.URL: www.scipedia.com/public/Kireenkov_2021a.
25. **Kireenkov A.A.** Preface: mathematical models and investigations methods of strongly nonlinear systems // AIP Conference Proceedings (2021), Vol. 2343, 120001.
26. **Surov M., Shiriaev A. and al.** Case study in non-prehensile manipulation: Planning and orbital stabilization of one-directional rollings for the Butterfly robot, in: Proceedings - IEEE International Conference on Robotics and Automation (2015), pp. 1484-1489.
27. **Amosov A.A., Zhavoronok S.I.** An approximate high-order theory of thick anisotropic shells // International Journal for Computational Civil and Structural Engineering (2003), Vol. 1, No. 5, pp. 28-38.
28. **Zhavoronok S.I., Leontiev A.N., Leontiev K.A.** Analysis of thick-walled rotation shells based on Legendre polynomials // International Journal for Computational Civil and Structural Engineering (2010), Vol. 6, No. 1-2, pp. 105-111.
29. **Zhavoronok S.I.** A general higher-order shell theory based on the analytical dynamics of constrained continuum systemsin: Shell Structures: Theory and Applications, Vol. 4. CRC Press / Balkema, Taylor & Francis Gr., Leiden (2018), pp. 189-192.
30. **Kireenkov A.A., Mikhailova E.Yu., Fedotenkov G.V.** method for reducing contact problems for spherical shells of the Timoshenko type to paired series-equations // Journal on Composite Mechanics and Design, Vol. 29(3), 390-401 (2023).
31. **Mikhailova E.Yu., Fedotenkov G.V.** Nonstationary Axisymmetric Problem of the Impact of a Spherical Shell on an Elastic Half-Space (Initial Stage of Interaction) // Mechanics of Solids (2011), Vol. 46, No. 2, pp. 239–247.
32. **Tarlakovskii D.V., Fedotenkov G.V.** Two-Dimensional Nonstationary Contact of Elastic Cylindrical or Spherical Shells // Journal of Machinery Manufacture and

Reliability (2014), Vol.43, No.2, pp. 145–152.

33. **Fedotenkov G.V., Mikhailova E.Yu, Kuznetsova El.L., Rabinskiy L.N.** Modeling the unsteady contact of spherical shell made with applying the additive technologies with the perfectly rigid stamp // International Journal of Pure and Applied Mathematics (2016), Vol. 111, No. 2, pp. 331-342.
34. **Mikhailova E.Yu., Tarlakovskii D.V., Fedotenkov G.V.** Transient contact problem for spherical shell and elastic half-space, in: Shell Structures: Theory and Applications, Vol. 4. CRC Press / Balkema, Taylor & Francis Gr., Leiden (2018), pp. 301-304.
35. **Tarlakovskii D.V., Fedotenkov G.V.** Nonstationary 3D motion of an elastic spherical shell // Mechanics of Solids (2015), Vol. 46, No, 5, pp. 779-787.
36. **Fedotenkov G.V., Zhavoronok S.I.** Transient contact of a cylindrical shell and a rigid body // AIP Conference Proceedings (2021), vol. 2343, 120010.

СПИСОК ЛИТЕРАТУРЫ

1. **Kireenkov A.A.**, AIP Conference Proceedings, Vol. 2611, p.100001 (2022)
2. **Kireenkov A.A.**, AIP Conference Proceedings, Vol. 2611, p.100002 (2022)
3. **Kireenkov A.A.**, AIP Conference Proceedings, Vol. 2343, p.120001 (2021)
4. **Kireenkov A.A.**, AIP Conference Proceedings, Vol. 2343, p.120002 (2021)
5. **Kireenkov A.A., Fedotenkov G.V., Shiriaev A.V., Zhavoronok S.I.**, International Journal for Computational Civil and Structural Engineering, Vol. 18(1), 14-26 (2022)
6. **Kireenkov A.**, Influence of the Combined Dry Friction on the Dynamics of the Rigid Ball Moving Along Two parallel Rails, in: 9th edition of the International Conference on Computational Methods for Coupled Problems in Science and Engineering (COUPLED PROBLEMS 2021). URL https://www.scipedia.com/public/Kireenkov_2021b.
7. **Kireenkov A., Zhavoronok S.** A Method of Parameters Identification for the Coupled Dry Friction Model for Pneumatic Tires, in: WCCM-ECCOMAS2020. URL https://www.scipedia.com/public/Kireenkov_Zhavoronok_2021a.
8. **Kireenkov A.A., Zhavoronok S.I.** Anisotropic combined dry friction in problems of pneumatics' dynamics // J. Vibration Engineering and Technology, Vol. 8, 365–372 (2020).
9. **Kireenkov A.A., Zhavoronok S.I.** Numeric-Analytical Methods of the Coefficients Definition of the Rolling Friction Model of the Pneumatic Aviation Tire, in: 8th International Conference on Coupled Problems in Science and Engineering, COUPLED PROBLEMS 2019 (2021), pp. 204-212.
10. **Kireenkov A.A., Ramodanov S.M.** Combined Dry Friction Models in the Case of Random Distribution of the Normal Contact Stresses Inside of Contact Patches, in: 8th International Conference on Coupled Problems in Science and Engineering, COUPLED PROBLEMS 2019 (2021), pp. 176-182.
11. **Kireenkov A.A., Zhavoronok S.I.** Implementation of analytical models of the anisotropic combined dry friction in problems of pneumatics' dynamics // MATEC Web of Conferences, Vol. 211 (2018), 08004
12. **Kireenkov A.A., Nushtaev D.V., Zhavoronok S.I.** A new approximate model of tyre accounting for both deformed state and dry friction forces in the contact spot on the background of the coupled model // MATEC Web of Conferences, Vol. 211 (2018), 08003.
13. **Kireenkov A.A.** Improved friction model of the aviation tyre contact with the landing

strip // IFAC-PapersOnLine Vol. 51, No. 2, pp. 890-894.

14. **Kireenkov A.A., Zhavoronok S.I.** Coupled Dry Friction Models in Problems of Aviation Pneumatics' Dynamics // International Journal of Mechanical Sciences (2017), Vol. 127, pp. 198-203.
15. **Kireenkov A.A.** Improved theory of the combined dry friction in problems of aviation pneumatics' dynamics, in: Proceedings of the 7th International Conference on Coupled Problems in Science and Engineering, COUPLED PROBLEMS 2017 (2017), pp. 1293-1298.
16. **Zhavoronok S.I., Kireenkov A.A.** On the effect of the anisotropic dry friction and the deformed state of tires on the shimmy initiation, in: Proceedings of the 7th International Conference on Coupled Problems in Science and Engineering, COUPLED PROBLEMS 2017 (2017), pp. 216-226.
17. **Ramodanov S.M., Kireenkov A.A.** Controllability of a rigid body in a perfect fluid in the presence of friction, in: Proceedings of the 7th International Conference on Coupled Problems in Science and Engineering, COUPLED PROBLEMS 2017 (2017), pp.179 – 184.
18. **Kireenkov A.A.** Further development of the theory of multicomponent dry friction, in: COUPLED PROBLEMS 2015 - Proceedings of the 6th International Conference on Coupled Problems in Science and Engineering (2015), pp. 203-209.
19. **Kireenkov A.A., Semendyaev S.V., Filatov V.V.** Experimental study of coupled two-dimensional models of sliding and spinning friction // Mechanics of Solids (2010), Vol. 45, No. 6, pp. 921–930.
20. **Kireenkov A.A.** Combined model of sliding and rolling friction in dynamics of bodies on a rough plane // Mechanics of Solids (2008), Vol. 43, No. 3, pp. 412-425.
21. **Kireenkov A.A.** Coupled models of sliding and rolling friction// Doklady Physics (2008), Vol. 53, No. 4, pp. 233-236
22. **Kireenkov A.A.** Modelling of the force state of contact of a ball rolling along the boundaries of two rails // AIP Conference Proceedings (2021), Vol. 2343,120002.
23. **Kireenkov A.** Influence of the Combined Dry Friction on the Dynamics of the Rigid Ball Moving Along Two parallel Rails, in: 9th edition of the International Conference on Computational Methods for Coupled Problems in Science and Engineering (COUPLED PROBLEMS 2021). URL https://www.scipedia.com/public/Kireenkov_2021b.
24. **Kireenkov A.** Dry Friction Model of a Contact of a Solid Ball Moving Along the Boundaries of Two Rails, in: WCCM-ECCOMAS2020.URL: www.scipedia.com/public/Kireenkov_2021a.
25. **Kireenkov A.A.** Preface: mathematical models and investigations methods of strongly nonlinear systems // AIP Conference Proceedings (2021), Vol. 2343, 120001.
26. **Surov M., Shiriaev A. and al.** Case study in non-prehensile manipulation: Planning and orbital stabilization of one-directional rollings for the Butterfly robot, in: Proceedings - IEEE International Conference on Robotics and Automation (2015), pp. 1484-1489.
27. **Amosov A.A., Zhavoronok S.I.** An approximate high-order theory of thick anisotropic shells // International Journal for Computational Civil and Structural Engineering (2003), Vol. 1, No. 5, pp. 28-38.
28. **Zhavoronok S.I., Leontiev A.N., Leontiev K.A.** Analysis of thick-walled rotation shells based on Legendre polynomials // International Journal for Computational Civil and Structural Engineering (2010), Vol. 6, No. 1-2, pp. 105-111.
29. **Zhavoronok S.I.** A general higher-order shell theory based on the analytical

dynamics of constrained continuum systemsin: Shell Structures: Theory and Applications, Vol. 4. CRC Press / Balkema, Taylor & Francis Gr., Leiden (2018), pp. 189-192.

30. **Kireenkov A.A., Mikhailova E.Yu., Fedotenkov G.V.** method for reducing contact problems for spherical shells of the Timoshenko type to paired series-equations // Journal on Composite Mechanics and Design, Vol. 29(3), 390-401 (2023).
31. **Mikhailova E.Yu., Fedotenkov G.V.** Nonstationary Axisymmetric Problem of the Impact of a Spherical Shell on an Elastic Half-Space (Initial Stage of Interaction) // Mechanics of Solids (2011), Vol. 46, No. 2, pp. 239–247.
32. **Tarlakovskii D.V., Fedotenkov G.V.** Two-Dimensional Nonstationary Contact of Elastic Cylindrical or Spherical Shells // Journal of Machinery Manufacture and Reliability (2014), Vol.43, No.2, pp. 145–152.
33. **Fedotenkov G.V., Mikhailova E.Yu, Kuznetsova El.L., Rabinskiy L.N.** Modeling the unsteady contact of spherical shell made with applying the additive technologies with the perfectly rigid stamp // International Journal of Pure and Applied Mathematics (2016), Vol. 111, No. 2, pp. 331-342.
34. **Mikhailova E.Yu., Tarlakovskii D.V., Fedotenkov G.V.** Transient contact problem for spherical shell and elastic half-space, in: Shell Structures: Theory and Applications, Vol. 4. CRC Press / Balkema, Taylor & Francis Gr., Leiden (2018), pp. 301-304.
35. **Tarlakovskii D.V., Fedotenkov G.V.** Nonstationary 3D motion of an elastic spherical shell // Mechanics of Solids (2015), Vol. 46, No, 5, pp. 779-787.
36. **Fedotenkov G.V., Zhavoronok S.I.** Transient contact of a cylindrical shell and a rigid body // AIP Conference Proceedings (2021), vol. 2343, 120010.

Alexey A. Kireenkov is a Senior Reseacher of the Ishlinsky Institute for Problems in Mechanics of Russian Academy of Sciences (IPMech RAS), Prospekt Vernadskogo 101, korp.1, 119526, Moscow, Russia; Associate Professor of the high mathematics departments of the Moscow Institute of Physics and Technology (National Investigation University). Phone: +7 (916) 868-58-39. e-mail: kireenk@ipmnet.ru

Grigory V. Fedotenkov is a Senior Researcher of the Laboratory of dynamical Tests of the Research Institute of Mechanics of Lomonosov Moscow State University, 119192, Michurinskiy Prospekt, 1, Moscow, Russia; Associate Professor of the Moscow Aviation Institute (National Research University). Phone: +7 (916) 459-83-63. e-mail: greghome@mail.ru

Киреенков Алексей Альбертович – старший научный сотрудник ФГБУН Институт проблем механики им. А.Ю. Ишлинского РАН, доцент кафедры высшей математики Московского физико-технического института (Национального исследовательского университета); ИПМех РАН, 119526, Россия Москва, Проспект Вернадского, 101, корп. 1, тел.: +7 (916) 868-58-39. e-mail: kireenk@ipmnet.ru

Федотенков Григорий Валерьевич – старший научный сотрудник Лаборатории динамических испытаний НИИ механики Московского Государственного университета им. М. В. Ломоносова, 119192, Москва, Россия, Мичуринский проспект, 1; доцент кафедры сопротивления материалов, динамики и прочности машин Московского авиационного института (национального исследовательского университета); тел.: +7 (916) 459-83-63. e-mail: greghome@mail.ru

DOI:10.22337/2587-9618-2024-20-3-35-44

EVALUATE THE INFLUENCE OF CONCRETE STRENGTH ON THE LEVEL OF CORROSION OF STEEL REINFORCEMENT IN REINFORCED CONCRETE BEAM STRUCTURES, TAKING INTO ACCOUNT THE APPLIED LOAD

Vo Van Nam, Nguyen Trong Tam
Ho Chi Minh City University of Transport, Ho Chi Minh City, VIETNAM

Abstract: In coastal areas, transportation infrastructure using reinforced concrete beam structures always works in environmental conditions with high corrosive agents, under the effect of load, the level of corrosion of steel reinforcement in the structure is high. The beam condition becomes more severe, which leads to a decrease in the beam's bending resistance. The level of corrosion of steel reinforcement in reinforced concrete beam structures depends on many influencing factors. These factors need to be seriously researched and evaluated to provide early warning results for designer, construction worker, operater for exploit the project safely and effectively. This article presents the results of research evaluating the influence of concrete strength on the level of corrosion of steel reinforcement in reinforced concrete beam structures, often taking into account the effect of load causing beam bending. Reinforced concrete beam samples were made with concrete at different strength levels: C30, C40 and C50 MPa; Then it was loaded with a yoke system with a loading level equivalent to 0.8Pmax of the destructive strength of the concrete sample. After the yokes were loaded, the beam samples were subjected to accelerated corrosion testing in a highly concentrated salt water environment. concentration equivalent to 3.5% NaCl for a period of 30 days, equivalent to an actual exploitation time of about 35 years. The corrosion rate of steel reinforcement is increased by supplying direct current to create an electrolytic corrosion environment, ensuring that the steel bars are corroded equivalent to the estimated calculated time. Beam samples after accelerated corrosion testing were evaluated for damage in terms of reinforcement volume.

Keywords: Concrete strength, reinforced concrete structure, steel corrosion level, applied load

ОЦЕНКА ВЛИЯНИЯ ПРОЧНОСТИ БЕТОНА НА УРОВЕНЬ КОРРОЗИИ СТАЛЬНОЙ АРМАТУРЫ В ЖЕЛЕЗОБЕТОННЫХ БАЛОЧНЫХ КОНСТРУКЦИЯХ С УЧЕТОМ ПРИЛОЖЕННОЙ НАГРУЗКИ

Во Ван Нам, Нгуен Чонг Там
Хошиминский университет транспорта, г. Хошимин, ВЬЕТНАМ

Аннотация: В прибрежных районах транспортная инфраструктура с применением железобетонных балочных конструкций всегда работает в условиях окружающей среды с повышенным содержанием агрессивных агентов, под действием нагрузки уровень коррозии стальной арматуры в конструкции увеличивается. Состояние балочных элементов становится более тяжелым, что приводит к снижению их сопротивления изгибу. Уровень коррозии стальной арматуры в железобетонных балочных конструкциях зависит от многих влияющих факторов. Эти факторы необходимо серьезно изучать и оценивать с целью раннего предупреждения для строителей, проектировщиков и операторов для обеспечения безопасной и эффективной эксплуатации проекта. В статье представлены результаты исследований по оценке влияния прочности бетона на уровень коррозии стальной арматуры железобетонных балочных конструкций с учетом влияния нагрузки, вызывающей изгиб балочных элементов. Образцы железобетонных балок изготавливались из бетона разной прочности: С30, С40 и С50 МПа; затем его нагружали с использованием системы хомутов с уровнем нагрузки, эквивалентным 0,8Pmax разрушающей прочности образца бетона. После нагружения образцы балочных элементов в течение 30 дней были подвергнуты ускоренным испытаниям на коррозию в водной среде с высокой концентрацией соли, эквивалентной 3,5% NaCl, что соответствует фактическому сроку эксплуатации около 35 лет. Скорость коррозии

стальной арматуры увеличивается за счет подачи постоянного тока для создания среды электролитической коррозии, обеспечивающей коррозию стальных стержней в течение расчетного времени. Образцы балок после ускоренных коррозионных испытаний оценивались на предмет повреждений по объему армирования.

Ключевые слова: Прочность бетона, железобетонная конструкция, уровень коррозии стали, приложенная нагрузка.

1. INTRODUCTION

The influence of the level of reinforcement corrosion on the behavior of reinforced concrete structures is an issue of great research interest in the world [1-23]. Because this is the basis for evaluating the load-bearing capacity of corroded reinforced concrete constructions in strongly aggressive environments such as sea areas and polluted areas.

With steel reinforcement used in reinforced concrete structures, the level of corrosion of the steel reinforcement is greatly influenced by the behavioral state and material structure of the protective concrete layer. When the reinforcement is still surrounded by solid protective layers of concrete, the alkaline environment in the concrete is high enough to create a protective film for the reinforcement. If this protective film is destroyed, the steel reinforcement will corrode [6,7,8,11,12,22,23]. One of the important reasons why the passive membrane is destroyed is the penetration of chloride ions from the outside environment into the position of the reinforcement. Micro cracks that appear in the protective concrete layer will facilitate chloride ions to penetrate faster, putting the structure at risk of corrosion sooner than expected [10,11,14,16]. Different types of reinforced concrete structures are also studied, in order to find differences in the design of reinforced concrete structures. In 2016, a group of authors from Cairo University, Egypt published research results on the difference between the corrosion process of steel reinforcement on prestressed reinforced concrete beams and this process on reinforced concrete. Traditional steel, Behavior of corroded bonded fully prestressed and conventional concrete beams; Research results have shown that the effect of corrosion due to aggressive environments has a strong effect and quickly reduces the bending resistance of conventional reinforced concrete beam structures. This has less impact on prestressed reinforced concrete beam structures under the same experimental environmental conditions. The team also pointed out that the reason why prestressed reinforced concrete is less affected is because cracks in the concrete develop less. In addition, high-strength steel is surrounded and protected by concrete mortar and pipe, so it is difficult for corrosive agents to come into contact to promote the corrosion of steel reinforcement [15]. Applying technology in building models to decode the behavior of reinforced concrete structures when the reinforcement is corroded has also been widely deployed in recent times: In 2018, an announcement by a research team from Chalmers University of Technology by using the finite element (FE) model to evaluate the behavior of reinforced concrete beams subject to steel bar corrosion. The research results concluded that the corrosion process changes the load-bearing cross section of the beam. reinforcement, reducing the bond force between concrete and reinforcement, thereby affecting the load-bearing capacity of reinforced concrete beams [17]. In 2020, a research team from the University of Technical Education. Ho Chi Minh City for proposing an algorithm and developing an independent calculation program to evaluate corrosion behavior affecting the bending capacity of reinforced concrete structures [18]. As stated, the material structure is a factor that directly affects the level of corrosion of steel reinforcement in reinforced concrete structures, so the strength of the concrete used to make beams - plays the role of a protective concrete layer. Protection that

prevents corrosive agents from coming into contact with the reinforcement is a parameter that needs to be evaluated and analyzed in detail.

This study will clarify the influence of concrete strength on the corrosion level of steel reinforcement in reinforced concrete structures. Reinforced concrete beam samples will be tested for accelerated corrosion with different loading levels before being immersed in a corrosive environment. The corroded beam samples were then evaluated for damage to the steel reinforcement due to corrosion.

The results of this research will contribute to the corrosion analysis of reinforced concrete structures in practice, taking into account the effects of load and environment; is the basis for predicting the lifespan and operating capacity of these structures.

2. EXPERIMENTAL PROGRAM

An experimental procedure was established to collect data to serve the assessment and analysis of the influence of concrete strength for making reinforced concrete beams on the level of corrosion of steel reinforcement in reinforced concrete beam components considering to the effect of load.

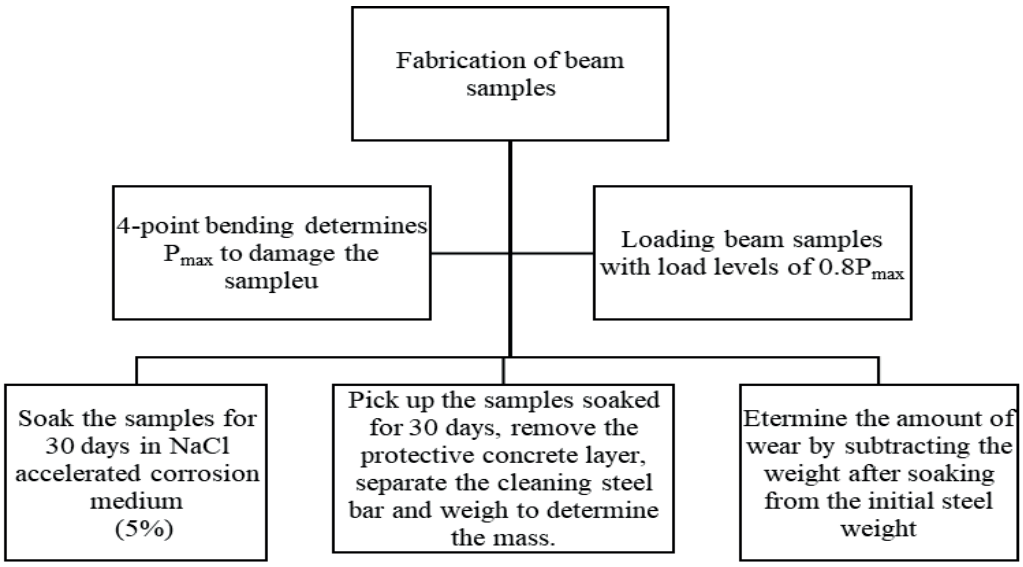


Figure 1. Procedure for performing the experiment

2.1. Materials for making samples

Concrete C30, C40, C50 has an expected compressive strength at 28 days fc' of 30, 40 and 50 MPa, respectively. The mix composition of concrete (mix batch 1m3) is designed according to ACI211.1-91 standard [13].

In there:

fc': Compressive strength of concrete.

C30, 40, 50: Concrete symbols with fc' are: 30, 40, 50 (MPa)

Table 1. Mix composition for 1m3 of concrete

Type of concrete	Material type			
	Stone (Kg)	Sand (Kg)	Cement (Kg)	Water (lit)
C30	1060	848	395	170
C40	1087	625	407	175
C50	1164	773	453,5	195

Average compressive strength of concrete when compressing and testing samples:

Table 2. Average compressive strength of concrete

Type of concrete	P_{max}^{N} (kN)	f'c (MPa)
C30	302,5	38.6
C40	410,6	50,39
C50	525,8	58,32

In there:
f'_c: Compressive strength of the sample
Steel used to make beams: D10, smooth round, f_y = 240 MPa. The steel bars are weighed to determine their weight before making the beam sample.
In there:
D10: Symbol of reinforcement diameter.
f_y: Tensile strength of steel.

2.2. Fabrication of beam samples

The beam samples manufactured for experiments have dimensions of 500x100x100 mm [13, 14, 16]. Quantity of 07 beams. In which: 01 beam determined the bending resistance force P_{max}^{k} of C30, 06 beam samples tested for accelerated corrosion considering the influence of applied load corresponding to 03 concrete levels C30, C40 and C50.
The number of beam samples for each concrete level is made in reserve for the purpose of providing compensation samples when unplanned incidents occur during the testing process.

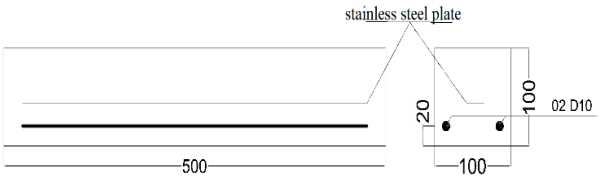


Figure 2. Dimensions and structure of experimental beams



Figure 3. Completed beam sample

2.3. Accelerated corrosion experiment

The corrosive environment is simulated by a concentrated NaCl solution (3,5%) combined with creating an electrode that activates the electrolytic corrosion environment, helping the corrosion process progress faster. The current intensity remains at 0.3A [11, 12, 14]. The corrosion rate of reinforcement is increased by applying electric current, ensuring that the reinforcement is corroded to a maximum of 25% reduction in diameter compared to the original within the expected time.

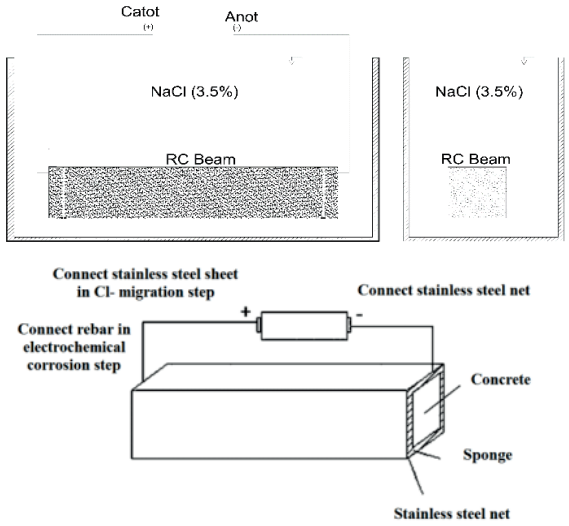


Figure 4. Description of Electrode Corrosion Equipment

After being manufactured for 28 days, beam samples will be loaded in pairs - 2 beams with a load level of $0.8P_{max}$ of sample C30 and immersed in an accelerated corrosive environment.

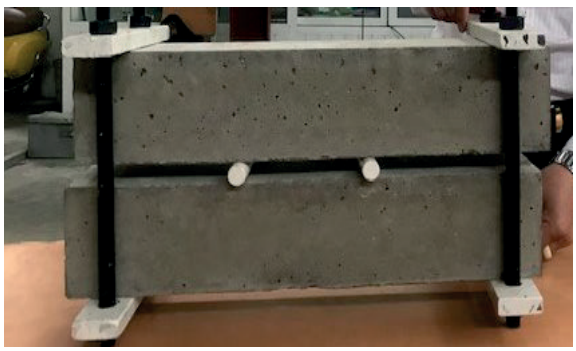


Figure 4. Loading beams for beam samples

The duration of the accelerated corrosion immersion test is specifically calculated based on the theory of corrosion of steel reinforcement in reinforced concrete structures.

The volume of steel consumed is related to the magnitude of current in electrochemical corrosion cells. Using Faraday's law to describe the mass loss of steel due to corrosion:

$$M_{loss} = \frac{MI_{corr}}{zF}t \quad (1)$$

In there:
- M_{loss} is the loss of consumed steel volume (g);
- M is the atomic mass of Fe ion, M = 56 g/mol;
- z is the valence of Fe,
- F is Faraday's constant, F = 96,500 C/mol
- t is the corrosion time in seconds (s).

Corrosion current density i_{corr} is defined as the corrosion current per unit steel surface. If the length unit L_0= 1 cm and the diameter unit d is mm, a relationship between I_{corr} (A) and i_{corr} ($\mu A/cm^2$) can be obtained as follows:

$$I_{corr} = 1 \times \pi \frac{d}{10} i_{corr} \times 10^{-6} = 10^{-7} \pi d i_{corr} \quad (2)$$

The percentage loss of reinforcement mass is ρ, we have the mass loss of reinforcement as:

$$M_{loss} = \rho M_s \quad (3)$$

With ρ_s=7.85g/cm^3 and L_0=1cm we get:

$$M_{loss} = \rho M_s = \rho \frac{\pi}{4}\left(\frac{d}{10}\right)^2 \rho_s = 0.0616 \rho d^2 \quad (4)$$

Combining equations (1), (4), with z = 2.5 (average value for Fe^{2+} and Fe^{3+}), the corrosion time t in years is related to ρ and icorr ($\mu A/cm^2$) as after:

$$t = \frac{zFM_{loss}}{MI_{corr}} = \frac{2.5 \times 96500 \times 0.0616 \rho d^2}{56 \times \pi d i_{corr} \times 10^{-7} \times 3600 \times 24 \times 365} = 26.799 \frac{\rho d}{i_{corr}} \quad (5)$$

Liu and Weyers (1998) [12] proposed the following corrosion rate:

$$i_{cor} = 0.926 \exp\left[7.98 + 0.7771 \ln(1.69 C_t) - \frac{3006}{T} - 0.000116 R_c + 2.24 t^{-0.215}\right] \quad (6)$$

In there:
- i_{cor} is the corrosion rate ($\mu A/cm^2$);
- C_t is the total chloride content at the depth of the steel surface (kg/m^3 of concrete);
- T is the ambient temperature (K);
- R_c is the ohmic resistance of the concrete cover layer (Ω);
- t is the time since the start of corrosion (years);

Liu (1996) [11] established the regression relationship between the ohmic resistance of concrete Rc and the total chloride content for field exposed samples as follows:

$$R_c = \exp\left[8.03 - 0.549 \ln(1 + 1.69 C_t)\right] \quad (7)$$

Lopez et al [10] studied the relationships between concrete resistance R_c and environmental relative humidity (H) based on experimental results. They give the following relationship:

$$R_c = 90.357 H^{-7.2548}\left[1 + \exp(5 - 50(1 - H)\right] \quad (8)$$

In equation (6), C_t total chloride content will change over time, C_t is based on Fick's second law of diffusion (considering the initial chloride concentration of concrete to be 0) as follows:

$$C(c,t) = \left\{C_s\left(1 - erf\frac{c}{2\sqrt{Dt}}\right)\right\} \times \frac{1}{100} \times \gamma_c \quad (9)$$

In there:
D - chloride diffusion coefficient in concrete;
C_s - chloride concentration on concrete surface;
c - Depth of the concrete layer protecting the steel bar;

t - time ($t = t_1+\Delta t$);
γ_c - the density of concrete.
The results of calculation and processing have determined the time for soaking beam samples in an accelerated corrosive environment with the aim of creating a corrosion process for the reinforcement sample reaching about 25% of the initial reinforcement volume in a specific time. Soak the sample for 30 consecutive days. During the accelerated corrosion immersion period, if an interruption occurs, the sample will be soaked for a corresponding period of time.

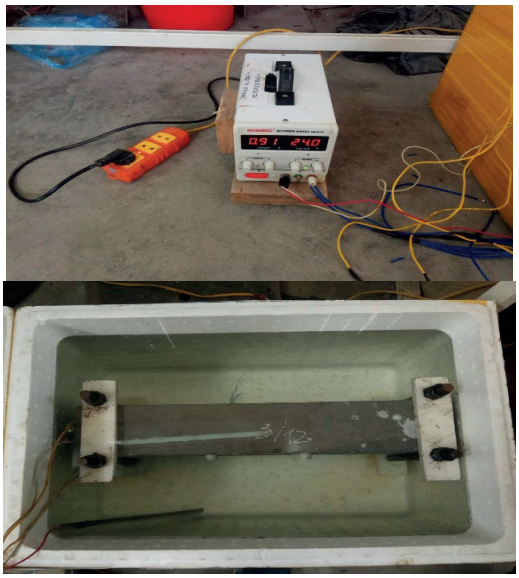


Figure 5. Girder specimen in corrosive environment

After soaking the beam samples for 30 days, they will be salvaged, the protective concrete layer will be removed, the steel bars will be removed and the surrounding steel rust and concrete adhering to the bars will be cleaned and then weighed to determine mass.



Figure 6. Sample after immersion in accelerated corrosive environment



Figure 7. Steel reinforcement is corroded after removing the concrete layer



Figure 8. Weigh the reinforcement sample to determine the level of corrosion

3. RESULTS AND DISCUSSION

The mass of steel consumed by corrosion in the accelerated corrosion test is calculated by the difference in mass between the steel types before and after the accelerated corrosion test. In fact, the corroded steel reinforcement is not balanced between sections. In this experiment, iron ore can be pre-formed by loading, so the mid-span position is considered as a representative disclosure in the steel corrosion price war. These data are set up in tables to conduct analysis and evaluation.

Table 3. Weight of corroded steel reinforcement

Sample symbol	Initial volume of reinforcement M_s (g)	Amount of corroded steel reinforcement M_{loss}(g)	Corrosion level of steel reinforcement ρ (%)
C30	560	141.5	25.2
C40	572	134,4	23,5
C50	568	130,07	22,9

A relationship chart between the strength of concrete for making reinforced concrete beams and the level of corrosion of steel reinforcement due to the influence of an environment containing chloride ions is built on experimental results of corroded beams in a corrosive environment move fast.

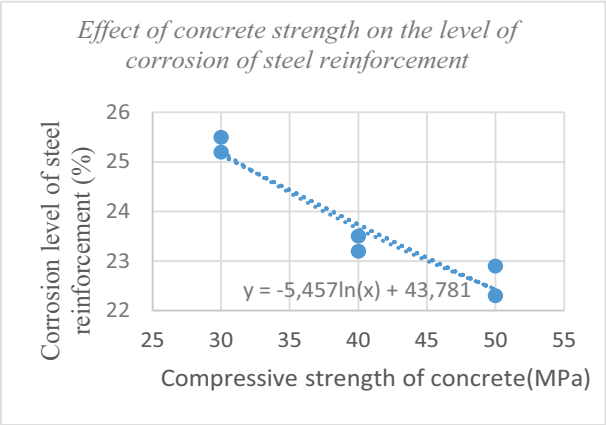


Figure 9. Effect of concrete strength on the level of corrosion of steel reinforcement after 35 years

Through the results of accelerated corrosion testing (same soaking time) of reinforced concrete beam samples with different strengths, loaded with the same load level of $0.8P_{max}$ of sample C30, we see: Corrosion level Reinforcement in reinforced concrete bridge beam components is inversely proportional to the strength of concrete used to make the beam. When concrete strength increases, the level of corrosion of reinforcement decreases specifically at 25% for C30 concrete and approximately 23.5% for C40 concrete and 23% for C50 concrete (same working conditions).

The slow decrease in the level of corrosion of reinforcement in beam samples with increasing strength is because the tensile strength of concrete increases slowly with the grade of concrete, so increasing the tensile capacity of concrete protects the position. The grain under the beam at the mid-span shear eye is insignificant, thereby having little impact on the ability of concrete to prevent crack development at the tensile grain of the beam.

4. CONCLUDE

The influence of concrete strength is significant on the level of corrosion of steel reinforcement in bending reinforced concrete beam structures, especially when reinforced concrete beams work in environments containing chloride ion corrosive agents;

The level of corrosion of steel reinforcement in reinforced concrete beam structures, taking into account the effect of load, is affected by many factors: thickness of protective concrete layer, temperature, humidity, ..., so it is necessary to present detailed evaluation studies with full parameters affecting the above process.

REFERENCES

1. **C.H. Truong, Q. Huynh, Q.V. Tran, P.P. Nguyen** (2008), Research and survey on the current state of corrosion and destruction of reinforced concrete structures and the possibility of erosion in the coastal environment Da Nang city. *Journal of science and technology*, University of Da Nang, 6(29).
2. **H.K. Dong, H.T.T. Duong (**2014**).** Corrosion of reinforced concrete and the method to avoid corrosion for reinforced concrete structures in VIETNAM'S sea. *VNCOLD.*
3. **T.T. Tran, D.T. Pham, M.N. Vu, V.Q. Truong, X.B. Ho, N.L. Tran, S.T. Nguyen, Q.D. To** (2021). Relation between water permeability and chloride diffusivity of concrete under compressive stress: Experimental investigation and mesoscale lattice modelling, *Construction and Building Materials.* https://doi.org/10.1016/j.conbuildmat.2020.121164
4. **T.T. Tran, T.M. Tran, X.T. Nguyen, D.H. Nguyen, B.T. Vu, and V.N. Vo. (**2022). Influences of pre-bending load and corrosion degree of reinforcement on the loading capacity of concrete beams.

Journal of the Mechanical Behavior of Materials. 31: pp. 554–563. https://doi.org/10.1515/jmbm-2022-0061
5. **Mutsuyoshi.** (2001). Present Situation of durability of post-tensioned pc bridges in Japan, Durability of post-tensioning tendons (Taerwe, L. ed.), *Fédération Internationale du Béton.*
6. **Uhlig, H.H.** (1971). Corrosion and Corrosion Control. *Wiley, New York*.
7. **Tuutti K.,** (1982), Corrosion of steel in concrete, *Swedish Cement and Concrete Researche Institute,* Ed., Stockholm.
8. **Bazant,** (1979). Physical Model for Steel Corrosion in Sea Structures- Theory. *Journal of the Structural Division*, june: pp. 1137-1153.
9. **Morinaga, S. (**1989). Prediction of Service Lives of Reinforced Concrete Buildings Based on Rate of Corrosion of Reinforcing Steel. *Special Report of the Institute of Technology: Skimiza Corporation, Japan*.
10. **López, W. and J.A. González**, (1993). Influence of the degree of pore saturation on the resistivity of concrete and the corrosion rate of steel reinforcement. *Cement and Concrete Research* 23 (2): pp. 368–376.
11. **Liu, Youping, (**1996). Modeling the Time-to-Corrosion Cracking of the Cover Concrete in Chloride Contaminated Reinforced Concrete Structures. *Virginia Polytechnic Institute and State University*.
12. **Weyers, Liu**, (1998). Modeling the dynamic corrosion process in chloride contaminated concrete structures. *Cement and Concrete Research,* 28 (3): pp. 365–379.
13. Concrete mix design (1991). Standard ACI211.1.
14. **T.D. Pham, S.T. Bui, T.T. Tran, N.V. Vo** (2023). Chloride ion diffusion in reinforced concrete beam structures subjected to bending: experiments and numerical simulations. *Journal of Transportation Sciences*, Volume 74, Number 5, pp. 644-654. https://doi.org/10.47869/tcsj.74.5.7
15. **M. Mohamed, H. El-Karmoty, A. El Zanaty, (**2016). Behavior of corroded bonded fully prestressed and conventional concrete beams. *HBRC Journal.* Issue:14, pp.137-149.
16. **Y. Xu, J. Shen, Y. Zheng, J. Mao, P. Wu.** (2018). Corrosion Characteristics of Reinforced Concrete Under the Coupled Effects of Chloride Ingress and Static Loading: Laboratory Tests and Finite Element Analysis. *Materials Science.* Vol. 24, No. 2. https://doi.org/10.5755/j01.ms.24.2.17963
17. **Hussain. H., Miteva. D.** (2018). Structural behavior of corroded reinforced concrete structures - A study based on detailed 3D FE analyses. *Master dissertation*. Chalmers University of Technology.
18. **T.H. Nguyen, A.T. Le, D.D. Nguyen** (2020). Bending strength diagnosis for corroded reinforced concrete beams with attendance of deterministic, random and fuzzy parameters. *Journal of SI & M.* Vol: 5, Issue: 3, pp.183-189. https://doi.org/10.1080/24705314.2020.1765268
19. **Zhou. Y., Gencturk. B., Willam. K., & Attar. A. (**2015). Carbonation-induced and chloride-induced corrosion in reinforced concrete structures. *Journal of Materials in Civil Engineering.* No: 27, Issue 9. https://doi.org/10.1061/(ASCE)MT.1943-5533.0001209
20. **Coronelli. D, Gambarova. P. (**2004). Structural assessment of corroded reinforced concrete beams: Modeling guidelines. *Journal of Structural Engineering*. Vol: *130*, pp. 1214–1224.
21. **A.El-Hefnawy.** (2000). A New Statistical Approach for Predicting the Residual Capacity of Reinforced Concrete Beams Having Corroded Main Steel. *Ph.D. Thesis*. Cairo University.
22. **Dang V.H, François R.** (2013). Influence of long-term corrosion in chloride environment on mechanical behaviour of RC beam. *Eng Struct.* 48: pp. 558–68
23. **Kim Anh T. Vu, Mark G. Stewart** (2000). Structural reliability of concrete bridges including improved chloride-induced

corrosion models, *Structural Safety*, 22, pp. 313-333.

СПИСОК ЛИТЕРАТУРЫ

1. **C.H. Truong, Q. Huynh, Q.V. Tran, P.P. Nguyen** (2008), Research and survey on the current state of corrosion and destruction of reinforced concrete structures and the possibility of erosion in the coastal environment Da Nang city. *Journal of science and technology*, University of Da Nang, 6(29).
2. **H.K. Dong, H.T.T. Duong (**2014**).** Corrosion of reinforced concrete and the method to avoid corrosion for reinforced concrete structures in VIETNAM'S sea. *VNCOLD.*
3. **T.T. Tran, D.T. Pham, M.N. Vu, V.Q. Truong, X.B. Ho, N.L. Tran, S.T. Nguyen, Q.D. To** (2021). Relation between water permeability and chloride diffusivity of concrete under compressive stress: Experimental investigation and mesoscale lattice modelling, *Construction and Building Materials.* https://doi.org/10.1016/j.conbuildmat.2020.121164
4. **T.T. Tran, T.M. Tran, X.T. Nguyen, D.H. Nguyen, B.T. Vu, and V.N. Vo. (**2022). Influences of pre-bending load and corrosion degree of reinforcement on the loading capacity of concrete beams. *Journal of the Mechanical Behavior of Materials*. 31: pp. 554–563. https://doi.org/10.1515/jmbm-2022-0061
5. **Mutsuyoshi.** (2001). Present Situation of durability of post-tensioned pc bridges in Japan, Durability of post-tensioning tendons (Taerwe, L. ed.), *Fédération Internationale du Béton.*
6. **Uhlig, H.H.** (1971). Corrosion and Corrosion Control. *Wiley, New York*.
7. **Tuutti K.,** (1982), Corrosion of steel in concrete, *Swedish Cement and Concrete Researche Institute,* Ed., Stockholm.
8. **Bazant,** (1979). Physical Model for Steel Corrosion in Sea Structures- Theory. *Journal of the Structural Division*, june: pp. 1137-1153.
9. **Morinaga, S. (**1989). Prediction of Service Lives of Reinforced Concrete Buildings Based on Rate of Corrosion of Reinforcing Steel. *Special Report of the Institute of Technology: Skimiza Corporation, Japan*.
10. **López, W. and J.A. González**, (1993). Influence of the degree of pore saturation on the resistivity of concrete and the corrosion rate of steel reinforcement. *Cement and Concrete Research* 23 (2): pp. 368–376.
11. **Liu, Youping, (**1996). Modeling the Time-to-Corrosion Cracking of the Cover Concrete in Chloride Contaminated Reinforced Concrete Structures. *Virginia Polytechnic Institute and State University*.
12. **Weyers, Liu**, (1998). Modeling the dynamic corrosion process in chloride contaminated concrete structures. *Cement and Concrete Research,* 28 (3): pp. 365–379.
13. Concrete mix design (1991). Standard ACI211.1.
14. **T.D. Pham, S.T. Bui, T.T. Tran, N.V. Vo** (2023). Chloride ion diffusion in reinforced concrete beam structures subjected to bending: experiments and numerical simulations. *Journal of Transportation Sciences*, Volume 74, Number 5, pp. 644-654. https://doi.org/10.47869/tcsj.74.5.7
15. **M. Mohamed, H. El-Karmoty, A. El Zanaty, (**2016). Behavior of corroded bonded fully prestressed and conventional concrete beams. *HBRC Journal.* Issue:14, pp.137-149.
16. **Y. Xu, J. Shen, Y. Zheng, J. Mao, P. Wu.** (2018). Corrosion Characteristics of Reinforced Concrete Under the Coupled Effects of Chloride Ingress and Static Loading: Laboratory Tests and Finite Element Analysis. *Materials Science.* Vol. 24, No. 2. https://doi.org/10.5755/j01.ms.24.2.17963

17. **Hussain. H., Miteva. D.** (2018). Structural behavior of corroded reinforced concrete structures - A study based on detailed 3D FE analyses. *Master dissertation*. Chalmers University of Technology.
18. **T.H. Nguyen, A.T. Le, D.D. Nguyen** (2020). Bending strength diagnosis for corroded reinforced concrete beams with attendance of deterministic, random and fuzzy parameters. *Journal of SI & M*. Vol: 5, Issue: 3, pp.183-189. https://doi.org/10.1080/24705314.2020.1765268
19. **Zhou. Y., Gencturk. B., Willam. K., & Attar. A. (**2015). Carbonation-induced and chloride-induced corrosion in reinforced concrete structures. *Journal of Materials in Civil Engineering.* No: 27, Issue 9. https://doi.org/10.1061/(ASCE)MT.1943-5533.0001209
20. **Coronelli. D, Gambarova. P. (**2004). Structural assessment of corroded reinforced concrete beams: Modeling guidelines. *Journal of Structural Engineering*. Vol: *130*, pp. 1214–1224.
21. **A.El-Hefnawy.** (2000). A New Statistical Approach for Predicting the Residual Capacity of Reinforced Concrete Beams Having Corroded Main Steel. *Ph.D. Thesis*. Cairo University.
22. **Dang V.H, François R.** (2013). Influence of long-term corrosion in chloride environment on mechanical behaviour of RC beam. *Eng Struct.* 48: pp. 558–68
23. **Kim Anh T. Vu, Mark G. Stewart** (2000). Structural reliability of concrete bridges including improved chloride-induced corrosion models, *Structural Safety*, 22, pp. 313-333.

Vo Van Nam, Doctor of Engineering, Department of Railways and Metro, Ho Chi Minh City University of Transport; 717066 Vietnam, Ho Chi Minh City, Vo Oanh, 2, tel. +842838991373, email: nam.vo@ut.edu.vn

Nguyen Trong Tam, Doctor of phylosophy, Head of the Department of Railways and Metro, Ho Chi Minh City University of Transport; 717066 Vietnam, Ho Chi Minh City, Vo Oanh, 2, tel. +842838991373, email: trongtam.nguyen@ut.edu.vn

Во Ван Нам, кандидат технических наук, Кафедра «Железная дорога и метрополитен», Хошиминский университет транспорта; 717066 Вьетнам, г. Хошимин, Во Оань, стр. 2, тел. +842838991373,email: nam.vo@ut.edu.vn

Нгуен Чонг Там, кандидат технических наук, заведующий кафедрой «Железная дорога и метрополитен», Хошиминский университет транспорта; 717066 Вьетнам, г. Хошимин, Во Оань, стр. 2, тел. +842838991373, e-mail: trongtam.nguyen@ut.edu.vn

International Journal for Computational Civil and Structural Engineering, 20(3) 45–55 (2024)

DOI:10.22337/2587-9618-2024-20-3-45-55

NUMERICAL SOLUTION OF THE FILTRATION-DEFORMATION PROBLEM IN THE CASE OF PHASED CONSTRUCTION OF A STORAGE DAM

Nikolay A. Aniskin, Stanislav A. Sergeev, Andrey V. Stupivtsev, Ilia A. Bokov

Moscow State University of Civil Engineering, Moscow, RUSSIA

Abstract. This paper presents the results of numerical modeling of the joint filtration-deformation problem for a storage dam taking into account its construction and filling of the pond bowl in 3 stages. Two variants of th e structure operation were considered: with the tubular drainage operating and excluded from operation. According to the results of researches the stability of the structure and parameters of filtration regime were evaluated. Recommendations on ensuring reliability and safety of the structure are formulated.

Keywords: numerical solution, finite element method, storage dam, filtration-deformation problem, depression surface, slope stability

ЧИСЛЕННОЕ РЕШЕНИЕ ФИЛЬТРАЦИОННО-ДЕФОРМАЦИОННОЙ ЗАДАЧИ ПРИ ПОЭТАПНОМ ВОЗВЕДЕНИИ ДАМБЫ НАКОПИТЕЛЯ

Н.А. Анискин, С.А. Сергеев, А.В. Ступивцев, И.А. Боков

Национальный исследовательский московский государственный строительный университет» (НИУ МГСУ), г. Москва, РОССИЯ

Аннотация. В данной работе представлены результаты численного моделирования совместной фильтрационно-деформационной задачи для дамбы накопителя с учетом ее возведения и наполнения чаши накопителя в 3 этапа. Рассматривалось два варианта работы сооружения: с действующим и исключенным из работы трубчатым дренажем. По результатам исследований дана оценка устойчивости сооружения и параметров фильтрационного режима. Сформулированы рекомендации по обеспечению надежности и безопасности сооружения.

Ключевые слова: численное решение, метод конечных элементов, дамба накопителя, фильтрационно-деформационная задача, депрессионная поверхность, устойчивость откоса

INTRODUCTION

For creation of accumulators of secondary material resources (“tailings” in the process of ore dressing, sludge in metallurgical production, fly ash in the operation of thermal power plants), dams from ground materials are used as enclosing structures. Also, industrial wastes can be used as materials for dam construction (as a rule, for building up the primary dam of the accumulator) if their properties allow it. As a rule, the construction of such storage dams is carried out in stages with their gradual filling. Such structures belong to hydraulic engineering structures and are subject to the same loads and impacts as earth dams. The peculiarity for the considered case is the gradual formation of stress-strain state of the erected soil massif. Also in the process of erection there is a change in the influence of water from the side of the storage bowl and the weighting and hydrodynamic pressure in the soil mass as a result of filtration flow. Operability of such structures depends to a great extent on the filtration regime. Certain requirements are imposed on the position of the depression curve, values of filtration flow rates, velocities and gradients [1, 2]. The results of

filtration calculations are necessary to assess the filtration strength of dam soils, to calculate transition zones and return filters, to calculate the stress-strain state and stability of the slopes of the earth dam.

One of the important structural elements of storage dams are drains necessary for lowering of the depressive surface position and organized drainage of filtered water. During operation of the structure, the drainage failure is possible, which can be caused by its colmatization [3, 4]. In this case the depression surface in the downstream prism of the dam rises, which can lead to undesirable consequences: threat of ground freezing in the zone of filtration flow outlet to the downstream in winter period.

This paper presents the results of filtration and deformation studies on a numerical model of a storage dam being built up during operation. Joint calculations of filtration, stress-strain state and stability of the dam slopes were carried out using the software package "PLAXIS 2D" based on the finite element method [5]. The results obtained made it possible to draw conclusions about the reliability of the structure and propose measures to improve its operation.

METHODS

The solution of this problem involves a joint filtration problem and the problem of determining the stress-strain state of the gradually built-up body of the storage dam. At each stage, the problem of unsteady filtration is solved with determination of filtration regime parameters necessary for calculation of the stress-strain state: position of the depression surface, values of filtration gradients and filtration volume hydrodynamic load in the design area.

In the most complicated cases, the filtration flow can pass through areas with different degrees of saturation of soil pores with water. This is the case when the water level in front of the structure changes in time. Then it is possible to conditionally divide the design area into 2 zones in which the filtration flow motion will be described by different dependencies [6, 7].

The basic differential equation of filtration [7] is used for the part of the design area of filtration, where the filtration flow movement occurs in a fully saturated water medium:

$$\frac{\delta}{\delta x}\left[k_x \frac{\delta h_t}{\delta x}\right] + \frac{\delta}{\delta y}\left[k_y \frac{\delta h_t}{\delta y}\right] + \frac{\delta}{\delta z}\left[k_z \frac{\delta h_t}{\delta y}\right] = S_s \frac{\delta h_t}{\delta t} \quad (1)$$

where $h_t = f(x, y, z, t)$ - head function in the considered area, varying along coordinates x, y, z and in time t; k_x, k_y, k_z - filtration coefficients of saturated soil in directions of axes x, y, z; S_s - saturation of soil.

Saturation can be expressed as follows: $S_s = \gamma_w (m_v + n\beta)$, where γ_w - specific weight of water, n - porosity, β - compressibility of water, m_v - volumetric compressibility coefficient of the soil of the filtration area.

Since water is not very compressible ($\beta = 4.7 \cdot 10^{-7}$ kPa - for cases of filtration flows), we can take $S_s = \gamma_w \cdot m_v$ in equation (1).

In the case when filtration in a region with incompletely saturated ground pores with water is considered, equation [7] is used for the solution:

$$\frac{\delta}{\delta x}\left[k(h_m) \frac{\delta h_m}{\delta x}\right] + \frac{\delta}{\delta y}\left[k(h_m) \frac{\delta h_m}{\delta y}\right] + \frac{\delta}{\delta z}\left[k(h_m)\left(\frac{\delta h_m}{\delta z} + 1\right)\right] = C(h_m) \frac{\delta h_m}{\delta t} \quad (2)$$

where $k(h_m)$ is the value of the filtration conductivity function; hm is the filtration head deficit (suction head); $C(h_m)$ is the slope of the soil volumetric water saturation curve.

At present, filtration problems are mainly solved using the finite element method (FEM) [8-13]. There are many program complexes (PCs) in which the solution of the steady filtration problem consists in solving the basic differential equation of filtration theory (1) using known boundary conditions. The position of the depression surface is determined by an iterative process.

Many studies conducted in recent years [14-18] have focused on the study of filtration processes, in a nonstationary state in incompletely saturated soils with a degree of water saturation $S_e < 0,8$. In this case, the complexity of the solution based on differential equation (2) consists in determining the parameters $k(h_m)$ and $C(h_m)$.

The model developed by Mualem in 1976 [19], which describes how the water permeability and water holding capacity of a soil depend on its degree of water saturation, is one of the widely used models in the field.

This model offers a relatively simple form for calculating the filtration conductivity of unsaturated soils. Additional research conducted by Van Genuchten in 1980 [20] compared the results based on Mualem's theory with direct measurements for a variety of differently characterized soils. The Van Genuchten model offers a way to describe the filtration characteristics for a wide range of soils, expressed through the relationship between the soil volumetric water saturation θ and the head deficit (suction head) h_m :

$$\theta = \theta_r + \frac{\theta_s - \theta_r}{\left[1 + (\alpha h_m)^n\right]^m}, \quad (3)$$

where θ_s – volume content of saturated water in the soil pores; θ_r - residual volume content of water in the soil pores; h_m - filtration head deficit (suction head); α, n and $m=1-1/n$ parameters of soil property curves (determined as a result of soil laboratory tests).

Filtration permeability of unsaturated soil is determined in accordance with the Van Genuchten model as follows:

$$k(h_m) = k_s \sqrt{S_e}\left[1 - (1 - S_e^{1/m})^m\right]^2, \quad (4)$$

where k_s – filtration conductivity (filtration coefficient) of saturated soil; S_e – degree of soil saturation, which is determined by dependence [20]:

$$S_e = \left[1 + (ah_m)^n\right]^{-m}, \quad (5)$$

Within the framework of this work, filtration studies were performed using the "PLAXIS 2D" software package based on the finite element method. The filtration calculations module of this complex "PlaxFlow" uses differential equations of saturated and unsaturated filtration (1-2) for solution. In the case of filtration in unsaturated soils, the Van Genuchten model described above (3-5) is used to determine the soil properties [20].

As a result of solving steady-state and transient filtration problems, a picture of filtration development in the dike and the foundation in the process of stage-by-stage construction of the dike and filling of the storage bowl was obtained. The position of the depression surface, distribution of heads, filtration gradients and velocities, volumetric filtration hydrodynamic load were determined for each stage.

Based on the obtained results of solving filtration problems at each stage, the stress-strain state of the dam and foundation was also evaluated and critical slip surfaces with stability coefficients were determined.

To solve the coupled filtration-deformation problem, the Plaxis 2d software package uses the calculation type "Fully coupled flow-deformation" using equation [5]:

$$\begin{bmatrix} K & Q \\ 0 & -H \end{bmatrix} \begin{bmatrix} v \\ p_w \end{bmatrix} + \begin{bmatrix} 0 & 0 \\ C & -S \end{bmatrix} \begin{bmatrix} \frac{dv}{dt} \\ \frac{dp_w}{dt} \end{bmatrix} = \begin{bmatrix} f_u \\ G + q_p \end{bmatrix} \quad (6)$$

where K is the stiffness matrix; H is the permeability matrix; Q, C is the coupling matrix and S the compressibility matrix; v is the displacement value; pw is the pore pressure; q_p is the flow function at the model boundaries; f_u is the loading vector; G is a vector that accounts for the effect of gravity on the flow in the vertical direction. This vector is part of the external flow.

On the basis of the joint unsteady deformation-filtration calculation, the stability coefficient of the upper slope of the dam was calculated.

To evaluate the stability of the slopes of the investigated soil structures in the PC "PLAXIS 2D" the "Safety" calculation is used, in which

the strength characteristics of the soils (angle of internal friction, cohesion and shear strength) are successively reduced until the minimum value of the stability coefficient is reached. The results of the stability calculation are the determination of the possible shear surface - the most weakened surface along which failure is possible, and the calculated stability coefficient. The possible shear surface is characterized by the minimum possible tangential stresses. The minimum design stability factor is defined as the ratio of the actual surface strength to the fracture strength.

RESEARCH OBJECT

Filtration and deformation studies have been carried out in relation to the enclosing dam of a tailings storage facility constructed to accommodate and store residual products of primary hydrometallurgical processing of ores. The barrier dam is an earth hydraulic engineering structure constructed by layer-by-layer backfilling with subsequent rolling. The cross section of the structure is shown in Figure 1. The maximum height of the embankment is 36.5 m with a crest elevation of 760 m, crest width of 13 m, and length along the dam axis of 645.8 m. The top slope of the dam is 1:3.0, the bottom slope is variable and is 1:2.5; 1:3.0. Berms 5 m wide are provided along the entire height of the dike with a spacing of 10-12.5 m. The thickness of the reclamation layers in the bowl is 32 m, the bowl filling level is 753.5 m. In the downstream prism of the dam, drainage is provided to ensure that the depression curve near the downstream slope is lowered below the seasonal freezing level.

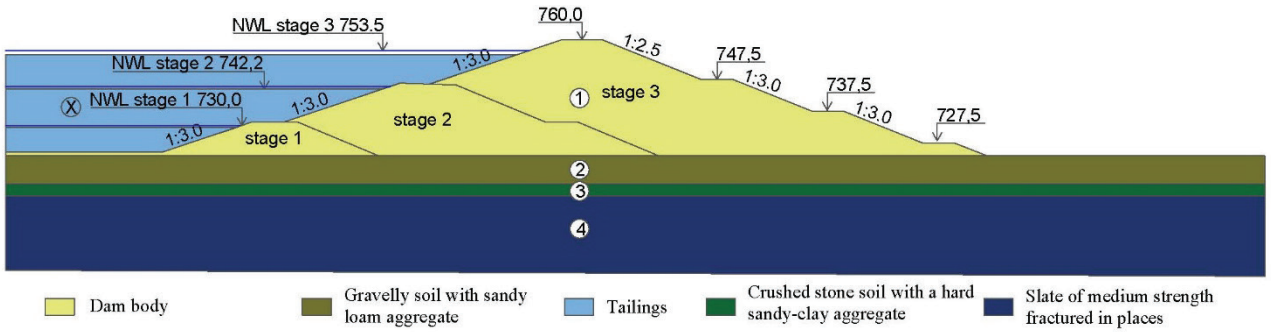


Figure 1. Cross-sectional profile of the tailings dam barrier

Table 1. Characteristics of soils

№ п.п	Soil type	Filtration coefficient m/day	Specific cohesion c, kPa	The angle of internal friction φ,°	Strain modulus E, kPa	Specific gravity ρ, kn/m^3
1	Sandy loam (dam body)	0,025	20	25	33500	21,3
2	Gravelly soil with sandy loam soil aggregate	0,08	16	33	29300	21
3	Crushed stone soil with a hard sandy-clay aggregate	0,09	15,0	20,3	30900	19,8
4	Slate of medium strength, fractured in places	0,00075	6535	35	50000	24,7
5	Tailings	0,003	21,1	19,5	7800	17,7

The volume of the technical reservoir at the design filling at the last stage is 10 million m3. The dam material is sandy loam. The base of the dam is predominantly gravel with sandy loam aggregate. There are interlayers of hard sandy loam up to 3 meters thick. At a depth of

more than 13 meters there is medium strength shale, fractured in some places. Physical and mechanical characteristics of the soils used in the calculation are presented in Table 1.

Problem statement

The process of phased construction of the storage dam to full height and filling of its bowl in 3 stages was modeled (Fig.1). The time step between the dam construction stages is 3 years. The schedule of dam construction and filling of the tailings storage facility is presented in Figure 2.

At each step, after filling the corresponding stage of the storage capacity, an unsteady filtration problem was solved with the determination of filtration flow parameters. The results of these calculations were used in the calculation of the stress-strain state and stability of the downstream slope of the dam for this stage using the calculation type "Fully coupled flow-deformation" in the PC "PLAXIS 2D" [5].

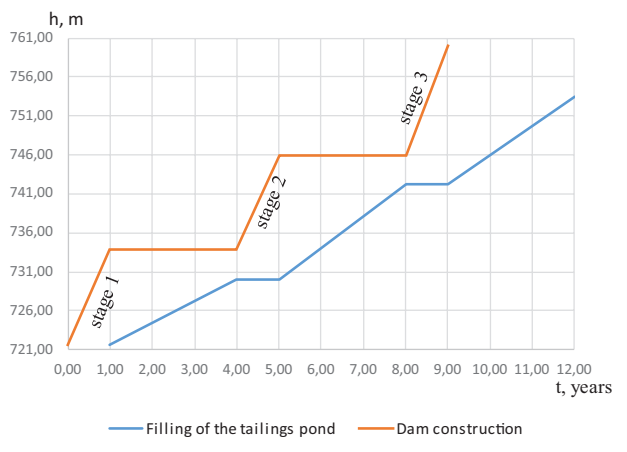


Figure 2. Schedule of dam construction and filling of the tailings pond bowl

Within the framework of the work two design cases were considered - the case of normal drainage operation and the case of drainage failure. The pipe drainage is located under the downstream prism at a distance of 64.0 m from the central axis of the dam (Fig. 1).

RESULTS

Filtration regime in case of full drainage operability.

Results of calculations of filtration regime for variant with full drainage operability are presented in Fig. 3-4.

Figure 3 shows the positions of the depression surface at the moments of time corresponding to the end of the filling stages (3, 6 and 9 years after the beginning of dam construction) and the moments of time 20, 25 and 30 years after the beginning of dam construction. It is possible to note gradual, rather long saturation of dam soil with water, which is caused by rather small value of dam soil filtration coefficient (k = 0.025 m/day). In case of normally operating drainage the soil of the downstream prism along the downstream slope is in dry condition. At that, its thickness up to the surface of the bottom slope all along exceeds the frost depth, which will ensure absence of ground freezing in winter period.

Figure 4 shows the distribution of filtration gradients in the dam massif at the time of stabilization of the filtration process (30 years from the start of construction). The maximum value of the gradient J_{max} = 1.48 was obtained at the outlet of the filtration flow into the drainage. To exclude filtration deformations at the outlet of filtration flow into drainage, this value should be used for calculation of drainage return filter and its device.

In accordance with the requirements to ensure the filtration strength of the soil [1] the inequality should be fulfilled:

$$J_{est,\,m} \leq J_{cr,m} / \gamma_n \qquad (7)$$

Where $J_{est,\,m}$ - average design head gradient of the seepage area; $J_{cr,m}$ - critical head gradient taken on the basis of laboratory studies of the dam soil or recommendations [1]; γ_n - reliability coefficient for the responsibility of the structure.

In our considered case $J_{est,\,m}$ = 0,29, $J_{cr,m}$ = 1,0 (according to [1] for sandy loam can be taken 2.0-

1.0), γ_n =1,25 (1st class of responsibility). Thus, the requirement (7) for this variant is fulfilled.

Results of filtration calculations of this variant testify to favorable filtration regime of the structure in case of proper operation of drainage.

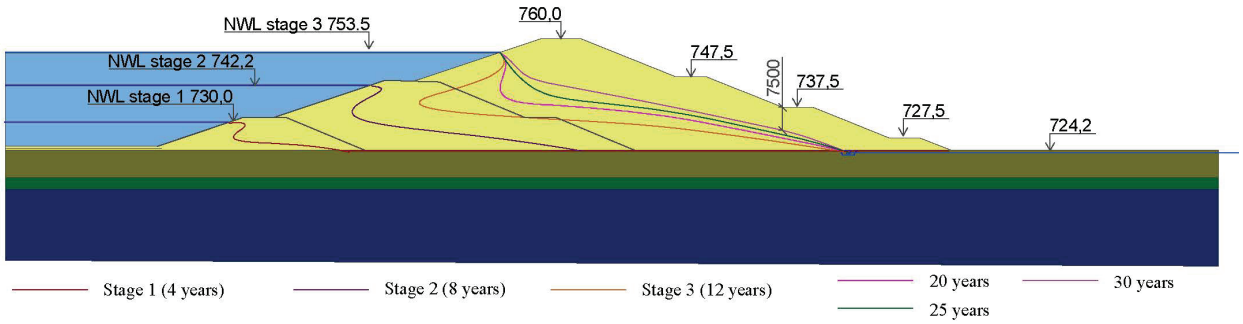


Figure 3: Position of the depression surface in the dam body in case of full operational capability of the drainage based on the results of unsteady calculation of filtration (transient flow) at stage filling and during the operation period

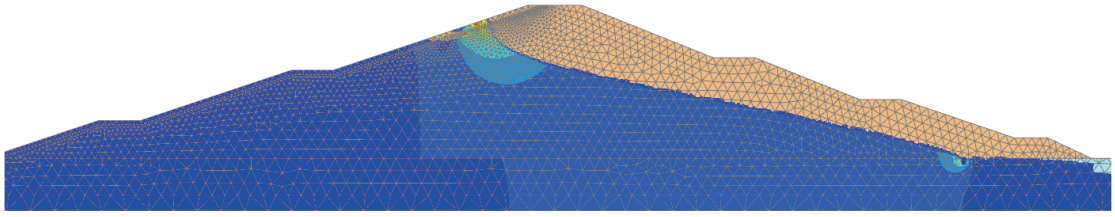


Figure 4. Distribution of head gradients in case of full serviceability of drainage according to results of unsteady filtration calculation (transient flow) at the moment of depression surface stabilization (30 years)

Filtration mode in case of complete drainage failure.

Drainage failure results in a significant increase in the position of the depression surface near the downstream slope of the dam (Figure 5-6). Over a significant length of the downstream slope, the distance from the slope surface to the depressional surface is less than the freezing depth. Operation of the structure under such conditions will result in freezing of the ground near the downslope slope and uplift of the depressional surface. If the frozen slope thaws in spring, it may lose its stability and collapse.

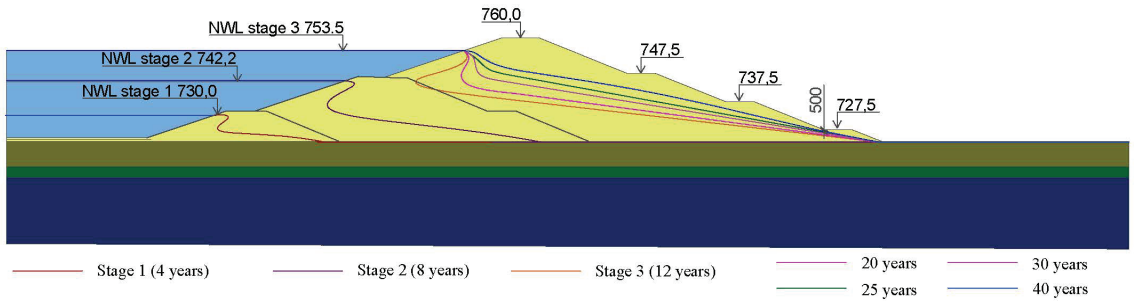


Figure 5. Position of the depression surface in the dam body in case of drainage failure based on the results of unsteady transient flow calculation during stage filling and operation period

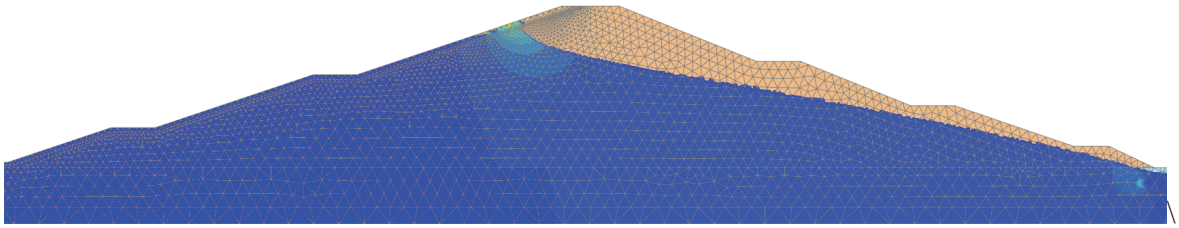


Figure 6. Distribution of head gradients in case of full serviceability of drainage according to the results of unsteady filtration calculation (transient flow) at the moment of stabilization of depressive surface (40 years)

Stabilization of dam soil saturation process comes for this variant in 40 years after the beginning of its construction. In order to ensure normal operation of the structure in case of drainage failure it is necessary to restore its serviceability or to pile additional soil massif on the part of the downstream slope, providing for the device of external drainage with a return filter. The value of maximum head gradient at the outlet of filtration flow, obtained for this option is equal to 1,67.

Requirements on average head gradient for this variant are also fulfilled ($J_{est,\,m}$ = 0,29).

Results of calculations of the stability of the downstream slope of the dam.

Using the results of the unsteady filtration calculations, the stability of the slopes of the dam body was calculated for the moments of time 10, 15, 20, 25, 30, 35, 40 years since the operation of the structure for each of the design cases. The results are presented in Figure 7,8 and Table 2.

For the variant with serviceable drainage during the operation period of the storage dam erected at full height, there is a gradual decrease in the stability coefficient over time from the value of 1.520 at the time of 10 years to the value of 1.351 at the time of 30 years, when the steady filtration regime is reached. The decrease is caused by gradual water saturation of the soil of the bottom prism and increase of hydrodynamic filtration force, which reduces the stability of the bottom slope. For this variant the stability requirements are fulfilled.

Table 2. Value of stability coefficients in unsteady filtration calculation.

Calculation option	Values of stability coefficients at service life						
	10 years	15 years	20 years	25 years	30 years	35 years	40 years
Operational drainage	1,520	1,406	1,383	1,369	1,351	1,351	1,351
Drainage failure	1,465	1,336	1,278	1,255	1,251	**1,249**	**1,247**

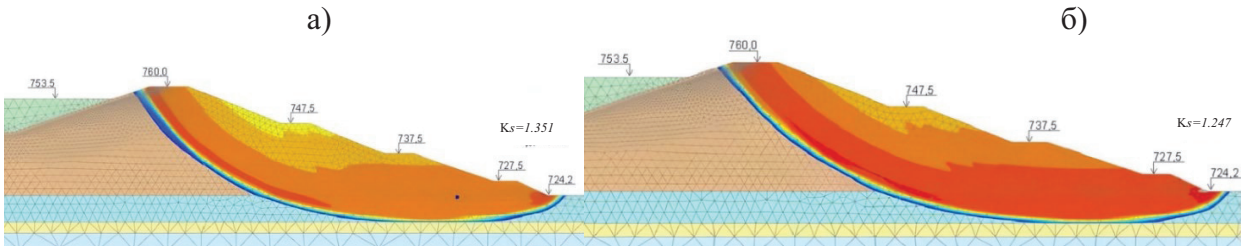


Figure 7. Slope shear surface: a - at the moment of stabilization of depression surface (30 years) in the dam body in case of proper operation of drainage, K_s= 1,351; b - at the moment of stabilization of depression surface (40 years) in the dam body in case of complete failure of drainage at non-stationary calculation of filtration, K_s= 1,247.

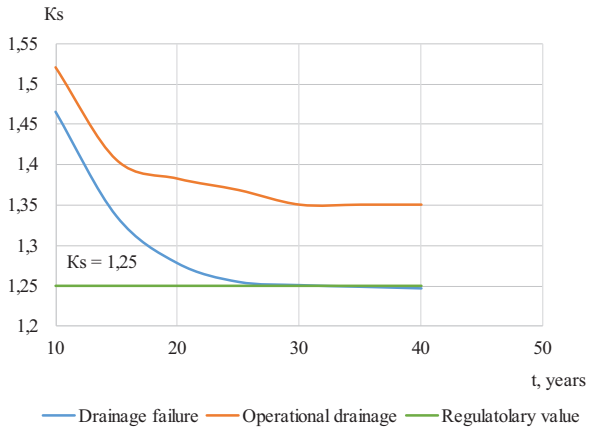


Figure 8. Graph of time dependence of dam slope stability coefficient in the process of operation

In case of non-working drainage at operation of the structure in time stability coefficient decreases from the value 1,465 (at the moment of time 10 years) to 1,249 - 1,247 (at moments of time 35-40 years). These obtained values are less than the normative stability coefficient K_s= 1,247 for this class of responsibility. Thus, operation of storage dam in considered variant with non-operating drainage is impossible.

RESULTS

Numerical solution of the joint filtration-deformation problem for the tailings dam being built up in stages is obtained. Two variants of the structure operation are considered: in case of normal operation of the pipe drainage and in case of its inoperability. The results of numerical investigations allowed to give an estimation of serviceability and safety of the structure during construction and operation.

Variant with working drainage satisfies all requirements to the structure on providing favorable filtration regime. In case of drainage failure the depression surface rises to the surface of the dam bottom slope, as a result of which the requirement to prevent freezing of the dam soil in winter period is not fulfilled.

Requirements on stability of the dam bottom slope in case of drainage failure are also not fulfilled: the value of slope stability coefficient at the moments of time 35-40 years is lower than the required normative value.

According to the results of solution of the joint deformation-filtration problem, it can be concluded that it is necessary to use tubular drainage or to change the design of the downstream prism of the dam

FUNDING

The research was funded by the National Research Moscow State University of Civil Engineering (grant for fundamental and applied scientific research, project No. 29-392/130).

REFERENCES

1. State Standart 39.13330.2012 «Rock fill dams»
2. **Trunkov, G.T.** Ensuring operational safety of tailing ponds for industrial waste storage in complex natural conditions. Hydrometeorology and Ecology, 2023, № 4(35). – C. 149-155. – EDN XSCAPB. https://journal.kazhydromet.kz/index.php/kazgidro/article/view/1812
3. **Dembski, B.** Evaluation of drainage performance in the reclamation dam of the Iron Bridge tailings dam. “Ore Enrichment.”. – 2007. – № 4. – C. 38-41. – EDN ICAKBX.
4. **Dzyubenko L.F., Kuznetsova Yu.A., Lavrentiev V.L.L., Sokolova V.A.** Assessment of efficiency of tubular drainage application in cryolithozone. Hydrotechnical construction, hydraulics and engineering hydrology // Izvestiya vuzov. Construction. - 2018. - № 1. - C. 84-95.
5. PLAXIS 2D 2022. Tutorial Manual. https://communities.bentley.com/cfs-file/__key/communityserver-wikis-components-files/00-00-00-05-58/PLAXIS2DCE_2D00_V21.00_2D00_01_2D00_Tutorial_2D00_2D.pdf

6. **Freeze, R.A., and Cherry, J.A.** Groundwater, Prentice-Hall, 1979, Englewood Cliffs, NJ.
7. **Stark T.D., Jafari N.H., Zhindon J.S.L., & Baghdady A.** Unsaturated and Transient Seepage Analysis of San Luis Dam. Journal of Geotechnical and Geoenvironmental Engineering. 2017; 143(2), 04016093. DOI: 10.1061/(ASCE)GT.1943-5606.0001602.
8. **Aniskin N.A., Antonov A.S.** Development geo-seepage models for solving seepage problems of large dam's foundations, on an example of ANSYS Mechanical APDL, Advanced Materials Research Vols. 1079-1080 (2015) pp 198-201
9. **Aniskin, N. & Malakhanov, Vyacheslav & Antonov, Anton.** (2016). Operational analysis of the tailings bund wall drainage system at mirny ore mining and processing enterprise. Vestnik MGSU. 91-102. 10.22227/1997-0935.2016.12.91-102.
10. **Zhang Ch., Chai J., Cao. J, Xu Z., Qin Y. and Lv Z.** 2020. Numerical Simulation of Seepage and Stability of Tailings Dams: A Case Study in Lixi, China. Water. DOI: 10.3390/B12030742
11. **Liu, Chong & Shen, Zhen-zhong & Gan, Lei & Xu, Liqun & Zhang, Kailai & Jin, Tian.** (2018). The Seepage and Stability Performance Assessment of a New Drainage System to Increase the Height of a Tailings Dam. Applied Sciences. 8. 1840. 10.3390/app8101840.
12. **Hu, S., Chen, Y., Liu, W., Zhou, S., & Hu, R.** (2014). Effect of seepage control on stability of a tailings dam during its staged construction with a stepwise-coupled hydro-mechanical model. International Journal of Mining, Reclamation and Environment, 29(2), 125–140. https://doi.org/10.1080/17480930.2013.870693
13. **Galavi, V.** 2016. Groundwater flow, fully coupled flow deformation and undrained analyses in PLAXIS 2D and 3D. 10.13140/RG.2.1.1940.7763.
14. **Al-Labban, Salama**, Seepage and Stability Analysis of the Earth Dams under Drawdown Conditions by using the Finite Element Method" (2018). Electronic Theses and Dissertations, 2004-2019. 6157.
15. **Terleev V.V., Narbut M. A., Topazh A. G., Mirshel' V.** Modeling of hydrophysical properties of soil as a capillary-porous body and improvement of the Moalem-Van Genuchten method: theory. Agrophysics, 2014, No. 2(14), pp. 35-44.
16. **Kosugi K.** 1999. General model for unsaturated hydraulic conductivity for soil with lognormal pore-size distribution. Soil Sci. Soc. Am. J. 63:270-277.
17. **Stark, T.D., Jafari, N.H., Leopold, A.L., and Brandon, T.L.** "Soil compressibility in transient unsaturated seepage analyses." Can. Geotech. J., 2014, 51(8), 858–868.
18. **Thieu, N.T.M., Fredlund, M.D., Fredlund, D.G., and Hung, V.Q.** "Seepage modeling in a saturated/unsaturated soil system." Proc., Int. Conf. on Management of the Land and Water Resources, 2001, 1–8.
19. **Mualem Y.** 1976. A new model for predicting hydraulic conductivity of unsaturated porous media. Water Resour. Res. 12:513-522.
20. **Van Genuchten, M.Th.** 1980. A closed form equation for predicting the hydraulic conductivity of unsaturated soils. Soil Sci. Soc. Am. J. 44:892-989.

СПИСОК ЛИТЕРАТУРЫ

1. State Standart 39.13330.2012 «Rock fill dams»
2. **Trunkov, G.T.** Ensuring operational safety of tailing ponds for industrial waste storage in complex natural conditions. Hydrometeorology and Ecology, 2023, № 4(35). – С. 149-155. – EDN XSCAPB. https://journal.kazhydromet.kz/index.php/kazgidro/article/view/1812
3. **Dembski, B.** Evaluation of drainage performance in the reclamation dam of the

Iron Bridge tailings dam. “Ore Enrichment.”. – 2007. – № 4. – С. 38-41. – EDN ICAKBX.

4. **Dzyubenko L.F., Kuznetsova Yu.A., Lavrentiev V.L.L., Sokolova V.A.** Assessment of efficiency of tubular drainage application in cryolithozone. Hydrotechnical construction, hydraulics and engineering hydrology // Izvestiya vuzov. Construction. - 2018. - № 1. - С. 84-95.
5. PLAXIS 2D 2022. Tutorial Manual. https://communities.bentley.com/cfs-file/__key/communityserver-wikis-components-files/00-00-00-05-58/PLAXIS2DCE_2D00_V21.00_2D00_01_2D00_Tutorial_2D00_2D.pdf
6. **Freeze, R.A., and Cherry, J.A.** Groundwater, Prentice-Hall, 1979, Englewood Cliffs, NJ.
7. **Stark T.D., Jafari N.H., Zhindon J.S.L., & Baghdady A.** Unsaturated and Transient Seepage Analysis of San Luis Dam. Journal of Geotechnical and Geoenvironmental Engineering. 2017; 143(2), 04016093. DOI: 10.1061/(ASCE)GT.1943-5606.0001602.
8. **Aniskin N.A., Antonov A.S.** Development geo-seepage models for solving seepage problems of large dam’s foundations, on an example of ANSYS Mechanical APDL, Advanced Materials Research Vols. 1079-1080 (2015) pp 198-201
9. **Aniskin, N. & Malakhanov, Vyacheslav & Antonov, Anton.** (2016). Operational analysis of the tailings bund wall drainage system at mirny ore mining and processing enterprise. Vestnik MGSU. 91-102. 10.22227/1997-0935.2016.12.91-102.
10. **Zhang Ch., Chai J., Cao. J, Xu Z., Qin Y. and Lv Z.** 2020. Numerical Simulation of Seepage and Stability of Tailings Dams: A Case Study in Lixi, China. Water. DOI: 10.3390/B12030742
11. **Liu, Chong & Shen, Zhen-zhong & Gan, Lei & Xu, Liqun & Zhang, Kailai & Jin, Tian.** (2018). The Seepage and Stability Performance Assessment of a New Drainage System to Increase the Height of a Tailings Dam. Applied Sciences. 8. 1840. 10.3390/app8101840.
12. **Hu, S., Chen, Y., Liu, W., Zhou, S., & Hu, R.** (2014). Effect of seepage control on stability of a tailings dam during its staged construction with a stepwise-coupled hydro-mechanical model. International Journal of Mining, Reclamation and Environment, 29(2), 125–140. https://doi.org/10.1080/17480930.2013.870693
13. **Galavi, V.** 2016. Groundwater flow, fully coupled flow deformation and undrained analyses in PLAXIS 2D and 3D. 10.13140/RG.2.1.1940.7763.
14. **Al-Labban, Salama**, Seepage and Stability Analysis of the Earth Dams under Drawdown Conditions by using the Finite Element Method" (2018). Electronic Theses and Dissertations, 2004-2019. 6157.
15. **Terleev V.V., Narbut M. A., Topazh A. G., Mirshel' V.** Modeling of hydrophysical properties of soil as a capillary-porous body and improvement of the Moalem-Van Genuchten method: theory. Agrophysics, 2014, No. 2(14), pp. 35-44.
16. **Kosugi K.** 1999. General model for unsaturated hydraulic conductivity for soil with lognormal pore-size distribution. Soil Sci. Soc. Am. J. 63:270-277.
17. **Stark, T.D., Jafari, N.H., Leopold, A.L., and Brandon, T.L.** “Soil compressibility in transient unsaturated seepage analyses.” Can. Geotech. J., 2014, 51(8), 858–868.
18. **Thieu, N.T.M., Fredlund, M.D., Fredlund, D.G., and Hung, V.Q.** “Seepage modeling in a saturated/unsaturated soil system.” Proc., Int. Conf. on Management of the Land and Water Resources, 2001, 1–8.
19. **Mualem Y.** 1976. A new model for predicting hydraulic conductivity of unsaturated porous media. Water Resour. Res. 12:513-522.
20. **Van Genuchten, M.Th.** 1980. A closed form equation for predicting the hydraulic conductivity of unsaturated soils. Soil Sci. Soc. Am. J. 44:892-989.

Aniskin Nikolay Alexeyevich, Professor, DSc, Acting Director of the Institute of Hydrotechnical and Power Engineering (IGES) of the National Research Moscow State University of Civil Engineering (NRU MGSU), 129337, Russia, Moscow, Yaroslavskoe shosse, 26, phone +7 (495) -287-49-14 ext. 14-19, e-mail: Aniskin@mgsu.ru

Sergeev Stanislav Alexeyevich, PhD, Associate Professor of the Department of Hydraulics and Hydraulic Engineering, Researcher at the Scientific and Educational Center "Geotechnics" of the National Research Moscow State University of Civil Engineering (NRU MGSU), 129337, Russia, Moscow, Yaroslavskoe shosse, 26, phone +7 (495) -287-49-14 ext. 14-19, e-mail: SergeevSA@mgsu.ru

Stupivtsev Andrey Vladimirovich, postgraduate student of the Institute of Hydrotechnical and Power Engineering (IGES) of the National Research Moscow State University of Civil Engineering (NRU MGSU), 129337, Russia, Moscow, Yaroslavskoe shosse, 26, phone +7 (495) -287-49-14 ext. 14-19, e-mail: StupivtsevAV@gmail.com

Bokov Ilia Alexeyevich, student of the Institute of Hydrotechnical and Power Engineering (IGES) of the National Research Moscow State University of Civil Engineering (NRU MGSU), 129337, Russia, Moscow, Yaroslavskoe shosse, 26, phone +7 (495) -287-49-14 ext. 14-19, e-mail: ibokov111111@gmail.com

Анискин Николай Алексеевич, профессор, доктор технических наук, исполняющий обязанности директора Института гидротехнического и энергетического строительства (ИГЭС) Национального исследовательского Московского государственного строительного университета (НИУ МГСУ), 129337, г. Москва, Ярославское ш., д. 26, тел. +7 (495)-287-49-14 доб.14-19. e-mail: Aniskin@mgsu.ru

Сергеев Станислав Алексеевич, кандидат технических наук, доцент кафедры «Гидравлики и гидротехнического строительства», научный сотрудник Научно-образовательного центра «Геотехника» Национального исследовательского Московского государственного строительного университета (НИУ МГСУ) 129337, г. Москва, Ярославское ш., д. 26, тел. +7 (495)-287-49-14 доб.14-19 e-mail: SergeevSA@mgsu.ru

Ступивцев Андрей Владимирович, аспирант кафедры «Гидравлики и гидротехнического строительства» Национального исследовательского Московского государственного строительного университета (НИУ МГСУ) 129337, г. Москва, Ярославское ш., д. 26, тел. +7 (495)-287-49-14 доб.14-19 e-mail: StupivtsevAV@gmail.com

Боков Илья Алексеевич, студент Института гидротехнического и энергетического строительства (ИГЭС) Национального исследовательского Московского государственного строительного университета (НИУ МГСУ), 129337, г. Москва, Ярославское ш., д. 26, тел. +7 (495)-287-49-14 доб.14-19. e-mail: ibokov111111@gmail.com

International Journal for Computational Civil and Structural Engineering, 20(3) 56–68 (2024)

DOI:10.22337/2587-9618-2024-20-3-56-68

NONLINEAR DYNAMIC ANALYSIS OF WIND ACTIONS ON A CABLE-STAYED GLASS FAÇADE SYSTEM

Oleg S. Goryachevsky, Alexander M. Belostotsky

National Research Moscow State University of Civil Engineering, Moscow, RUSSIA

Abstract: This paper presents the results of a nonlinear dynamic analysis of wind actions on a cable-stayed glass façade. The wind impact was determined by a transient eddy-resolving numerical simulation using a hybrid RANS-LES model SBES. The revealed dynamic response of the façade system confirms the relevance of dynamic calculations compared to simplified static approaches.

Keywords: computational fluid dynamics (CFD), wind action, wind response, cable-stayed glass façade system, nonlinear dynamic analysis

НЕЛИНЕЙНЫЙ ДИНАМИЧЕСКИЙ РАСЧЕТ ВАНТОВОГО СВЕТОПРОЗРАЧНОГО ФАСАДА НА ВЕТРОВЫЕ ВОЗДЕЙСТВИЯ

О.С. Горячевский, А.М. Белостоцкий

Национальный исследовательский Московский государственный строительный университет, г. Москва, РОССИЯ

Аннотация: В статье представлены результаты нелинейного динамического расчета вантового светопрозрачного фасада на ветровое воздействие. Ветровое воздействие было определено в результате численного моделирования в нестационарной вихреразрешающей постановке по гибридной модели SBES. Выявленный динамический отклик фасадной системы подтверждает актуальность динамических расчетов по сравнению с упрощенными статическими подходами.

Ключевые слова: вычислительная гидродинамика, ветровое воздействие, отклик на ветровое воздействие, вантовый светопрозрачный фасад, нелинейный динамический анализ

1. INTRODUCTION

The widespread use of complex and costly façade systems in modern construction challenges engineers to correctly calculate their robustness, stiffness and stability. The situation becomes even more complicated if the façade structures are flexible (possessing low eigenfrequencies) and their mechanical behaviour is significantly non-linear; for instance, cable-stayed glass façades (CSGF), Fig. 1.

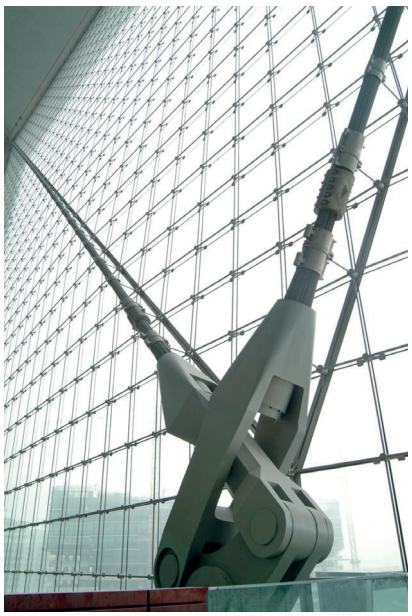
As a rule, wind loads are the most important for façade structures. Physical modelling utilising wind tunnels (PM) is currently the most common and well-studied method for determining wind loads for non-typical structures. Along with its advantages, PM has a number of disadvantages, among which are the reduced scale of the models, limited consideration of the surrounding buildings and terrain, measurement of the required parameters in a small number of points (usually a few dozen).

In the last 30 years, interest in numerical modelling of wind loads (NM) has grown significantly [1,2]. NM has almost unlimited possibilities to take into account surrounding buildings, topography, climatic effects and a number of other factors, allows obtaining results in millions of points, processing and visualising

them freely. High computational complexity and use of simplifying hypotheses that reduce accuracy have for a long time restrained the introduction of NM in construction practice [3,4]. However, the development of computational techniques, turbulence models, numerical methods and software currently allows full use of NM as a tool for determining wind actions [5,6]. Today, NM is implemented in foreign [7,8] and Russian regulatory documents [9,10], and is actively used in many construction companies.



(a) exterior view



(b) interior view

Figure 1. Beijing Poly Plaza Hotel, China

The research on a CSGF's stress-strain state started in the 2000s. Let us highlight the main ones in chronological order (2009-2023).

In [11], Feng et al. found that glazing elements increase the façade stiffness up to 30% and the damping performance from 0.1% to 3.5-4.5% compared to an unglazed cable network. In [12] Feng, based on the nonlinear differential equation of vibration, analysed the response spectra to seismic load. It was found that the influence of nonlinearities decreases when the natural frequencies of vibration increase. In [13], Feng experimentally and numerically (using ANSYS Mechanical) revealed a significant difference in the glazing's stress-strain state when using spiders and clamping plates.

Amadio and Bedon investigated the potential of elastic-plastic dampers to reduce the response to blast effects on the basis of dynamic analysis [14,15]. It was found that cables are the most vulnerable to blast effects, and the use of dampers can reduce the maximum forces in them while maintaining flexures.

The most extensive study of CSGFs is done in Yussof's thesis [16]. In his work, an overview of the application, implementation and types of CSGFs is presented. A set of experimental and parametric numerical studies in Simulia ABAQUS are carried out. Static load, impact load on the glass and cable removal are considered.

In [17], Wang experimentally and numerically investigated the dynamic behaviour of CSGFs. Several first eigenfrequencies and modes, as well as damping coefficients, were determined. It was found that the sealant has almost no effect on the vibrations and can be disregarded.

The study by Xiang [18] focuses on evaluating the effect of the building load-bearing system on the response of a CSGF to seismic loading.

In 2023, numerical studies of wind actions on CSGFs in a direct dynamic formulation appeared. In [19], Rizzo used wind pressures obtained in a wind tunnel, while in [20] Zhou generated synthetic wind loads using a random Gaussian process model. Rizzo's study focused

mainly on modelling, while Zhou's study focused on finding simplified mathematical models. Zhou also showed that the behaviour of a CSGF is reliably described by thin membrane theory when the cables are dense.
Among the published studies of CSGFs, no papers were found in which wind loads were determined on the basis of NM. Thus, the choice of NM for determining wind loads determines the scientific novelty of the paper.

2. METHODOLOGY AND OBJECT

2.1 Object and task description

The object is a CSGF of an office building (Fig. 2). The building is being constructed on the territory of the new modern town of Rublevo-Arkhangelskoye in the western part of Moscow (Fig. 3).



Figure 2. Investigated Building with CSGF



Figure 3. Render of Rublevo-Arkhangelskoye

The polygonal in plan building is 122 m long, 58 m wide and 34 m tall. The maximum height of the CSGF is 19.34 m, and the minimum height is 2.99 m.
In a structural sense, the façade consists of:

- vertical pre-stressed load-bearing steel cables with a diameter of 30 mm;
- single glazing units with maximum dimensions of 2880 × 1480(h) mm and a total glass thickness of 28 mm;
- cable attachment assemblies to glass panes (spiders);
- cable attachment assemblies to reinforced concrete and steel structures.

According to SP 20.13330, the construction site is located in wind zone I (w_0 = 230 Pa), terrain type C.
Among the loads, dead weight, internal and external wind loads were taken into account. The internal wind pressure was calculated according to paragraph B.1.9 of SP 20.13330, and the external wind pressure was calculated on the basis of PM.
Cable pretension is set from 5 to 20 tf (higher in areas of maximum flexure).

The stress-strain state received was assessed according to the following criteria:

- relative flexures of cables (< 1/200 length, demanded by SP 20.13330);
- relative flexures of insulating glass units (< 1/250, which is equal to 5.92 mm, demanded by GOST 24866-2014);
- maximum forces in cables (< R_{dh} = 40.76 tf, demanded by SP 16.13330).

A computationally economical methodology was used to determine the wind loads on the façade:
1. Initially, hazardous wind directions were determined by steady-state RANS simulations (SST k-ω model);
2. For the identified hazardous wind directions, the refined values of peak wind pressures and pressure time series for each glazing element were determined based by transient simulations (using a hybrid RANS-LES model SBES).

The dynamic stress-strain state of the façade system was then analysed, taking into account cable pretension, damping and geometric nonlinearity from time-dependent wind pressures.

2.2 CFD model description

NM of the wind actions was carried out in ANSYS Fluent using the finite volume (FV) method. The geometrical model of the building is shown in Fig. 4. Different polyhexagonal meshes were used for steady-state and transient simulations (Figs. 5-6).

The modelling was carried out at a geometric scale of 1:100 (integral loads were scaled during processing).

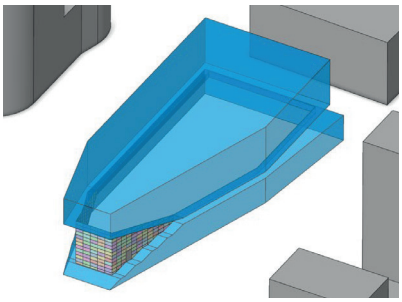


Figure 4. Calculation area near the GSCF

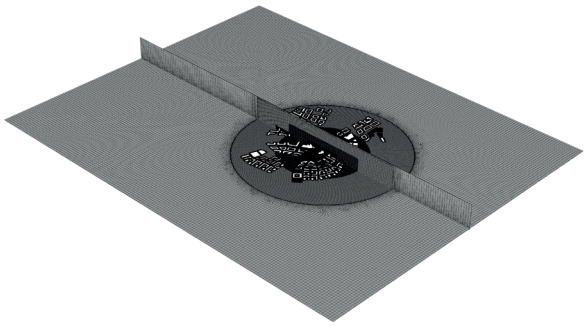


Figure 5. Mesh for RANS (10.2m cells)

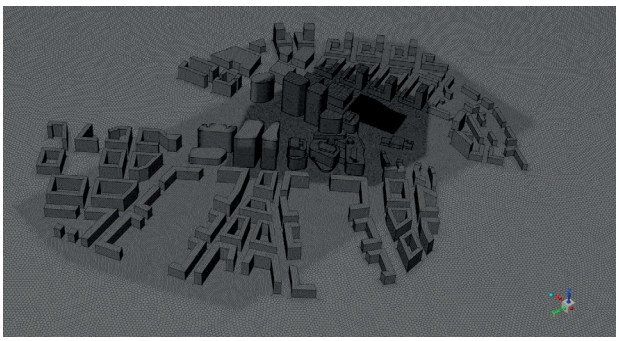


Figure 6. Mesh for SBES (9.2-9.5m cells)

Steady-state (RANS) simulations were performed using the SST k-ω turbulence model [21].

Transient simulations were performed using a hybrid RANS-LES model SBES [22]. The RANS model SST k-ω in the near-wall and vortex-free zones and the LES model WALE [23] in the other regions were coupled (mixed).

The hybrid SBES model is based on spatial mixing of turbulent viscosity:

$$\nu_t^{SBES} = f_{SDES}\nu_t^{RANS} + f_{SDES}\nu_t^{LES}, \qquad (1)$$

where ν_t^{RANS} is the turbulent viscosity of RANS models (determined by the Boussinesq hypothesis); ν_t^{LES} is the subgrid viscosity of LES models; f_{SDES} is a special function providing the transition between LES and RANS zones (shielding function).

For steady-state simulations, the Coupled pressure-velocity solver was used. For transient simulations, the segregated SIMPLEC solver was used.

Spatial numerical discretisation schemes over space were applied [24]:

- (RANS) Second Order Upwind for the momentum equation;
- (SBES) Bounded Central Differencing for the momentum equation (coefficient 0.75);
- Second Order Upwind for the turbulent transport equations;
- Second Order Upwind for the interpolation of pressures;
- Least Squares Method to calculate gradients in the centroids of FVs.

Time integration for SBES was performed using Bounded Second Order Implicit scheme. The time step $\Delta t = 0.0002$ s (physical 0.02 s).

The following boundary conditions for the computational domain were applied:

1.The velocity profile at the inlet: $U(z)$, taken from the building code;

2. Turbulence intensity 1% (total turbulence is modelled directly by the flow moving through the surrounding buildings);

3.Backflow pressure at the outlet: $\overline{p} = 0$;

4.Free slip wall conditions were set for the lateral and upper boundaries;
5.No-slip wall conditions were set for the ground and building surfaces.

2.3 Peak wind load calculation

RANS simulations were performed for 36 wind directions (in 10° increments), and transient simulations were performed only for the identified hazardous directions.
Peak wind pressures $p_{e,+(-)}$ from RANS simulations were estimated using a semi-empirical model [25]:

$$\begin{aligned} p_{e,+} &= \Delta\overline{p} + \theta_{+}\sigma_p; \\ p_{e,-} &= \Delta\overline{p} - \theta_{-}\sigma_p; \\ \sigma_P &= \left(2I_U + I_U^2\right)\Delta\overline{p}; \end{aligned} \tag{2}$$

$$I_U = \sqrt{\frac{\rho_{air}k}{3\left|\Delta\overline{p}\right|}}, \tag{3}$$

where $\theta_+ = 0.5$, $\theta_- = 1.5$ are calibration coefficients; k is the turbulent kinetic energy near the wall, $\Delta\overline{p}$ is the mean pressure at the wall.
The accuracy of the (2-3) model is sufficient to identify the hazardous wind directions.
Based on (2-3), the peak integral wind loads on each of the 3 sides of the façade were calculated:

$$\begin{aligned} F_{n,+(-)} &= \int_S w_{e,+(-)}dS = \\ &= v_{+(-)}\left(1+\zeta\right)\int_S p_{e,+(-)}dS, \end{aligned} \tag{4}$$

where S is the area of the facade side (one of three); $\zeta = 1.31$ is wind pressure pulsation coefficient for terrain type C; $v_{+(-)} = 0.75(0.65)$ is correlation coefficient (both taken from SP 20.13330).
For RANS simulations, 450 iterations with stepwise relaxation enhancement were calculated.
Based on the results of transient simulations, integral values of peak wind loads and peak pressures on glazing elements were determined, which were further used in static calculations:

$$\begin{aligned} F_{n,+} &= \max_j \int_S \Delta p(t_j)dS; \\ F_{n,-} &= \min_j \int_S \Delta p(t_j)dS; \end{aligned} \tag{5}$$

$$w_{e,+(-)} = \frac{1}{S}\int_S \Delta p(t_k)dS; \tag{6}$$

where S is the area of the façade side / glazing element; t_j is the j-th physical timestep; t_k is the k-th timestep at which the maximum of integral forces (5) is achieved for the façade side on which the corresponding glazing element is located.
Formulas (5-6) do not contain pulsation and pressure correlation coefficients because the corresponding effects are modelled directly.
The total physical time during transient simulations was 5.2-5.7 s (~$2.7\cdot10^4$ time steps, real-scale 7.8-8.5 min). During the post-processing, the first 0.5 s were discarded.

2.4 FEM model description

Stress-strain state calculations of the GSCF were carried out in the ANSYS Mechanical using the following finite element types: SHELL181 (for glazing elements), LINK180 (for cables), BEAM188 (for columns, spiders and door frames), MASS21 (to simulate the mass of the non-load-bearing part of spiders and luminaires).
The total dimensionality of the finite element model (Figs. 7-8) is 57440 nodes / 52925 FEs / ~334000 variables.

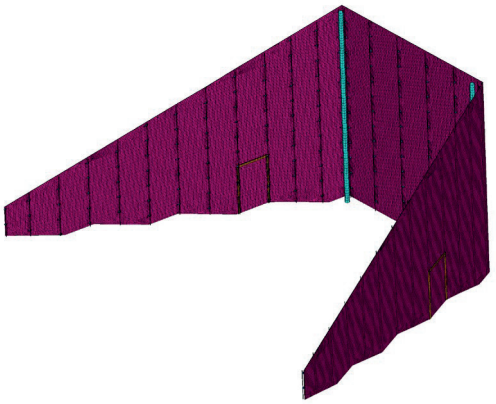


Figure 7. FEM model - general view

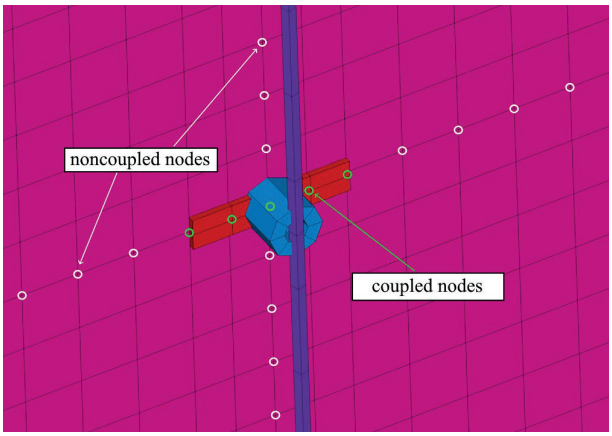


Figure 8. FEM model - cable and glass connection diagram

Columns and cables are fixed in all degrees of freedom at the points of attachment to the load-bearing structures of the building. The windows are attached using roller supports (free in the façade plane) at the upper and lower façade marks, except for the corner points of each window, which are attached using hinged supports.

All calculations were carried out in a geometrically nonlinear formulation taking into account cable pretension.

For dynamic calculations, the time step was set to $\Delta t = 0.01$ s (see Section 3.2).

Numerical Newton-Raphson method was used for resolving the nonlinearity and Newmark method was used for time integration.

Damping was accounted for by the Rayleigh hypothesis with a damping coefficient in fractions of the critical $\xi = 0.035$ [11].

3. RESULTS AND DISCUSSION

3.1 Peak wind load results

The analysis of peak values of integral loads (Fig. 9) obtained from the static simulations revealed 4 hazardous wind directions: 130°, 200°, 230° and 310°. For each of these directions, a refined transient simulation was carried out (Table 1).

It should be clarified that the loads given in Table 1 do not take into account the dynamic response of the structure.

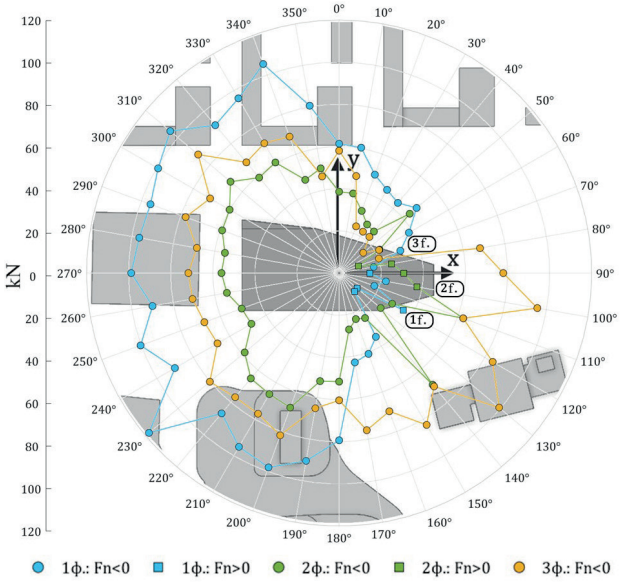


Figure 9. Pie chart of F_n [kN] obtained in the steady simulations

Table 1. Peak wind loads on the façade sides

Wind attack angle, °	Simulation	F_n, kN		
		1f.	2f.	3f.
130	SST	55.1	-25.8	-99.3
	SBES	54.8	-64.5	-105
200	SST	-98.1	-67.9	-81.9
	SBES	-66.8	-69.8	-71.0
230	SST	-118.0	-58.6	-80.2
	SBES	-70.5	-52.3	-69.0
310	SST	-105	-67.4	-87.4
	SBES	-75.2	-54.2	-60.9

Examples of the resulting time series and spectra are shown in Figs. 10-13.

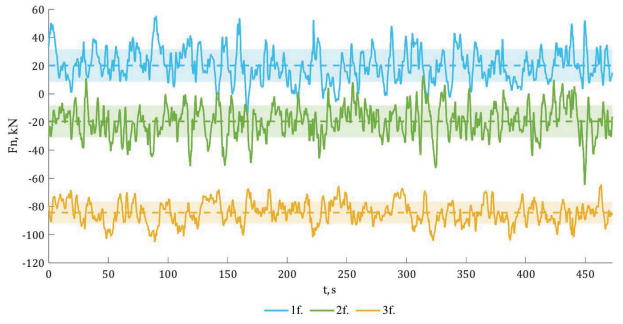


Figure 10. Steady-state fluctuations of integral wind loads on the facade sides, kN (130°)

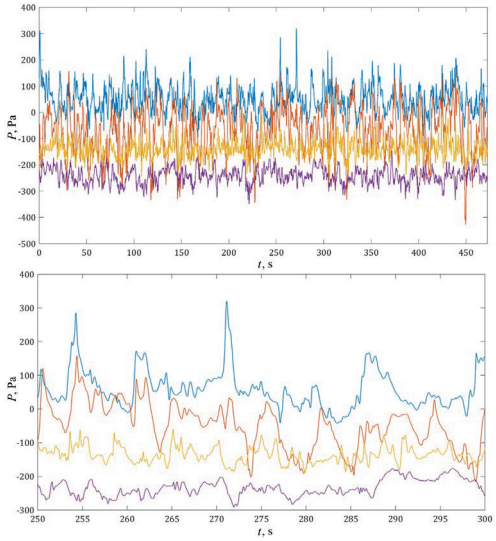


Figure 11. Steady-state wind pressure fluctuations for 4 characteristic glazing elements, Pa (130°)

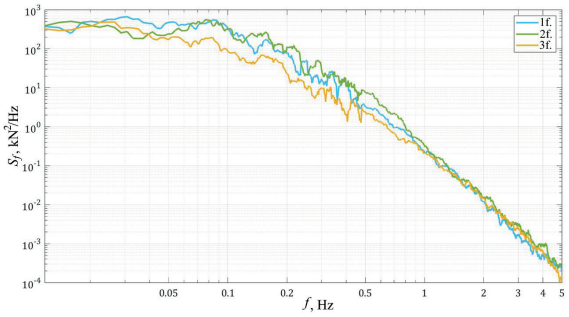


Figure 12. Power spectral power density of integral wind loads on facade sides, kN^2 /Hz (130°)

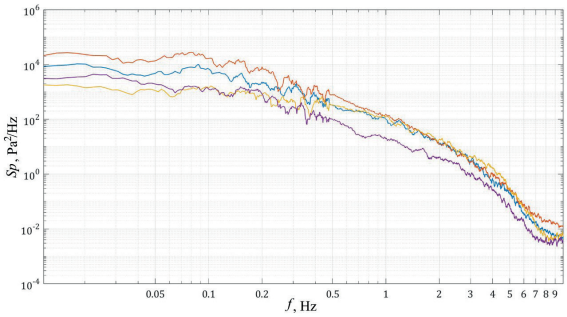


Figure 13. Pressure power spectral power density for 4 characteristic glazing elements, Pa^2 /Hz (130°)

Analysis of the peak integral wind loads show that the wind loads obtained through the transient simulations may differ significantly from the RANS approach.

Analysis of time series and spectra of wind loads shows significant fluctuations of wind loads in a wide frequency range. This corresponds to the physical nature of the phenomenon and can potentially lead to resonant vibrations of flexible structures.

Examples of velocity and pressure distributions in a horizontal section at a height of 15 m are shown in Figs. 14-15. Fig. 16 shows the pressure distributions over the façade surface.

(a) SST: $\overline{V}$

(b) SBES: $\overline{V}$

(c) SBES: σ_V

(d) SBES: $V(t_i)$

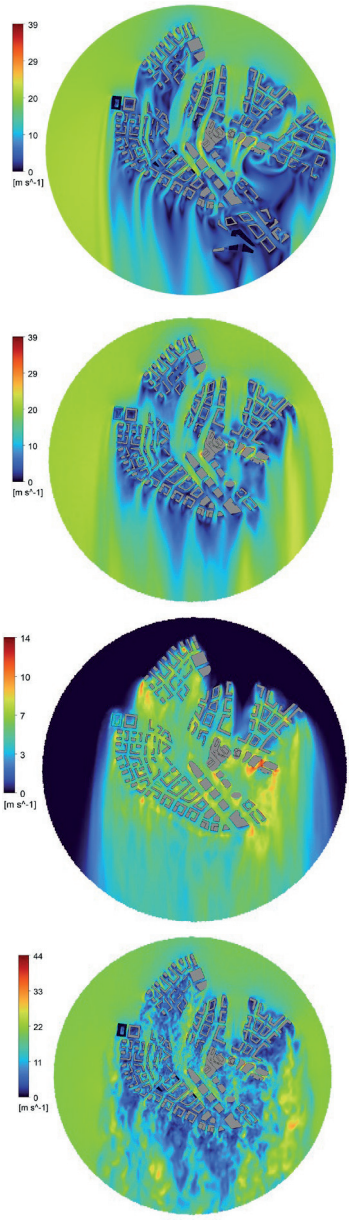


Figure 14. Instantaneous, mean and standard deviation values of velocity [m/s] in horizontal section, 130°

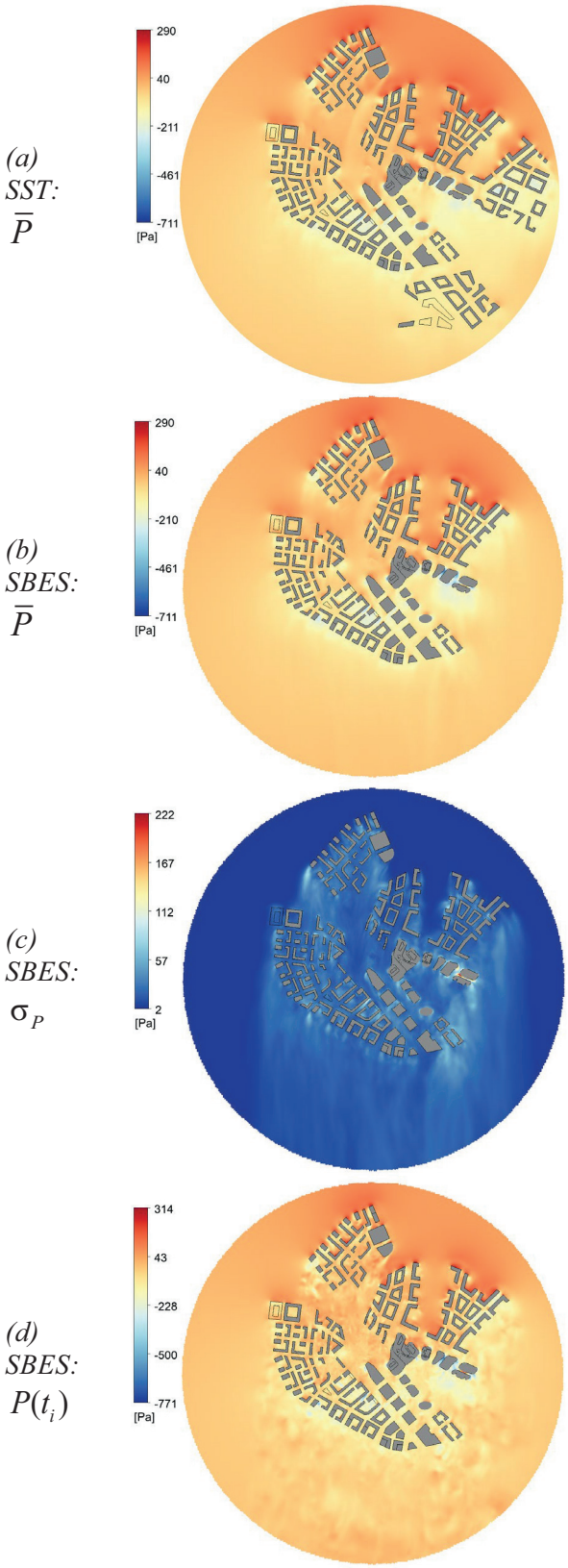


Figure 15. Instantaneous, mean and standard deviation values of pressure [Pa] in horizontal section, 130°

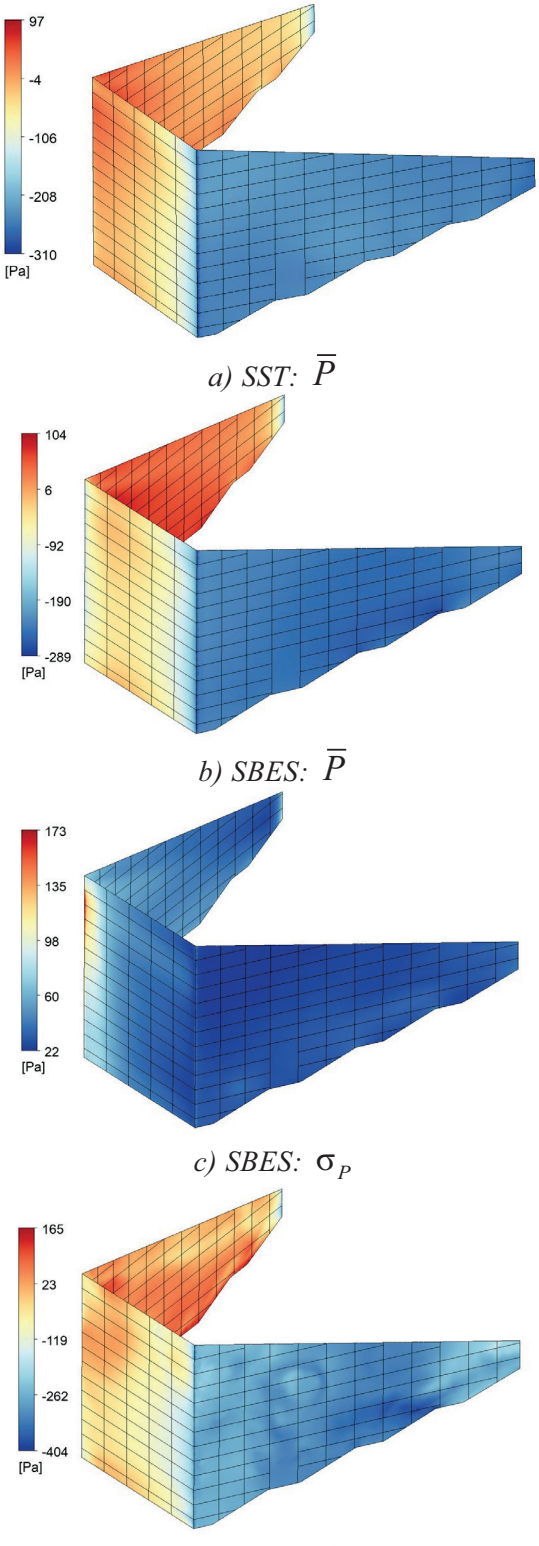
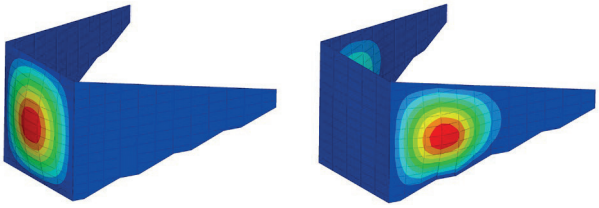


Figure 16. Instantaneous, mean and standard deviation values of pressure [Pa] on the façade surface, 130°

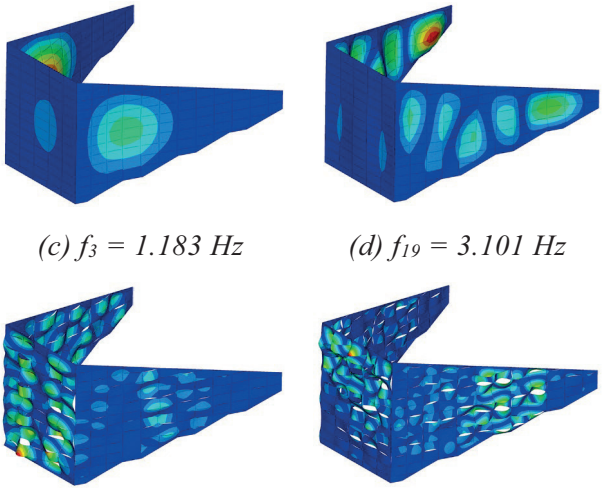
3.2 Modal analysis results

To determine the time step required for transient calculations, the modes and eigenfrequencies were initially analysed (Fig. 17).

Starting from 18 Hz, only the highest modes of individual glazing elements are observed, and it makes no practical sense to take them into account. Therefore, the timestep $\Delta t = 0.01$ s is chosen, which corresponds to ~6 steps for the smallest considered eigenfrequency (1/18.0 Hz = 0.056 s, 308th form)



(a) f_1 = 1.053 Hz *(b) f_2 = 1.178 Hz*



(c) f_3 = 1.183 Hz *(d) f_{19} = 3.101 Hz*

(d) f_{117} = 10.026 Hz *(e) f_{308} = 18.049 Hz*

Figure 17. Characteristic frequencies and modes

3.3 Stress-strain state results

Figs. 18-20 show the maximum values of the flexures of the glazing elements and cables and the forces in the cables over time. Figs. 21-23 show corresponding examples of time series.

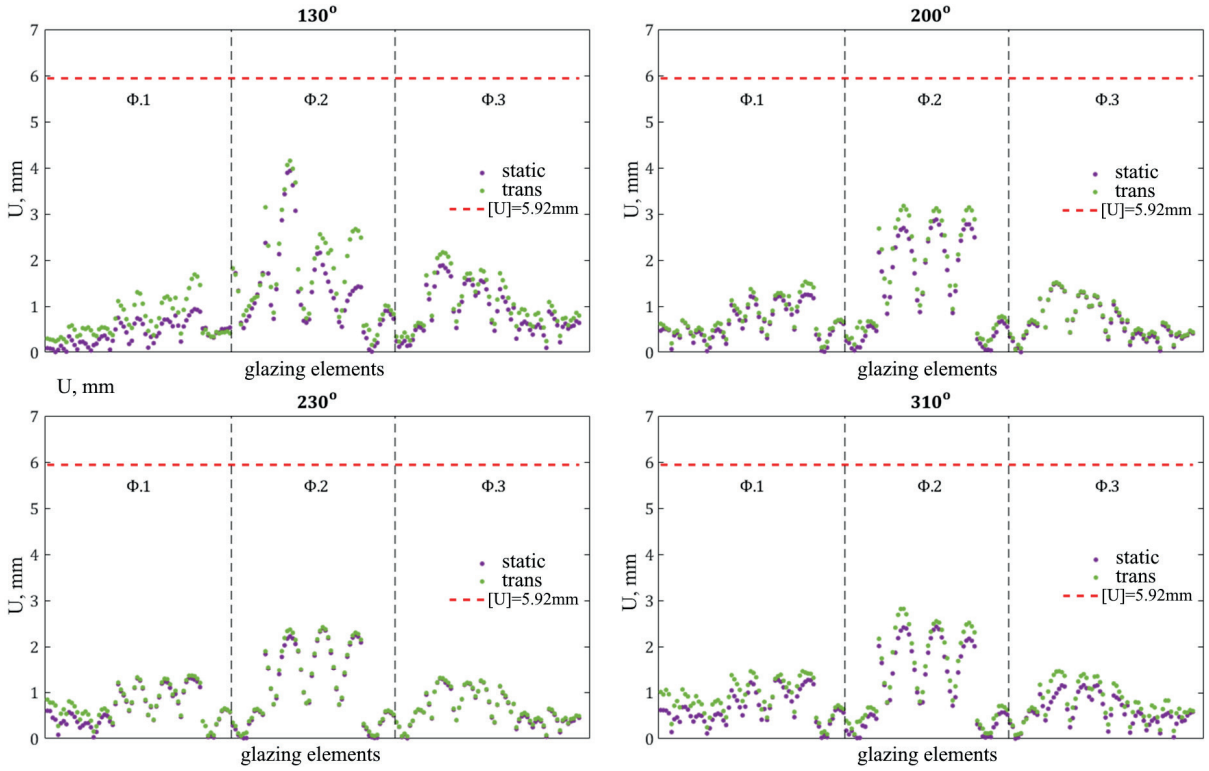


Figure 18. Flexures of glazing elements with limit value markings

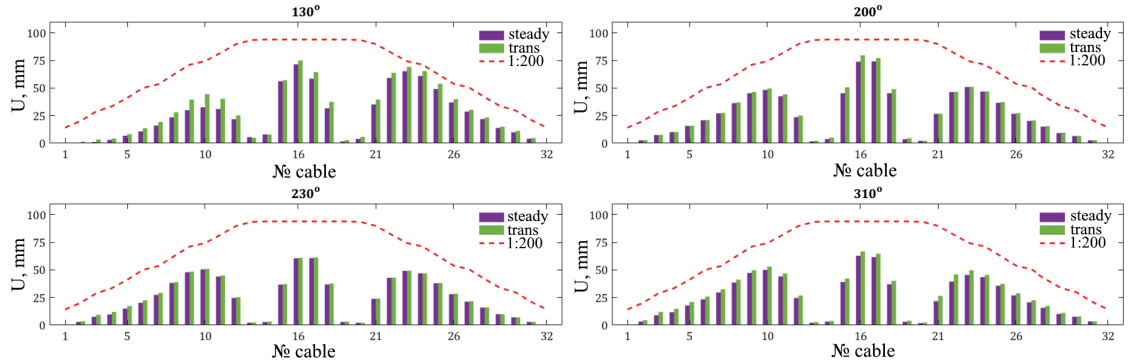


Figure 19. Maximum flexures of cables with limit value markings

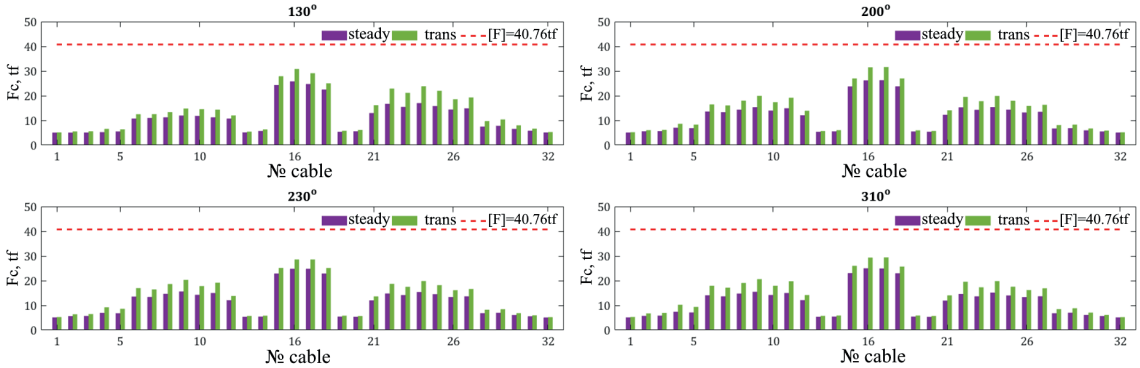


Figure 20. Maximum forces in cables with limit value markings

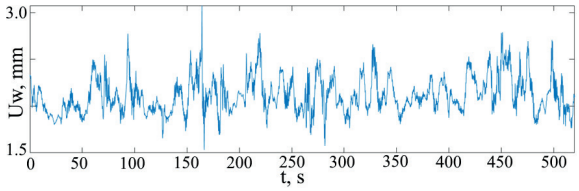


Figure 21. Flexures of a characteristic glazing element, mm (200°)

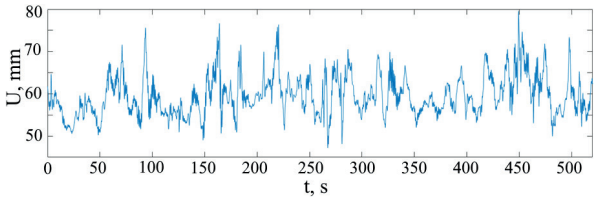


Figure 22. Flexures of a characteristic cable, mm (200°)

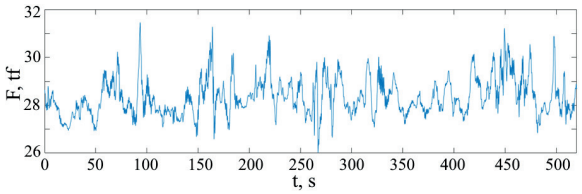


Figure 23. Forces in a characteristic cable, tf (200°)

Analysis of the results in Figs. 18-23 show that:

1. High-frequency resonance effects are periodically manifested under wind actions.
2. Presence of significant dynamic effects is revealed: flexures of glazing elements increased up to 2 times, flexures of cables to 40%, forces in cables to 40%.
3. The cable strength and façade stiffness do not exceed the criterion values even from the refined dynamic analysis.

3. CONCLUSIONS

The approach to the stress-strain state calculation of cable-stayed glass façades presented in this paper can be applied to any flexible structures.

It is shown that the application of nonlinear dynamic calculations allows to take into account the dynamic response to wind actions, which is the main one for flexible façade structures.

Numerical modelling of wind actions using LES turbulence model is a very costly approach and is often unavailable. Application of RANS models together with empirical methods (formulae 2-3) to determine hazardous wind directions and selective application of hybrid RANS-LES methods to determine design wind loads can reduce modelling time by orders of magnitude.

ACKNOWLEDGEMENTS

The research was funded by the National Research Moscow State University of Civil Engineering (grant for fundamental and applied scientific research, project No. 05-392/130).

REFERENCES

1. **Blocken B.** 50 years of computational wind engineering: past, present and future // J. Wind Eng. Wind Eng. Ind. Aerodyn., 2014, V. 129, pp. 69-102.
2. **Belostotsky A.M., Akimov P.A., Afanasyeva I.N..** Vychislitel'naya aerodinamika v zadachah stroitel'stva, Moscow: Izdatel'stvo ASV, 2017, 720 p. (in Russian).
3. **Cochran L., Derickson R.** A physical modeller's view of computational wind engineering // J. Wind Eng. Wind Eng. Ind. Aerodyn., 2011, V. 99, Issue 4, pp. 139-153.
4. **Meroney R.N., Derickson R.** Virtual reality in wind engineering: the windy world within the computer // J. Wind Eng. Wind Eng., 2014, V. 11, pp. 11-26.
5. **Thordal, M.S., Bennetsen, J.C., Capra, S., Koss, H.H.H..** Towards a standard CFD setup for wind load assessment of high-rise buildings: Part 1 - Benchmark of the CAARC building // Journal of Wind Engineering and Industrial Aerodynamics, 2020, V. 205, P. 104283.
6. **Bruno L. et al.** Codes and standards on computational wind engineering for structural design: State of art and recent trends // Wind and Structures, 2023, V., No. 2, pp. 37, No. 2, pp. 133-151.
7. CNR DT 207 R1/2018 Istruzioni per la valutazione delle azioni e degli effetti del vento sulle costruzioni, 2019. (in Italian)
8. ASCE/SEI 7-22 Minimum Design Loads and Associated Criteria for Building and other Structures, 2022.
9. Matematicheskoe (chislennoe)" modelirovanie vetrovyh nagruzok i vozdejstvii. Metodicheskoe posobie. Moscow: FAU "FCS", 2020, 61 p.
10. STO 02066523-089-1-2024 Numerical modelling of wind and snow actions, 2024
11. **Feng R.-q., Zhang L.-l., Wu Y., Shen S.-z.** Dynamic performance of cable net facades // Journal of Constructional Steel Research, 2009, V. 65, № 12. pp. 2217-2227.
12. **Feng R.-q., Ye J.-h., Wu Y., Shen S.-z.** Nonlinear response spectra of cable net facades // Soil Dynamics and Earthquake Engineering, 2012, V. 32, pp. 71-86.
13. **Feng R.-q., Ye J.-h., Wu Y., Shen S.-z.** Mechanical Behaviour of Glass Panels Supported by Clamping Joints in Cable Net Facades // Journal of Constructional Steel Research, 2012, V. 12, № 1. pp. 15-24.
14. **Amadio C., Bedon C.** Elastoplastic dissipative devices for the mitigation of blast resisting cable-supported glazing façades // Engineering Structures, 2012, V. 39, pp. 103-115.
15. **Bedon C., Amadio C**. Exploratory numerical analysis of two-way straight cable-net façades subjected to air blast loads // Engineering Structures, 2014, V. 79, pp. 276-289
16. **Yussof, M.M.** Cable-net supported glass façade systems. A thesis submitted in partial fulfilment for the degree of Doctor of Philosophy. United Kingdom, University of Surrey, 2015. P. 249
17. **Wang Y. et al.** Experimental and numerical studies on the static and the

dynamic behaviours of embedded cable support (ECS) glass facade system // Engineering Structures, 2019 V. 178, pp. 521-533.
18. **Xiang Y. et al.** Effect of the primary structure on the seismic response of the cable-net façade // Engineering Structures, 2020, V. 220, pp. 110989.
19. **Rizzo F., Bedon C.** Performance of cable-supported glass façades under time-depending wind action // Glass Structures & Engineering, 2023, V. 8, No. 1, pp. 81-98.
20. **Zhou Q. et al.** Frequency calculation method and wind-induced dynamic response of cable net façades considering the façade stiffness // Structures, 2023, V., V. 55, pp. 718-726.
21. **Menter F.R.** Review of the shear-stress transport turbulence model experience from an industrial perspective // J. Wind Eng. Wind Eng. Ind. Aerodyn., 2009, V. 23, pp. 305-316.
22. **Menter F., Hüppe A., Matyushenko A., Kolmogorov D**. An overview of hybrid RANS-LES models developed for industrial CFD // Appl. Sci., 2021, V. 11, p. 2459, 2021.
23. **Nicoud F., Ducros F.** Subgrid-scale stress modelling based on the square of the velocity gradient tensor // Flow, Turbulence and Combustion, 1999, V., No. 62, no. 62, №. 3, pp. 183-200.
24. **Menter F.R.** Best Practice: Scale-Resolving Simulations in ANSYS CFD. Version 2.00. Technical paper. ANSYS, 2015, 47 p.
25. **Goryachevsky O.S.** Numerical modelling of wind loads on windows // International Journal for Computational Civil and Structural Engineering, 2023, V. 19, No. 3, pp. 19, No. 3, pp. 114-129

СПИСОК ЛИТЕРАТУРЫ

1. **Blocken B.** 50 years of computational wind engineering: past, present and future // J. Wind Eng. Ind. Aerodyn., 2014, V. 129, pp. 69-102.
2. **Белостоцкий А.М., Акимов П.А., Афанасьева И.Н.** Вычислительная аэродинамика в задачах строительства, М.: Издательство АСВ, 2017, 720 с.
3. **Cochran L., Derickson R**. A physical modeler's view of computational wind engineering // J. Wind Eng. Ind. Aerodyn., 2011, V. 99, Issue 4, pp. 139-153.
4. **Meroney R.N., Derickson R**. Virtual reality in wind engineering: the windy world within the computer // J. Wind Eng., 2014, V. 11, pp. 11-26.
5. **Thordal, M.S., Bennetsen, J.C., Capra, S., Koss, H.H.H.** Towards a standard CFD setup for wind load assessment of high-rise buildings: Part 1 – Benchmark of the CAARC building // Journal of Wind Engineering and Industrial Aerodynamics, 2020, V. 205, P. 104283.
6. **Bruno L. et al.** Codes and standards on computational wind engineering for structural design: State of art and recent trends // Wind and Structures, 2023, V. 37, № 2, pp. 133-151.
7. CNR DT 207 R1/2018 Istruzioni per la valutazione delle azioni e degli effetti del vento sulle costruzioni, 2019. (in Italian)
8. ASCE/SEI 7-22 Minimum Design Loads and Associated Criteria for Building and other Structures, 2022.
9. Математическое (численное)" моделирование ветровых нагрузок и воздействий. Методическое пособие, М.: ФАУ «ФЦС», 2020, 61 с.
10. СТО 02066523-089-1-2024 Численное моделирование ветровых и снеговых воздействий, НИУ МГСУ, НИЦ СтаДиО, 2024
11. **Feng R.-q., Zhang L.-l., Wu Y., Shen S.-z.** Dynamic performance of cable net facades // Journal of Constructional Steel Research, 2009, V. 65, № 12. pp. 2217-2227.
12. **Feng R.-q., Ye J.-h., Wu Y., Shen S.-z**. Nonlinear response spectra of cable net

facades // Soil Dynamics and Earthquake Engineering, 2012, V. 32, pp. 71-86.
13. **Feng R.-q., Ye J.-h., Wu Y., Shen S.-z.** Mechanical Behavior of Glass Panels Supported by Clamping Joints in Cable Net Facades // Journal of Constructional Steel Research, 2012, V. 12, № 1. pp. 15-24.
14. **Amadio C., Bedon C.** Elastoplastic dissipative devices for the mitigation of blast resisting cable-supported glazing façades // Engineering Structures, 2012, V. 39, pp. 103-115.
15. **Bedon C., Amadio C.** Exploratory numerical analysis of two-way straight cable-net façades subjected to air blast loads // Engineering Structures, 2014, V. 79, pp. 276–289
16. **Yussof, M.M.** Cable-net supported glass façade systems. A thesis submitted in partial fulfilment for the degree of Doctor of Philosophy. United Kingdom, University of Surrey, 2015. P. 249
17. **Wang Y. et al.** Experimental and numerical studies on the static and the dynamic behaviors of embedded cable support (ECS) glass facade system // Engineering Structures, 2019 V. 178, pp. 521-533.
18. **Xiang Y. et al.** Effect of the primary structure on the seismic response of the cable-net façade // Engineering Structures, 2020, V. 220, pp. 110989.
19. **Rizzo F., Bedon C**. Performance of cable-supported glass façades under time-depending wind action // Glass Structures & Engineering, 2023, V. 8, № 1, pp. 81-98.
20. **Zhou Q. et al.** Frequency calculation method and wind-induced dynamic response of cable net façades considering the façade stiffness // Structures, 2023, V. 55, pp. 718-726.
21. **Menter F.R.** Review of the shear-stress transport turbulence model experience from an industrial perspective // J. Wind Eng. Ind. Aerodyn., 2009, V. 23, pp. 305-316.
22. **Menter F., Hüppe A., Matyushenko A., Kolmogorov D.** An overview of hybrid RANS–LES models developed for industrial CFD // Appl. Sci., 2021, V. 11, p. 2459, 2021.
23. **Nicoud F., Ducros F.** Subgrid-scale stress modelling based on the square of the velocity gradient tensor // Flow, turbulence and Combustion, 1999, V. 62, №. 3, pp. 183-200.
24. **Menter F.R.** Best Practice: Scale-Resolving Simulations in ANSYS CFD. Version 2.00. Technical paper. ANSYS, 2015, 47 p.
25. **Горячевский О.С.** Численное моделирование ветровых давлений на окна. Валидация для типового многоэтажного здания квадратной формы // International Journal for Computational Civil and Structural Engineering, 2023, Т. 19, № 3, с. 114-129

Oleg Sergeevich Goryachevsky – Deputy Director at A.B. Zolotov REC CM of the National Research Moscow State University of Civil Engineering; 129337, Russia, Moscow, Yaroslavskoe shosse, 26.
E-mail: osgoryachevskij@mail.ru

Олег Сергеевич Горячевский – заместитель директора НОЦ КМ им. А.Б. Золотова Национального исследовательского Московского государственного строительного университета; 129337, Россия, г. Москва, Ярославское шоссе, д. 26.
E-mail: osgoryachevskij@mail.ru

Alexander Mikhailovich Belostotsky – DSc, Professor, Full Member of the Russian Academy of Architecture and Construction Sciences. Scientific adviser at A.B. Zolotov REC CM of the National Research Moscow State University of Civil Engineering; 129337, Russia, Moscow, Yaroslavskoe shosse, 26.
E-mail: amb@stadyo.ru

Александр Михайлович Белостоцкий – Научный руководитель НОЦ КМ им. А.Б. Золотова Национального исследовательского Московского государственного строительного университета; 129337, Россия, г. Москва, Ярославское шоссе, д. 26.
E-mail: amb@stadyo.ru

International Journal for Computational Civil and Structural Engineering, 20(3) 69–83 (2024)

DOI:10.22337/2587-9618-2024-20-3-69-83

AN INNOVATIVE HYBRID MACHINE LEARNING TECHNIQUES FOR PREDICTING CONSTRUCTION COST ESTIMATES

Kittisak Lathong, Kittipol Wisaeng

Mahasarakham Business School, Mahasarakham University, Mahasarakham, THAILAND

Abstract: The importance of precise cost estimations in construction investment sector cannot be overstated, serving as the cornerstone for crucial investment decisions. Unfortunately, inaccurate estimations often lead to significant losses due to flawed investment objectives. Consequently, the pursuit of an effective investment decision support system has become a paramount research focus, aiming to aid construction investors in making informed and timely choices. This study focuses on a novel hybrid machine learning (HML) approach, amalgamating various base models such as artificial neural networks (ANNs), support vector machines (SVMs), multiple linear regression (MLR), decision trees (DTs) and random forest (RF) to construct a sophisticated construction cost forecasting model. Remarkably, empirical findings demonstrate the exceptional accuracy of the hybrid ANN-DT model, reaching an impressive 92.1% and surpassing individual models. This breakthrough holds the promise of substantial advantages and increased profitability within the construction industry, particularly benefitting professionals in civil engineering, architecture, and construction investing. By combining the predictive strength of ANNs with the transparent decision rules of DTs, this hybrid model effectively addresses the industry's need for precise predictions and understandable forecasting methodologies, representing a significant advancement in enhancing informed decision-making processes within the construction domain.

Keywords: construction cost estimation, machine learning, hybrid learning model, residential buildings

ИННОВАЦИОННЫЕ ГИБРИДНЫЕ МЕТОДЫ МАШИННОГО ОБУЧЕНИЯ ДЛЯ ПРОГНОЗИРОВАНИЯ СТОИМОСТИ СТРОИТЕЛЬСТВА

К. Латонг, К. Висенг

Бизнес-школа Махасаракхам, Университет Махасаракхам, Махасаракхам, ТАИЛАНД

Аннотация: Сложно переоценить важность точной оценки затрат в сфере инвестиций в строительстве, поскольку это служит краеугольным камнем для принятия важнейших инвестиционных решений. К сожалению, неточные оценки часто приводят к значительным убыткам из-за неверных инвестиционных целей. Поэтому создание эффективной системы поддержки принятия инвестиционных решений стало первостепенным направлением исследований, призванных помочь инвесторам в строительство сделать обоснованный и своевременный выбор. Данное исследование посвящено новому гибридному подходу машинного обучения (HML), объединяющему различные базовые модели, такие как искусственные нейронные сети (ANN), машины векторов поддержки (SVM), множественная линейная регрессия (MLR), деревья решений (DT) и случайный лес (RF), для построения сложной модели прогнозирования стоимости строительства. Примечательно, что эмпирические результаты демонстрируют исключительную точность гибридной модели ANN-DT, достигающую впечатляющих 92,1% и превосходящую отдельные модели. Это обещает существенные преимущества и повышение рентабельности в строительной отрасли, что будет полезным для специалистов в области гражданского строительства, архитектуры и инвестирования в строительство. Сочетая предсказательную силу ANN с прозрачными правилами принятия решений DT, эта гибридная модель эффективно удовлетворяет потребности отрасли в точных прогнозах и понятных методологиях прогнозирования, представляя собой значительное достижение в улучшении процессов принятия обоснованных решений в строительной сфере.

Ключевые слова: оценка стоимости строительства, машинное обучение, гибридная модель обучения, жилые здания

1. INTRODUCTION

Precisely estimating the construction cost of residential buildings through machine learning harnesses the real estate landscape of Thailand. The importance of residential living or housing structures within the flat-building paradigm is crucial to human life, representing a fundamental aspect of human shelter. The burgeoning real estate sector in Thailand has seen a significant surge in construction, notably following the COVID-19 situation that impacted the country and the globe, resulting in economic slowdowns. However, the current market dynamics present challenges in accurately appraising property values. In this context, the assessment process of property valuation is transitioning from traditional methodologies to predictive machine learning techniques.

The cost estimation method [1] serves as a fundamental cornerstone in engineering endeavors associated with entire projects. It exerts significant influence across various aspects, encompassing planning, project feasibility studies, bidding, design, construction management, and cost control. The outcomes of such estimations play a crucial role in assisting project planners and stakeholders in evaluating project feasibility and efficiently managing costs within the intricate scope of detailed project design. Given the inherent scarcity of data available for comprehensive project coverage in the initial phases, construction managers rely extensively on their experience to conduct these estimations. This practice greatly facilitates accurate project cost estimation, offering enhanced convenience in project cost evaluations [2]. Comprehensive cost estimation entails complex assessments involving materials, overhead costs, labor quantities, space, public utilities, sales considerations, temporary parameters, and arrays of associated costs all encapsulated within the project's structural framework and timeline.

Preliminary or rough construction cost estimation entails an initial approximation of project expenses, even as the finer details of the components remain incompletely delineated. The accuracy of this preliminary estimate is reliant upon the estimator's expertise and may incorporate pertinent data extrapolated from analogous completed undertakings. This estimation process commonly manifests a range of variability, typically spanning between 10% and 30% [3], [4], as depicted in Fig. 1. However, Kawee Wangnivejankul [4] posits that this variability may potentially extend up to 50%, thereby introducing an elevated level of risk into the construction undertaking. Consequently, prudent consideration should be accorded to potentially circumventing the preliminary estimation process when feasible, given its propensity to exert a significant influence on the inherent risk profile associated with the construction endeavor. The process of detailed construction cost estimation becomes tenable when equipped with a comprehensive and exhaustive design schema. This entails an intricate dissection of construction materials into quantifiable units, subsequently affording the quantification of costs spanning materials, labor, machinery, operations, profit margins, tax implications, and financial interests, among other factors.

Empirical cost models rely on statistical analysis and historical data curve-fitting, predominantly using capacity as the primary variable. Concurrently, cost estimation by area or volume entails computing project expenses based on the dimensions of a structure or material, encompassing surface area (in square footage) or volume (in cubic meters) considerations. Area-based estimation involves multiplying the cost per unit area by the total area, while volume-based estimation multiplies the cost per unit volume by the total required volume. These widely employed methods in construction facilitate precise budgeting and planning for various development projects, particularly for materials like concrete, paint, and roofing. Parametric models leverage multiple variables, often employing empirical or hybrid empirical/factored approaches, providing tailored specificity for different applications compared to typical parametric or factored cost

models. Factored cost models, commonly utilized in water treatment and oil and gas sectors, rely on capital cost estimates for major equipment and incorporate factors for the remaining capital costs, usually requiring design development and vendor quotations. Material take-off, employed post-significant design activity, involves tallying components and furnishing material schedules, along with cost quotations for each line item. While highly accurate, this method necessitates a well-developed design [5]. Empirical and parametric models are predominantly favored in the early stages of development, with the Association for the Advancement of Cost Engineering (AACE) [6] offering guidelines on estimate accuracy at various project stages. Figure 1 outlines estimate uncertainty and the typical level of design detail provided.

The utilization of advanced machine learning and regression techniques enhances the capability to predict property values of flat-building structures, depending on influential factors within diverse market domains. This study explores innovative decision tree algorithm models, which are unsupervised learning paradigms that function without stringent parameter dependence. These algorithms serve for both classification and regression analysis, synthesizing the core principles of decision-making algorithms [7] derived from the inherent nature of data. The overarching objective is to construct an efficient model capable of expertly predicting target variable values. Machine learning (ML) has found widespread applications across various industrial and business sectors. ML technology has undergone extensive development, expanding predictive capabilities in diverse applications. The intriguing study illustrates the efficacy of ML methods in forecasting or classifying various factors, such as interest rates and real estate prices within specified contexts. Construction cost estimation stands as a pivotal issue under scrutiny, featuring a comprehensive and intricately detailed examination of ML capabilities. Furthermore, construction cost projections pose nonlinear challenges influenced by various construction years and features, both direct and indirect.

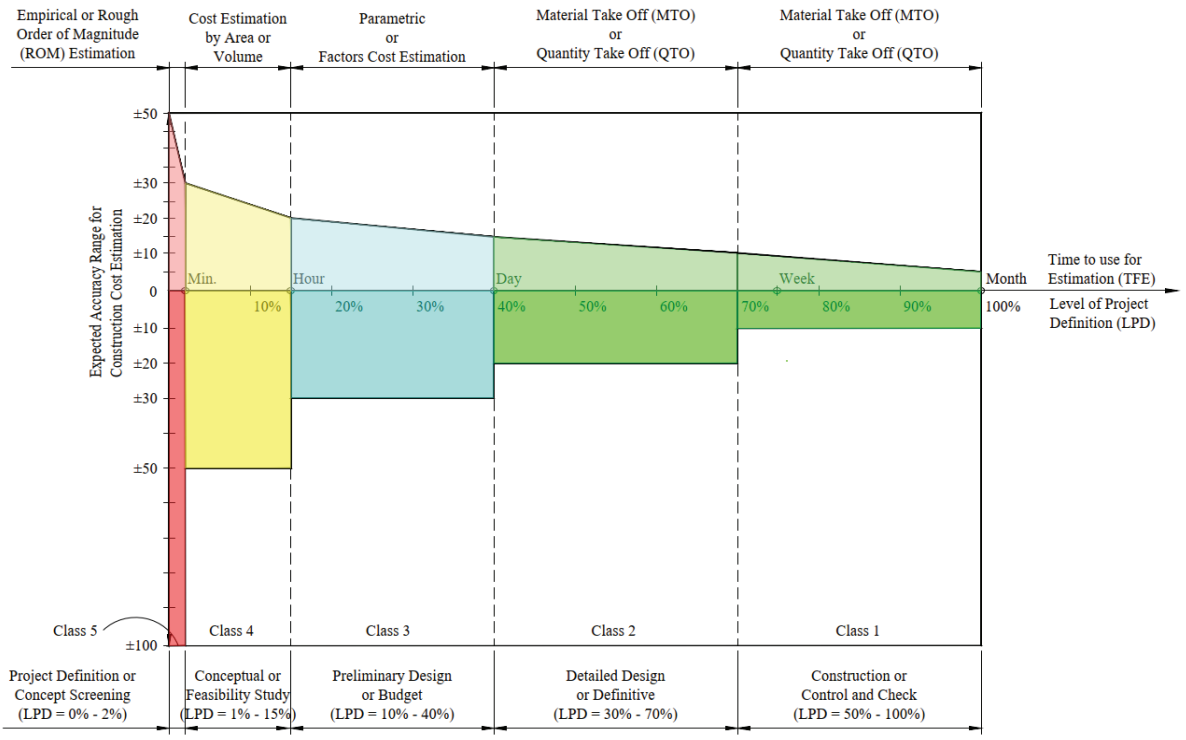


Figure 1. The relationship between construction cost estimate accuracy, the time allocated for estimation, and the project's developmental stage

Machine learning (ML) is a subset of artificial intelligence (AI) that collaborates with algorithms and technologies to extract valuable insights from data. ML is suitable for calculations associated with data because it cannot process data efficiently and independently without ML. Hence, the reliance on algorithms enabling ML to be a predictive algorithm capable of quantitatively processing data for predictions, as stated by Xu et al. [8]. ML has significantly transformed various industries and emerged as a powerful tool in the construction sector, automating processes. ML technology is crucial for processing vast amounts of data, saving time, and enhancing processing resource efficiency. Moreover, it may be particularly suitable for the construction industry in predicting financial costs and time, achieving optimal efficiency [9].

Within the realm of construction cost estimation, Tayefeh Hashemi et al. [10] conducted an in-depth analysis of research papers over a span of 30 years, from 1985 to 2020. These papers aimed to apply ML techniques for cost estimation in construction projects. The overarching goal of these studies was to develop predictive models capable of accurately estimating costs, especially before bidding, facilitating informed decision-making by project managers based on project data. Notably, widely used ML techniques have been employed in reviewed literature, including Artificial Neural Networks (ANN), Regression Analysis (RA), Case-Based Reasoning (CBR), and Support Vector Machines (SVM). This analysis aligns with the findings of Elfaki et al. [11] in their survey of construction cost estimation over the past decade, emphasizing the enduring prominence of classic ML techniques, particularly ANN and SVM, within the field.

The several research studies have illuminated the complexity and significance inherent in predicting real estate prices, acknowledging the diverse factors that wield influence within the housing market. Sifei Lu et al. [12] underscored the necessity for refined methodologies extending beyond the conventional House Price Index. Their emphasis lay in accurately predicting individual house prices, considering a spectrum of factors like location, house type, size, construction year, and local amenities. They proposed a hybrid Lasso and Gradient Boosting regression model, showcased by its exceptional performance in the Kaggle Challenge "House Prices: Advanced Regression Techniques," ranking among the top 1% among all participants, signifying promising predictive capabilities.

Sruthi Chiramel et al. [13] recognized the challenges faced by homebuyers due to inflation and escalating housing prices. Their study aimed to predict house prices in Iowa, USA, utilizing regression analysis and various explanatory variables. It detailed the effectiveness of models like Linear Regression and Ridge Regularization, emphasizing their significance in employing machine learning techniques for addressing house price prediction challenges.

On a different note, Gergo Pinter et al. [14] introduced a pioneering machine learning approach that employed Call Detail Records (CDR) to investigate how mobility characteristics influence real estate price prediction. Utilizing AI and fundamental mobility entropy factors linked to dwellers' and workers' attributes, their model, employing a multi-layered perceptron (MLP) with particle swarm optimization (PSO), revealed substantial correlations between mobility factors and real estate prices. Similarly, Choujun Zhan et al. [15] highlighted the crucial role of accurate house price prediction models in shaping national real estate policies. Their research introduced a framework leveraging Hybrid Bayesian Optimization (HBO) models, including Stacking (HBOS), Bagging (HBOB), and Transformer (HBOT), aiming to enhance forecasting performance through hyperparameter tuning. A comparative analysis against benchmark models underscored the superior predictive performance of HBOS models, supported by a comprehensive multi-

source dataset encompassing Hong Kong real estate transactions from 1996 to 2021.

Despite the notable predictive capabilities of classical models utilized in previous research, attempts to enhance their efficiency have fallen short. In contrast, ML models have demonstrated varying degrees of effectiveness, particularly in real estate valuation and prediction within the residential domain, relying predominantly on readily available ML methodologies. However, existing literature has primarily focused on evaluating value and forecasting real estate using foundational ML techniques, overlooking the significance of integrating hybrid machine learning models derived from general-purpose models to streamline and elevate work practices. Presently, predictive models using ML for construction cost estimation in Thailand are gaining attention, albeit predominantly relying on widely used basic learning techniques. The implementation of hybrid learning methods lacks comprehensive comparative demonstrations, a crucial aspect within the learning domain. This knowledge gap necessitates the refinement of ML models for precise real estate price forecasting. Current studies endeavor to bridge these gaps comprehensively and address these challenges.

The aforementioned issues arise when business owners, project managers, or homeowners seek precise and detailed construction cost estimations, which consume considerable time and often require the involvement of engineers, architects, or estimators. Developing predictive models for flat-house construction cost estimation using cutting-edge ML techniques proves beneficial. This AI technique facilitates automated computer learning, enabling direct cost predictions from household area data, reducing the necessity for human intervention in the design process. Simultaneously, it maintains cost estimates closely aligned with traditional estimation methods

This research aims to achieve the objective of proposing innovative directions for low-rise building construction cost estimation using hybrid machine mearning (HML) techniques. The study endeavors to comprehensively compare the performance among various HML. Upon attaining these objectives, the study intends to present valuable insights into residential price estimations, aiming to enhance the accuracy and efficiency of real estate forecasts within the housing market ultimately. These advancements provide invaluable insights and tools for scholars, practitioners, engineers, architects, and investors aiming to gain a deeper comprehension of housing market dynamics. This deeper understanding enables more accurate predictions of market trends.

The remaining sections of this paper adhere to a structured framework. Section 2 provides an overview of the dataset and hybrid machine learning methodologies. Section 3 presents the empirical findings, culminating in Section 4, the conclusion.

2. METHODS

In this section, the dataset description for house price forecasting is defined. Following this, a data pre-processing method is proposed for house price prediction utilizing individual machine learning models and hybrid machine learning techniques. Within this framework, the analysis focuses on assessing the performance enhancement of 10 hybrid models for house price forecasting, evaluated using 8 measures to gauge predictive accuracy.

2.1. Dataset

The proposed model was applied using a dataset obtained from the Bureau of Public Works in Bangkok, focusing on low-rise housing and their corresponding prices. This dataset includes 15 key features defining different aspects of the low-rise buildings: construction cost (y), number of stories (x1), total usable area covering all floors (x2), area dedicated to bedrooms (x3), allocated bathroom area (x4), space for living rooms or restrooms (x5), kitchen and dining area (x6), laundry facilities

area (x7), balcony area (x8), space for stairs and corridors (x9), areas covered by roofing (x10, x11), parking area (x12), overall building height (x13), roof height (x14), and average floor height (x15). These features collectively describe various physical and functional attributes of the low-rise structures, forming the basis for the predictive model's analysis.

2.2. Data analysis

In this study, we conducted a comparative analysis of various HML algorithms like ANN, SVM, MLR, DT, and RF to predict construction costs for low-rise building projects. The aim was to identify the most precise and dependable method for estimating construction expenses. The dataset used in this analysis includes information on low-rise housing and their corresponding prices obtained from the Bureau of Public Works in Bangkok. It comprises 120 samples and encompasses 15 distinct attributes. Statistical measures of the dataset, including minimum, mean, maximum, and standard deviation, are visually represented in Figure 2.

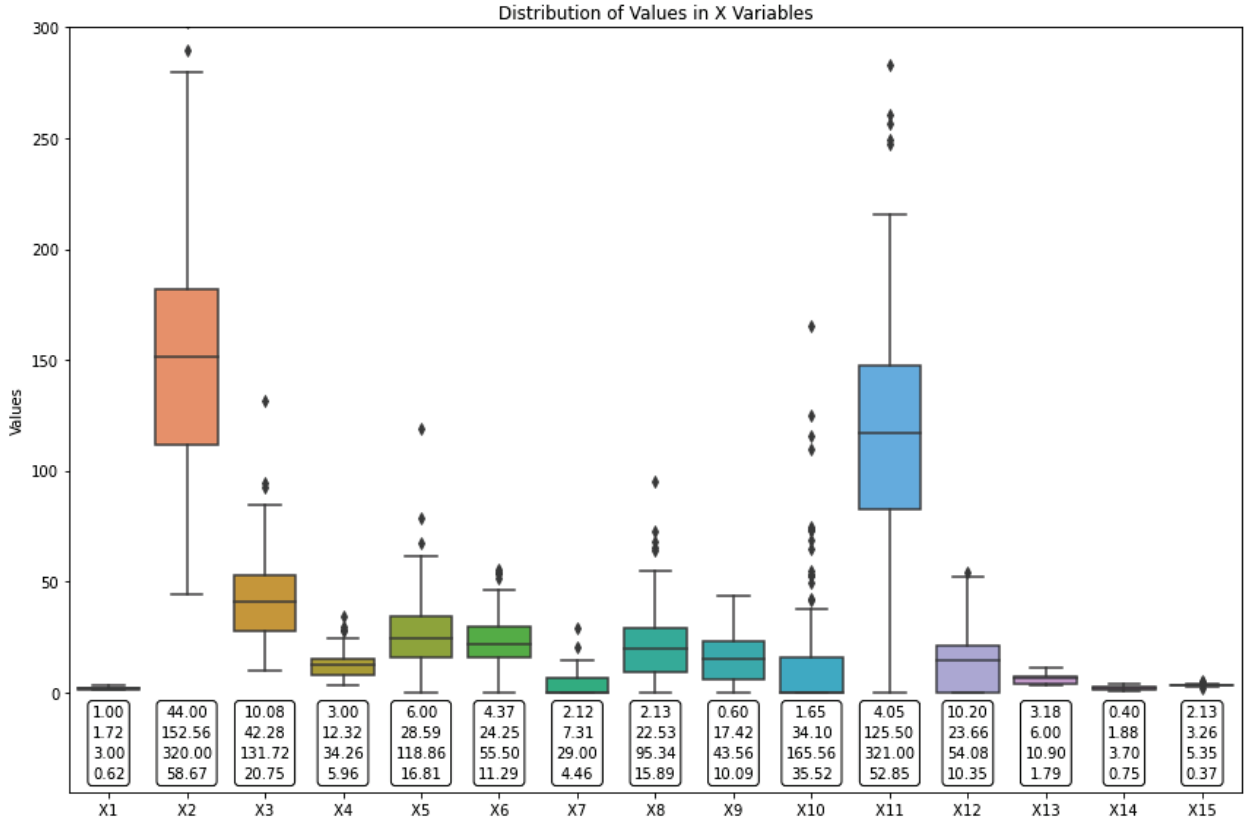


Figure 2. Visualization of the dataset

2.3. Data pre-processing

The meticulous data preprocessing steps involved managing missing data and precise segmentation into training and testing sets. The initial focus in predicting low-rise building prices was on selecting high-quality datasets sourced meticulously from reliable sources. These datasets encompass features like room area, building height, and amenities, all influential in determining the prices of low-rise buildings. Ultimately, the dataset was split into training, validation, and testing sets, facilitating model evaluation, training, hyperparameter fine-tuning, and accurate performance assessment.

2.4. Machine learning techniques base model

ML algorithms excel in modeling intricate and ambiguous systems, even when nonlinear relationships are unknown. In this study, five distinguished ML algorithms, namely ANNs,

SVMs, MLR, DT, and RF, are employed to create the proposed models. Leveraging these diverse algorithms enhances the predictive power of the approach. Additionally, detailed explanations of the design parameters for each algorithm are provided. The workflow process of the fundamental base ML is depicted in Figure 3.

Artificial Neural Networks (ANN) are a class of machine learning algorithms inspired by the human brain's neural structure. Comprising interconnected nodes (neurons) arranged in layers, ANNs are capable of learning complex patterns and relationships in data. They operate by receiving input data, processing it through these interconnected layers, and producing an output [14, 16].

Support Vector Machines (SVM) are supervised learning models used for classification and regression tasks. SVMs classify data by finding the optimal hyperplane that best separates different classes in a dataset [17]. They work well in both linearly and non-linearly separable datasets by transforming input data into higher dimensions to find an optimal boundary.

Multiple Linear Regression (MLR) is a statistical method used for modeling the relationship between a dependent variable and multiple independent variables [18]. It extends simple linear regression by accommodating more than one predictor variable, predicting a continuous output by estimating the coefficients of each predictor variable.

Decision Trees (DT) are tree-like structures used for both classification and regression tasks. They make decisions by splitting the dataset based on feature values, creating a tree structure of if-else decision nodes that lead to leaf nodes providing predictions [19].

Random Forest (RF) is an ensemble learning technique based on the concept of constructing multiple decision trees. It builds multiple trees and merges their predictions to improve accuracy and prevent overfitting by aggregating the predictions from various trees. Random forests are versatile and suitable for classification and regression problems [20].

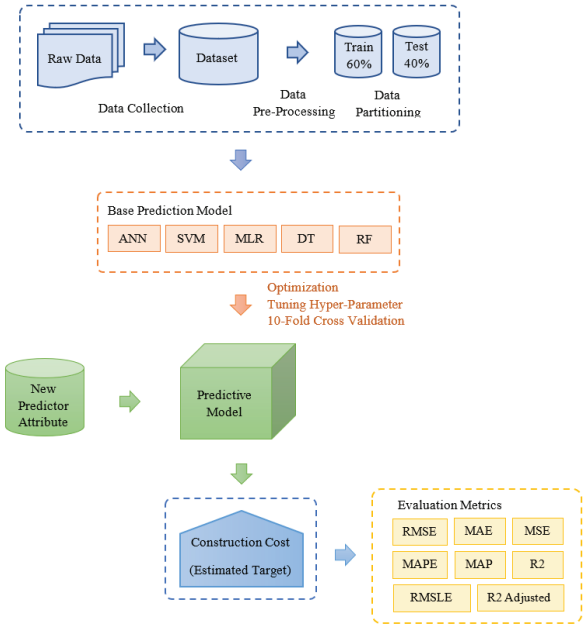


Figure 3. The classic base ML work flow

2.5. Hybrid machine learning model

Hybrid machine learning (HML) represents an innovative technique in machine learning where multiple models are amalgamated to enhance predictive accuracy, robustness, and generalization compared to employing a single model. Each hybrid method incorporates a distinct strategy to combine predictions from individual base models, employing various techniques. The workflow of HML is illustrated in Figure 4.

In the realm of predictive modeling, the quest for accuracy and robustness drives innovation. Recent advancements have shown that combining distinct machine learning algorithms into a hybrid model can significantly improve predictive performance. This study delves into the synthesis of hybrid models, each integrating two distinguished algorithms - an approach that has exhibited promising results in enhancing predictive power across various domains. Utilize a diverse set of ten hybrid models, including combinations like ANN-SVM, ANN-MLR, ANN-DT, ANN-RF, SVM-MLR, SVM-DT, SVM-RF, MLR-DT, MLR-RF, and DT-RF.

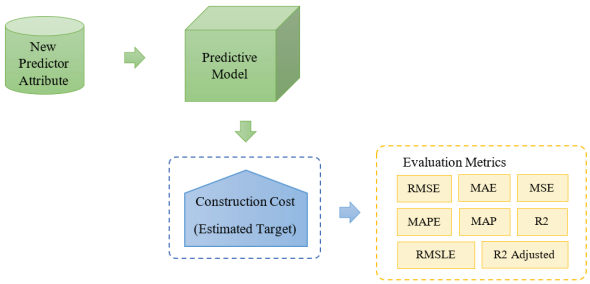


Figure 4. The HML work flow

ANN-SVM, the fusion of ANN and SVM aims to leverage the strength of both models. ANN, known for its ability to learn complex relationships in data, is combined with SVM, revered for its robustness in handling non-linear data. By merging ANN's capacity to comprehend intricate patterns with SVM's proficiency in handling high-dimensional datasets, the hybrid model offers a formidable approach to prediction tasks, effectively capturing nuanced relationships while maintaining resilience against overfitting.

ANN-RF, the hybridization of RF with ANN capitalizes on the strengths of both models. RF, a robust ensemble technique, brings its prowess in handling high-dimensional data and mitigating overfitting. By combining it with ANN's proficiency in learning complex relationships, this hybrid model endeavors to achieve improved generalization and predictive accuracy. The integration aims to refine predictions by mitigating biases from individual models, thus enhancing overall predictive performance.

ANN-DT, the fusion of ANN and DT seeks to leverage ANN's capacity for learning complex relationships and DT's interpretability and handling of non-linearities. By combining ANN's deep learning capabilities with DT's tree-based structure, this hybrid approach aims to capture intricate patterns while ensuring transparency and ease of interpretation in the decision-making process.

ANN-MLR, the amalgamation of ANN with MLR attempts to amalgamate ANN's ability to capture complex data patterns with MLR's simplicity in handling linear relationships. This union endeavors to exploit ANN's proficiency in learning intricate features while augmenting it with the interpretability and clarity of linear relationships provided by MLR, creating a balanced predictive model.

SVM-MLR, the coupling of SVM and MLR strives to unite SVM's robustness in handling complex data structures and MLR's capacity for understanding linear relationships. By merging the strengths of SVM's effective classification boundaries with MLR's straightforward interpretation, this hybrid approach aims to create a model that adeptly navigates both linear and non-linear aspects in data.

SVM-DT, the fusion of SVM and DT capitalizes on SVM's ability to handle high-dimensional data and DT's interpretability in handling complex decision boundaries. This pairing aims to amalgamate SVM's resilience against overfitting with DT's capacity to partition data into smaller subsets, providing a model capable of handling complex data structures while retaining interpretability.

SVM-RF, the fusion of SVM with RF aims to merge SVM's ability to handle high-dimensional data and RF's ensemble-based learning. By combining SVM's robustness in creating effective decision boundaries with RF's ensemble of diverse decision trees, this hybrid model aspires to enhance predictive performance by leveraging the strengths of both algorithms.

MLR-DT, a fundamental tool for understanding linear relationships, is coupled with DT, famed for its interpretability and non-parametric nature. The combination aims to harness the interpretive simplicity of linear regression while augmenting it with DT's capability to handle non-linearities and interactions within the data. This amalgamation promises a balanced model that navigates both linear and non-linear aspects, providing a comprehensive view of the predictive landscape.

MLR-RF, the fusion of MLR with RF seeks to unify MLR's ability to model linear relationships with RF's ensemble-based learning approach. MLR, known for its simplicity and interpretability in modeling linear relationships,

is combined with RF's ensemble of decision trees, which excels in capturing complex nonlinearities and interactions within data. This amalgamation aims to create a hybrid model that harmonizes the interpretability of linear regression with the predictive power of ensemble-based learning.

DT-RF, the fusion of DT with RF seeks to combine DT's tree-based structure and interpretability with RF's ensemble learning approach. This hybridization aims to leverage the interpretability and ease of understanding provided by DT while harnessing the robustness and predictive power of RF's ensemble learning, potentially enhancing overall model performance.

In conclusion, the amalgamation of these leading machine learning algorithms into hybrid models presents a compelling approach to enhancing predictive capabilities. The combinations offer complementary strengths, effectively addressing various complexities inherent in diverse datasets. The pursuit of hybrid models, combining two powerful algorithms at a time, marks a significant stride toward achieving more accurate and resilient predictive models in the architecture of machine learning.

2.6. Performance measure

Mean Absolute Error (MAE) is the average of the absolute differences between the predicted and actual values. It measures the average magnitude of errors without considering their direction [19].

Mean Squared Error (MSE) is a measure of the average squared difference between the actual and predicted values [19]. It squares the difference between predicted and actual values for each data point, sums those squares, and then divides by the number of data points (or samples). It penalizes larger errors heavily due to the squaring effect.

Root Mean Squared Error (RMSE) is the square root of the MSE. It provides an interpretable metric in the same units as the target variable [13]. RMSE is more sensitive to outliers compared to MAE.

R-squared (R2) represents the proportion of variance in the dependent variable that is predictable from the independent variables in the model. It ranges from 0 to 1, with higher values indicating a better fit of the model to the data [18, 21].

Mean Absolute Deviation (MAD) calculates the mean of the absolute deviations between predicted and actual values. It measures the average difference between predicted and actual values.

Mean Absolute Percentage Error (MAPE) computes the average percentage difference between predicted and actual values. It's useful for understanding the relative error between predictions and true values [19].

Root Mean Squared Logarithmic Error (RMSLE) calculates the average difference of the logarithmic values of predicted and actual values. It's commonly used when the target variable has a wide range of values [20].

Adjusted R-squared (R2 Adjusted). Adjusted is a modified version of R2 that adjusts for the number of predictors in the model. It penalizes the addition of unnecessary predictors that do not improve the model significantly.

The predictive performance of the model is assessed using eight evaluation measures, defined as follows

$$MAE = \frac{1}{N}\sum_{i=1}^{N}\left|y_{i(pred)} - y_{i(actual)}\right| \quad (1)$$

$$MSE = \frac{1}{N}\sum_{i=1}^{N}\left(y_{i(pred)} - y_{i(actual)}\right)^2 \quad (2)$$

$$RMSE = \sqrt{\frac{1}{N}\sum_{i=1}^{N}\left(y_{i(pred)} - y_{i(actual)}\right)^2} \quad (3)$$

$$R^2 = 1 - \frac{\sum (y_{i(pred)} - y_{i(actual)})^2}{\sum (y_{i(\text{average})} - y_{i(actual)})^2} \quad (4)$$

$$MAD = \frac{1}{N}\sum_{i=1}^{N} median_n\left(y_{i(actual)} - y_{i(pred)}\right) \quad (5)$$

$$MAPE = \frac{1}{N}\sum_{i=1}^{N}\frac{\left|y_{i(actual)} - y_{i(pred)}\right|}{\max(\tau, \left|y_{i(actual)}\right|}} \quad (6)$$

$$RMSLE = \sqrt{\frac{1}{N}\sum_{i=1}^{N}(\log_e(1+y_{i(actual)}) - \log_e(1+y_{i(\text{pred})}))^2} \quad (7)$$

$$R^2_{adjusted} = 1 - \left[\frac{(1-R^2)(n-1)}{n-m-1}\right] \quad (8)$$

where yi(actual) is the actual low-rise building construction cost, yi(pred) is the predicted low-rise building construction cost, yi(average) is the average low-rise building construction cost, N is the total number of observations, m is the number of sample features and τ is an arbitrarily small but strictly positive number to avoid undefined results [15, 18].

The success of predicting construction cost estimation relies significantly on selecting the most fitting algorithm. The evaluation of various algorithms is carried out meticulously, employing pertinent assessment metrics like R2, MSE, or MAE on the validation dataset. The algorithm that displays exceptional predictive capabilities and robust generalization becomes the chosen prediction model. Overall, these methodologies span crucial phases from data selection and preprocessing to model training and algorithm selection, providing a comprehensive solution for low-rise building price prediction. This systematic approach enables real estate professionals, investors, and analysts to make well-informed decisions backed by accurate predictions of low-rise building prices.

3. RESULT AND DISCUSSION

In this section, we delve deeply into the outcomes derived from the meticulous development and training of machine learning hybrid models, utilizing a pre-processed dataset. The focal point lies in presenting a comprehensive comparative analysis of the performance of all ten hybrid machine learning algorithms. This comprehensive analysis encapsulates an all-encompassing parameter tuning process aimed at bolstering the robustness in performance evaluation. Furthermore, employing 10-fold cross-validation enhances the reliability of this performance assessment.

The primary objective of this study is to forecast low-rise building construction costs utilizing the advantages of ten sets of hybrid machine learning models. To measure their efficacy, we employed eight distinct statistical metrics, as detailed in Table 1, aiming to assess the accuracy of each model in estimating the housing construction costs in Thailand. As indicated in Table 1, the ANN-DT model emerged as the most prominent hybrid model, exhibiting an impressive accuracy of 0.921. Following closely, the ANN-MLR showcased a commendable accuracy of 0.916, while both the ANN-RT and MLR-DT demonstrated accuracies of 0.907. Conversely, the models utilizing the SVM algorithms displayed relatively lower accuracies, especially the SVM-RF model, registering the lowest accuracy at 0.696.

Table 1. The summary of the HML algorithms performance

No.	Model	R2	R2_Adj	MSE	RMSE	MAE	MAD	MAPE	RMSLE
1	ANN-SVM	0.804	0.713	85611185529	292593.89	195276.88	195276.88	0.18	0.24
2	ANN-MLR	0.916	0.877	36642276522	191421.72	135165.07	135165.07	0.10	0.13
3	**ANN-DT**	**0.921**	**0.885**	**34164053244**	**184835.21**	**125468.65**	**125468.65**	**0.11**	**0.15**
4	ANN-RF	0.905	0.861	41433259536	203551.61	137532.68	137532.68	0.11	0.15
5	SVM-MLR	0.753	0.637	108144129649	328852.75	198573.01	198573.01	0.16	0.21
6	SVM-DT	0.759	0.646	105538683718	324867.18	192032.70	192032.70	0.18	0.24
7	SVM-RF	0.696	0.554	132884310435	364533.00	211720.14	211720.14	0.18	0.25
8	MLR-DT	0.907	0.864	40622706349	201550.75	126171.77	126171.77	0.09	0.12
9	MLR-RF	0.875	0.816	54831353216	234160.96	143613.72	143613.72	0.09	0.12
10	DT-RF	0.868	0.807	57601528945	240003.19	138988.05	138988.05	0.11	0.16

Consequently, these research findings enable us to draw two significant conclusions. Firstly, the ANN-DT model outperforms all other models, consistently securing the top rank across almost all eight-evaluation metrics. This indicates that ANN-DT demonstrates increased stability and superior overall performance within the housing price dataset. Secondly, these findings suggest that the ANN-DT hybrid model is the most suitable for estimating low-rise building construction costs in Thailand, surpassing other hybrid learning models.

The comparison of accuracy performance among the 10 hybrid machine learning models is depicted in Figure 5. This representation illustrates their effectiveness in predicting the construction cost of low-rise residential buildings, showcasing varying predictive capabilities. However, aiming for predictions with an error rate of less than 10 percent, aligned with AACE's recommendations for finished design and model approximation, reveals only 4 models that meet this criterion. These models consist of ANN-DT, ANN-MLR, ANN-RF, and MLR-DT.

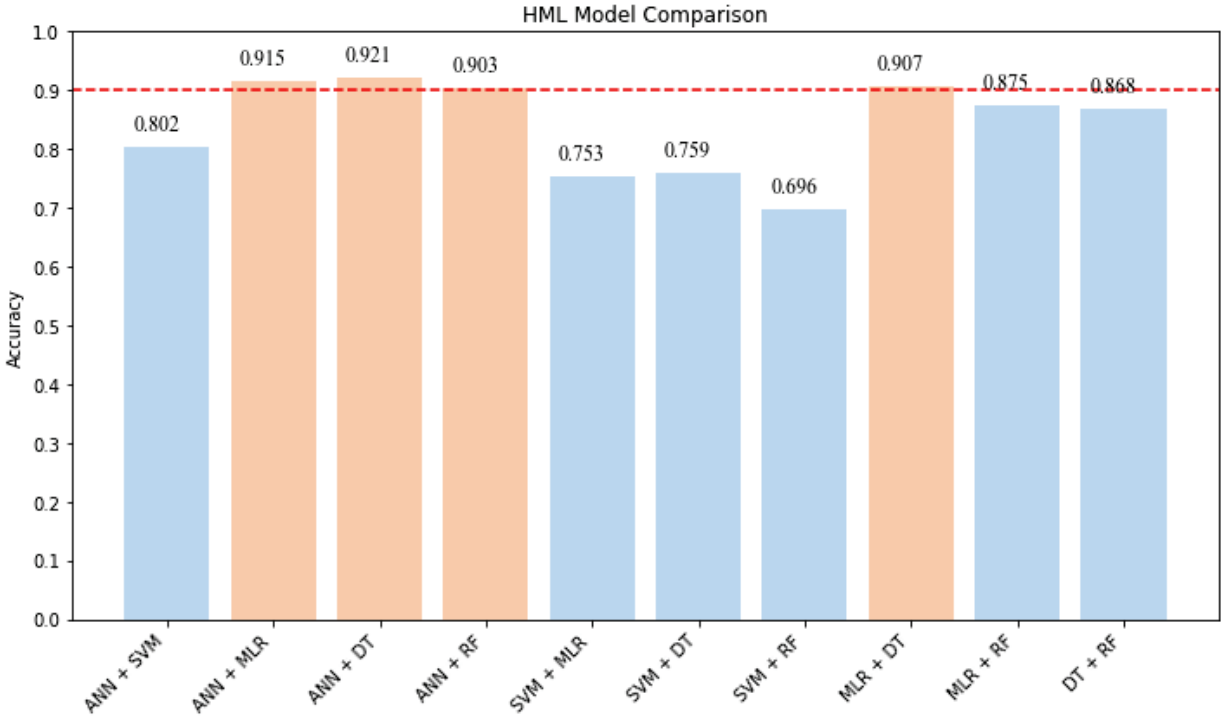


Figure 5. Comparison of accuracy among the HML models

In summary, the research involved evaluating predictions made by 10 hybrid machine learning models employing diverse methodologies to forecast the prices of low-rise buildings. The findings emphasize the exceptional performance of ANN-DT, positioning it as an appealing choice for practical applications in this domain. Furthermore, models such as ANN-MLR, ANN-RF, and MLR-DT demonstrate outstanding accuracy, surpassing acceptable standards for estimating construction costs follow the AACE recommended. This substantiates their standing as valuable options worthy of consideration.

4. CONCLUSION

In conclusion, this study harnessed the predictive potential of ten HML models to anticipate low-rise building construction cost. Predicting construction costs for residential housing holds significant importance within the

economic landscape. Extensive research has explored machine learning applications in modeling house price predictions. However, this study encounters specific limitations. Firstly, diverse machine learning models exhibit distinct strengths and weaknesses, and a model's performance in a specific metric or dataset doesn't ensure universal efficacy. Secondly, enhancing machine learning model performance heavily relies on hyperparameters, posing challenges in optimizing models through traditional grid or random search methods.

To address prevailing challenges in current house price prediction methodologies, characterized by high similarity in price trends across different regions, this study introduces a comprehensive and innovative framework for accurate house price forecasting. Initially, basic models including ANN, SVM, MLR, DT, and RF were utilized to develop ten hybrid machine learning models incorporating techniques such as ANN-SVM, ANN-MLR, ANN-DT, ANN-RF, SVM-MLR, SVM-DT, SVM-RF, MLR-DT, and DT-RF. Next, eight evaluation metrics including MSE, RMSE, MAE, $R2$, MAD, MAPE, $R2adjusted$, RMSLE were employed to analyze and compare the performance of these models.

The findings pinpointed the remarkable accuracy of ANN-DT with a high score of 0.921 among all tested models. This hybrid technique amalgamated expertise from different models, showcasing outstanding results. Additionally, ANN-MLR, ANN-DT, and MLR-DT demonstrated competitive accuracy, scoring 0.916, 0.907, and 0.904, respectively. These outcomes underscore significant performance enhancements achievable through mass techniques compared to details designing and tweaking models to limit deviations to under 10%, as recommended by AACE.

The study contributes valuable insights applicable to both academia and industry, particularly in refining house price prediction accuracy. It represents a significant stride in real estate market research by addressing existing limitations and establishing a foundational methodological framework for future house price prediction studies. Although this study demands substantial computational resources, future endeavors aim to explore more efficient model architectures, optimization techniques, and increased data utilization. Further research will encompass three facets: integrating a multi-source data fusion framework, employing diverse datasets for comprehensive model performance assessment, and exploring factors influencing real estate values to provide policy recommendations.

ACKNOWLEDGEMENTS

This research project was financially supported by Mahasarakham University of Thailand under Grant No. 6603024.

CONFLICTS OF INTEREST

The authors declare no conflict of interest.

REFERENCES

1. **M.-Y. Cheng, H.-C. Tsai, and W.-S. Hsieh**, "Web-based conceptual cost estimates for construction projects using Evolutionary Fuzzy Neural Inference Model," Automation in Construction, vol. 18, no. 2, pp. 164-172, 2009.
2. **S.S. Arage and N.V. Dharwadkar,** "Cost estimation of civil construction projects using machine learning paradigm," in 2017 International Conference on I-SMAC (IoT in Social, Mobile, Analytics and Cloud)(I-SMAC), 2017: IEEE, pp. 594-599.
3. **Sirithikon Sittikarnkul,** "Construction Cost Estimation for Government Building Using Prediction Modeling Techniques," Master of Engineering, Graduate School, Chiang Mai University, 2021.

4. **Kawee Wangnivejankul**, Construction Cost Estimating. Bangkok: SE-EDUCATION, 2023.
5. **R.P. Huehmer**, "Detailed estimation of desalination system cost using computerized cost projection tools," in 12th annual conference, DesalinationVisions for the Future, 2011, pp. 14-15.
6. **R.P.N.R.-.** AACE International, Cost Estimate Classification System - As Applied for the Petroleum Exploration and Production Industry. Morgantown, WV: AACE International, August 7, 2020.
7. **P. Chandu and N.B. Devi,** "Improved Prediction Accuracy of House Price Using Decision Tree Algorithm over Linear Regression Algorithm," in 2023 Eighth International Conference on Science Technology Engineering and Mathematics (ICONSTEM), 2023: IEEE, pp. 1-6.
8. **Y. Xu, Y. Zhou, P. Sekula, and L. Ding,** "Machine learning in construction: From shallow to deep learning," Developments in the built environment, vol. 6, p. 100045, 2021.
9. **L. Kittisak and W. Kittipol,** "The Prediction of Low-Rise Building Construction Cost Estimation Using Extreme Learning Machine," Adv. technol. innov., Dec. 2023.
10. **S. Tayefeh Hashemi, O. M. Ebadati, and H. Kaur,** "Cost estimation and prediction in construction projects: A systematic review on machine learning techniques," SN Applied Sciences, vol. 2, pp. 1-27, 2020.
11. **A.O. Elfaki, S. Alatawi, and E. Abushandi**, "Using intelligent techniques in construction project cost estimation: 10-year survey," Advances in Civil engineering, vol. 2014, 2014.
12. **S. Lu, Z. Li, Z. Qin, X. Yang, and R.S.M. Goh**, "A hybrid regression technique for house prices prediction," in 2017 IEEE international conference on industrial engineering and engineering management (IEEM), 2017: IEEE, pp. 319-323.
13. **S. Chiramel, D. Logofătu, J. Rawat, and C. Andersson,** "Efficient Approaches for House Pricing Prediction by Using Hybrid Machine Learning Algorithms," in Intelligent Information and Database Systems: 12th Asian Conference, ACIIDS 2020, Phuket, Thailand, March 23–26, 2020, Proceedings 12, 2020: Springer, pp. 85-94.
14. **G. Pinter, A. Mosavi, and I. Felde,** "Artificial intelligence for modeling real estate price using call detail records and hybrid machine learning approach," Entropy, vol. 22, no. 12, p. 1421, 2020.
15. **C. Zhan, Y. Liu, Z. Wu, M. Zhao, and T. W. Chow**, "A hybrid machine learning framework for forecasting house price," Expert Systems with Applications, vol. 233, p. 120981, 2023.
16. **J. Kalliola, J. Kapočiūtė-Dzikienė, and R. Damaševičius,** "Neural network hyperparameter optimization for prediction of real estate prices in Helsinki," PeerJ computer science, vol. 7, p. e444, 2021.
17. **B.B. Nair, V. Mohandas, and N. Sakthivel,** "A genetic algorithm optimized decision tree-SVM based stock market trend prediction system," International journal on computer science and engineering, vol. 2, no. 9, pp. 2981-2988, 2010.
18. **K. Lathong and K. Wisaeng,** "The Prediction of Low-Rise Building Construction Cost Estimation Using Extreme Learning Machine," Adv. technol. innov., Dec. 2023.
19. **S. Papadopoulos, E. Azar, W.-L. Woon, and C.E. Kontokosta,** "Evaluation of tree-based ensemble learning algorithms for building energy performance estimation," Journal of Building Performance Simulation, vol. 11, no. 3, pp. 322-332, 2018.
20. **Q. Truong, M. Nguyen, H. Dang, and B. Mei,** "Housing price prediction via improved machine learning techniques," Procedia Computer Science, vol. 174, pp. 433-442, 2020.

21. **L. El Mouna, H. Silkan, Y. Haynf, M.F. Nann, and S.C. Tekouabou**, "A Comparative Study of Urban House Price Prediction using Machine Learning Algorithms," in E3S Web of Conferences, 2023, vol. 418: EDP Sciences, p. 03001.

СПИСОК ЛИТЕРАТУРЫ

1. **M.-Y. Cheng, H.-C. Tsai, and W.-S. Hsieh**, "Web-based conceptual cost estimates for construction projects using Evolutionary Fuzzy Neural Inference Model," Automation in Construction, vol. 18, no. 2, pp. 164-172, 2009.
2. **S.S. Arage and N.V. Dharwadkar,** "Cost estimation of civil construction projects using machine learning paradigm," in 2017 International Conference on I-SMAC (IoT in Social, Mobile, Analytics and Cloud)(I-SMAC), 2017: IEEE, pp. 594-599.
3. **Sirithikon Sittikarnkul,** "Construction Cost Estimation for Government Building Using Prediction Modeling Techniques," Master of Engineering, Graduate School, Chiang Mai University, 2021.
4. **Kawee Wangnivejankul**, Construction Cost Estimating. Bangkok: SE-EDUCATION, 2023.
5. **R.P. Huehmer**, "Detailed estimation of desalination system cost using computerized cost projection tools," in 12th annual conference, DesalinationVisions for the Future, 2011, pp. 14-15.
6. **R.P.N.R.-.** AACE International, Cost Estimate Classification System - As Applied for the Petroleum Exploration and Production Industry. Morgantown, WV: AACE International, August 7, 2020.
7. **P. Chandu and N.B. Devi,** "Improved Prediction Accuracy of House Price Using Decision Tree Algorithm over Linear Regression Algorithm," in 2023 Eighth International Conference on Science Technology Engineering and Mathematics (ICONSTEM), 2023: IEEE, pp. 1-6.
8. **Y. Xu, Y. Zhou, P. Sekula, and L. Ding,** "Machine learning in construction: From shallow to deep learning," Developments in the built environment, vol. 6, p. 100045, 2021.
9. **L. Kittisak and W. Kittipol,** "The Prediction of Low-Rise Building Construction Cost Estimation Using Extreme Learning Machine," Adv. technol. innov., Dec. 2023.
10. **S. Tayefeh Hashemi, O. M. Ebadati, and H. Kaur,** "Cost estimation and prediction in construction projects: A systematic review on machine learning techniques," SN Applied Sciences, vol. 2, pp. 1-27, 2020.
11. **A.O. Elfaki, S. Alatawi, and E. Abushandi**, "Using intelligent techniques in construction project cost estimation: 10-year survey," Advances in Civil engineering, vol. 2014, 2014.
12. **S. Lu, Z. Li, Z. Qin, X. Yang, and R.S.M. Goh**, "A hybrid regression technique for house prices prediction," in 2017 IEEE international conference on industrial engineering and engineering management (IEEM), 2017: IEEE, pp. 319-323.
13. **S. Chiramel, D. Logofătu, J. Rawat, and C. Andersson,** "Efficient Approaches for House Pricing Prediction by Using Hybrid Machine Learning Algorithms," in Intelligent Information and Database Systems: 12th Asian Conference, ACIIDS 2020, Phuket, Thailand, March 23–26, 2020, Proceedings 12, 2020: Springer, pp. 85-94.
14. **G. Pinter, A. Mosavi, and I. Felde,** "Artificial intelligence for modeling real estate price using call detail records and hybrid machine learning approach," Entropy, vol. 22, no. 12, p. 1421, 2020.
15. **C. Zhan, Y. Liu, Z. Wu, M. Zhao, and T. W. Chow**, "A hybrid machine learning framework for forecasting house price," Expert Systems with Applications, vol. 233, p. 120981, 2023.
16. **J. Kalliola, J. Kapočiūtė-Dzikienė, and R. Damaševičius,** "Neural network hyperparameter optimization for prediction

of real estate prices in Helsinki," PeerJ computer science, vol. 7, p. e444, 2021.
17. **B.B. Nair, V. Mohandas, and N. Sakthivel,** "A genetic algorithm optimized decision tree-SVM based stock market trend prediction system," International journal on computer science and engineering, vol. 2, no. 9, pp. 2981-2988, 2010.
18. **K. Lathong and K. Wisaeng,** "The Prediction of Low-Rise Building Construction Cost Estimation Using Extreme Learning Machine," Adv. technol. innov., Dec. 2023.
19. **S. Papadopoulos, E. Azar, W.-L. Woon, and C.E. Kontokosta,** "Evaluation of tree-based ensemble learning algorithms for building energy performance estimation," Journal of Building Performance Simulation, vol. 11, no. 3, pp. 322-332, 2018.
20. **Q. Truong, M. Nguyen, H. Dang, and B. Mei,** "Housing price prediction via improved machine learning techniques," Procedia Computer Science, vol. 174, pp. 433-442, 2020.
21. **L. El Mouna, H. Silkan, Y. Haynf, M.F. Nann, and S.C. Tekouabou**, "A Comparative Study of Urban House Price Prediction using Machine Learning Algorithms," in E3S Web of Conferences, 2023, vol. 418: EDP Sciences, p. 03001.

Kittipol Wisaeng received a Ph.D. in Electrical and Computer Engineering from Thailand in 2016. He is currently an Associate Professor in Computer Science. His main research interests center on advancing artificial intelligence methods and systems integration in applications that lie predominantly in medical image segmentation. He has carried out a unique portfolio of research programs, generally focusing on deep learning and machine learning. He addresses such issues as optimization techniques, retinal segmentation, breast cancer detection, blood vessel extraction, exudates identification, optic disc localization, and brain tumor classification in challenging environments. He has published over 26 technical papers in this area and has seven H-index. He received the senior researcher award, outstanding publication award, the highest publication of research in the Scopus database, the highest h-index award, and the highest citation per article organized by Mahasarakham University. He was a Guest Reviewer of Applied Soft Computing in 2014, IEEE Transactions on Instrumentation and Measurement in 2023, Journal of Intelligent & Fuzzy Systems in 2022, Soft Computing in 2020, Computers, Materials & Continua in 2022, Intelligent Automation & Soft Computing in 2023, and IET Image Processing in 2023. He can be contacted at email: kittipol.w@acc.msu.ac.th

Kittisak Lathong rereceived a B.Eng. degree in Civil Engineering from Srinakharinwirot University, Thailand, a B.P.H. degree in Occupational Health and Safety from Sukhothai Thammathirat Open University, Thailand, a M.Eng. degree in Civil Engineering from KMITL, Thailand, a M.P.A. degree in Public Administration from Ramkhamhaeng University, Thailand and culminating with a Ph.D. degree in Business Administration and Innovation from The Mahasarakham University, Thailand. With over 15 years of dedicated experience in the fields of design and construction, he possesses exceptional expertise. His professional proficiency is a testament to his extensive hands-on involvement and comprehensive understanding of the industry. His research pursuits encompass various topics, notably civil engineering, construction engineering, building information modeling, machine learning, and artificial intelligence. His dedication to advancing these domains underscores his commitment to driving innovation and progress within the field. He can be contacted at email: kittisak.lathong@gmail.com.

Киттипол Висаенг, доктор философии в области электротехники и вычислительной техники, доцент в области компьютерных наук. Электронная почта: kittipol.w@acc.msu.ac.th.

Киттисак Латхонг, магистр в области гражданского строительства, доктор философии в области управления бизнесом и инноваций, Электронная почта: kittisak.lathong@gmail.com.

DOI:10.22337/2587-9618-2024-20-3-84-96

DIAGNOSTICS AND RENOVATION METHODS FOR STEEL PIPELINES

Vladimir A. Orlov, Sergey P. Zotkin, Dmitry V. Podolyan

National Research Moscow State University of Civil Engineering, Moscow, RUSSIA

Abstract. The article explores the analytical challenges and potential applications of diagnostic equipment and tools for cost-effective restoration of aging pressure pipeline systems at minimum costs for water transportation. The study focuses on a section of a water supply network made of steel pipes that requires repair and restoration due to corrosion damage and wall thinning.

The paper presents an analysis of effective non-destructive pipeline diagnostic methods, details the design and technical specifications of the domestic diagnostic system HeatScan. Provided are sample magnetograms that indicate defect zones and the absolute residual wall thickness at the defect locations. The benefits of the HeatScan system over the Inspector Systems flaw detector are also shown.

To identify the most cost-effective pipeline repair method, three alternative technologies for inserting polymer pipes into the existing pipeline are considered, along with a calculation of the energy consumption for water transportation. It is noted that the most cost-efficient repair method could be the Swagelining technology, which involves pre-compressing the polymer pipe with the subsequent straightening. Information on the return-on-investment period for the diagnostic system when used in pipeline restoration projects is provided.

Keywords: pipelines, diagnostics, repair methods, energy consumption, return on investment period

ДИАГНОСТИКА СТАЛЬНЫХ ТРУБОПРОВОДОВ И МЕТОДЫ ИХ РЕНОВАЦИИ

В.А. Орлов, С.П. Зоткин, Д.В. Подолян

Национальный исследовательский Московский государственный строительный университет (НИУ МГСУ), г. Москва, РОССИЯ

Аннотация. В статье рассматриваются поисковые задачи анализа и возможного использования оборудования и приборной базы по диагностике для решения вопросов эффективной реконструкции ветхих напорных трубопроводных сетей при минимальных денежных затратах на транспортировку воды. Объектом исследований является участок стальной водопроводной сети, который подлежит ремонтно-восстановительным операциям в связи с наличием дефектов в виде коррозионных повреждений и утонения стенок.

Представлен анализ эффективных методов диагностики трубопроводов методами неразрушающего контроля, описана конструкция и приведены технические характеристики и результаты работ отечественного диагностического комплекса HeatScan. Приведены образцы магнитограмм, свидетельствующих о наличии дефектных зон и абсолютных величин остаточной толщины стенок в местах дефектов. Представлены преимущества комплекса HeatScan по сравнению с дефектоскопом Inspector Systems.

В целях выявления наиболее экономичного метода ремонта трубопровода рассмотрены три альтернативные технологии протягивания в старый трубопровод полимерных труб и проведен расчет потребления электроэнергии на транспортировку воды. Выявлено, что наиболее экономичным методом ремонта, может служить применение технологии предварительного сжатия полимерной трубы и последующего распрямления Swagelining. Представлены данные о сроке окупаемости диагностического комплекса при его использовании на линейных объектах реконструкции трубопроводов.

Ключевые слова: трубопроводы, диагностика, методы ремонта, энергопотребление, срок окупаемости

INTRODUCTION

Organizations and enterprises involved in construction, repair, and modernization of urban and rural pipeline infrastructure are tasked with maintaining efficient operation of utility networks. This is achieved through extensive use of diagnostic systems to assess the technical

condition of specific sections of underground pipelines, including culvert crossings, and to select the optimal repair method for these networks [1].

Particular emphasis is placed on conducting diagnostics under challenging conditions (for instance, in wells where pipeline access is difficult), during emergency excavations requiring prompt measurements, and when laying steel pipelines in urban areas with uniform and non-uniform layers of backfill soil, where steel degradation may occur, etc. [2]. The primary objective of diagnosing pressure pipelines is to promptly identify any operational failures and minimize the impact in an emergency. It is necessary to consider such factors as the type and parameters of defects, the actual thickness of the pipe wall after prolonged use, and the residual life of steel pipelines. The concluding phase of pipeline network restoration programs involves selecting the most urgent reconstruction project and the best method of pipeline restoration, focusing on trenchless repair technologies, i.e., without excavation work (with or without access inside the pipeline).

The modernization of diagnostic work on aging operational sections of water supply and drainage networks, including culverts, should be carried out by using (or purchasing) new process equipment and its subsequent testing. This requires a thorough analysis of the market for diagnostic devices, up-to-date regulatory and technical documentation, scientific literature, as well as information available on the official websites of companies that manufacture equipment for inspecting and repairing underwater pipeline crossings and offer diagnostic, installation, and repair services for such facilities [3].

Comprehensive diagnostics of underwater pipeline crossings can be categorized as either external or internal. External diagnostics involve locating the pipeline, inspecting its surface (either visually or with simple measuring tools), instrumentally examining the pipeline surface and insulation, and monitoring channel processes. Internal diagnostics are carried out by putting instruments and devices inside the pipeline to assess its technical condition. The surface and internal examination of underwater pipeline crossings is conducted using non-destructive testing methods: magnetographic, ultrasonic, electromagnetic, and radiographic [4].

Several non-destructive testing methods can be used to assess the technical condition and position of underwater pipeline crossings relative to the seabed profile, according to an analysis of the diagnostic equipment used [5, 6]:

1) Magnetographic methods (based on recording changes in magnetic field lines in the zone of pipe wall and insulation defects).
2) Ultrasonic methods (based on changes in the reflection of ultra-short sound waves in the zone of pipe defects).
3) Electromagnetic methods (similar to magnetographic ones, but involve the use of electromagnetic sensors rather than magnetite sensors).
4) Radiographic methods (based on the use of γ-radiation).

There are two primary categories of methods for inspecting pipelines using electromagnetic phenomena [7, 8]:

- methods that measure the electromagnetic fields generated by the pipelines themselves; these methods are based on measurements of the fields created by the pipelines, and
- methods for measuring electromagnetic fields induced on the pipeline using specialized systems and devices.

Several other methods have been utilized for detecting leaks from underwater pipeline crossings, such as analyzing pressure diagrams along the pipeline's length at its initial and final points, as well as optical methods that involve introducing a fluorescent dye into the pumped medium and subsequently detecting it under a certain light spectrum above the pipeline's location [9-13].

Acoustic methods, which are based on recording sound signals arising from liquid turbulence when it flows into a low-pressure space [14,

15], and physical methods, which use measuring devices to track pressure levels and flow in the pipeline system [16], are also utilized.

It's crucial to note that in Russia, there is no approved regulatory and technical documentation governing the inspection procedures for underwater water supply and sewerage culverts. Existing regulations, such as SP 272.1325800.20161, are centered around visual diagnostic methods for drainage systems, as well as methodological guidelines for assessing the technical state of other systems like heating, hot water, cold water, and wastewater disposal.

The external inspection of underwater pipelines involves monitoring parameters such as pipeline shape, characteristics of the water body's bottom beneath the pipeline, thickness of the soil layer covering the pipeline, condition of corrosion protection, overall technical state of the pipeline, and geotechnical properties of the surrounding soil.

Inline diagnostics of such structures are typically conducted in several stages. First, the internal cavity of the diagnostic area is cleaned to a level mandated by regulatory and technical documentation. This is followed by the deployment of special profile-measuring and defect-detecting devices (including robotic devices), with a subsequent prompt analysis of the gathered data. Then, a stress-corrosion device is deployed. Finally, a comprehensive analysis of the diagnostic study results is conducted and documented in specific reports.

Inline inspection makes it possible to monitor parameters such as pipe geometry alterations, metal loss due to corrosion, presence of cracks and erosion, as well as pipeline profile, including shifts in plan or elevation caused by soil erosion.

Russian scientists are working on innovative instrument systems that facilitate diagnostic studies of underwater culverts. Specifically, a method [17] for evaluating the technical condition of underwater utilities has been developed that makes it possible to promptly obtain real-time information about the object's condition, even as the vessel is passing over the pipeline being diagnosed. This method employs hydroacoustic tools to measure seabed topography and assess the technical condition of the pipeline, including the state of its insulation coating, based on electromagnetic field parameters.

The paper [18] showcases the successful use of the long-wave ultrasound system *Wavemaker* developed by *Guided Ultrasonics Ltd.* from the *UK* for diagnosing and monitoring hard-to-reach pipelines. One of the key benefits of the *Wavemaker* system is its ability to gather data on the condition of a pipeline up to 50 meters long by installing a special ring with piezoelectric transducers at a single network point, eliminating the need to move it along the entire pipeline length. The system package comprises a control unit and *WavePro* software for a personal computer. The system can identify zones of crack formation, corrosion, and mechanical damage with metal loss of up to 5%, as well as welded joint defects. A significant advantage of this system is that there's no need to strip all insulation from the pipeline, as it is enough to strip it only at the ring's installation point. The existence of flange connections does not impact the effectiveness of the diagnostics. The manufacturer also offers various types of fastening ring transducers for ultrasonic scanning.

Russian organizations engaged in the operation and examination of underwater pipeline crossings have gained positive experience using domestic electronic information systems (IS "Duker" and IS "Duker 2.0") [19]. These systems not only store and organize information about the facility but also provide a comprehensive assessment of the technical condition of underwater crossings, and generate report documentation, including data visualization.

Currently, the diagnostics of underwater gas and oil pipelines are performed using advanced and highly precise equipment, including multibeam and narrow-beam echosounders, hydroacoustic (ultrasonic) profilers, side- and circular-scan sonars, devices for measuring water flow direction and speed, as well as satellite navigation systems [20-22].

Side-scan sonars are advised for use in deep waters and large water bodies. Conversely, 360-degree sonars are suitable for use in areas with limited depth and confined spaces. Side-scan sonars generate ultrasonic pulses directed at the seabed at a sharp angle and then record the reflected signals. There are analog and digital versions of sonars, with the latter considered more advanced.

For specialists working in construction and pipeline maintenance, where precise location and depth of underground objects is crucial, radio telescopes like the *Radiodetection RD*8100 [23, 24] are an essential tool.

Pipeline swabs (also known as smart pigs) have gained popularity for in-line diagnostics of gas and oil pipelines [25]. These devices provide simultaneous information about the pipeline's spatial configuration, the geometry of the pipe walls, and allow for monitoring of the network's technical condition through integrated non-destructive testing systems (typically of magnetic or ultrasonic types).

A detailed description of these devices' functions and their application in design solutions can be found in the article [26].

METHODS AND MATERIALS.

To choose the optimal diagnostic complex design, we studied the main types of products offered by both Russian and international manufacturers for the diagnostics and repair of water supply and sewerage pipelines. As a result of collection, processing, and analysis of information, it was proposed to use Russian-made equipment, specifically the *HeatScan* diagnostic complex from the Russian company Octanta. The study was carried out with the direct participation of representatives from JSC Mosvodokanal.

The *HeatScan* complex is designed for measuring pipeline wall thickness in zones of area thinning and for detecting defects during continuous in-line diagnostics of steel pipelines using a magnetic inspection method (Figure 1). No prior preparation of the pipe is required. The diagnostic robot in the complex is equipped with six tracks, enabling it to traverse areas with large deposits on the pipeline walls, and can monitor the condition of metal through a deposit layer up to 30 mm thick.

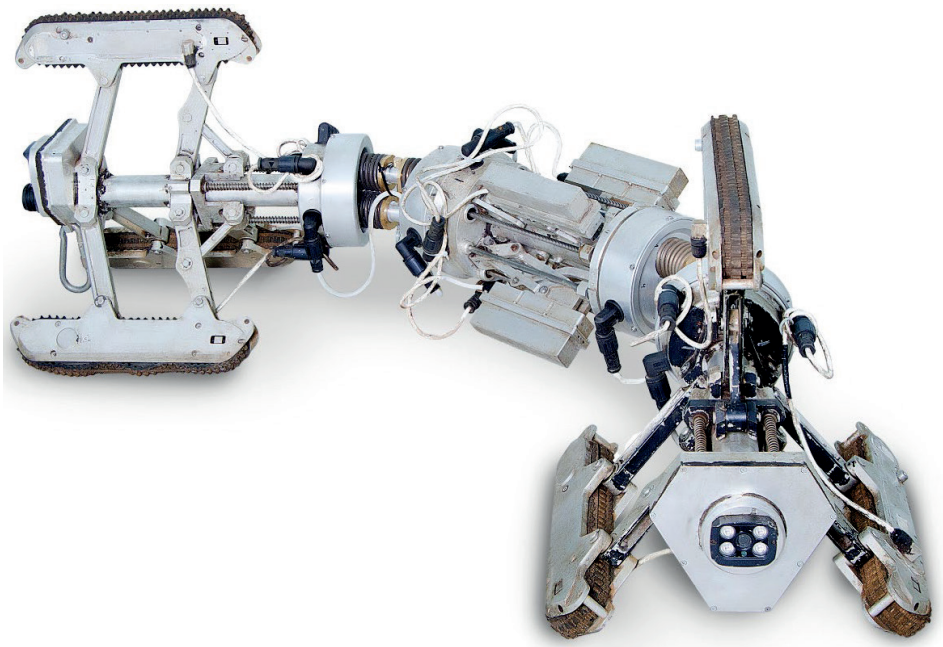


Figure 1. HeatScan robot

The robot is operated by a technician inside the autolaboratory, which is a mobile control panel for the complex, located near the robot's pipe entry point. The robot is loaded into the pipe through a 600×600 mm process cut, either inside a heat recovery chamber or at pipeline pits.

Table 1 summarizes the robot's technical capabilities for pipeline diagnostics.

Table 1. Technical specifications and capabilities of the HeatScan complex.

Range of inspected pipe diameters, mm	400-1600
Range of pipe wall thickness, mm	3-16
Length of inspection, m	500
Thickness of deposits on the pipe's inner surface, mm	15 (up to 30 with reduced sensitivity)
Size of detected/measured defects, mm	- a through defect of 6 mm diameter
Performance, m/h	no less than 100
Number of branches passed, pcs	2
Passing through tees	yes
Measurement error from the remaining wall thickness in the defect zone, %	20
Relative humidity, %	100%
Range of working temperatures, °*C*	0-70

Presented below are the additional technical specifications for the *HeatScan* diagnostic system (КМВТД-01), which has valid calibration certificates:

- manufactured in 2018 by NPO *Oktanta LLC* in the Russian Federation,
- equipped with programs for remote control, data processing, and pipeline technical condition report generation, including defect coordinates (*MFC control*),
- design type: portable,
- performance: no less than 100 m/h;
- voltage: 220 V, 50 Hz,
- power consumption: no more than 1 kVA.

RESULTS

Experimental studies of the *HeatScan* diagnostic system efficiency for in-pipe diagnostics were carried out at the Mosvodokanal JSC facility.

The diagnosed facility was a 158.4 m long steel pressure pipeline for process water (Figure 2). Pipeline design parameters: outer diameter 500 mm, wall thickness 10 mm. The diagram in Figure 3 illustrates the coding of loading points and travel routes (No. 1 and No. 2) as an example.

Figure 3 also shows the points where hydraulic tests were conducted and the locations of vertical attachments (risers).



Figure 2. The pipeline's location

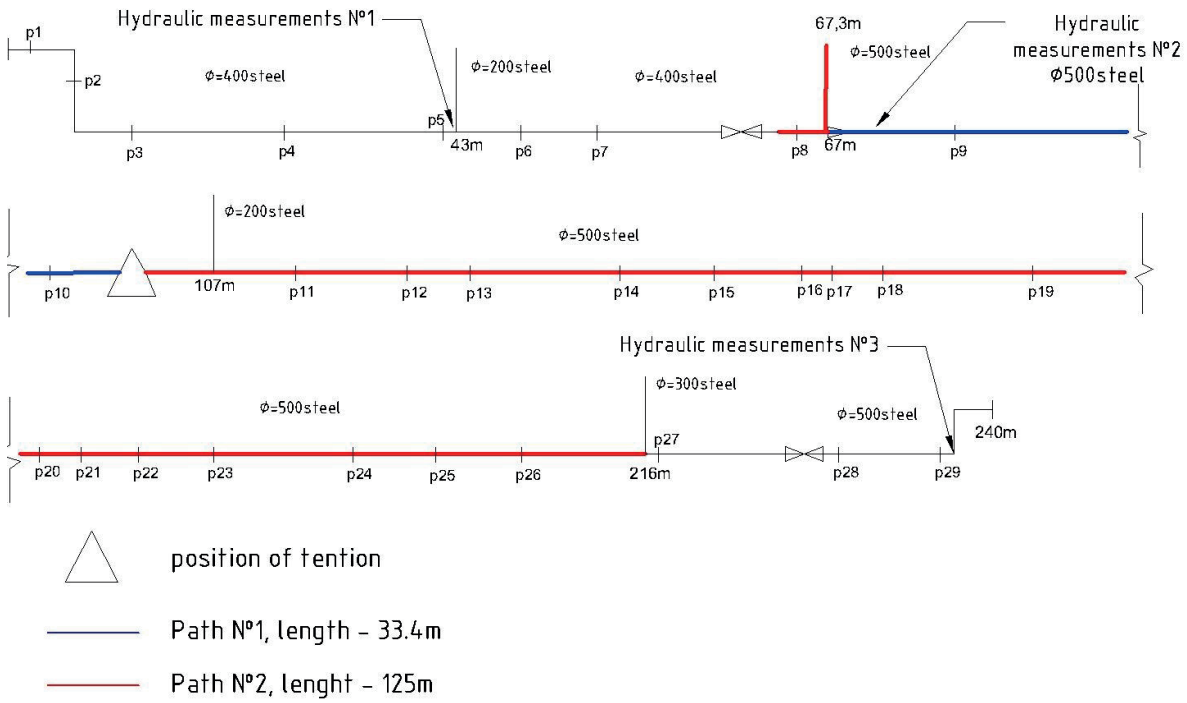


Figure 3. Loading point and travel routes

The magnetic inspection revealed critical defects that are detailed in Tables 2 and Table 3. The process of recording and coding the inspection results involved documenting the travel distance covered by the diagnostic system (m), as well as the angular coordinates of points within the pipeline's circumference (degrees). Measurements were taken from the cross-sections of the pipeline for each of the two routes. The angular coordinate was measured counterclockwise, with the top of the pipe circumference taken as zero.

Table 2. Indicators at outer diameter of a new pipeline d_1=1000 mm

Route number	Zone number	Distances and angular coordinates of points along the pipeline's circumference meters/degrees	Minimum remaining wall thickness, mm	Comments
1	1	15.6/186	5.5	-
	2	38/261	3.7	-
		38/13	6.3	-
	3	42.5/149	3.8	-
		42.8/233	3.7	-
		43.1/163	5.1	-
2	4	48.2/219	2.5	*Corrosion area with spot thinning and substantial defect area*
		48.4/123	< 1	
		48.2/204	< 1	
		48.6/196	< 1	
		49.2/179	< 1	
		49.1/135	< 1	
	5	51.9/195	3.7	-
		51.6/52	4.0	-

Table 3. Experimental data for the second route (zones 6-9)

Route number	Zone number	Distances and angular coordinates of points along the pipeline's circumference meters/degrees	Minimum remaining wall thickness, mm	Comments
2	6	61.1/261	3.9	-
	7	79.7/167	2.9	-
		80.2/85	3.5	-
		80.5/191	3.6	-
	8	84.4/204	3.2	-
	9	118.3/244	5.4	-

Below are selected magnetograms of defective zones with the most significant defects (see Figures 4 and 5).

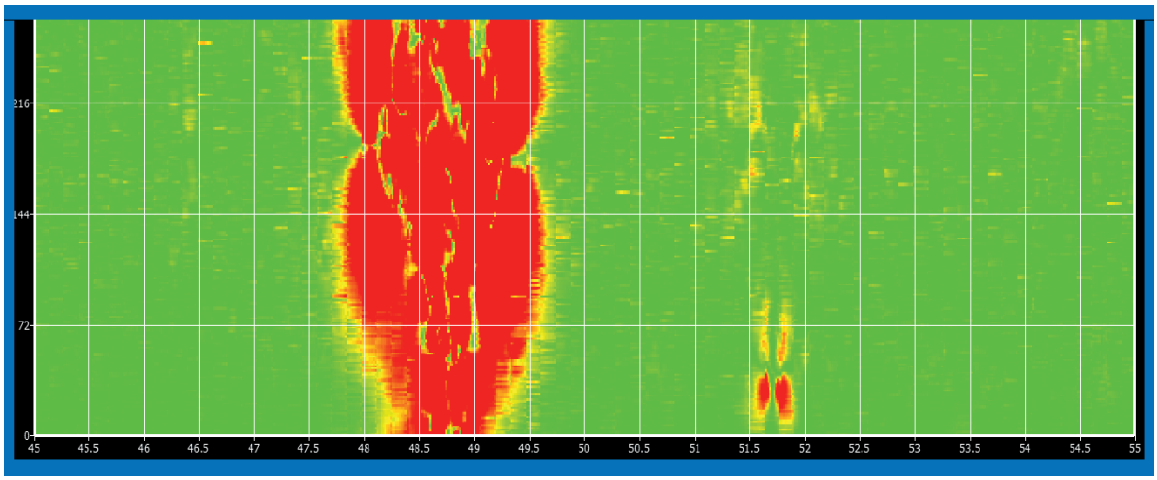


Figure 4. Illustration of defects and their areas on route 2 (Zone 4)

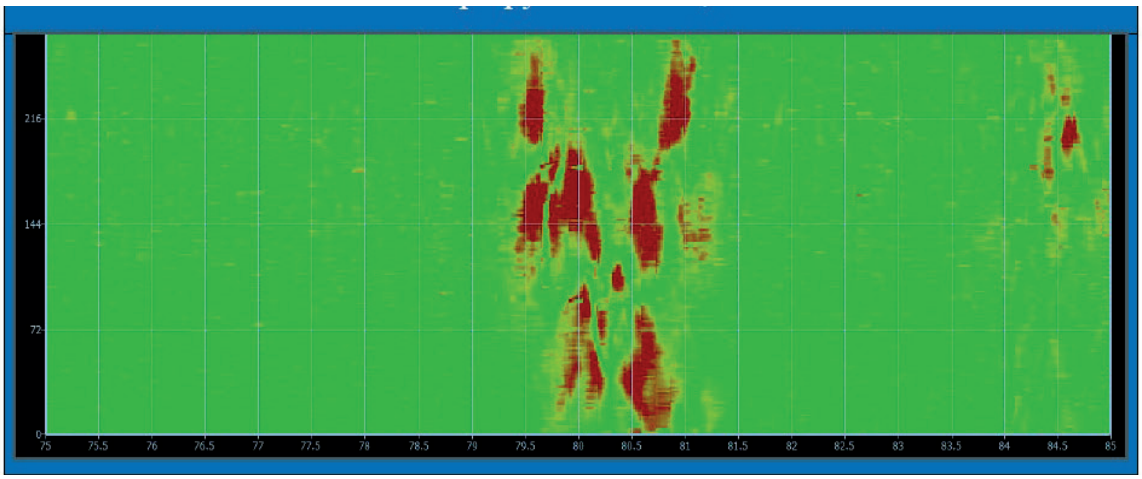


Figure 5. Illustration of defects and their areas on route 2 (Zones 7 and 8)

Thus, as the magnetograms indicate, the most defective zones for the earliest pipeline failure are the coordinates of 5 points along route 2 (zone number 4), which have a bright trace and, accordingly, the minimum values of the residual wall thickness (less than 1 mm), which is less than 10% of the original wall thickness and it indicates the exhaustion of the pipeline's resource. Thus, the wide and bright trace on the magnetogram of Figure 4 indicates the need to replace the dilapidated pipeline as soon as possible or reconstruct it using appropriate methods. In turn, Figure 5 shows only minor small traces, for example, from 3.7 to 6.3 mm (zones 1, 2 and 3 along route 1), which allows us to assess the condition of the pipeline as satisfactory at this point in time. As for the data on route 2 (zone numbers 6-9), the so-called "average values" of the residual wall thickness are observed here. In this case, the technical condition of the pipeline should be considered as potential for reconstruction.

When comparing the diagnostic results of the *HeatScan* system with those of the *Inspector Systems* flaw detector, which was also tested at the research site as an alternative device for assessing pipeline condition, it is clear that *HeatScan is superior*. Specifically, for larger defect areas, the differential signal from the *Inspector Systems* flaw detector showed quite low values that did not accurately represent the actual corrosion zone.

Regarding the restoration methods, the most suitable solution for a timely repair could be pulling new polymer pipes inside the old steel pipeline, which has an inner diameter of 480 mm, using the appropriate technologies [27], i.e.:

- A deformed *U*-shaped pipe with an outer diameter of 450 mm, an inner diameter of 428 mm (*SDR* 41), and a wall thickness of 11 mm.
- A pipe pre-compressed using *Swagelining* technology with an outer diameter of 500 mm, an inner diameter of 454.32 mm (*SDR* 41) after straightening, and a new wall thickness of 12.84 mm.
- A *Primus Line* hose with an outer diameter of 450 mm, an inner diameter of 437 mm, and a wall thickness of 6.5 mm.

It's important to note that there will be no significant alterations in the hydraulic characteristics of the pipeline when using the repair methods presented, as the hydraulic friction coefficient λ of new pipes is considerably lower than that of old steel ones.

The optimal choice among the technologies presented above is determined by calculating the annual energy savings ΔE_{1m} for each unit length of the restored pipeline. The energy calculation is performed using the following formulas (1 and 2) [28].

$$\Delta E_{1m}=[9.81\cdot Q^3(A_s - A_n)\cdot 24\cdot 365]/\eta_p \qquad (1)$$

where ΔE_{1m} is the amount of electricity saved, kWh/year; Q is the flow rate of water supplied by the pipeline, m^3/s; A_s and A_n are the resistivity coefficients of the old and new pipes, respectively; η_p is the efficiency factor of the pumping unit; 24 is the number of pump operating hours per day, h; 365 is the number of days in a year.

$$A_s = 0.0017d^{-5.1359}, \quad A_n = 0.0004d^{-5.7276} \qquad (2)$$

where d is the inner diameter of the pipeline, m.

In the calculations, it was assumed that the flow rate of transported water Q=0.23 m^3/s, the efficiency factor of the pumping unit η_p = 0.9, the inner diameter of the old pipeline d=480 mm and the new diameters d of polymer pipes when using the relevant renovation technologies were 438, 454.32 and 437 mm.

Therefore, by substituting the initial data into formulas (1 and 2), the following energy saving values are obtained for water transportation through the pipeline after its restoration using:

– a deformed *U*-shaped pipe

$\Delta E_{1m} = [9.81\cdot 0.23^3(0.0017\cdot 0.48^{-5.1359} - 0.0004\cdot 0.428^{-5.7276})\cdot 24\cdot 365] / 0.9 = 25.644$ kWh per year per each meter of pipeline length

– a precompressed pipe

$\Delta E_{1m} = [9.81 \cdot 0.23^3 (0.0017 \cdot 0.48^{-5.1359} - 0.0004 \cdot 0.45432^{-5.7276}) \cdot 24 \cdot 365] / 0.9 =$ 43.015 kWh per year per each meter of pipeline length

– a hose

$\Delta E_{1m} = [9.81 \cdot 0.23^3 (0.0017 \cdot 0.48^{-5.1359} - 0.0004 \cdot 0.437^{-5.7276}) \cdot 24 \cdot 365] / 0.9 = 32.386$ kWh per year for each meter of pipeline length

Therefore, the maximum energy saving potential during water transportation through the restored pipeline will be achieved by utilizing the *Swagelining technology.* In this scenario, the average energy savings will be 25-40% higher than when using the previously discussed alternative repair technologies.

The expected savings of water supply network operating organizations purchasing the *HeatScan* diagnostic complex (КМВТД-01) amounts to 46.0 million rubles. When purchasing the complex, it is highly desirable that the equipment's return on investment period does not exceed one year. Therefore, relevant market research was conducted, specifically analyzing the potential use of the complex for diagnosing steel pipeline networks in the area serviced by Mosvodokanal JSC.

Concerning the return on investment period, a preliminary calculation was made, based on the length of steel networks that need diagnosing, with the condition that the cost of the *HeatScan* complex is not exceeded.

Based on the budget data incorporated into the automated "Stroyinformresurs" program and the current prices for 2023, diagnosing (video inspection of a steel pipeline 158.4 m long and 500 mm in diameter with preliminary washing and drying operations) costs 81,346.73 rubles.

To achieve the desired return on investment period for diagnostic equipment using the *HeatScan* complex and implementing the aforementioned restoration technologies, the total length of steel pipeline networks diagnosed annually should not exceed 89 km (0.1584 × 46,000,000 / 81,346.73). This figure falls within the range of annual diagnostic and pipeline restoration targets set by Mosvodokanal JSC.

CONCLUSIONS

1. Following an analysis of advanced diagnostic tools for assessing the condition of pressurized steel pipelines, Russian-made equipment — the *HeatScan* diagnostic complex — was identified and tested on an actual site.
2. Based on the results obtained from the operation of the *HeatScan* diagnostic complex, which identifies the locations and nature of steel pipeline defects, three trenchless repair technologies were suggested as alternative renovation options, which involve pulling new polyethylene pipes into the existing pipeline.
3. The calculations showed that the most significant economic benefit in terms of energy savings for water transportation through the pipeline post-restoration was achieved when using *Swagelining* technology.
4. An estimate has been made of the length of pipeline networks that can be diagnosed to ensure a return on investment for the diagnostic complex.
5. The main directions for the implementation of the results of the conducted research may be the widespread use in the practice of water utilities of the described in-line diagnostic complexes and alternative options for the reconstruction of pressure pipelines of water supply systems that ensure the effect of energy saving.

REFERENCES

1. **Primin O.G.** Water Leaks *Federal State Budgetary Educational Institution of Higher Education "Moscow State University of Civil Engineering (National Research University)"*, 2022. 167 p.
2. **Zvirko O., Tsyrulnyk O., Nykyforchyn H.** Non-destructive evaluation of the condition of operational pipeline steel,

taking into account the stage of degradation. *Procedia Structural Integrity*. 2020; 26:219-224. DOI: 10.1016/j. prostr.2020.06.025.
3. **Ryltseva Yu.A.** Advanced methods and tools for diagnosing and repairing underwater pipeline crossings // *Bulletin of MGSU*. 2021. V. 16. Issue 9. Pp. 1236-1263. DOI: 10.22227/1997-0935.2021.9.1236-1263.].
4. **Bhadran V., Shukla A., Karki H.** Non-contact flaw detection and condition monitoring of subsurface metallic pipelines using magnetometric method. *Materials Today*: Proceedings. 2020; 28:860-864. DOI: 10.1016/j.matpr.2019.12.313.
5. **Chen L., Arzaghi E., Mahdi M., Garaniya V., Abbassi R.** Condition monitoring of subsea pipelines considering stress observation and structural deterioration. *Journal of Loss Prevention in the Process Industries*. 2018; 51:178-185. DOI: 10.1016/j.jlp.2017.12.006
6. **Davis P., Brockhurst J.** Subsea pipeline infrastructure monitoring: A framework for technology review and selection. *Ocean Engineering*. 2015; 104:540-548. DOI: 10.1016/j.oceaneng.2015.04.025
7. **Ivliev E.A.** Detection, tracking, and inspection of underwater pipelines and cables using electromagnetic methods. *Underwater Research and Robotics*. 2009. Issue 2 (8). Pp. 22-33.
8. **Yang Q., Sun M., He M., Yang Q.** Evolution features of riverbeds near underwater crossing line pipes: *An experimental study. Natural Gas Industry B*. 2020. Vol. 7. Pp. 246-253. DOI: 10.1016/j.ngib.2019.10.006
9. **Zezin V.G.; Lazukov V.A.** Determination of continuous media flow rate using variable pressure drop method. Chelyabinsk: *Publishing House of South Ural State University*, 2007. 102 p.
10. **Mogutin Yu.B., Guseva O.A., Veselova A.V., Vlasyev M.V.** Coordinating underwater maintenance operation at offshore oil and gas deposits. *Shipbuilding*. 2017. Issue 3 (832). Pp. 25-31.
11. **Verde C., Molina L., Carrera R.** Practical Issues of Leaks Diagnosis in Pipelines. *IFAC Proceedings Volumes*. 2011. Vol. 44. Issue 1. Pp. 12337-12342. DOI: 10.3182/20110828-6-IT-1002.01688
12. **Mahmutoglu Y., Turk K.** Positioning of leakages in underwater natural gas pipelines for time-varying multipath environment. *Ocean Engineering*. 2020. Vol. 207. P. 107454. DOI: 10.1016/j.oceaneng.2020.107454
13. **Lu H., Iseley T., Behbahani S., Fu L.** Leakage detection techniques for oil and gas pipelines: State-of-the-art. *Tunnelling and Underground Space Technology*. 2020. Vol. 98. P. 103249. DOI: 10.1016/j. tust.2019.103249
14. **Khallyev N.Kh.** Overhaul of the linear section of trunk gas and oil pipelines: *Study guide. Moscow*: Max Press, 2011. 448 p.
15. **Marinenko E.E.** Gas supply: Study guide. Volgograd: *Volgograd Institute of Civil Engineering and Architecture*, 2008. 222 pages.
16. **Pashilov M.V.** Actions to ensure safe operation of the Varandey oil terminal's undersea pipeline // *New Science: Current Status and Development Paths*. 2015. Issue 5. Pp. 155-158.
17. **Gaidukevich S.V., Nikonenko A.D., Shalagin V.N.** Maintenance of Gazprom's pipeline river and sea crossings. *State analysis and development proposals. Territoriya NEFTEGAZ*. 2013. Issue 11. Pp. 86-91.
18. **Valyshkov I.L.** "Wavemaker" — a long-wave ultrasonic system for pipeline diagnostics and monitoring. *Exposition Neft Gaz*. 2015; 5(44):81-83. (rus.).
19. **Kudryashov S.P., Gaidukevich S.V.** Diagnostics of underwater crossings of Gazprom's trunk gas pipelines. *Gas Industry*. 2018. Issue 53 (778). Pp. 88-89.
20. **Wang P., Chi C., Jiyuan L., Huang H.** Improving performance of three-

dimensional imaging sonars through deconvolution. *Applied Acoustics*. 2021. Vol. 175. P. 107812. DOI: 10.1016/j.apacoust. 2020.107812

21. **Tang Z., Lu J., Wang Z., Ma G.** Three dimensional height information reconstruction based on mobile active sonar detection // *Applied Acoustics*. 2020. Vol. 169. Pp. 107459. DOI: 10.1016/j.apa-coust. 2020.107459
22. **Joe H., Kim J., Yu S.-Ch.** Sensor Fusion-based 3D Reconstruction by Two Sonar Devices for Seabed Mapping // *IFAC-PapersOnLine*. 2019. Vol. 52. Issue 21. Pp. 169-174. DOI: 10.1016/j.ifacol.2019.12.302
23. **Titova Yu.S., Miroshnichenko T.A., Tailenkunova A.S., Kudreshov N.N**. Diagnostics of the condition of trunk gas pipelines crossing water barriers. *Bulletin of scientific conferences*. 2019. Issue 4-2 (44). Pp. 110-115
24. **Zakharov M.N., Martynov D.S.** Determining the maximum displacements of a metal collapsible pipeline from its initial position. Proceedings of Higher Educational Institutions. *Oil and Gas Studies*. 2022; (1): 67-80. https://doi.org/10.31660/0445-0108-2022-1-67-80
25. **Bussugu U.D.** Problems of creating underwater systems for monitoring the condition of marine pipelines. *Bulletin of Science and Education*. 2019; 2-2(56):93-100
26. **Yurieva R.A., Vedernikova K.A., Andreev Yu.S.** Project design and process solutions. Project design and process solutions in the development of robotic systems for pipeline condition monitoring. *Cybernetics and Programming*. 2016. Issue 6. P. 56- DOI 10.7256/2306-4196.2016.6/20982 URL: http:nbpublish.com/library read_article.php?id=20982
27. **Khramenkov S.V., Primin O.G., Orlov V.A.** Pipeline systems restoration. – Moscow: *ASV Publishing*, 2008, 215 pages.
28. **Orlov V.A.** Trenchless technologies and energy conservation. -Moscow: *ASV Publishing*, 2021, 95 p.

СПИСОК ЛИТЕРАТУРЫ

1. **Примин О.Г.** Утечки воды. *ФГБОУ ВО «НИУ МГСУ»*, 2022. 167 с.
2. **Zvirko O., Tsyrulnyk O., Nykyforchyn H.** Non-destructive evaluation of operated pipeline steel state taking into account degradation stage. *Procedia Structural Integrity*. 2020; 26:219-224. DOI: 10.1016/j. prostr.2020.06.025.
3. **Рыльцева Ю.А.** Современные способы и средства диагностики и ремонта подводных переходов трубопроводов // *Вестник МГСУ*. 2021. Т. 16. Вып. 9. С. 1236–1263. DOI: 10.22227/1997-0935.2021.9.1236-1263.].
4. **Bhadran V., Shukla A., Karki H.** Non-contact flaw detection and condition monitoring of subsurface metallic pipelines using magnetometric method. *Materials Today*: Proceedings. 2020; 28:860-864. DOI: 10.1016/j.matpr.2019.12.313.
5. **Chen L., Arzaghi E., Mahdi M., Garaniya V., Abbassi R**. Condition monitoring of subsea pipelines considering stress observation and structural deterioration. *Journal of Loss Prevention in the Process Industries*. 2018; 51:178-185. DOI: 10.1016/j.jlp.2017.12.006
6. **Davis P., Brockhurst J.** Subsea pipeline infrastructure monitoring: A framework for technology review and selection. *Ocean Engineering*. 2015; 104:540-548. DOI: 10.1016/j.oceaneng.2015.04.025
7. **Ивлиев Е.А.** Обнаружение, отслеживание и обследование подводных трубопроводов и кабелей электромагнитными методами. *Подводные исследования и робототехника*. 2009. № 2 (8). С. 22–33.
8. **Yang Q., Sun M., He M., Yang Q.** Evolution features of riverbeds near

underwater crossing line pipes: *An experimental study. Natural Gas Industry B*. 2020. Vol. 7. Pp. 246–253. DOI: 10.1016/j.ngib.2019.10.006

9. **Зезин В.Г., Лазуков В.А.** Определение расхода сплошных сред методом переменного перепада давления.- Челябинск: *Издательство ЮУрГУ*. 2007. 102 с.
10. **Могутин Ю.Б., Гусева О.А., Веселова А.В., Власьев М.В.** Организация подводных сервисных работ на морских нефтегазовых месторождениях. *Судостроение*. 2017. № 3 (832). С. 25–31.
11. **Verde C., Molina L., Carrera R.** Practical Issues of Leaks Diagnosis in Pipelines. *IFAC Proceedings Volumes*. 2011. Vol. 44. Issue 1. Pp. 12337–12342. DOI: 10.3182/20110828-6-IT-1002.01688
12. **Mahmutoglu Y., Turk K.** Positioning of leakages in underwater natural gas pipelines for time-varying multipath environment. *Ocean Engineering*. 2020. Vol. 207. P. 107454. DOI: 10.1016/j.oceaneng.2020.107454
13. **Lu H., Iseley T., Behbahani S., Fu L.** Leakage detection techniques for oil and gas pipelines: State-of-the-art. *Tunnelling and Underground Space Technology*. 2020. Vol. 98. P. 103249. DOI: 10.1016/j.tust.2019.103249
14. **Халлыев Н.Х.** Капитальный ремонт линейной части магистральных газонефтепроводов: *учебное пособие. М.*: Макс Пресс, 2011. 448 с.
15. **Мариненко Е.Е.** Газоснабжение: учебное пособие. Волгоград: *ВолгГАСУ*, 2008. 222 с.
16. **Пашилов М.В.** Мероприятия по обеспечению безопасной эксплуатации морского подводного трубопровода Варандейского нефтеотгрузочного терминала // *Новая наука: современное состояние и пути развития*. 2015. № 5. С. 155–158.
17. **Гайдукевич С.В., Никоненко А.Д., Шалагин В.Н.** Техническое обслуживание речных и морских переходов трубопроводов ОАО «Газпром». *Анализ состояния и предложения по развитию. Территория НЕФТЕГАЗ*. 2013. № 11. С. 86–91.
18. **Valyshkov I.L.** «Wavemaker» — long-wave ultrasonic system for diagnostics and monitoring of pipelines. *Exposition Neft Gaz*. 2015; 5(44):81-83. (rus.).
19. **Кудряшов С.П., Гайдукевич С.В.** Диагностика подводных переходов магистральных газопроводов ПАО «Газпром». *Газовая промышленность*. 2018. № S3 (778). С. 88–89.э
20. **Wang P., Chi C., Jiyuan L., Huang H.** Im-proving performance of three-dimensional imaging sonars through deconvolution. *Applied Acoustics*. 2021. Vol. 175. P. 107812. DOI: 10.1016/j.apacoust. 2020.107812
21. **Tang Z., Lu J., Wang Z., Ma G.** Three dimensional height information reconstruction based on mobile active sonar detection // *Applied Acoustics*. 2020. Vol. 169. Pp. 107459. DOI: 10.1016/j.apa-coust. 2020.107459
22. **Joe H., Kim J., Yu S.-Ch.** Sensor Fusion-based 3D Reconstruction by Two Sonar Devices for Seabed Mapping // *IFAC-PapersOnLine*. 2019. Vol. 52. Issue 21. Pp. 169–174. DOI: 10.1016/j.ifacol.2019.12.302
23. **Титова Ю.С., Мирошниченко Т.А., Тайленкунова А.С., Кудрешов Н.Н.** Диагностика состояния магистральных газопроводов, проходящих через водные преграды. *Вестник научных конференций*. 2019. № 4–2 (44). С. 110–115
24. **Захаров М.Н., Мартынов Д.С.** Определение предельных смещений металлического сборно-разборного трубопровода относительно его начального положения. Известия высших учебных заведений. *Нефть и газ*. 2022; (1):67-80. https://doi.org/10.31660/0445-0108-2022-1-67-80
25. **Bussugu U.D.** Problems of creating underwater systems for monitoring the

condition of marine pipelines. *Bulletin of Science and Education*. 2019; 2-2(56):93-100

26. **Юрьева Р.А., Ведерникова К.А., Андреев Ю.С.** Проектно-конструкторские и технологические решения. Проектно-конструкторские и технологические решения при разработке роботизированных систем контроля состояния трубопроводов. *Кибернетика и программирование*. 2016. № 6. С. 56- DOI 10.7256/2306-4196.2016.6/20982 URL: http:nbpublish.com/library read_article.php?id=20982
27. **Храменков С.В., Примин О.Г., Орлов В.А.** Реконструкция трубопроводных систем.-М: *Издательство АСВ*, 2008, 215 с.
28. **Орлов В.А.** Бестраншейные технологии и энергосбережение.-М: *Издательство АСВ*, 2021, 95 с.

Orlov Vladimir A., Professor, Doctor of Technical Sciences; National Research Moscow State Construction University (NIU MSCU), Russia, 129337, Moscow, 26 Yaroslavskoe Shosse, ph. +7(917) 538-43-16; E-mail: OrlovVA@mgsu.ru.

Орлов Владимир Александрович, профессор, доктор технических наук; Федеральное государственное бюджетное образовательное учреждение высшего образования «Национальный исследовательский Московский государственный строительный университет» (НИУ МГСУ), Россия, 129337, Москва, Ярославское шоссе, 26; тел. +7(917) 538-43-16; E-mail: OrlovVA@mgsu.ru.

Zotkin Sergey P., Professor, Candidate of Technical Sciences; Russia, National Research Moscow State Construction University (NIU MSCU), Russia, 129337, Moscow, 26 Yaroslavskoe Shosse; ph. +7(916) 868-34-48; E-mail: ZotkinSP@mgsu.ru.

Зоткин Сергей Петрович, профессор, кандидат технических наук; Россия, Федеральное государственное бюджетное образовательное учреждение высшего образования «Национальный исследовательский Московский государственный строительный университет» (НИУ МГСУ), 129337, Москва, Ярославское шоссе, 26; тел. +7(916) 868-34-48; E-mail: ZotkinSP@mgsu.ru.

Podolyan Dmitry V., PhD student; National Research Moscow State Construction University (NIU MSCU), Russia, 129337, Moscow, 26 Yaroslavskoe Shosse; ph. +7(917) 543-94-84; E-mail: dim.p-2010@yandex.ru.

Подолян Дмитрий Владимирович, аспирант; Федеральное государственное бюджетное образовательное учреждение высшего образования «Национальный исследовательский Московский государственный строительный университет» (НИУ МГСУ), Россия, 129337, Москва, Ярославское шоссе, 26; тел. +7(917) 543-94-84; E-mail: dim.p-2010@yandex.ru

International Journal for Computational Civil and Structural Engineering, 20(3) 97–115 (2024)

DOI:10.22337/2587-9618-2024-20-3-97-115

RATIONAL DESIGN OF NONLINEAR-DEFORMABLE STRUCTURALLY HETEROGENEOUS ELEMENTS OF STRUCTURES

Andrey V. Mishchenko [1], Maxim S. Veshkin [1], Vladimir L. Mondrus [2], Leonid Yu. Stupishin [2]

[1] Novosibirsk State University of Architecture and Civil Engineering (Sibstrin), Novosibirsk, RUSSIA
[2] National Research Moscow State University of Civil Engineering, Moscow, RUSSIA

Abstract: The article deals with the problem of rational design of a nonlinearly deformable heterogeneous composite Timoshenko rod under force impact. The rod has a structure that is symmetrical relative to the force plane, formed by the connection of quasi-homogeneous parts (phases, layers) with different physical properties, taking any geometric shape in space. The structural materials that form the rod have nonlinear elastic properties. To describe the main component of the stress tensor – the normal stress in the longitudinal direction – in each phase, the same type of approximation by entire rational polynomials is taken depending on the deformation. On their basis, compact nonlinear equations were obtained that connect integral forces with generalized deformations of the axial line of the rod. In this system, the rigidity characteristics of higher exponent are figured as coefficients.
Nonlinear equilibrium conditions written for the case of large displacements and rotation angles in combination with linear kinematic relations are resolved in the form of the initial parameter method.
Based on the strength condition written in the form of a quasi-uniaxial criterion, the designing criterion is formulated for the heterogeneous rod. This criterion is continuous along the longitudinal coordinates and it is discrete along the transverse coordinates. A two-stage algorithm is developed to solve the design problem of the rational design of a nonlinearly deformable layered rod. It makes it possible to identify the geometric functions of the longitudinal profiling of the rod layers presented in a discrete form. Resolution relations were obtained to find the functions of the width and height of the profiled layers.
Numerical results are presented to solve the design problem of calculating a compressed-bent I-section rod, in which the flanges and I-beam webs were made of various materials. The presence of geometric restrictions on variable values from below ensured non-degeneracy of the flanges at the pre-support areas. The three characteristic areas were detected in the rod with the implementation of the calculated continuous criterion in the form of two-, one- and zero-point conditions along the transverse coordinate. It is shown that the consideration of the shear stresses in the rod of this flexibility is not relevant.

Keywords: layered rod, physical nonlinearity, geometric nonlinearity, continuous criterion of strength, rational design

РАЦИОНАЛЬНОЕ ПРОЕКТИРОВАНИЕ НЕЛИНЕЙНО-ДЕФОРМИРУЕМЫХ СТРУКТУРНО-НЕОДНОРОДНЫХ ЭЛЕМЕНТОВ КОНСТРУКЦИЙ

А.В. Мищенко [1], М.С. Вешкин [1], В.Л. Мондрус [2], Л.Ю. Ступишин [2]

[1] Новосибирский государственный архитектурно-строительный университет (Сибстрин), г. Новосибирск, РОССИЯ
[2] Национальный исследовательский Московский государственный строительный университет, г. Москва, РОССИЯ

Аннотация: Рассматривается задача рационального проектирования нелинейно деформируемого неоднородного составного стержня Тимошенко при силовом воздействии. Стержень имеет структуру, симметричную относительно силовой плоскости, образованную соединением различных по физическим свойствам квазиоднородных частей (фаз, слоев), принимающих в пространстве произвольную геометрическую форму. Конструкционные материалы, образующие стержень, обладают нелинейно-упругими свойствами. Для описания основной компоненты тензора напряжений – нормального напряжения про-

дольного направления, в каждой фазе приняты однотипные аппроксимации целыми рациональным полиномами в зависимости от деформации. На их основе получены компактные нелинейные уравнения, связывающие интегральные усилия с обобщенными деформациями осевой линии стержня. В качестве коэффициентов в данной системе фигурируют жесткостные характеристики высших порядков.
Нелинейные условия равновесия, записанные для случая больших перемещений и углов поворота в сочетании с линейными кинематическими соотношениями разрешены в форме метода начальных параметров.
На основе условия прочности, записанного в форме квазиодноосного критерия, для неоднородного стержня сформулирован проектный критерий – непрерывный по продольной и дискретный по поперечной координатам. Разработан двухэтапный алгоритм решения проектной задачи рационального проектирования нелинейно деформируемого слоистого стержня. Он позволяет выявлять представленные в дискретной форме геометрические функции продольного профилирования слоев стержня. Получены разрешающие соотношения для нахождения функций ширины и высоты профилируемых слоев.
Приведены численные результаты решения проектной задачи расчета сжато-изогнутого стержня двутаврового сечения, в котором полки и стенка двутавра были выполнены из различных материалов. Наличие геометрических ограничений на варьируемые величины снизу обеспечивало невырождение полок в приопорных областях. В стержне было выявлено три характерных участка с выполнением расчетного непрерывного критерия в форме двух-, одно- и нульточечного условия по поперечной координате. Показано, что в стержне данной гибкости учет касательных напряжений не является актуальным.

Ключевые слова: слоистый стержень, физическая нелинейность, геометрическая нелинейность, непрерывный критерий прочности, рациональное проектирование

INTRODUCTION

Bearing structures used in construction, as a rule, experience complex thermal power and kinematic effects. The effective consideration of the operational requirements for structures currently dictates the use of new approaches and principles of mathematical modeling. Among them, we highlight the more significant ones, which allow radically increasing the performance of the structures. They are: 1). *The principle of structural heterogeneity* of the designed system, according to which the system is formed of parts (elements, blocks, layers, phases, etc.) made of various materials combined into a single structure. 2). *The principle of rational geometric profiling* of the system elements, as a result of which it acquires a calculated configuration (geometric, physical, structural). The combined use of these two principles allows us to create structural systems with a stress-strain state adapted to external impacts, and, as a result, to ensure regulatory requirements in the best possible way.

A large number of works known in the literature are devoted to the calculation of various heterogeneous structural systems, considering their physical structure (discrete- and dispersive-heterogeneous, reinforced, layered), structural purpose, physical features of the materials deformation, the nature of external impacts [1, 2], the differences in calculation approaches, hypotheses, and research methods. In most works, when solving the direct problems of stress-strain state calculation, the universal finite element method is used [3, 4, 5, 6, 7, 8, 9]. At the same time, analysis methods without the use of discretization procedures are also used to perform research tasks.

For example, [10] discusses the construction of an improved analysis of layered composites using a variation approach, considering piecewise linear displacements and shear effects. In the work [8], a layer-by-layer trigonometric approximation of shear deformations was performed with the satisfaction of the defining physical relations. The proposals to refine the Tymoshenko shear model are proposed in [6, 11]. The methods to homogenize the heterogeneous structures are also widely used [3, 4]. The model of the parametric method of cells, based on the theory of zigzag distributions of displacements by the thickness coordinate, was used in [12] in combination with spline approximations.

Modern materials from which composite systems are made often have nonlinear deformation properties. In order to take into account such effects, the work [13] proposes a universal

method for their description and the formation of physical correlations in heterogeneous rods.

The methods of inverse problems - optimal and rational design - are of a particular interest in the structure design. They are rather complex in combination with the above-mentioned principles of mathematical modeling for heterogeneous designs. They are covered extremely insufficiently in the literature. In this direction, there is a number of works devoted to the search for rational geometry of elements in wooden [14] and concrete [15, 16] structures based on the strength criterion. In the works [17, 18, 19] an energy approach was used to assess the efficiency of the configuration and the internal structure of the construction. The possibilities to significantly increase the strength and rigidity of heterogeneous structures are presented in sources [7, 20, 21], and in work [22] an effective method based on a gradient reinforcement scheme is proposed for a hybrid heterogeneous rod.

It should be noted that the studies devoted to the comprehensive consideration of the above mentioned principles of modeling profiled heterogeneous rod elements of the structures are not presented in the literature.

MATERIALS AND METHODS OF THE RESEARCH

1. Mathematical model of a heterogeneous rod

The heterogeneous rod has a structure formed by the connection of quasi-uniform parts (phases) of finite sizes, different in physical properties, which takes a variety of geometric shapes in space (Fig. 1). With the use of certain technological methods, the phases are combined into a single heterogeneous structure. The rod can be a part of the rod system or be an independent structural element.

In the local coordinate system *xyz*, the longitudinal axis of the *s*-phase rod is aligned with the *x* axis, and the structure has symmetry properties relative to the *xy* plane, in which the rod experiences a straight longitudinal-transverse bend. A straight line having a arbitrary reference to the physical structure specified in a specific calculation is taken as the geometric axis of the rod [13].

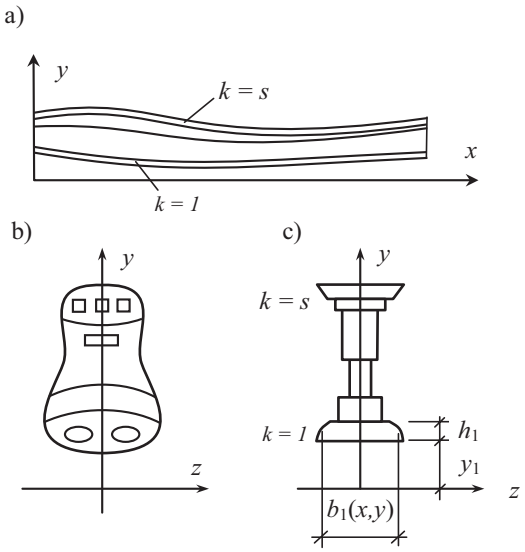


Figure 1. Heterogeneous rod scheme.
a – front projection of the rod in the plane xy,
b, c – variants of the rod cross section

We assume that the following restrictions are met with respect to the physical and geometric parameters of the rod:

1). Rod is thin $(h/l<1/10)$ and submits to the hypotheses of S.P. Timoshenko. The validity of it is confirmed by numerical analysis [23].

2). Structural materials that form the phases of the rod have nonlinear elastic properties described under single-axis stress state in the framework of the deformation theory of plasticity by finite dependences of the form $\sigma_k=\sigma_k(\varepsilon)$, $(k\in[1,s])$, which bind the deformation $\varepsilon=\varepsilon_x$ and conditional stress $\sigma_k=\sigma_{x,k}$ in the material of the k-phase under single-axis stress state. The physical parameters of these dependencies for different materials have values of the same order.

3). When forming the calculated dependencies, the deformations are considered small, and the displacements are considered large values, keeping to the relations

$$\varepsilon_x \ll 1,\ v \ll l,\ \sin\theta \approx \theta,\ \cos\theta \approx 1.$$

The dependences for values of longitudinal ε_x and transverse ε_y deformations, shear strain γ_{yx}, longitudinal u and transverse v displacements of the reference axis points, the angles of rotation of cross sections θ we present in the form

$$\begin{gathered} u(x,y)=u_0-\theta\, y, \quad v(x)=v_0, \\ \varepsilon_x(x,y)=\varepsilon_0-\kappa\, y, \quad \varepsilon_y(x,y)=0, \\ \gamma_{xy}(x,y)=\frac{dv_0}{dx}-\theta=\gamma_0(x), \\ \varepsilon_0(x)=\frac{du_0}{dx}, \quad \kappa(x)=\frac{d\theta}{dx}, \end{gathered} \tag{1}$$

where $u_0(x)$, $v_0(x)$ – displacement of the points of the geometric axis in the direction of the axes x, y; $\varepsilon_0(x)$, $\kappa(x)$ – deformation and curvature of the axis of the rod; $\gamma_0(x)$ – shear strain averaged along the y coordinate.

2. Physical dependencies

The expressions for integral force factors and differential equations of equilibrium of the rod are written in the form

$$\begin{gathered} \left[N,M,Q\right](x)=\sum_{k=1}^{s}\iint_{A_k}\left[\sigma_x^{(k)},-\sigma_x^{(k)}y,\tau_{yx}^{(k)}\right]dA, \\ \frac{dN}{dx}=-q_x, \quad \frac{dQ}{dx}=q_y, \quad \frac{dM}{dx}=Q+m_z. \end{gathered} \tag{2}$$

Here q_x, q_y, m_z – are the distributed forces acting in the direction of the x, y and the moment in the xy plane; A_k – the square of the k-phase in the normal section.

The main component of the stress tensor for the k- phase under force action is represented in the form of decomposition

$$\sigma_x^{(k)}(\varepsilon)=p_{k,0}^{\pm}+p_{k,1}^{\pm}\varepsilon+p_{k,2}^{\pm}\varepsilon^2+\ldots=\sum_{i=0}^{r}p_{k,i}^{\pm}\varepsilon^i, \tag{3}$$

with the specified parameters $p_{k,i}^{+}$, $p_{k,i}^{-}$ for the tensile and compression areas.

The advantage of taking power functions in (3) is that the first three of them with numbers $i=0,1,2,...$ are traditionally used in various theories and have a definite physical meaning. The following allow you to refine the approximations of phase material diagrams. As special cases, the calculation model (3) describes: rigid plastic, linearly elastic, including - multimodule deformation.

When holding in (3) linear and quadratic terms, the power dependence of F.I. Gerstner, $\sigma=E\varepsilon+p\varepsilon^2$, used in [14] for the calculation of wooden frames with shifted centers of cross sections, as well as in the calculations of concrete elements and structures, is obtained, generalized to the case of difference resistance of materials [15, 16].

If the material deformation law can be approximated by an odd function, in (3) it is advisable to hold only terms with odd indices, thereby eliminating the need for special detection of the position of the neutral axis. Acceptance in (3) members with numbers gives the dependencies of A.R. Rzhanitsyn, P.A. Lukash.

Using stress approximations $\sigma_x^{(k)}(\varepsilon)$ *the Ilyushin function* ω_k used in nonlinear calculations can be found, which is entered based on the expression

$$\sigma_x^{(k)}(\varepsilon)=E_k\varepsilon(1-\omega_k). \tag{4}$$

Given that $p_{k,1}^{\pm}=E_k^{\pm}$ we receive

$$\omega_k(\varepsilon)=1-\sum_{i=1}^{r}\frac{p_{k,i}^{\pm}}{p_{k,1}^{\pm}}\varepsilon^{i-1}.$$

Substituting stresses (3) into the first two equations (2) when considering kinematic hypotheses (1), gives a system of nonlinear equations that connects the longitudinal force and the bending moment with generalized deformations ε_0, κ

$$\begin{cases} \sum\limits_{i=0}^{r}\sum\limits_{j=0}^{i}(-1)^j c_{ij} D_{ij} \varepsilon_0^{i-j} \kappa^j = N, \\ -\sum\limits_{i=0}^{r}\sum\limits_{j=0}^{i}(-1)^j c_{ij} D_{ij+1} \varepsilon_0^{i-j} \kappa^j = M. \end{cases} \quad (5)$$

Coefficients in (5) are integral *stiffness characteristics of a cross section of nonlinear elastic materials of i -physical and j-geometric order*.

$$D_{ij}(x) = \sum_{k=1}^{s} p_{k,i}^{\pm} \iint\limits_{A_k} y^j dA = \sum_{k=1}^{s} D_{ij}^{(k)} . \quad (6)$$

Numerical coefficients $c_{i\,j}$ $(j = 0,...,i)$ – are *the Newton binomiall* coefficients $(a+b)^j$.

Calculating rigidity of the k-phase $D_{ij}^{(k)}$ in (6) it is necessary to perform an additional height breakdown $h_k = h_k^+ + h_k^-$ at the intersection of the layer with the neutral axis on the areas with the same deformation sign

$$D_{ij}^{(k)} = p_{k,i}^{+} \int\limits_{h_k^+} b_k(x,y) y^j dy + p_{k,i}^{-} \int\limits_{h_k^-} b_k(x,y) y^j dy .$$

The system of physical equations (5) is a generalization of known classical cases. Thus, when $r = 0$, the equations contain rigidity

$$D_{00} = \sum_{k=1}^{s} (\pm \sigma_{k,s}^{\pm} A_k), \quad D_{01} = \sum_{k=1}^{s} (\pm \sigma_{k,s}^{\pm} S_k)$$

and describe the limit states of the layered section made of rigid plastic materials.

When holding in (3) linear members, the system (5) becomes quasi-linear with rigidity characteristics of the heterogeneous section from linearly elastic different-module materials

$$D_{10} = \sum_{k=1}^{s} E_k^{\pm} A_k , \quad D_{11} = \sum_{k=1}^{s} E_k^{\pm} S_k ,$$

$$D_{12} = \sum_{k=1}^{s} E_k^{\pm} I_k .$$

If you additionally perform reduction to the central axes (which gives $D_S = 0$, but it is not advisable when you solve inverse problems of the design type), we get the solution of S.P. Timoshenko.

Depending on the properties of phase materials, different (not necessarily sequential) sets of homogeneous blocks can be used in (5).

When organizing numerical procedures in iterative algorithms, physical dependencies (3) are presented in quasi-linear form

$$\sigma_x^{(k)}(\varepsilon) = \overline{E}_k(\varepsilon) \cdot \varepsilon \quad (7)$$

with variable secant elastic module depending on the deformation

$$\overline{E}_k(\varepsilon) = \sum_{i=0}^{r} p_{k,i}^{\pm} \varepsilon^{i-1} . \quad (8)$$

Applying expression (7) for forces (2) gives the system of quasi-linear equations

$$\begin{cases} \overline{D}_A \varepsilon_0 - \overline{D}_S \kappa = N, \\ -\overline{D}_S \varepsilon_0 - \overline{D}_I \kappa = M, \end{cases} \quad (9)$$

with functional *secant stiffness characteristics* $\overline{D}$

$$\left[\overline{D}_A, \overline{D}_S, \overline{D}_I\right](x,\varepsilon) =$$

$$= \sum_{i=1}^{r}\sum_{j=0}^{i-1}(-1)^j c_{i-1,j} \left[D_{i\,j}, D_{i\,j+1}, D_{i\,j+2}\right] \varepsilon_0^{i-j-1} \kappa^j , \quad (10)$$

depending on generalized deformations ε_0, κ.

In expressions (10) higher-exponent characteristics are used (6).

For odd cubic approximation $\sigma_x^{(k)} = p_{k,1}^{\pm} \varepsilon + p_{k,3}^{\pm} \varepsilon^3$ stiffness expressions (10) take the form

$$\begin{aligned} \overline{D}_A &= D_{10} + \varepsilon_0^2 D_{30} - 2\varepsilon_0 \kappa D_{31} + \kappa^2 D_{32}, \\ \overline{D}_S &= D_{11} + \varepsilon_0^2 D_{31} - 2\varepsilon_0 \kappa D_{32} + \kappa^2 D_{33}, \\ \overline{D}_I &= D_{12} + \varepsilon_0^2 D_{32} - 2\varepsilon_0 \kappa D_{33} + \kappa^2 D_{34}. \end{aligned} \quad (11)$$

3. Shear stress

Obtaining shear stresses under equilibrium conditions, with non-linear dependencies (3), is a laborious procedure that is not advisable for secondary stress components of energy significance. More efficient and consistent with the initial assumptions is an alternative approach based on the equilibrium condition of the upper displaced part of $y \in [y, y_{s+1}]$ the rod element with a length of *dx*

$$\tau_{yx}^{(k)}(x,y) = \\ = -\frac{1}{b_k(x,y)}\frac{\partial}{\partial x}\left(\int_{y}^{y_{s+1}(x)} \sigma_x(x,y)b(x,y)dy\right). \quad (12)$$

We approximate the linear shear force (derivative of the integral in (12)) in the form

$$\frac{\partial N^{\text{sec}}(x,y)}{\partial x} = b_0\tau_0(x)f_\tau(y) \quad (13)$$

using a dimensionless function of the transverse distribution of shear forces $f_\tau(y)$, that satisfies the boundary conditions $f_\tau(y_1) = f_\tau(y_{s+1}) = 0$. The parameter $\tau_0(x)$ characterizes the longitudinal distribution of shear forces, and b_0 is a geometric parameter. Combining (12), (13), excluding the parameter τ_0 using condition (2) we obtain the formula of the shear stress

$$\tau_{yx}^{(k)}(x,y) = \frac{Q(x)}{b_k(x,y)}\frac{f_\tau(y)}{F_\tau}, \quad F_\tau = \int_{y_1}^{y_{s+1}} f_\tau dy. \quad (14)$$

In heterogeneous structures which have fragments of Z-layering (Fig. 2), for which lines $y(z) = \text{const}$ cross different phases, the formula (14) should be improved by introducing the shear stiffness coefficient at the *y* level

$$k_\tau(y,z) = \frac{G_k(y,z)}{\sum_j G_k(y,z)b_j(y)}.$$

Here, the summation is performed on the phases crossed by the line $y(z) = \text{const}$. Assuming, in accordance with the accepted hypotheses, the constancy of shears (1), we obtain shear stresses in Z-layered structures

$$\tau_{yx}^{(k)}(x,y,z) = \frac{Q(x)f_\tau(y)}{F_\tau}\frac{G_k(y,z)}{\sum_j G_j(y,z)b_j(x,y)}.$$

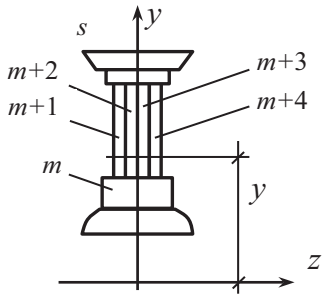


Figure 2. Cross-layered structure with Z-layered fragment

When the shear stiffness of the section is found, we assume the equivalence of the Ilyushin functions in the dependencies (4) and in the law for shear stresses, by

$$\tau_{yx}^{(k)} = G_k(1-\omega_k)\gamma_{yx}.$$

The increment of the elastic deformation energy in the heterogeneous section during the shear is presented in two forms: through the integral force *Q* and stress $\tau_{yx}^{(k)}$

$$Q\Delta\gamma_0 = \sum_{k=1}^{s}\iint_{A_k}\tau_{yx}^{(k)}\Delta\gamma_{yx}dA. \quad (15)$$

Here $\Delta\gamma_0 = \Delta Q / \bar{D}_Q(\gamma)$ is the deformation increment of the average shear in the Timoshenko rod, $\bar{D}_Q$ is section shear stiffness, $\Delta\gamma_{yx}(x,y) = \Delta\tau_{yx}^{(k)} / G_k / (1-\omega_k)$ – shear strain increment at a heterogeneous section point. Substituting stress (14) into (15), we obtain variable *secant shear stiffness*

$$\bar{D}_Q = \frac{F_\tau^2}{\sum_{k=1}^{s} \int_{y_k}^{y_{k+1}} \frac{f_\tau^2}{b_k G_k (1-\omega_k)} dy}, \qquad (16)$$

with which the third physical relation is recorded

$$\bar{D}_Q \gamma_0 = Q, \qquad (17)$$

complements the system of equations (5), and binds shear strain γ_0 with transverse force Q.

4. Relations for internal forces and displacements

The differential equations of equilibrium of the rod in the deformed state are

$$\begin{cases} N' + (\theta Q)' = -q_x, \\ Q' - (\theta N)' = q_y, \\ M' = Q + m_z, \end{cases} \qquad (\ldots)' = \frac{\partial}{\partial x}.$$

Their integration considering small values of the first order when the following conditions are satisfied

$$N(0) = N_0 - Q_0\theta_0, \quad Q(0) = Q_0 + N_0\theta_0, \quad M(0) = M_0$$

gives the expressions of internal force factors in the form of the initial parameters method. Applying the method of iterative refinement, we write them for the t-step in the form

$$\begin{aligned} N^{[t]}(x) &= N_0^{[t]} - Q_0^{[t]}\theta^{[t-1]} - F_x - \theta^{[t-1]}F_y - \\ &- \int_{x_{qx}}^{x} q_x dx - \theta^{[t-1]} \int_{x_{qy}}^{x} q_y dx, \\ Q^{[t]}(x) &= N_0^{[t]}\theta^{[t-1]} + Q_0^{[t]} - \theta^{[t-1]}F_x + F_y - \\ &- \theta^{[t-1]} \int_{x_{qx}}^{x} q_x dx + \int_{x_{qy}}^{x} q_y dx, \end{aligned} \qquad (18)$$

$$\begin{aligned} M^{[t]}(x) &= M_0^{[t]} + N_0^{[t]}v^{[t-1]} + Q_0^{[t]}x + M_z + \int_{x_m}^{x} m_z dx + \\ &+ F_y(x - x_{F_y}) - F_x[v^{[t-1]}(x) - v^{[t-1]}(x_{F_x})] - \\ &- \int_{x_{qx}}^{x} q_x(\xi)[v^{[t-1]}(x) - v^{[t-1]}(\xi)]d\xi + \int_{x_{qy}}^{x} q_y(\xi)(x-\xi)d\xi. \end{aligned}$$

In case there are several similar loads on the rod, in (18) several terms of the corresponding type should be used. The differentiation of the influence areas of loads is completed with the use of the Heaviside step function (to reduce the entry not specified in (18)).

The determination of displacements is performed using quasi-linear equations (9). Expressing from (9), (17) generalized deformations through *secant section pliability*

$$\bar{\delta}_A = \frac{1}{\bar{D}_A - \bar{D}_S^2/\bar{D}_I}, \quad \bar{\delta}_S = \frac{\bar{D}_S}{\bar{D}_I\bar{D}_A - \bar{D}_S^2}, \quad \bar{\delta}_I = \frac{1}{\bar{D}_I - \bar{D}_S^2/\bar{D}_A}, \quad \delta_Q = \frac{1}{\bar{D}_Q} \qquad (19)$$

and substituting them into kinematic dependencies (1), we obtain the angle of rotation and displacements at t-step

$$\begin{aligned} \theta^{[t]}(x) &= \theta_0^{[t]} + \int_0^x \delta_S^{[t-1]} N^{[t-1]} dx + \int_0^x \delta_I^{[t-1]} M^{[t-1]} dx, \\ u^{[t]}(x) &= u_0^{[t]} + \int_0^x \delta_A^{[t-1]} N^{[t]} dx + \int_0^x \delta_S^{[t-1]} M^{[t]} dx, \\ v^{[t]}(x) &= v_0^{[t]} + \theta_0^{[t]}x + \int_0^x\int_0^x \delta_S^{[t-1]} N^{[t-1]} dxdx + \\ &+ \int_0^x\int_0^x \delta_I^{[t-1]} M^{[t-1]} dxdx + \int_0^x \delta_Q^{[t-1]} Q^{[t-1]} dx. \end{aligned} \qquad (20)$$

Substituting here the internal forces (18) gives the final expressions of displacements (they are not given here), which depend on the initial parameters $N_0^{[t]}$, $Q_0^{[t]}$, $M_0^{[t]}$, $u_0^{[t]}$, $\theta_0^{[t]}$, $v_0^{[t]}$, loads,

secant pliability (19) and displacements in the previous step.
Initial parameters are from six boundary conditions

$$N^{[t]}(x_*)+\theta^{[t-1]}(x_*)Q^{[t]}(x_*)=\mp F_{x^*},$$
$$\theta^{[t-1]}(x_*)N^{[t]}(x_*)-Q^{[t]}(x_*)=\mp F_{y^*},$$
$$M^{[t]}(x_*)=\pm m_{z^*}, \qquad (21)$$

when recording which the upper signs are used on the left end, and the lower signs on the right.

5. Rational design of layered rod based on continuous strength criterion

In a cross-layered rod at a given force effect, it is required to determine a particular set of geometric functions from the full set

$$r_k(x),\ \ r\in[b,h],\ \ (k=1,...,s), \qquad (22)$$

internal force factors (18) and displacements (20), satisfying boundary conditions (21). In addition, geometric functions must satisfy the constraints

$$r_k \ge r_{\min},\quad r\in[b,h]. \qquad (23)$$

The strength condition of the material of the *k*-layer with the calculated resistance R_k is presented in the form

$$\frac{1+\phi_k}{2}\sqrt{\sigma_x^2+\beta_k\tau_{yx}^2}+\frac{1-\phi_k}{2}\left|\sigma_x\right|\le R_k^{\pm}.$$

Presenting stresses σ_x and R_k with the use of (7) through secant moduli of elasticity

$$\overline{E}_k(\varepsilon)=\frac{\sigma_x^{(k)}}{\varepsilon},\quad \overline{E}_k(\varepsilon_{\text{adm}}^{(k)})=\frac{R_k}{\varepsilon_{\text{adm}}^{(k)}}, \qquad (24)$$

we obtain the strength condition recorded through the deformation

$$\operatorname{sgn}(\varepsilon_x)\,\varepsilon_x(x,y)\le\mu_\tau^{(k)}\mu_\varepsilon^{(k)}\varepsilon_{\text{adm}}^{(k)\pm},\ (k=1,...,s). \qquad (25)$$

Here $\varepsilon_{\text{adm}}^{(k)\pm}$ is allowable deformation levels of the material of the *k*-layer under tensile and compression;

$$\mu_\tau^{(k)}(x,y)=$$
$$=\frac{1}{2\phi_k}\left[(1+\phi_k)\sqrt{1-\phi_k\beta_k\left(\frac{\tau_{yx}(x,y)}{R_k^{\pm}}\right)^2}+\phi_k-1\right] \qquad (26)$$
$$\mu_\tau^{(k)}(x,y)\in(0,1]-$$

the coefficient considering the decrease of the allowable material deformation $\varepsilon_{\text{adm}}^{(k)\pm}$ at shear stresses; and

$$\mu_\varepsilon^{(k)}(x,y)=\frac{\overline{E}_k(\varepsilon_{\text{adm}}^{(k)\pm})}{\overline{E}_k(\varepsilon)}\in(0,1]- \qquad (27)$$

the coefficient reflecting non-linearity of stress function $\sigma_x(\varepsilon)$, recorded through secant moduli of elasticity at finite (limit) and current points (24).
Based on the strength condition for the biaxial stress state (25), determine the *continuous multipoint design* criterion (CDC) of the heterogeneous non-linearly deformed the *s*-phase rod.
Definition. The generalized limit state in the area of heterogeneous nonlinear elastic rod that occupies the space *X*, *Y*, is realized if condition (25) is performed in the form of the strict equality

$$\operatorname{sgn}(\varepsilon_x)[\varepsilon_0(x)-\kappa(x)y]=\mu_\tau^{(k)}\mu_\varepsilon^{(k)}\varepsilon_{\text{adm}}^{(k)\pm},$$
$$x\in X,\quad y=\xi_1,...,\xi_{n_y}=Y_*\in Y$$

continuously along the longitudinal coordinate $x\in X$, in discrete number of levels n_y along transverse coordinate $y=\xi_1,...,\xi_{n_y}=Y_*\in Y$. For all other points $x\in X$, $y\notin Y_*$ condition (25) is real in the form of inequality.
The multiplicity Y_* in the cross-layered structures is typically formed from the layer interfaces $y_1,...,y_{s+1}$. The multiplicity of the criterion

n_y depending on the conditions of the problem, takes values from 1 to $s+1$, while the criterion is referred to as n_y - point CDC. In general, to satisfy these equalities, except for the varying geometric functions, requires a change in the physical structure of the rod. For fixed-structure rods, the maximum multiplicity n_y is two.

Application *s*+1- and *s* - point criterion. As $s+1$ variable parameters (22) we take the width of external layers b_1, b_s and the height h_k of all, except one, layers ($k=1,..,k_0-1,k_0+1,..s$). The height h_{k_0} and width of the inner layers are set. According to CDC we compose a system $n_y=s+1$ of equations (23), for certainty, considering the case of different-valued deformations in the section with a change of sign within the layer k_0

$$\begin{cases} \varepsilon_0(x)-\kappa(x)y_1=\pm\mu_\tau^{(1)}\mu_\varepsilon^{(1)}\varepsilon_{\text{adm}}^{(1)\pm}, \\ \ldots\ldots\ldots \\ \varepsilon_0(x)-\kappa(x)y_{k_0}=\pm\mu_\tau^{(k_0)}\mu_\varepsilon^{(k_0)}\varepsilon_{\text{adm}}^{(k_0)\pm}, \\ \varepsilon_0(x)-\kappa(x)y_{k_0+1}=\mp\mu_\tau^{(k_0)}\mu_\varepsilon^{(k_0)}\varepsilon_{\text{adm}}^{(k_0)\mp}, \\ \ldots\ldots\ldots \\ \varepsilon_0(x)-\kappa(x)y_{s+1}=\mp\mu_\tau^{(s)}\mu_\varepsilon^{(s)}\varepsilon_{\text{adm}}^{(s)\mp}. \end{cases} \quad (28)$$

Here, with positive (negative) curvature, the upper (lower) signs are taken. The relationships for other types of strain distribution are also written analogically. With unambiguous distributions k_0 and k_0+1 both equations are replaced by one, and the criterion becomes the *s*-point. At the same time, the height of one of the layers is excluded from the variable parameter.

The solution of the problem will be performed with phased accounting of the values of the coefficients $\mu_\tau^{(k)}(x,y)$, $\mu_\varepsilon^{(k)}(x,y)$ at the computational points. At the first stage, their values are taken equal to one.

▪ Using k_0 and k_0+1 the equations of the system (28), we determine the curvature and deformation

$$\kappa_*(x)=\frac{\pm\mu_\tau^{(k_0)}\mu_\varepsilon^{(k_0)}\varepsilon_{\text{adm}}^{(k_0)\pm}\pm\mu_\tau^{(k_0)}\mu_\varepsilon^{(k_0)}\varepsilon_{\text{adm}}^{(k_0)\mp}}{h_{k_0}},$$
$$\varepsilon_{0*}=\frac{\pm\mu_\tau^{(k_0)}\mu_\varepsilon^{(k_0)}\varepsilon_{\text{adm}}^{(k_0)\pm}y_{k_0+1}\pm\mu_\tau^{(k_0)}\mu_\varepsilon^{(k_0)}\varepsilon_{\text{adm}}^{(k_0)\mp}y_{k_0}}{h_{k_0}} \quad (29)$$

Then, using the remaining equations, we find $(s-1)$ of the desired heights

$$h_{k+1}=\frac{\pm\mu_\tau^{(k_0)}\mu_\varepsilon^{(k_0)}\varepsilon_{\text{adm}}^{(k+1)\mp}\mp\mu_\tau^{(k_0)}\mu_\varepsilon^{(k_0)}\varepsilon_{\text{adm}}^{(k)\mp}}{\kappa_*},$$
$$k=k_0,..,s-1, \quad (30)$$
$$h_{k-1}=\frac{\pm\mu_\tau^{(k_0)}\mu_\varepsilon^{(k_0)}\varepsilon_{\text{adm}}^{(k-1)\pm}\mp\mu_\tau^{(k_0)}\mu_\varepsilon^{(k_0)}\varepsilon_{\text{adm}}^{(k)\pm}}{\kappa_*},$$
$$k=k_0,..,2.$$

If received $h_k<0$ we need to change the physical structure of the package or reduce the multiplicity of the criterion.

▪ The internal force factors at the *t*-step in the design area are written in the form (18), and the functions of displacements and rotation angles, assuming $\varepsilon_0=\varepsilon_{0*}$, $\kappa=\kappa_*$, in the form

$$u^{[t]}(x)=u_0^{[t]}+\int_0^x\varepsilon_{0*}^{[t]}dx,\quad \theta^{[t]}(x)=\theta_0^{[t]}+\int_0^x\kappa_*^{[t]}dx,$$

$$v^{[t]}(x)=v_0^{[t]}+\theta_0^{[t]}x+\int_0^x dx\int_0^x\kappa_*^{[t]}dx-Q_0^{[t]}\int_0^x\delta_Q^{[t-1]}dx-$$

$$-F_y\int_{x_{Fy}}^x\delta_Q^{[t-1]}dx-\int_{x_{q_y}}^x\delta_Q^{[t-1]}\int_{x_{q_y}}^x q_y dxdx.$$

▪ Physical relations (5), when substituting limit generalized deformations (29), give a system of equations to determine the two remaining variable parameters

$$\begin{cases} \Psi_N(N,\varepsilon_{0*},\kappa_*,b_1,b_s,h_1,...,h_s,x)=0, \\ \Psi_M(M,\varepsilon_{0*},\kappa_*,b_1,b_s,h_1,...,h_s,x)=0. \end{cases} \quad (31)$$

▪ Calculation of stiffness characteristics $\bar{D}_A$, $\bar{D}_S$, $\bar{D}_I$ (10), $\bar{D}_Q$, shear (14) and normal stresses

$$\sigma_x^{(k)}(x,y)=\sum_{i=0}^{r} p_{k,i}^{\pm}[\varepsilon_0(x)-\kappa(x)y]^i .$$

▪ Verification of constraint (23) and criteria to achieve the required accuracy of calculations.

Application of two-point criterion. As variable parameters, any two *geometric functions* from set (22) are accepted. In this case, a two-point CDC and a system (23) are used in the form of two equations recorded for the two $\xi_1, \xi_2 = Y_*$ most dangerous levels

$$\varepsilon_{0*}-\kappa_* y_i = \pm\mu_\tau^{(k)}\mu_\varepsilon^{(k)}\varepsilon_{\text{adm}}^{(k)\pm}, \qquad (32)$$
$$i=\xi_1,\ \xi_2, \quad x\in X_*, \quad y_i\in Y_*.$$

The difference between two-point setting is the ability to perform the solution for any given physical structure of the layered package.

After determination of limit deformation and curvature from (32), further steps bypassing (30), are performed similarly to the procedure for multipoint criterion.

The obtained solution is realized if the obtained geometric functions continuously along the x coordinate satisfy the problem constraints (23). Otherwise, we need to decrease the multiplicity and switch to the single-point criterion ($n_y=1$).

Then, for the corresponding function (for example, the first one), the equality is assumed

$$r_{i,k_1}(x)=r_{\min} \qquad (33)$$

with simultaneous setting of deformation

$$\varepsilon_{i,\xi_2}(x)=\pm\mu_\tau^{(k)}\mu_\varepsilon^{(k)}\varepsilon_{\text{adm},\xi_2}^{(k)\pm}. \qquad (34)$$

Substituting (33), (34) into (31) gives a mixed system of resolving equations for the geometric function $r_{k_2}(x)$ and deformation $\varepsilon_{i,\xi_1}(x)$:

$$\begin{cases}\Psi_N(N_i,\varepsilon_{i,\xi_1},r_{i,k_2},x)=0,\\ \Psi_M(M_i,\varepsilon_{i,\xi_1},r_{i,k_2},x)=0.\end{cases}$$

If the two constraints cannot be satisfied (23), a zero-point ($n_y=0$) inequality criterion (25) is applied at the area. Taking in this case for the desired geometric equality functions

$$r_{i,k_1}(x)=r_{\min}, \quad r_{i,k_2}(x)=r_{\min},$$

we have a direct formulation of the problem.

Scheme to solve the problem of rational design. Using preliminary information about the stress-strain state of the rod, we will select sections in it (with indefinite boundaries) with the implementation of CDC of various degrees of multiplicity. Then we add to them the areas with the same laws of effort. The total number of areas is denoted by n_u. For each of them, based on (18), (20), we compose expressions of efforts and displacements containing constants $N_{i,0}$, $Q_{i,0}$, $M_{i,0}$, $u_{i,0}$, $\theta_{i,0}$, $v_{i,0}$ ($i=1,...,n_u$). Secant pliability (19) and displacements in the right parts should be considered known according to the calculation results at the previous step.

To determine $6n_u$ the constant, $n_y n_u$ of variable functions and n_u-1 boundaries of the areas, we will form groups of conditions. *The first group* of conditions, a total number $7n_u-1$, is invariant to the type of the design criterion and consists of six boundary conditions for the rod as a whole (21) and $6(n_u-1)$ conditions for the conjugation of power and kinematic functions at the boundaries of the areas. This group of conditions is supplemented, formed on the basis of constraints (23), n_u-1 equation to define x_i – boundaries of the area,

$$r_i(x_i)=r_{\min}, \quad i=1,...,n_u-1, \quad r\in[b,h].$$

The second group of $n_y n_u$ conditions depending on the accepted design criterion, is represented

by n_y equations (23), (31) for each of n_u design areas.

6. Forms of resolving equations

Varying the width of the layers. The desired functions of the width of two layers with numbers k_1, k_2 we set in the form

$$b_k(x,y) = b_k^x(x)\,\overline{b}_k^{\,y}(y), \quad (k = k_1, k_2)$$

with the desired layer width function $b_k^x(x)$ and the defined dimensionless transverse profiling function $\overline{b}_k^{\,y}(y)$.

The resolution system (31), derived from the physical equalities (9), takes the form

$$\begin{cases} \varphi_{11} b_{k_1}^x + \varphi_{12} b_{k_2}^x = \varphi_1(x), \\ \varphi_{21} b_{k_1}^x + \varphi_{22} b_{k_2}^x = \varphi_2(x), \end{cases} \tag{35}$$

$$\varphi_{11} = \sum_{i=1}^{r}\sum_{j=0}^{i} (-1)^j c_{i,j} \varepsilon_{0*}^{i-j} \kappa_*^j \overline{D}_{i,j}^{(k_1)},$$

$$\varphi_{12} = \sum_{i=1}^{r}\sum_{j=0}^{i} (-1)^j c_{i,j} \varepsilon_{0*}^{i-j} \kappa_*^j \overline{D}_{i,j}^{(k_2)},$$

$$\varphi_{21} = -\sum_{i=1}^{r}\sum_{j=0}^{i} (-1)^j c_{i,j} \varepsilon_{0*}^{i-j} \kappa_*^j \overline{D}_{i,j+1}^{(k_1)},$$

$$\varphi_{22} = -\sum_{i=1}^{r}\sum_{j=0}^{i} (-1)^j c_{i,j} \varepsilon_{0*}^{i-j} \kappa_*^j \overline{D}_{i,j+1}^{(k_2)},$$

$$\varphi_1 = N - \sum_{i=1}^{r}\sum_{j=0}^{i} (-1)^j c_{i,j} \varepsilon_{0*}^{i-j} \kappa_*^j \overline{D}_{i,j}^{(0)},$$

$$\varphi_2 = M + \sum_{i=1}^{r}\sum_{j=0}^{i} (-1)^j c_{i,j} \varepsilon_{0*}^{i-j} \kappa_*^j \overline{D}_{i,j+1}^{(0)},$$

$$\overline{D}_{ij}^{(k)} = p_{k,i}^{\pm} \int_{h_k} \overline{b}_k^{(y)} y^j dy,$$

$$D_{ij}^{(0)}(x) = \sum_{k \notin k_1, k_2} p_{k,i}^{\pm} \int_{h_k} b_k^x(x,y) y^j dy.$$

Varying the height of the layers. When varying the heights $h_{k_1}(x)$, $h_{k_2}(x)$ of the numbered layers k_1, k_2 we obtain a non-linear system of resolution equalities (31) of degree $n_g + 1$, where n_g – is the highest geometric order of the stiffness characteristic (6). Matrix of Jacobi, used in solving system (31) has components

$$\frac{\partial \Psi_N}{\partial h_l} = \sum_{i=0}^{\eta}\sum_{j=0}^{i} (-1)^j c_{ij} \frac{\partial D_{ij}}{\partial h_l} \varepsilon_{0*}^{i-j} \kappa_*^j,$$

$$\frac{\partial \Psi_M}{\partial h_l} = \sum_{i=0}^{\eta}\sum_{j=0}^{i} (-1)^{j+1} c_{ij} \frac{\partial D_{ij+1}}{\partial h_l} \varepsilon_{0*}^{i-j} \kappa_*^j, \tag{36}$$

$$(l = k_1, k_2)$$

$$\frac{\partial D_{ij}}{\partial h_l} = \sum_{k=1}^{s} p_{k,i}^{\pm} \left[\frac{\partial y_{k+1}}{\partial h_l} b_k(x, y_{k+1}) y_{k+1}^j - \frac{\partial y_k}{\partial h_l} b_k(x, y_k) y_k^j \right].$$

Depending on the number of the variable layer and the position of the reference surface, we have derivatives $\partial y_k / \partial h_l = -1, 0, 1$. For example, for a three-layer section that has the dimensions of rectangular sections of layers: $b_k(x)$, $h_k(x)$ ($k = 1,2,3$), of which all functions are defined, and $h_1(x)$ and $h_3(x)$ are to be determined, taking on the basis of (3) the quadratic law, binding the reference surface to the middle of the inner layer, we obtain

$$[y_1, y_2, y_3, y_4] =$$

$$= [-h_1 - 0{,}5h_2; -0{,}5h_2; 0{,}5h_2; 0{,}5h_2 + h_3]$$

$$\frac{\partial}{\partial h_1}[y_1, y_2, y_3, y_4] = [-1; 0; 0; 0],$$

$$\frac{\partial}{\partial h_1}[D_{10}, D_{11}, D_{12}](x) = p_{11} b_1 [1, y_1, y_1^2],$$

$$\frac{\partial}{\partial h_3}[y_1, y_2, y_3, y_4] = [0; 0; 0; 1],$$

$$\frac{\partial}{\partial h_3}[D_{10}, D_{11}, D_{12}](x) = p_{31} b_3 [1, y_4, y_4^2],$$

$$\frac{\partial}{\partial h_1}[D_{20}, D_{21}, D_{22}, D_{23}](x) = p_{12} b_1 [1, y_1, y_1^2, y_1^3],$$

$$\frac{\partial}{\partial h_3}[D_{20}, D_{21}, D_{22}](x) = p_{32} b_3 [1, y_4, y_4^2].$$

Thus we obtain the components of Matrix of Jacobi (36)

$$\frac{\partial \Psi_N}{\partial h_1} = p_{11} b_1 (\varepsilon_{0*} - \kappa_* y_1) + p_{12} b_1 (\varepsilon_{0*} - \kappa_* y_1)^2,$$

$$\frac{\partial \Psi_N}{\partial h_3} = p_{31} b_3 (\varepsilon_{0*} - \kappa_* y_4) + p_{32} b_3 (\varepsilon_{0*} - \kappa_* y_4)^2,$$

$$\frac{\partial \Psi_M}{\partial h_1} = -p_{11} b_1 y_1 (\varepsilon_{0*} - \kappa_* y_1) - p_{12} b_1 y_1 (\varepsilon_{0*} - \kappa_* y_1)^2,$$

$$\frac{\partial \Psi_M}{\partial h_3} = -p_{31} b_3 y_4 (\varepsilon_{0*} - \kappa_* y_4) - p_{32} b_3 y_4 (\varepsilon_{0*} - \kappa_* y_4)^2.$$

RESULTS AND DISCUSSION

Fig. 3 shows the design scheme of the compressed-bent rod. We assume that initially the rod was homogeneous, it had a prismatic shape with a rectangular cross section. Then, in order to increase the bearing capacity, it was strengthened by adding two outer plates made of another (stronger) material. As a result, the rod took the form of a heterogeneous I-beam.

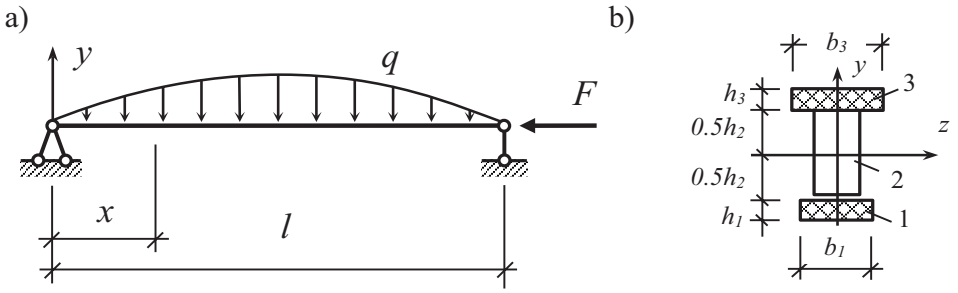


Figure 3. Design scheme of the compressed-bent rod (a); cross section (b)

Table. Data on the geometric and physical parameters of the layered rod

k	Type of the material	$p_{k,1}$ hPa	$p_{k,3}$ hPa	$\varepsilon_{adm}^{(k)}$	b_k mm	h_k mm
1	1	22	-162000	0,0053	$b_1(x)$	10
2	2	11	-105000	0,0045	50	300
3	1	22	-162000	0,0053	$b_1(x)$	10

It is required, at given loads, structure and materials, to perform rational profiling of the width $b_1(x)$, $b_3(x)$ of the outer layers using two-point strength criterion (32) and the satisfaction of limitations (23): $b_1(x) \geq b_{\min}$, $b_3(x) \geq b_{\min}$. Minimum values of the width are defined $b_{\min} = b_2$.

The rod with the length $l = 6$ m is loaded with axial force $F = 60$ kN and transverse load of variable intensity $q = 18\sin(\pi x / l)$ kN/m. The y axis is compatible with the force plane, and the x axis is compatible with the center axis of the inner ($k = 2$) layer. The diagrams of material deformation of I-beam elements are represented by identical symmetric cubic dependencies $\sigma_x^{(k)} = p_{k,1}\varepsilon + p_{k,3}\varepsilon^3$ (3) with two parameters. Table shows the physical and geometric parameters of the three layers, fig. 4 shows the approximations of the function $\sigma(\varepsilon)$ with the limit points marked.

The stress-strain state functions of the rod are represented in discrete form at m = 21 design points

$$\Phi \in [N, Q, M, \theta, v, \varepsilon_0, \kappa, b].$$

The solution of the design problem is possible to comply on the basis of a two-stage algorithm. *The first stage* is to solve *the direct problem* on the basis of physical and geometric nonlinearity with fixed design parameters – discrete functions b_1, b_3. At this stage, secant stiffness characteristics (11), which depend on generalized deformations

and internal forces, are specified iteratively. The latter depends on movements and rotation angles.

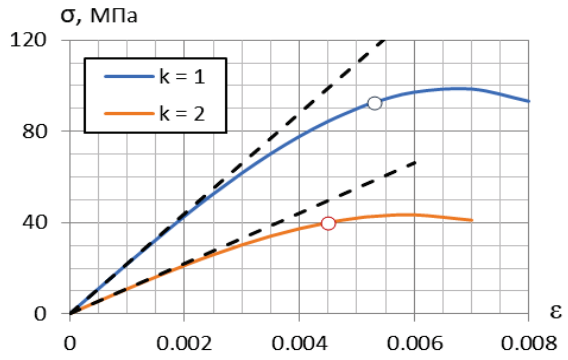


Figure 4. Graphs $\sigma_x(\varepsilon)$ *for the material of the I-beam flange (k = 1) and the wall (k = 2)*

Considering boundary conditions

$$N_0 = -F\,,\quad Q_0 = \frac{q_0 l}{\pi}\,,\quad M_0 = 0\,,$$

using expressions (18) for t_1-step we obtain the calculated expressions of internal forces

$$N^{[t_1]}(x) = -F - \frac{q_0 l}{\pi}\theta^{[t_1-1]}\cos\frac{\pi x}{l}\,,$$
$$Q^{[t_1]}(x) = \frac{q_0 l}{\pi}\cos\frac{\pi x}{l} - F\theta^{[t_1-1]}\,, \qquad (37)$$
$$M^{[t_1]}(x) = -Fv^{[t_1-1]} + \frac{q_0 l^2}{\pi^2}\sin\frac{\pi x}{l}\,.$$

At *the second stage (design stage)* solution of the system of equations (35) the discrete design functions are obtained b_1, b_3 considering the calculated (32) on the limit values of generalized deformations ε_{0*}, κ_*. At this stage, the internal forces are taken from the previous stage. Further, the constraints (23) are checked and, if they are violated for one or (and) another parameter in the interval $x \in X_r$, the equality is accepted $b_{k,j} = b_{\min}$ ($k = 1, 3$; $j \in X_r$). The final check of the calculation is the control of accuracy achievement of iterative calculation of the required parameters values of the width of the layers $b_{1,j}$, $b_{3,j}$.

Initially, the calculation was performed without considering the influence of shear stresses of (32) $\mu_\tau^{(k)} = \mu_\varepsilon^{(k)} = 1$. According to the specified limit deformations $\varepsilon_{\text{adm}}^{(k)}$ (Table) the polygon of limit deformations is formed (fig. 5). It shows the limit line of deformations $\varepsilon_*(y) = \varepsilon_{0*} - \kappa_* y$, it has internal contacts with the polygon at two points $y_{\xi_1} = y_2$, $y_{\xi_2} = y_3$, located in the second layer. The coordinates of the layer boundaries are indicated by y_j ($j = 1,\ldots,4$). In this problem, the limit state regulates the inner layer. External layers ($k = 1$, $k = 3$) are in the pre-limit state.

Under the accuracy equal to 0.01, the computational procedure required $t_1 = 4 \div 7$ refinement iterations at the first stage and $t_2 = 5$ at the second stage.

The influence of geometric nonlinearity due to the presence of interchange in the force formulas (37), led to an increase in the bending moment by 11.3% in the middle of the span and a shear force by 12.0% in the support sections. Physical nonlinearity caused a decrease in secant stiffness characteristics $\bar{D}_A$, $\bar{D}_S$, $\bar{D}_I$ (11) in relation to the stiffness of linear theory D_A, D_S, D_I by values 9.1; 16.0; 14.1% respectively in section $x = l/2$.

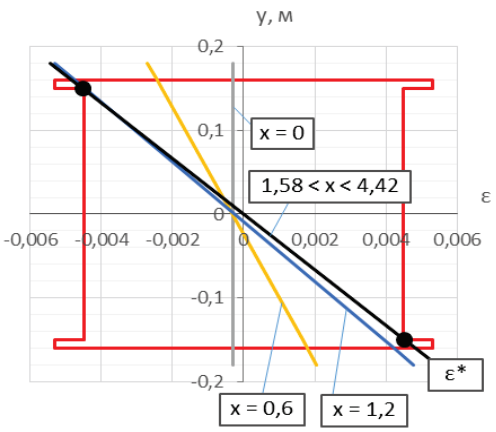


Figure 5. Polygon of limit deformations of the three-layer section with deformation curves ε(y)

The calculated width profiles of the outer layers $b_1(x)$, $b_3(x)$ are shown in Fig. 6. In the middle part of the rod ($1.58 \le x \le 4.42$) under the action of large bending moments, both limits (23):

$b_1 \geq 0.05$ m, $b_3 \geq 0.05$ m, were performed and the criterion (32) was implemented in the form of two-point ($n_y = 2$).

The decrease of the bending moments observed at the approach to the support led to the decrease of the calculated width of the layers. And, on two symmetric areas $0.93 \leq x \leq 1.58$, $4.42 \leq x \leq 5.07$ were obtained $b_1 < 0.05$ м, that demanded the acceptance of $b_1 = 0.05$ m. Further, this situation was in addition shown also for width of the upper layer on two pre-support areas $0 \leq x \leq 0.93$, $5.07 \leq x \leq 6$. At these areas, it was accepted $b_1 = b_3 = 0.05$ m. м. These areas with the indication of the multiplicity degree of the strength criterion is shown in Fig. 6.

Figure 5 shows deformation lines $\varepsilon(y)$ in sections $x = 0; 0.6; 1.2$ and on the area $1.58 \leq x \leq 4.42$. The entire middle area $1.58 \leq x \leq 4.42$ is characterized by *invariant* deformation distribution with fulfillment of the two-point strength criterion. The line for section $x = 1.2$ reflects one-point, and for sections $x = 0; 0.6$ reflects zero-point criteria.

Fig. 7 shows the curves of normal stresses $\sigma_x(x, y)$, calculated in the cross sections of the rod with coordinates $x = 0; 0.6; 1.2$ and in the design area $1.58 \leq x \leq 4.42$. The curves have a nonlinear character, as the stresses increase, the degree of nonlinearity increases. This is clearly visible in the area of the second layer $-0.15 \leq y \leq 0.15$. Nonlinearity is also manifested in the outer layers, but due to their low height, it is less noticeable. To illustrate the nonlinearity of stress laws in the outer layers, the sections of the curves are formally continued beyond these layers and are shown in dotted lines.

At the boundaries of the layers, when the physical parameters of the materials are changed $p_{k,1}$, $p_{k,3}$ (Table), according to the formula (3), breaks are observed at the curves $\sigma_x(y)$. At all points of the heterogeneous rod volume, the strength limit is performed $\operatorname{sgn}(\varepsilon_x)\,\sigma_x^{(k)}(x, y) \leq \mu_\tau^{(k)} \mu_\varepsilon^{(k)} R^{(k)\pm}$, in which the design stress are found according to the laws specified for stresses (Fig. 4) and the values of limit deformations (Table): $R^{(k=1)\pm} = \pm 92.5$ mPa, $R^{(k=2)\pm} = \pm 40.0$ mPa. In accordance with the two-point criterion of strength at the design area $1.58 \leq x \leq 4.42$ in two levels according to the y coordinate, the continuous equality of stresses is realized

$$\sigma_x^{(2)}(x; -0.15) = 40 \text{ mPa},$$
$$\sigma_x^{(2)}(x; +0.15) = -40 \text{ mPa}.$$

The analysis of the stress state showed that for the heterogeneous rod at a) a specified ratio of geometric parameters $l / (h_1 + h_2 + h_3) = 18.75$ and b) specified loads, the consideration of shear stresses and shear deformations is not relevant. In support of this, Fig. 7 shows the curve of shear stress (14), that acts in the support section of the rod with the greatest shear force, as well as the analysis of the coefficient $\mu_\tau(x, y_3)$ (26) is performed in the criterion (32). When calculating it, according to Mises' theory, it was admitted $\phi_k = 1$, $\beta_k = 3$. For the calculated level $y = y_3$ the function is obtained $\mu_\tau^{(2)}(x; 0.15)$ (Fig. 8). Its accounting makes amendments to the results of the calculation less than 0.03 %, which indicates the validity of the assumption $\mu_\tau^{(k)} = 1$.

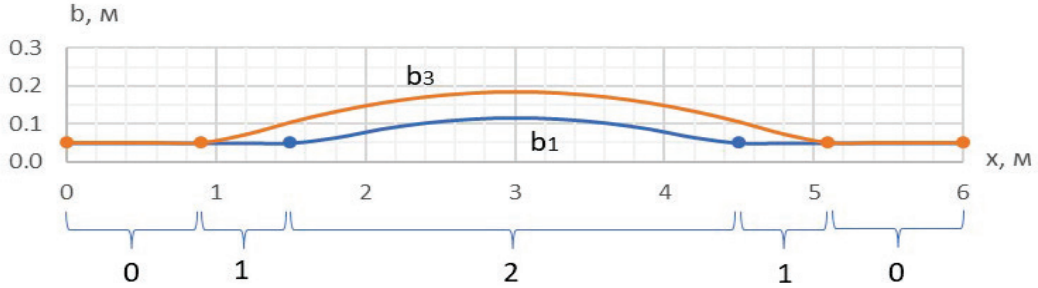


Figure 6. Design profiling of the external layers width b_1, b_3 by two-point strength criterion

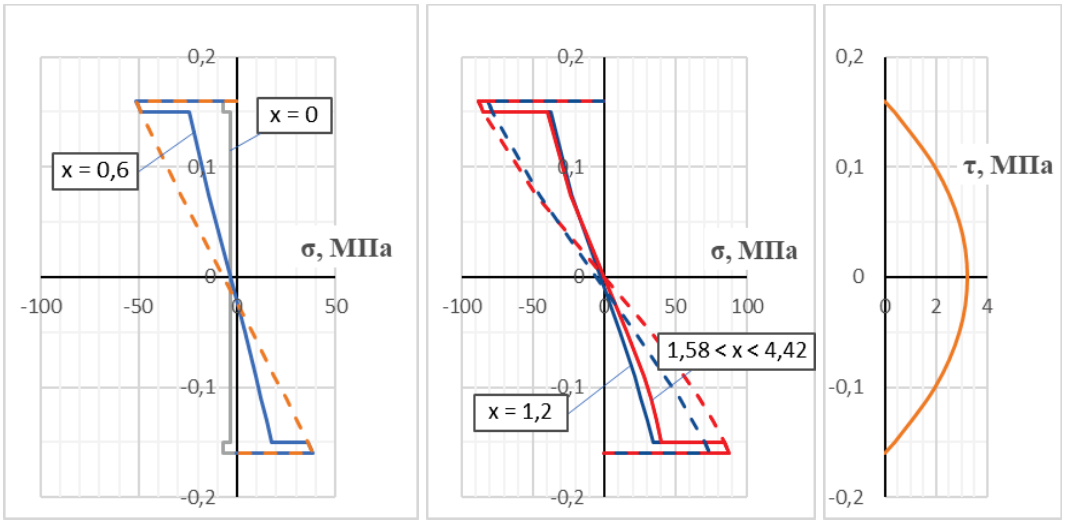


Figure 7. Curves of normal stresses $\sigma_x(x, y)$ *in the cross sections of the rod with coordinates* $x = 0; 0.6; 1.2$ *(m) and in the design area* $1.58 \le x \le 4.42$ *(m). Curve* $\tau_{yx}(0, y)$ *in the support section of the rod at* $Q = Q_{\max}$

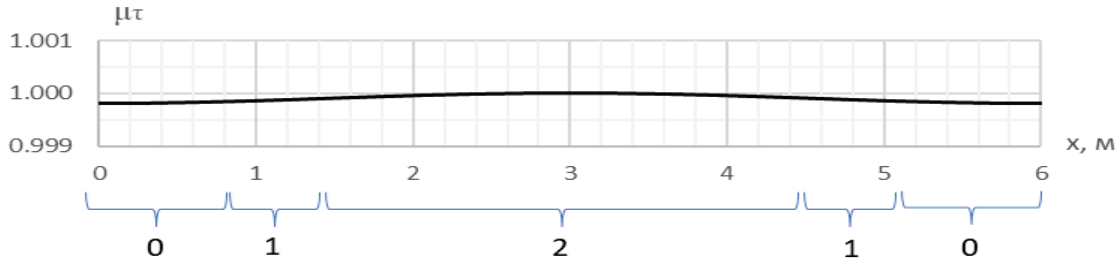


Figure 8. Graph of a correction factor change $\mu_\tau(x, y_3)$ *to consider the shear stresses in the strength criterion*

In other cases, the consideration of shear stresses and shear deformations can be completed according to the algorithm described above. Such cases are characterized by: a) the specifics of loading, if there are areas with a dangerous combination of several conditions, including shear forces, in the design areas; b) the consideration of rods of relatively shorter length, which will lead to an increase in the relative contribution of shear stresses in the strength criterion; c) the structure of the rod sections that has local thin-walled areas with significant shear stresses.

CONCLUSION

The developed method allows solving design nonlinear problems for heterogeneous rods with finding a rational profile (geometric configuration) of the rod layers. A computationally convenient formulation of physical dependencies in combination with an iterative method to clarify the functions of internal forces and displacements makes it possible to reduce the complexity in the problem solution of rational design of a nonlinearly deformable heterogeneous rod, i.e. a structural element of engineering structure.

The developed design can be used to solve problems of strengthening structures by adding external layers-plates to the elements of the initial system, which has the configuration and location determined by the solution of the opposite problem based on specified requirements for strength, rigidity and others.

REFERENCES

1. **J. Šulda, V. Adámek, R**. Kroft Transient response of non-prismatic heterogeneous viscoelastic rods and identification of their material properties // European Journal of Mechanics - A/Solids, Vol. 105, 2024, 105241, ISSN 0997-7538, https://doi.org/10.1016/j.euromechsol.2024.105241.
2. **J.M. Whitney, C.T. Sun.** A higher order theory for extensional motion of laminated composites // Journal of Sound and Vibration. – Vol. 30. – Issue 1, 1973. – P. 85-97, ISSN 0022-460X, https://doi.org/10.1016/S0022-460X(73)80052-5.
3. **Rong Chiu, Wenbin Yu** Heterogeneous Beam Element for Multiscale Modeling of Non-prismatic Composite Beam-like Structures // International Journal of Solids and Structures. – Vol. 285, 2023, 112490, ISSN 0020-7683, https://doi.org/10.1016/j.ijsolstr.2023.112490.
4. **Mouad Fergoug, Augustin Parret-Fréaud, Nicolas Feld, Basile Marchand, Samuel Forest** Hierarchical modeling of heterogeneous structures driven by a modeling error estimator // Computer Methods in Applied Mechanics and Engineering. – Vol. 418, Part B, 2024, 116529, ISSN 0045-7825, https://doi.org/10.1016/j.cma.2023.116529.
5. **V. Adámek, A. Berezovski, M. Mračko, R. Kolman** A two-layer elastic strip under transverse impact loading: Analytical solution, finite element, and finite volume simulations // Mathematics and Computers in Simulation. – Vol. 189, 2021. – P. 126-140, ISSN 0378-4754, https://doi.org/10.1016/j.matcom.2020.10.007.
6. **Xin Liu, Wenbin Yu** A novel approach to analyze beam-like composite structures using mechanics of structure genome // Advances in Engineering Software. – Vol. 100, 2016. – P. 238-251, ISSN 0965-9978, https://doi.org/10.1016/j.advengsoft.2016.08.003.
7. **P. Vidal, L. Gallimard, O. Polit,** Composite beam finite element based on the Proper Generalized Decomposition // Computers & Structures. – Vol. 102–103, 2012. – P. 76-86, ISSN 0045-7949, https://doi.org/10.1016/j.compstruc.2012.03.008.
8. **R.P. Shimpi, A.V. Ainapure** A beam finite element based on layerwise trigonometric shear deformation theory // Composite Structures. – Vol. 53. – Issue 2, 2001. – P. 153-162, ISSN 0263-8223, https://doi.org/10.1016/S0263-8223(00)00186-0.
9. **E.A. Fancello, J.P. Ponthot, L. Stainier** A variational framework for nonlinear viscoelastic models in finite deformation regime // Journal of Computational and Applied Mathematics, Vol. 215, Issue 2, 2008, p. 400-408, ISSN 0377-0427, https://doi.org/10.1016/j.cam.2006.04.064.
10. **S. Srinivas** A refined analysis of composite laminates // Journal of Sound and Vibration. – Vol. 30. – Issue 4, 1973. – P. 495-507, ISSN 0022-460X, https://doi.org/10.1016/S0022-460X(73)80170-1.
11. **Wei Ding, Sansit Patnaik, Fabio Semperlotti** Transversely heterogeneous nonlocal Timoshenko beam theory: A reduced-order modeling via distributed-order fractional operators // Thin-Walled Structures. – Vol. 197, 2024, 111608, ISSN 0263-8231, https://doi.org/10.1016/j.tws.2024.111608.
12. **Aryan Kheyabani, Eyass Massarwa, Adnan Kefal** Multiscale structural analysis of thick sandwich structures using parametric HFGMC micromechanics and isogeometric plate formulation based on refined zigzag theory // Composite Structures. – Vol. 297, 2022. – 115988, ISSN 0263-8223, https://doi.org/10.1016/j.compstruct.2022.115988.
13. **Mishchenko A.V.** Sposob formirovaniya nelinejnyh fizicheskih sootnoshenij v pryamyh i obratnyh zadachah rascheta mnogofaznyh sterzhnej // Vestnik Yuzhno-Ural'skogo gosudarstvennogo universiteta. Seriya: Stroitel'stvo i arhitektura. – 2014. – Vol. 14. № 3. – p. 12-16.

14. **Mishchenko A.V., Nemirovskij Yu.V.** Raschet i proektirovanie derevyannyh sterzhnevyh sistem s uchetom fizicheskoj nelinejnosti // Stroitel'naya mekhanika i raschet sooruzhenij. – 2007. – № 6 (215). – p. 46-52.
15. **Nemirovskij Yu.V., Tihonov S.V.** Opredelenie nesushchej sposobnosti mnogoetazhnyh zdanij iz fizicheski nelinejnyh betonnyh sterzhnej // Vestnik Chu-vashskogo gosudarstvennogo pedagogicheskogo universiteta im. I.Ya. Yakovleva. Seriya: Mekhanika predel'nogo sostoyaniya. – 2022. – № 2 (52). – p. 19-35.
16. **Mishchenko A.V., Nemirovskij Yu.V.** Nelinejnoe deformirovanie betonnyh elementov pri prodol'no-poperechnom izgibe // Izvestiya vuzov. Stroitel'stvo. – 2013. – № 4. – p. 3-12.
17. **Mishchenko A.V.** Energeticheskaya optimizaciya strukturno-neodnorodnoj dvuhsharnirnoj ramy // Stroitel'naya mekhanika i konstrukcii. – 2022. – № 3 (34). – p. 71-81. DOI 10.36622/VSTU.2022.34.3.005.
18. **L.Yu. Stupishin, V.L. Mondrus** Energy properties of symmetric deformable systems // International Journal for Computational Civil and Structural Engineering, 20(1), 2024, DOI: https://doi.org/10.22337/2587-9618-2024-20-1-35-45.
19. **Yur'ev A.G., Panchenko L.A., Zin'kova V.A.** Strukturnyj sintez sterzhnevyh sistem // Vestnik Belgorodskogo gosudarstvennogo tekhnologicheskogo univer-siteta im. V.G. Shuhova. – 2022. – № 10. – p. 34-40. DOI: 10.34031/2071-7318-2022-7-10-34-40.
20. **S. Wang, H.B. Huang, F. Yin, X.S. Hou, Z. Zhang, L.M. Luo, C. Chen** Modification of the mechanical properties of Ti/Ta multilayer composites with heterogeneous lamella structure, International // Journal of Refractory Metals and Hard Materials. – Vol. 110, 2023, 105996, ISSN 0263-4368, https://doi.org/10.1016/j.ijrmhm.2022.105996.
21. **Amal M.K. Esawi, Mahmoud M. Farag** Carbon nanotube reinforced composites: Potential and current challenges // Materials & Design. – Vol. 28. – Issue 9, 2007, P. 2394-2401, ISSN 0261-3069, https://doi.org/10.1016/j.matdes.2006.09.022.
22. **Sidorov I.N., Andrianova K.A., Gaifutdinov A.M., Usmonov R.S., Amirova L.M.** Modeling and experimental investigations of mechanical properties of hybrid composite rods with gradient composition // Materials Today Communications, Vol. 39, 2024, 108738, ISSN 2352-4928, https://doi.org/10.1016/j.mtcomm.2024.108738.
23. **Mishchenko A.V., Kalinkin S.A.** Analiz napryazhenno-deformirovannogo sostoyaniya racional'nyh proektov sloistoneodnorodnyh sterzhnej // Modelirova-nie i mekhanika konstrukcij. 2017. № 5. URL: http://mechanics.pguas.ru/ Plone/nomera-zhurnala /no5 /stroitelnaya-mehanika/5.3/at_download/file.

СПИСОК ЛИТЕРАТУРЫ

1. **J. Šulda, V. Adámek, R**. Kroft Transient response of non-prismatic heterogeneous viscoelastic rods and identification of their material properties // European Journal of Mechanics - A/Solids, Vol. 105, 2024, 105241, ISSN 0997-7538, https://doi.org/10.1016/j.euromechsol.2024.105241.
2. **J.M. Whitney, C.T. Sun.** A higher order theory for extensional motion of laminated composites // Journal of Sound and Vibration. – Vol. 30. – Issue 1, 1973. – P. 85-97, ISSN 0022-460X, https://doi.org/10.1016/S0022-460X(73)80052-5.
3. **Rong Chiu, Wenbin Yu** Heterogeneous Beam Element for Multiscale Modeling of Non-prismatic Composite Beam-like Structures // International Journal of Solids and Structures. – Vol. 285, 2023, 112490, ISSN 0020-7683, https://doi.org/10.1016/j.ijsolstr.2023.112490.
4. **Mouad Fergoug, Augustin Parret-Fréaud, Nicolas Feld, Basile Marchand, Samuel Forest** Hierarchical modeling of heterogeneous structures driven by a modeling error es-

timator // Computer Methods in Applied Mechanics and Engineering. – Vol. 418, Part B, 2024, 116529, ISSN 0045-7825, https://doi.org/10.1016/j.cma.2023.116529.

5. **V. Adámek, A. Berezovski, M. Mračko, R. Kolman** A two-layer elastic strip under transverse impact loading: Analytical solution, finite element, and finite volume simulations // Mathematics and Computers in Simulation. – Vol. 189, 2021. – P. 126-140, ISSN 0378-4754, https://doi.org/10.1016/j.matcom.2020.10.007.
6. **Xin Liu, Wenbin Yu** A novel approach to analyze beam-like composite structures using mechanics of structure genome // Advances in Engineering Software. – Vol. 100, 2016. – P. 238-251, ISSN 0965-9978, https://doi.org/10.1016/j.advengsoft.2016.08.003.
7. **P. Vidal, L. Gallimard, O. Polit,** Composite beam finite element based on the Proper Generalized Decomposition // Computers & Structures. – Vol. 102–103, 2012. – P. 76-86, ISSN 0045-7949, https://doi.org/10.1016/j.compstruc.2012.03.008.
8. **R.P. Shimpi, A.V. Ainapure** A beam finite element based on layerwise trigonometric shear deformation theory // Composite Structures. – Vol. 53. – Issue 2, 2001. – P. 153-162, ISSN 0263-8223, https://doi.org/10.1016/S0263-8223(00)00186-0.
9. **E.A. Fancello, J.P. Ponthot, L. Stainier** A variational framework for nonlinear viscoelastic models in finite deformation regime // Journal of Computational and Applied Mathematics, Vol. 215, Issue 2, 2008, p. 400-408, ISSN 0377-0427, https://doi.org/10.1016/j.cam.2006.04.064.
10. **S. Srinivas** A refined analysis of composite laminates // Journal of Sound and Vibration. – Vol. 30. – Issue 4, 1973. – P. 495-507, ISSN 0022-460X, https://doi.org/10.1016/S0022-460X(73)80170-1.
11. **Wei Ding, Sansit Patnaik, Fabio Semperlotti** Transversely heterogeneous nonlocal Timoshenko beam theory: A reduced-order modeling via distributed-order fractional operators // Thin-Walled Structures. – Vol. 197, 2024, 111608, ISSN 0263-8231, https://doi.org/10.1016/j.tws.2024.111608.
12. **Aryan Kheyabani, Eyass Massarwa, Adnan Kefal** Multiscale structural analysis of thick sandwich structures using parametric HFGMC micromechanics and isogeometric plate formulation based on refined zigzag theory // Composite Structures. – Vol. 297, 2022. – 115988, ISSN 0263-8223, https://doi.org/10.1016/j.compstruct.2022.115988.
13. **Мищенко А.В**. Способ формирования нелинейных физических соотношений в прямых и обратных задачах расчета многофазных стержней // Вестник Южно-Уральского государственного университета. Серия: Строительство и архитектура. – 2014. – т. 14. – № 3. – с. 12-16.
14. **Мищенко А.В., Немировский Ю.В.** Расчет и проектирование деревянных стержневых систем с учетом физической нелинейности // Строительная механика и расчет сооружений. – 2007. – № 6 (215). – с. 46-52.
15. **Немировский Ю.В., Тихонов С.В.** Определение несущей способности многоэтажных зданий из физически нелинейных бетонных стержней // Вестник Чувашского государственного педагогического университета им. И.Я. Яковлева. Серия: Механика предельного состояния. – 2022. – № 2 (52). – с. 19-35.
16. **Мищенко А.В., Немировский Ю.В.** Нелинейное деформирование бетонных элементов при продольно-поперечном изгибе // Известия вузов. Строительство. – 2013. – № 4. – с. 3–12.
17. **Мищенко А.В.** Энергетическая оптимизация структурно-неоднородной двухшарнирной рамы // Строительная механика и конструкции. – 2022. – № 3 (34). – с. 71-81. DOI 10.36622/VSTU.2022.34.3.005
18. **L.Yu. Stupishin, V.L. Mondrus** Energy properties of symmetric deformable systems

// International Journal for Computational Civil and Structural Engineering, 20(1), 2024, DOI: https://doi.org/10.22337/2587-9618-2024-20-1-35-45.

19. **Юрьев А.Г., Панченко Л.А., Зинькова В.А.** Структурный синтез стержневых систем // Вестник Белгородского государственного технологического университета им. В.Г. Шухова. – 2022. – № 10. – С. 34-40. DOI: 10.34031/2071-7318-2022-7-10-34-40.
20. **S. Wang, H.B. Huang, F. Yin, X.S. Hou, Z. Zhang, L.M. Luo, C. Chen** Modification of the mechanical properties of Ti/Ta multilayer composites with heterogeneous lamella structure, International // Journal of Refractory Metals and Hard Materials. – Vol. 110, 2023, 105996, ISSN 0263-4368, https://doi.org/10.1016/j.ijrmhm.2022.105996.
21. **Amal M.K. Esawi, Mahmoud M. Farag** Carbon nanotube reinforced composites: Potential and current challenges // Materials & Design. – Vol. 28. – Issue 9, 2007, P. 2394-2401, ISSN 0261-3069, https://doi.org/10.1016/j.matdes.2006.09.022.
22. **I.N. Sidorov, K.A. Andrianova, A.M. Gaifutdinov, R.S. Usmonov, L.M. Amirova.** Modeling and experimental investigations of mechanical properties of hybrid composite rods with gradient composition // Materials Today Communications, Vol. 39, 2024, 108738, ISSN 2352-4928, https://doi.org/10.1016/j.mtcomm.2024.108738.
23. **Мищенко А.В., Калинкин С.А.** Анализ напряженно-деформированного состояния рациональных проектов слоисто-неоднородных стержней // Моделирование и механика конструкций. 2017. № 5. URL: http: //mechanics.pguas.ru/ Plone/nomera-zhurnala /no5 /stroitelnaya-mehanika/5.3/at_download/file.

Mishchenko Andrey Viktorovich – Doctor of Technical Sciences, Associate Professor, Professor of the Department of Structural Mechanics, Novosibirsk State University of Architecture and Civil Engineering (Sibstrin) (NSUACE (Sibstrin)). 253, 113, str. Leningradskaya, Novosibirsk, 630008 Russia. E-mail: a.michshenko@sibstrin.ru, +7(383) 266-33-80

Veshkin Maxim Sergeevich – Candidate of Technical Sciences, Associate Professor of the Department of Structural Mechanics, Novosibirsk State University of Architecture and Civil Engineering (Sibstrin) (NSUACE (Sibstrin)). 253, 113, str. Leningradskaya, Novosibirsk, 630008 Russia. E-mail: m.veshkin@sibstrin.ru, +7(383) 266-33-80

Mondrus Vladimir Lvovich – Doctor of Technical Sciences, Professor, Corresponding Member of RAASN, Head of the Department of Structural and Theoretical Mechanics, Institute of Industrial and Civil Engineering, National Research Moscow State Construction University (NIU MSCU). 405, 26, Yaroslavskoe Shosse, Moscow, 129337, Russia. E-mail: m.mondrusvl@mgsu.m, +7 (495) 287-49-14 ext. 3074

Stupishin Leonid Yulianovich– Doctor of Technical Sciences, Professor, Professor of the Department of Construction and Theoretical Mechanics, Institute of Industrial and Civil Engineering, National Research Moscow State Construction University (NIU MSCU). 405, 26, Yaroslavskoe Shosse, Moscow, 129337, Russia. E-mail: stupishinlyu@mgsu.ru, +7 (495) 287-49-14 ext. 3074

Мищенко Андрей Викторович – д.т.н., доцент, профессор кафедры строительной механики, Новосибирский государственный архитектурно-строительный университет (Сибстрин) (НГАСУ (Сибстрин)). 253, 113, ул. Ленинградская, Новосибирск, 630008 Россия. E-mail: a.michshenko@sibstrin.ru, +7(383) 266-33-80

Вешкин Максим Сергеевич – к.т.н., доцент кафедры строительной механики, Новосибирский государственный архитектурно-строительный университет (Сибстрин) (НГАСУ (Сибстрин)). 253, 113, ул. Ленинградская, Новосибирск, 630008 Россия. E-mail: m.veshkin@sibstrin.ru, +7(383) 266-33-80

Мондрус Владимир Львович – д.т.н., профессор, член корр. РААСН, зав. каф. строительной и теоретической механики, институт Промышленного и гражданского строительства, Национальный Исследовательский Московский Государственный Строительный Университет (НИУ МГСУ). 405, 26, Ярославское шоссе, Москва, 129337, Россия. E-mail: m.mondrusvl@mgsu.m, +7 (495) 287—49-14 доб. 3074

Ступишин Леонид Юлианович – д.т.н., профессор, профессор кафедры строительной и теоретической механики, институт Промышленного и гражданского строительства, Национальный Исследовательский Московский Государственный Строительный Университет (НИУ МГСУ). 405, 26, Ярославское шоссе, Москва, 129337, Россия. E-mail: stupishinlyu@mgsu.ru, +7(495) 287-49-14 доб. 3074

DOI:10.22337/2587-9618-2024-20-3-116-124

MODEL OF CAKE FILTRATION IN POROUS MEDIUM

Liudmila I. Kuzmina [1], Yuri V. Osipov [2]

[1] HSE University, Moscow, RUSSIA
[2] Moscow State University of Civil Engineering, Moscow, RUSSIA

Abstract: Strengthening of loose soil and creation of water-resistant underground walls are associated with filtration of small particles in a porous medium. Liquid solution pumped into a well under pressure spreads through hollow channels and strengthens the soil upon hardening. Many porous filters retain particles near the entrance. The particles deposited on the filter surface form a crust, which does not allow suspended particles to penetrate deep into the porous medium. A model of cake filtration - the formation of a surface crust during filtration of a monodisperse suspension in a homogeneous porous medium is considered. This model is a modification of the standard mathematical description of deep bed filtration with linear accessible fractional flow decreasing to zero. An exact solution is obtained using the method of characteristics. Asymptotics is constructed for a long time. It is shown that the dynamics and profiles of suspended and deposited particles concentrations exponentially decrease.

Keywords: cake filtration, deep bed filtration, porous medium, exact solution, asymptotics

МОДЕЛЬ ПОВЕРХНОСТНОЙ ФИЛЬТРАЦИИ В ПОРИСТОЙ СРЕДЕ

Л.И. Кузьмина [1], Ю.В. Осипов [2]

[1] Национальный исследовательский университет «Высшая школа экономики», г. Москва, РОССИЯ
[2] Национальный исследовательский Московский государственный строительный университет, г. Москва, РОССИЯ

Аннотация: Укрепление рыхлого грунта и создание водонепроницаемых подземных стен связаны с фильтрацией мелких частиц в пористой среде. Жидкий раствор, закаченный в скважину под давлением, распространяется по полым каналам и при застывании укрепляет грунт. Многие пористые фильтры задерживают частицы вблизи входа пористой среды. Осажденные частицы на поверхности фильтра образуют корку, которая не пропускает частицы вглубь пористой среды. Рассматривается модель образования поверхностной корки при фильтрации монодисперсной суспензии в однородной пористой среде. Модель является модификацией стандартного математического описания глубинной фильтрации, включающей убывающую до нуля функцию допустимого потока. Методом характеристик найдено точное решение. Построена асимптотика при большом времени. Показано, что динамика и профили концентраций взвешенных и осажденных частиц экспоненциально убывают.

Ключевые слова: поверхностная фильтрация, глубинная фильтрация, пористая среда, точное решение, асимптотика

1. INTRODUCTION

Filtration of liquids with particles is used in construction technologies to strengthen soil during the construction of structures and reconstruction of roads. The injected grout penetrates far into the soil through hollow pores and closes them, strengthening the underground layer and preventing the penetration of groundwater [1-5].

Effective filters used in water wells and in the treatment of industrial and domestic wastewater collect particles on the surface of the filter and purify the water of impurities. The formation of a sediment on the surface of a porous medium, which does not allow particles to pass deeper, is called cake filtration. As a rule, the crust is formed by large particles that cannot penetrate into narrow pores [6-8]. The surface layer of deposited particles is also a porous medium that

can allow small particles to pass through. If small particles spread along the entire length of the porous medium, then cake filtration and deep bed filtration occur simultaneously [9, 10]. Standard deep bed filtration models assume that a porous medium has large pores through which a carrier fluid easily transfers particles from inlet to outlet [11-13]. During layer-by-layer deposition, small particles can block large pores on the surface and limit the transfer of suspended particles deep into the porous medium [14]. In [15] a model of surface deposition is considered, which relates the growth of retained concentration at the inlet with the decreasing velocity of suspended particles. To describe the cake filtration, this article proposes the deep bed filtration model with vanishing accessible fractional flow [16, 17]. The model includes the mass exchange equation of suspended and deposited particles and the kinetic equation of deposit growth with the Langmuir filtration function [18]. The accessible fractional flow is proportional to the linear filtration function and vanishes to zero when the deposit limit is reached. For the new model, an exact solution and asymptotics for large times are obtained.

As a rule, filtration equations do not allow an exact solution and are solved numerically [19-21]. The presence of an exact solution for the cake filtration model under consideration allows us to check the accuracy of numerical methods and adjust the program code.

2. CAKE FILTRATION MODEL

Consider the cake filtration model in an infinite homogeneous porous medium. In the domain $\Omega = \{x \geq 0,\ t \geq 0\}$, the model in a dimensionless form is specified by a system of first-order partial differential equations with unknown volumetric concentrations of suspended and deposited particles $C(x,t),\ S(x,t)$:

$$\frac{\partial C}{\partial t} + \frac{\partial}{\partial x}\left(\left(1 - \frac{S}{S_m}\right)C\right) + \frac{\partial S}{\partial t} = 0, \qquad (1)$$

$$\frac{\partial S}{\partial t} = \lambda\left(1 - \frac{S}{S_m}\right)C \qquad (2)$$

with the conditions

$$x = 0 : C = 1, \quad t = 0 : C = 0,\ S = 0. \qquad (3)$$

Here $\lambda > 0$ is the filtration coefficient and $S_m > 0$ is the maximum limiting deposit.

According to the condition (3), at the inlet of the porous medium $x = 0$, equation (2) takes the form

$$\frac{\partial S_0}{\partial t} = \lambda\left(1 - \frac{S_0}{S_m}\right). \qquad (4)$$

Solution to the equation (4) with the condition (3) is

$$S_0(t) = S_m\left(1 - e^{-\lambda t / S_m}\right). \qquad (5)$$

Let's reduce problem (1)-(3) to one equation with unknown S. Substitute the equation (2) into (1)

$$\frac{\partial C}{\partial t} + \frac{1}{\lambda}\frac{\partial}{\partial x}\frac{\partial S}{\partial t} + \frac{\partial S}{\partial t} = 0$$

and change the order of differentiation in the mixed derivative

$$\frac{\partial C}{\partial t} + \frac{1}{\lambda}\frac{\partial}{\partial t}\frac{\partial S}{\partial x} + \frac{\partial S}{\partial t} = 0.$$

Integration over time gives

$$C + \frac{1}{\lambda}\frac{\partial S}{\partial x} + S = K(x). \qquad (6)$$

The integration constant is obtained from the conditions (3): $K(x) = 0$.

Express C from the equation (2):

$$C = \frac{\partial S / \partial t}{\lambda(1 - S / S_m)} \qquad (7)$$

and substitute in (6)

$$\frac{\partial S / \partial t}{\lambda(1 - S / S_m)} + \frac{1}{\lambda}\frac{\partial S}{\partial x} + S = 0 .$$

Transform the equation:

$$\frac{\partial S}{\partial t} + \left(1 - \frac{S}{S_m}\right)\frac{\partial S}{\partial x} + \lambda S\left(1 - \frac{S}{S_m}\right) = 0 . \qquad (8)$$

The solution S is zero at $t \le x$ and is positive at $t > x$. The boundary $t = x$ is the front of deposit concentration.

To solve equation (8) in the domain $\Omega^+ = \{x > 0,\, t > x\}$, we will use the method of characteristics [22, 23] and make a change of variables: $(x,t) \to (\tau, t_0)$. Here τ is a variable along the characteristic, and t_0 is the initial value on the time axis. The characteristics are given by the equations

$$\dot{t} = 1,\ \dot{x} = 1 - \frac{S}{S_m},\ t(0) = t_0,\ x(0) = 0,$$

where ( ) is the derivative with respect to τ. In the characteristic variables, equation (8) takes the form

$$\dot{S} + \lambda S\left(1 - \frac{S}{S_m}\right) = 0,\ \ S(0) = S_0(t_0) . \qquad (9)$$

The solution to problem (9) is obtained by the method of separation of variables:

$$S = S_m \frac{e^{\lambda t_0 / S_m} - 1}{e^{\lambda\tau} + e^{\lambda t_0 / S_m} - 1} . \qquad (10)$$

Using solution (10), the characteristics are obtained:

$$t = \tau + t_0,\ \ x = \frac{1}{\lambda}\ln\frac{e^{\lambda\tau} + e^{\lambda t_0 / S_m} - 1}{e^{\lambda t_0 / S_m}} . \qquad (11)$$

Express τ from the first equation (11) and substitute it into the second one:

$$x = \frac{1}{\lambda}\ln\left(e^{\lambda(t - t_0(1 + 1/S_m))} - e^{-\lambda t_0 / S_m} + 1\right).$$

Transform the equation to the form

$$F(z) = e^{\lambda t} z^{1+S_m} - z + 1 - e^{\lambda x} = 0, \quad z = e^{-\lambda t_0 / S_m} .$$

In the domain Ω^+ on the interval (0;1) the function $F(z)$ is differentiable and $F''(z) > 0$, at the ends of the interval $F(0) < 0,\ F(1) > 0$. Consequently, there is a single root $z^+(x,t),\ 0 < z^+ < 1$ of the transcendental equation $F(z) = 0$.

Now the characteristic variables τ, t_0 can be expressed in terms of Cartesian x, t:

$$t_0(x,t) = -\frac{S_m}{\lambda}\ln z^+(x,t),$$
$$\tau(x,t) = t + \frac{S_m}{\lambda}\ln z^+(x,t).$$

In variables x, t, solution (10) takes the form

$$S = S_m \frac{1 - z^+}{(z^+)^{1+S_m} e^{\lambda t} - z^+ + 1} . \qquad (12)$$

Transform formula (12) using (11)

$$S(x,t) = S_m e^{-\lambda x}(1 - z^+) . \qquad (13)$$

The solution $C(x,t)$ is determined by the formulae (7) and (13):

$$C(x,t) = \frac{S_m z^+}{(1 + S_m)(e^{\lambda x} - 1) + S_m z^+} . \qquad (14)$$

For large time *t,* the asymptotic expansion of the solution [24] is given by the formulae

$$S(x,t) = S_m e^{-\lambda x} \cdot \cdot\left(1-(e^{\lambda x}-1)^{1/(1+S_m)} e^{-\lambda t/(1+S_m)}\right) + O\left(e^{-2\lambda t/(1+S_m)}\right), \quad (15)$$

$$C(x,t) = \frac{S_m (e^{\lambda x}-1)^{-S_m/(1+S_m)}}{(1+S_m)} e^{-\lambda t/(1+S_m)} + O\left(e^{-2\lambda t/(1+S_m)}\right). \quad (16)$$

Example 1. Let $S_m = 1$. Then (11) is a quadratic equation with the positive root

$$z^+(x,t) = \frac{1+\sqrt{1+4e^{\lambda t}(e^{\lambda x}-1)}}{2e^{\lambda t}}.$$

Characteristic variables are expressed using the formulae

$$t_0 = \frac{1}{\lambda}\ln\frac{2e^{\lambda t}}{1+\sqrt{1+4e^{\lambda t}(e^{\lambda x}-1)}},$$

$$\tau = t - \frac{1}{\lambda}\ln\frac{2e^{\lambda t}}{1+\sqrt{1+4e^{\lambda t}(e^{\lambda x}-1)}}.$$

Solution (13) and (14) takes the form

$$S = S_m\left(e^{-\lambda x} - \frac{\sqrt{1+4e^{\lambda t}(e^{\lambda x}-1)}+1}{2e^{\lambda t}e^{\lambda x}}\right), \quad (17)$$

$$C = \frac{1}{\sqrt{1+4e^{\lambda t}(e^{\lambda x}-1)}}. \quad (18)$$

On the concentration front $t = x$ the solution is

$$C = \frac{1}{2e^{\lambda x}-1}, \quad S = 0.$$

When $x = const$, $t \to \infty$ the solutions tend to the limits $C \to 0$, $S \to e^{-\lambda x}$. The asymptotics of the solution at $t \to \infty$ has the form

$$C = \frac{e^{-\frac{\lambda t}{2}}}{2\sqrt{e^{\lambda x}-1}} + O\left(e^{-\frac{3\lambda t}{2}}\right),$$

$$S = e^{-\lambda x} - e^{-\frac{\lambda t}{2}}\sqrt{e^{-\lambda x}-e^{-2\lambda x}} + O\left(e^{-\frac{3\lambda t}{2}}\right).$$

3. NUMERICAL RESULTS

Two-dimensional graphs of the solution to the cake filtration problem in a porous medium make it possible to determine the dynamics (at a constant coordinate *x*) and the profiles (at a constant time *t*) [25, 26]. The model is calculated at $\lambda = 1$, $S_m = 1$. Fig. 1 shows the dependence of concentrations on time at various points of the porous medium.

According to Fig. 1. when $t < x$ at the considered point *x* of the porous medium there are no particles and the solution is zero. At the moment $t = x$ the concentration front arrives at point *x* and the concentration of suspended particles *C* changes abruptly. At $t > x$ at point *x* the suspended and retained particles are present and the solution is positive. When moving away from the inlet of the porous medium, i.e. as *x* increases, the concentrations of suspended and deposited particles decrease exponentially.

At a fixed time *t,* non-zero concentrations of suspended and retained particles are located behind the concentration front at $x < t$ (Fig. 2).

Graphs of the limit retention profiles at $t \to \infty$ for various λ are shown in Fig. 3.

In the cake filtration model, retention profiles decrease exponentially and decrease with increasing λ.

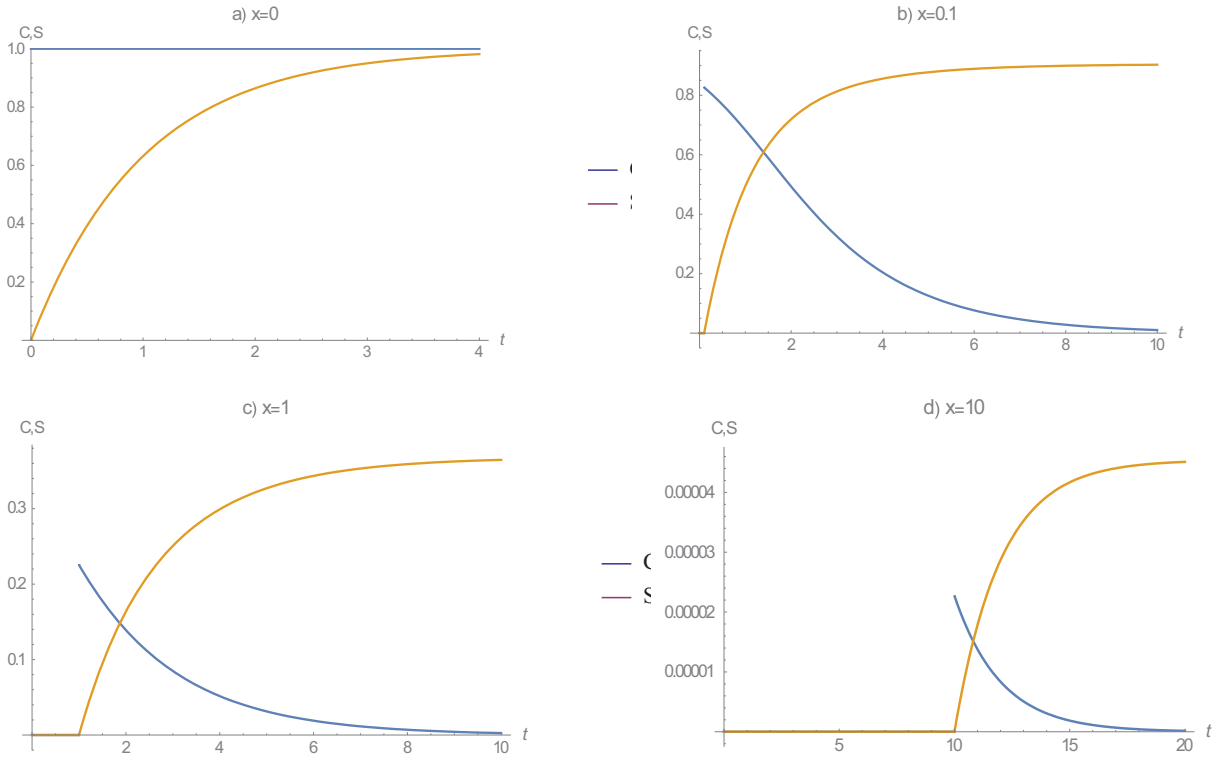


Figure 1. Dynamics of suspended and retained particles concentrations. a) $x = 0$ b) $x = 0.1$ c) $x = 1$ d) $x = 10$

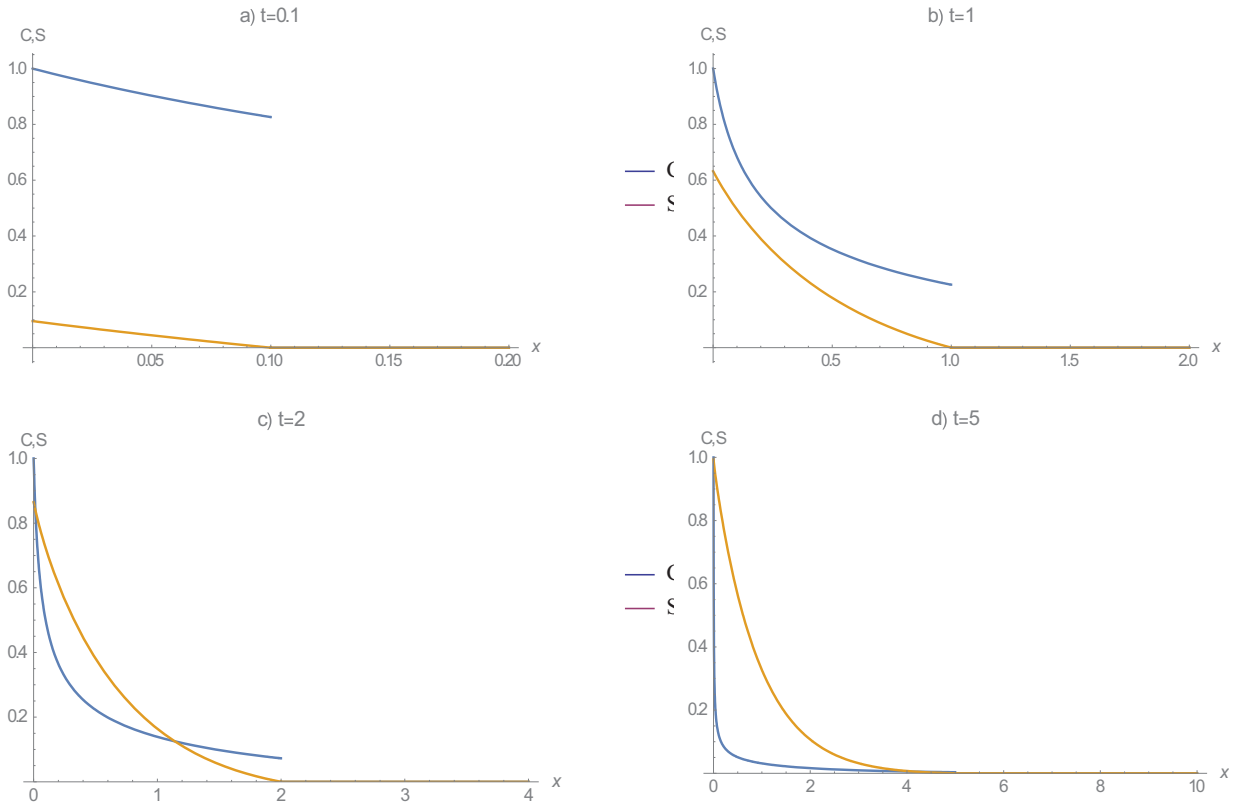


Figure 2. Profiles of suspended and retained particles. a) $t = 0.1$ b) $t = 1$ c) $t = 2$ d) $t = 5$.

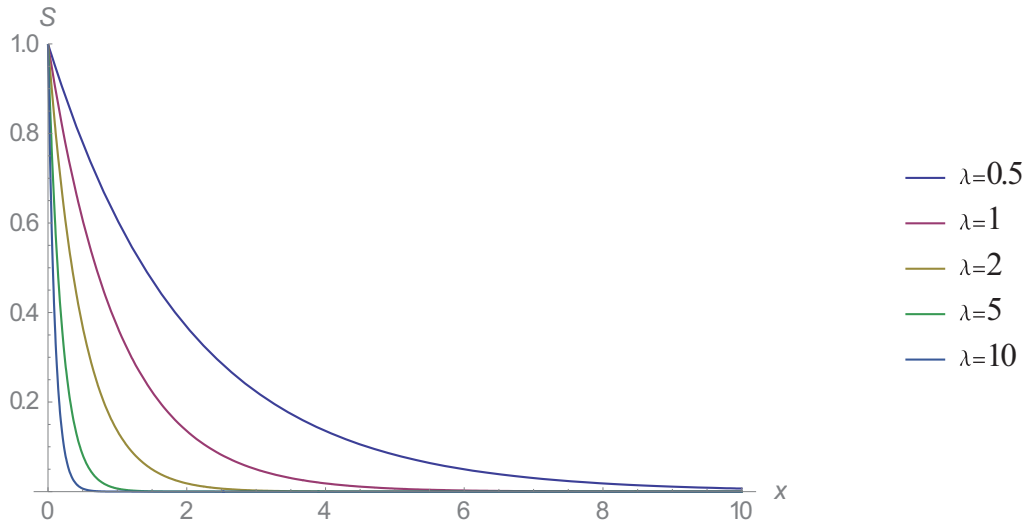


Figure 3. Limit retention profiles at different filtration coefficients.

DISCUSSION

The proposed cake filtration model is a modification of the deep bed filtration model. Thus, both different types of filtration processes are described in a unified way by population balance equations.

At high fluid speeds, trapped particles can be detached from the framework of the porous medium and become suspended again [14, 15, 27, 28]. The model with sediment erosion will be considered separately.

Two free parameters can adapt the model to the results of laboratory experiments [29, 30].

4. CONCLUSIONS

The study of the cake filtration model allows us to draw the following conclusions.

– Cake filtration model is constructed as a modified deep bed filtration model.
– Particles are deposited on the surface and near the inlet of the porous medium.
– The concentration of suspended particles decreases with time and tends to zero.
– An exact solution in explicit form is obtained.
– The asymptotics of the solution at $t \to \infty$ is constructed.

REFERENCES

1. **Zhou Z., Zang H., Wang S., Du X., Ma D., Zhang J.** Filtration Behavior of Cement-Based Grout in Porous Media // Transport in Porous Media, 2018, vol. 125, pp. 435–463.
2. **Xie B., Cheng H., Wang X., Yao Z., Rong C., Zhou R., Zhang L., Guo L., Yu H., Xiong, W., Xiang X.** Theoretical Research on Diffusion Radius of Cement-Based Materials Considering the Pore Characteristics of Porous Media // Materials, 2022, vol. 15, 7763.
3. **Zhu G., Zhang Q., Liu R., Bai J., Li W., Feng X.** Experimental and Numerical Study on the Permeation Grouting Diffusion Mechanism considering Filtration Effects // Geofluids, 2021, 6613990.
4. **Wang X., Cheng H., Yao Z., Rong C., Huang X., Liu X.** Theoretical Research on Sand Penetration Grouting Based on Cylindrical Diffusion Model of Tortuous Tubes // Water, 2022, vol. 14, 1028.
5. **Faramarzi L., Rasti A., Abtahi S.M.** An Experimental Study of the Effect of Cement and Chemical Grouting on the Improvement of the Mechanical and Hydraulic Properties of Alluvial Formations // Journal of Construction & Building Materials, 2016, vol. 126, pp. 32–43.

6. **Tien C.** Introduction to Cake Filtration, Elsevier, Amsterdam, 2006.
7. **Yim S.** A theoretical and experimental study on cake filtration with sedimentation // Korean Journal of Chemical Engineering, 1999, vol. 16, pp. 308–315.
8. **Civan F.** Reservoir formation damage, third ed, Gulf Professional Publishing, Burlington, MA, USA, 2014.
9. **Sacramento R.N., Yang Y., You Z., Waldmann A., Martins A.L., Vaz A.S.L., Zitha P.L.J., Bedrikovetsky P.** Deep bed and cake filtration of two-size particle suspension in porous media // Journal of Petroleum Science and Engineering, 2015, vol. 126, pp. 201–210.
10. **Khuzhayorov B.K., Saydullaev U., Ibragimov G., Wahi N.** An Axisymmetric Problem of Suspension Filtering with Formation of Elastic–Plastic Cake Layer // Symmetry, 2022, vol. 14(6), 1202.
11. **Herzig J.P., Leclerc D.M., Le Goff P.** Flow of Suspensions Through Porous Media – Application to Deep Filtration // Journal of Industrial & Engineering Chemistry, 1970, vol. 62(8), pp. 8–35.
12. **Bedrikovetsky P.** Upscaling of stochastic micro model for suspension transport in porous media // Transport in Porous Media, 2008, vol. 75, pp. 335–369.
13. **Kuzmina L.I., Osipov Y.V., Gorbunova T.N.** Asymptotics for filtration of polydisperse suspension with small impurities // Applied Mathematics and Mechanics (English Edition), 2021, vol. 42(1), pp. 109–126.
14. **Bizmark N., Schneider J., Priestley R.D., Datta S.S.** Multiscale dynamics of colloidal deposition and erosion in porous media // Science advances, 2020, vol. 6(46), eabc2530.
15. **Kuzmina L.I., Osipov Y.V., Pesterev A.R.** Deep bed filtration model for cake filtration and erosion // Applied Mathematics and Mechanics (English Edition), 2024, vol. 45(2), pp. 355–372.
16. **You Z., Bedrikovetsky P., Kuzmina L.** Exact Solution for Long-Term Size Exclusion Suspension-Colloidal Transport in Porous Media // Abstract and Applied Analysis, 2013, 680693.
17. **Galaguz Y.P., Kuzmina L.I., Osipov Y.V.** Problem of Deep Bed Filtration in a Porous Medium with the Initial Deposit // Fluid Dynamics, 2019, vol. 54(1), pp. 85–97.
18. **Kuzmina L.I., Osipov Yu.V.** Determining the Lengmur coefficient of the filtration problem // International Journal for Computational Civil and Structural Engineering, 2020, vol. 16(4), pp. 48–54.
19. **Galaguz Y.P.** Realization of the TVD-scheme for a numerical solution of the filtration problem // International Journal for Computational Civil and Structural Engineering, 2017, vol. 13(2), pp. 93–102.
20. **Safina G.L.** Filtration problem with nonlinear filtration and concentration functions // International Journal for Computational Civil and Structural Engineering, 2022, vol. 18(1), pp. 129–140.
21. **Osipov Yu., Safina G., Galaguz Yu.** Calculation of the filtration problem by finite differences methods // MATEC Web Conference, 2018, vol. 251(3), 04021.
22. **Courant R., Hilbert D.** Partial differential equations, Reprint of the 1962 Original, Edited, Wiley-InterScience, New York, 1989.
23. **Polyanin A.D., Manzhirov A.V.** Handbook of mathematics for engineers and scientists, Chapman & Hall/CRC, Boca Raton, FL, 2006.
24. **Maslov V.P., Arnold V.I., Buslaev V.S.** Theory of perturbations and asymptotic methods, Dunod, Paris, 1972.
25. **Kuzmina L.I., Osipov Y.V., Astachov M.D.** Bidisperse filtration problem with non-monotonic retention profles // Annali di Mathematica Pura ed Applicata (1923-), 2022, vol. 201, pp. 2943–2964.
26. **Kuzmina L.I., Osipov Y.V., Astachov M.D.** Retention profiles of multiparticle filtration in porous media // Mathematical Methods in the Applied Sciences, 2024, vol. 47, pp. 8319–8341.
27. **Kuzmina L., Osipov Y.** Filtration in porous medium with particle release //

Advances in Transdisciplinary Engineering, 2022, vol. 31, pp. 40–48.
28. **Kuzmina L.I., Osipov Y.V.** Particles Transport with Deposit Release in Porous Media // Lecture Notes in Civil Engineering, 2021, vol. 170, pp. 539–547.
29. **Vaz A., Bedrikovetsky P., Fernandes P.D., Badalyan A., Carageorgos T.** Determining model parameters for non-linear deep-bed filtration using laboratory pressure measurements // Journal of Petroleum Science and Engineering, 2017, vol. 151, pp. 421–433.
30. **Yang S., Russell T., Badalyan A., Schacht U., Woolley M., Bedrikovetsky P.** Characterization of fines migration system using laboratory pressure measurements // Journal of Natural Gas Science and Engineering, 2019, vol. 65, pp. 108–124.

СПИСОК ЛИТЕРАТУРЫ

1. **Zhou Z., Zang H., Wang S., Du X., Ma D., Zhang J.** Filtration Behavior of Cement-Based Grout in Porous Media // Transport in Porous Media, 2018, vol. 125, pp. 435–463.
2. **Xie B., Cheng H., Wang X., Yao Z., Rong C., Zhou R., Zhang L., Guo L., Yu H., Xiong, W., Xiang X.** Theoretical Research on Diffusion Radius of Cement-Based Materials Considering the Pore Characteristics of Porous Media // Materials, 2022, vol. 15, 7763.
3. **Zhu G., Zhang Q., Liu R., Bai J., Li W., Feng X.** Experimental and Numerical Study on the Permeation Grouting Diffusion Mechanism considering Filtration Effects // Geofluids, 2021, 6613990.
4. **Wang X., Cheng H., Yao Z., Rong C., Huang X., Liu X.** Theoretical Research on Sand Penetration Grouting Based on Cylindrical Diffusion Model of Tortuous Tubes // Water, 2022, vol. 14, 1028.
5. **Faramarzi L., Rasti A., Abtahi S.M.** An Experimental Study of the Effect of Cement and Chemical Grouting on the Improvement of the Mechanical and Hydraulic Properties of Alluvial Formations // Journal of Construction & Building Materials, 2016, vol. 126, pp. 32–43.
6. **Tien C.** Introduction to Cake Filtration, Elsevier, Amsterdam, 2006.
7. **Yim S.** A theoretical and experimental study on cake filtration with sedimentation // Korean Journal of Chemical Engineering, 1999, vol. 16, pp. 308–315.
8. **Civan F.** Reservoir formation damage, third ed, Gulf Professional Publishing, Burlington, MA, USA, 2014.
9. **Sacramento R.N., Yang Y., You Z., Waldmann A., Martins A.L., Vaz A.S.L., Zitha P.L.J., Bedrikovetsky P.** Deep bed and cake filtration of two-size particle suspension in porous media // Journal of Petroleum Science and Engineering, 2015, vol. 126, pp. 201–210.
10. **Khuzhayorov B.K., Saydullaev U., Ibragimov G., Wahi N.** An Axisymmetric Problem of Suspension Filtering with Formation of Elastic–Plastic Cake Layer // Symmetry, 2022, vol. 14(6), 1202.
11. **Herzig J.P., Leclerc D.M., Le Goff P.** Flow of Suspensions Through Porous Media – Application to Deep Filtration // Journal of Industrial & Engineering Chemistry, 1970, vol. 62(8), pp. 8–35.
12. **Bedrikovetsky P.** Upscaling of stochastic micro model for suspension transport in porous media // Transport in Porous Media, 2008, vol. 75, pp. 335–369.
13. **Kuzmina L.I., Osipov Y.V., Gorbunova T.N.** Asymptotics for filtration of polydisperse suspension with small impurities // Applied Mathematics and Mechanics (English Edition), 2021, vol. 42(1), pp. 109–126.
14. **Bizmark N., Schneider J., Priestley R.D., Datta S.S.** Multiscale dynamics of colloidal deposition and erosion in porous media // Science advances, 2020, vol. 6(46), eabc2530.
15. **Kuzmina L.I., Osipov Y.V., Pesterev A.R.** Deep bed filtration model for cake filtration and erosion // Applied Mathematics and Mechanics (English Edition), 2024, vol. 45(2), pp. 355–372.

16. **You Z., Bedrikovetsky P., Kuzmina L.** Exact Solution for Long-Term Size Exclusion Suspension-Colloidal Transport in Porous Media // Abstract and Applied Analysis, 2013, 680693.
17. **Galaguz Y.P., Kuzmina L.I., Osipov Y.V.** Problem of Deep Bed Filtration in a Porous Medium with the Initial Deposit // Fluid Dynamics, 2019, vol. 54(1), pp. 85–97.
18. **Kuzmina L.I., Osipov Yu.V.** Determining the Lengmur coefficient of the filtration problem // International Journal for Computational Civil and Structural Engineering, 2020, vol. 16(4), pp. 48–54.
19. **Galaguz Y.P.** Realization of the TVD-scheme for a numerical solution of the filtration problem // International Journal for Computational Civil and Structural Engineering, 2017, vol. 13(2), pp. 93–102.
20. **Safina G.L.** Filtration problem with nonlinear filtration and concentration functions // International Journal for Computational Civil and Structural Engineering, 2022, vol. 18(1), pp. 129–140.
21. **Osipov Yu., Safina G., Galaguz Yu.** Calculation of the filtration problem by finite differences methods // MATEC Web Conference, 2018, vol. 251(3), 04021.
22. **Courant R., Hilbert D.** Partial differential equations, Reprint of the 1962 Original, Edited, Wiley-InterScience, New York, 1989.
23. **Polyanin A.D., Manzhirov A.V.** Handbook of mathematics for engineers and scientists, Chapman & Hall/CRC, Boca Raton, FL, 2006.
24. **Maslov V.P., Arnold V.I., Buslaev V.S.** Theory of perturbations and asymptotic methods, Dunod, Paris, 1972.
25. **Kuzmina L.I., Osipov Y.V., Astachov M.D.** Bidisperse filtration problem with non-monotonic retention profles // Annali di Mathematica Pura ed Applicata (1923-), 2022, vol. 201, pp. 2943–2964.
26. **Kuzmina L.I., Osipov Y.V., Astachov M.D.** Retention profiles of multiparticle filtration in porous media // Mathematical Methods in the Applied Sciences, 2024, vol. 47, pp. 8319–8341.
27. **Kuzmina L., Osipov Y.** Filtration in porous medium with particle release // Advances in Transdisciplinary Engineering, 2022, vol. 31, pp. 40–48.
28. **Kuzmina L.I., Osipov Y.V.** Particles Transport with Deposit Release in Porous Media // Lecture Notes in Civil Engineering, 2021, vol. 170, pp. 539–547.
29. **Vaz A., Bedrikovetsky P., Fernandes P.D., Badalyan A., Carageorgos T.** Determining model parameters for non-linear deep-bed filtration using laboratory pressure measurements // Journal of Petroleum Science and Engineering, 2017, vol. 151, pp. 421–433.
30. **Yang S., Russell T., Badalyan A., Schacht U., Woolley M., Bedrikovetsky P.** Characterization of fines migration system using laboratory pressure measurements // Journal of Natural Gas Science and Engineering, 2019, vol. 65, pp. 108–124.

Liudmila I. Kuzmina, Candidate of Physical and Mathematical Sciences, Associate Professor, Department of Applied Mathematics, National Research University Higher School of Economics, 101000, Russia, Moscow, Myasnitskaya st., 20, tel. +7(495) 77295 90 * 15219, e-mail: lkuzmina@hse.ru.

Yuri V. Osipov, Candidate of Physical and Mathematical Sciences, Professor, Department of Computer Science and Applied Mathematics, Moscow State University of Civil Engineering, 129337, Russia, Moscow, Yaroslavskoe Shosse, 26, tel. +7(499)1835994, e-mail: yuri-osipov@mail.ru.

Кузьмина Людмила Ивановна, доцент, кандидат физико-математических наук, Департамент прикладной математики МИЭМ им. А.Н. Тихонова, Национальный исследовательский университет «Высшая школа экономики»; 101000, г. Москва, ул. Мясницкая, д. 20, тел. +7(495) 77295 90 *15219; e-mail: lkuzmina@hse.ru.

Осипов Юрий Викторович, профессор, кандидат физико-математических наук, кафедра информатики и прикладной математики Национального исследовательского Московского государственного строительного университета; 129337, Россия, г. Москва, Ярославское шоссе, д. 26; тел. +7(499)1835994; e-mail: yuri-osipov@mail.ru.

DOI:10.22337/2587-9618-2024-20-3-125-144

RC BUILDINGS RESPONSE TO EARTHQUAKES: NONLINEAR STATIC ANALYSIS CONSIDERING VARYING SOIL TYPES AND SEISMIC CODES

Amer Yassin [1], Rifat Resatoglu [2]

[1] Department of Civil Engineering, Faculty of Civil and Environmental Engineering, Nicosia, NORTHERN CYPRUS
[2] Department of Civil Engineering, Faculty of Civil and Environmental Engineering, Nicosia, NORTHERN CYPRUS

Abstract: Reinforced concrete (RC) building construction remains predominant in Northern Cyprus, offering resilience against natural disasters when appropriately designed and implemented. This paper presents a seismic analysis of RC building systems across different stories, configurations, and soil classes, according to three seismic design codes: The Northern Cyprus Seismic Code 2015 (NCSC-2015), Eurocode 8 (EC 8), and Turkish Buildings Earthquake Code 2018 (TBEC-2018). The study compares regular and irregular forms of Moment Resisting Frame (MRF) and MRF combined with Shear Walls (MRF+SW) systems in various configurations: G+3, G+7, and G+11 for regular buildings, and only G+11 for irregular buildings. Pushover analysis using ETABSv18 was employed to assess base shear, displacement, and plastic hinge behavior. The results indicate that structural regularity enhances resistance and longevity compared to irregular configurations, with shear walls augmenting resistance against earthquake loads in both regular and irregular buildings. Furthermore, soil class emerges as a significant factor influencing results across the codes. While variations among the codes were not consistently observed, EC 8 and TBEC-2018 often appeared more conservative, with TBEC-2018 demonstrating greater adaptability to advanced technologies and a more detailed parameter consideration.

Keywords: Earthquake, Pushover analysis method, Reinforced concrete, Soil classes, Seismic codes, Northern Cyprus, ETABSv18

ОТКЛИК ЖЕЛЕЗОБЕТОННЫХ КАРКАСОВ ЗДАНИЙ ПРИ ЗЕМЛЕТРЯСЕНИЯХ: НЕЛИНЕЙНЫЙ СТАТИЧЕСКИЙ АНАЛИЗ С УЧЕТОМ РАЗЛИЧНЫХ ТИПОВ ГРУНТОВ И СЕЙСМИЧЕСКИХ НОРМ

Амер Ясин [1], Рифат Ресатоглу [2]

[1] Кафедра гражданского строительства, факультет гражданского и экологического строительства, г. Никосия, СЕВЕРНЫЙ КИПР
[2] Кафедра промышленного и гражданского строительства, факультет промышленного, гражданского и экологического строительства, г. Никосия, СЕВЕРНЫЙ КИПР

Аннотация: Железобетонные здания по-прежнему преобладают на Северном Кипре, поскольку они обладают устойчивостью к стихийным бедствиям при правильном проектировании и строительстве. В данной статье представлен расчет сейсмостойкости железобетонных несущих систем зданий различной этажности, конфигурации при различных категориях грунта в соответствии с тремя кодексами сейсмического проектирования: нормы сейсмостойкого строительства Северного Кипра 2015 года (NCSC-2015), Еврокод 8 (EC 8) и Турецкие нормы сейсмостойкого строительства 2018 года (TBEC-2018). В исследовании сравниваются регулярные и нерегулярные рамные каркасы с диафрагмами жесткости в различных конфигурациях: G+3, G+7 и G+11 для обычных зданий и G+11 для нерегулярных каркасов зданий. Для оценки сдвига основания, перемещений и работы пластических шарниров был применен pushover - анализ с использованием программного комплекса ETABSv18. Результаты показывают, что регулярность каркасов зданий повышает их устойчивость к воздействиям и долговечность по сравнению с нерегулярными конфигурациями каркасов. Диафрагмы жесткости повышают устойчивость к сейсмическим нагрузкам как в регулярных, так и в нерегулярных каркасах зданий. Кроме того, категория грунта является значимым фактором, влияющим на результаты расчета согласно всем рассмотренным кодексам проектирования. Хотя различия между кодексами не столь существенны, EC 8 и TBEC-2018

часто оказываются достаточно консервативными. При этом TBEC-2018 демонстрирует большую адаптируемость к передовым технологиям и более детальному рассмотрению параметров.

Ключевые слова: землетрясение, pushover анализ, железобетон, категории грунтов, сейсмические кодексы, Северный Кипр, ETABSv18

INTRODUCTION

Reinforced concrete structures are frequently seen worldwide due to the high capacity they can carry and the large number of floors they can consist of. Consequently, a comprehensive understanding of RC structure design is crucial, as failure in any component or joint can lead to catastrophic collapse, resulting in significant loss of life. Particularly, the consideration of earthquake loads in RC structure design has become paramount due to the substantial casualties often associated with seismic events. While it's impossible to guarantee complete safety during earthquakes, adherence to seismic code regulations can substantially enhance building safety. For instance, the recent earthquake in Turkey and Northern Syria on February 6th, 2023, measuring 7.7 magnitude and followed by a 7.6 magnitude aftershock with over 9000 subsequent tremors, highlighted the consequences of neglecting code requirements. The failure to comply with seismic codes led to outcomes surpassing initial expectations. In general, strict adherence to code regulations is imperative to ensure structural resilience. Furthermore, code standards must be periodically updated to facilitate earthquake-resistant building design. However, in the case of Turkish codes, the comprehensive update process can be lengthy (Aksoylu et al., 2020).

ETABS has garnered considerable recognition and undergone substantial evolution over a span exceeding three decades, as delineated by Mule et al. (2020). A plethora of prior scholarly investigations have directed their focus toward leveraging ETABS for conducting structural analyses. Furthermore, its amenability to accommodating various design codes has facilitated the seamless execution of analyses across diverse regulatory frameworks, owing to its comprehensive repository encompassing such codes.

Seismic activity poses a complex load on structures, necessitating precise analysis to predict structural response accurately (Kocer, 2021). This seismic movement is categorized into various grades based on intensity. The first grade represents low movement, typically resulting in minimal to no damage. The second grade signifies moderate movement, which may lead to some non-structural damage. Finally, the third grade denotes intensive movement, causing both structural and non-structural damage (Yassin & Sadeghi, 2023).

The focus of this study is Northern Cyprus, which shares a direct border with Southern Cyprus. Both regions exhibit similarities in geographical nature, soil type, and environmental factors. Additionally, they are situated amidst two fault lines stemming from the East Anatolian Fault line. Despite these similarities, Northern Cyprus and Southern Cyprus adhere to different earthquake regulations, utilize distinct design codes, and consider various designing parameters. Furthermore, Northern Cyprus imports certain materials from Turkey, aligned with TBEC-2018 standards. Despite existing studies comparing different earthquake codes, there is a scarcity of research pertaining to NCSC-2015. Thus, there is a compelling need to compare NCSC-2015, EC 8, and TBEC-2018, as they all play integral roles or indirectly influence the same geographical area.

In the context of structural design practices in Cyprus, the NCSC-2015 standard is predominantly applied within the jurisdiction of Northern Cyprus, albeit supplemented by the importation of construction materials from

Turkey, as inferred from references within TEC-2007. Conversely, the EC8 standard finds prevalence in Southern Cyprus. Despite this, there remains a notable absence of direct comparisons between these codes in existing literature. Existing research has shown significant differences and inconsistencies, highlighting the need for a thorough investigation across different factors like soil type, number of storeys, and geographical locations. Therefore, this study seeks to strengthen and expand on previous findings, improving the reliability and applicability of the conclusions drawn from the analysis.

The following are some previous studies:

A comparative study between two Seismic design codes EC8 and NCSC-2015 was carried out by Reşatoğlu & Hamed, 2019. The results of base shear for EC8 and NCSC-2015 were similar. Another study carried out by Aksoylu et al, 2020 compares TBEC-2018, ASCE 7-16, and TEC-2007 using the linear equivalent method to analyze buildings with a different number of stories. The results show that the maximum base shear force was achieved at TEC-2007 for buildings that consist of 3 and 5 stories, whereas the maximum base shear force was achieved at TBEC-2018 for buildings that consist of 7 and 9 stories.

A study conducted by Atmaca & Atmaca in 2019 pointed out that the TBEC-2018 introduces two new earthquake analysis methods, namely Nonlinear and Linear, which were not present in TEC-2007. Moreover, TBEC-2018 offers several advantages, including specifying the earthquake site and the soil type with six classes instead of four. Additionally, it accounts for both long and short periods of acceleration coefficients. Ultimately, the study's findings indicate that the 2018 code is more cautious compared to the previous one.

In conclusion, Nicosia (Gonyeli region) and Yeni Iskele (Long Beach region) were selected in this study due to the population growth and the different soil type properties they have. For example, the Long Beach region has alluvial soil while some locations in southern Turkey that were affected by the 6th of February earthquake have the same soil. This soil type is listed as the softest soil type in the three codes, while it significantly amplifies the shaking of the ground during earthquakes (Büyüksaraç et al, 2014).

The primary aim of this study is to compare the analysis outcomes of NCSC-2015, EC 8, and TBEC-2018, with the following objectives:

1. Conducting seismic analysis through nonlinear static analysis (Push Over) of both three-dimensional (3D) regular and irregular moment-resisting frame (MRF) systems, as well as regular and irregular moment-resisting frame with shear walls (MRF+SW) systems using ETABSv18 Software.
2. Comparing the resulting base shear and displacement values obtained from the analysis.
3. Observing the formation of plastic hinges to identify the weakest joints within the building structures.

SEISMICITY OF CYPRUS

The predicted period for the return of a rock condition earthquake is estimated to be 475 years. The studied area, Cyprus, is surrounded by three tectonic plates: the Anatolian plate moving westward, the African plate moving northward, and the Arabian plate moving northward at a faster pace. These plates are interconnected by fault lines, including the East Anatolian fault line, which has two extension fault lines traversing through the island. Previous studies, such as those by Cagnan et al. (2010), have suggested that the East Anatolian Fault has active extensions both to the south and north of Cyprus. These fault lines span across several countries, including Turkey, Syria, Cyprus, Lebanon, Palestine, and Jordan, as depicted in Figure 1.

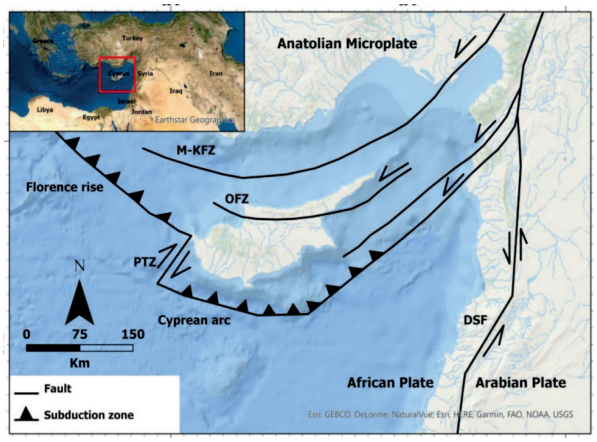


Figure 1. The Fault Lines Between the Anatolian Plate, Arabian Plate, and African Plate (Evelpidou. 2022)

SESMIC DESIGN CODES

Codes serve as the foundation of design regulations, providing engineers with essential guidelines for their calculations. It is crucial for codes to undergo continuous study and updating over time to ensure they evolve and remain relevant. In the realm of civil engineering, earthquake codes have been established for quite some time. In Turkey, for instance, earthquake codes date back to as early as 1940, with the most recent version being in 2018, marking the 10th iteration (Işık, 2021).

NCSC-2015 and EC8 have a seismic zone map that shows different areas based on earthquake severity, where each area has a specific peak ground acceleration (PGA). The map is divided into four seismic zones according to NCSC-2015 and three seismic zones according to EC8, where the selected locations in this study are located in the first zone in NCSC-2015 and the second zone in EC8 as shown in Fig 2 and Fig 3.

The TBEC-2018 introduces changes in the process compared to NCSC-2015 and EC8. Instead of PGA values, it now employs short-period spectral acceleration (Ss) and long-period spectral acceleration (S1). Furthermore, it's the first code to incorporate horizontal and vertical design spectra, appearing to be better aligned with modern technologies. It's launched with more detailed information for each province in Turkey. Unfortunately, this code and its map are specific to Turkey, but the approach can be adapted and applied to other codes in different regions.

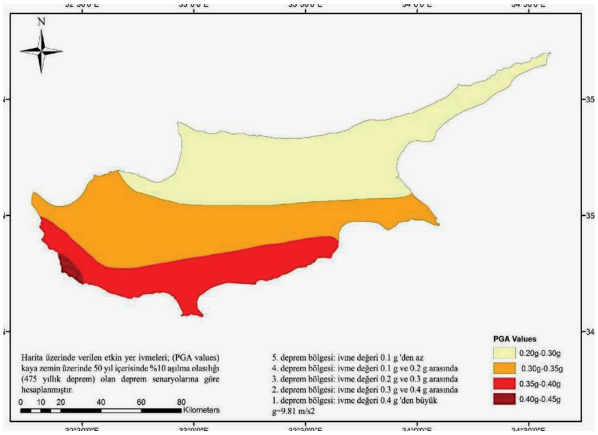


Figure 2. Seismic Zoning Map of Cyprus According to NCSC-2015 (NCSC-2015)

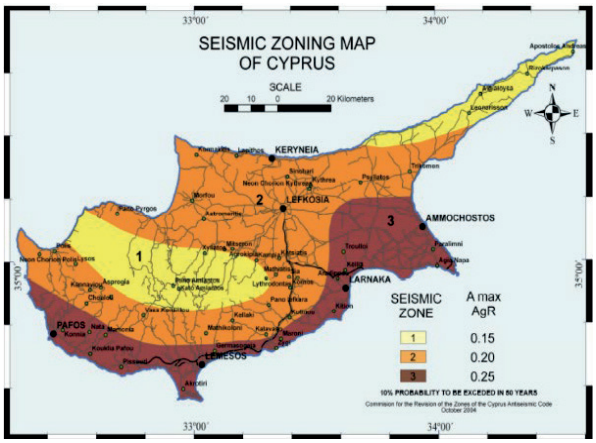


Figure 3. Seismic Zoning Map of Cyprus According to EC8 (Cyprus National Annex, Eurocode 8)

To conclude, numerous new concepts have been added in TBEC-2018 such as the classification of building height, earthquake ground motion level, vertical elastic design spectrum, earthquake design class, and the application of earthquake hazard on a regional basis was the most important addition to this code (Büyüksaraç, 2022).

In order to obtain the ratio of spectral acceleration to PGA check Fig 4, which represents the ratio between spectral acceleration and PGA of return periods ranging from 100 to 1000 years from the database of more than 50 studies. (Lubkowski & Aluisi, 2012).

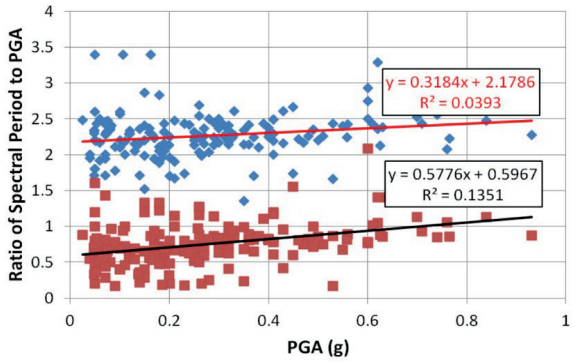


Figure 4. The Ratio of Spectral Period to PGA from Seismic Hazard Database (Lubkowski & Aluisi, 2012)

Blue diamonds represent the ratio between Ss and PGA, and therefore, by identifying the PGA, Ss can be obtained from this equation:

SS/PGA= 0.3386 PGA + 2.1696

On the other hand, red squares represent the ratio between S1 and PGA, and therefore, by identifying the PGA, S1 can be obtained from this equation:

$$S1/PGA= 0.5776\ PGA + 0.5967$$

NONLINEAR STATIC ANALYSIS

The pushover analysis method is the method that aims to push the structure till it reaches the maximum resistance, and according to the applied earthquake properties such as PGA, soil type, spectral acceleration, etc, the building has two possibilities:

1. If a building reaches a collapsed state, therefore, this building is unsafe, and the applied earthquake loads have pushed the structure till it collapses.
2. If a building reaches its maximum limit without collapsing during an earthquake, it means that the structure has endured the maximum earthquake loads without showing any critical hinges. This indicates that the building is considerably safe and that the applied earthquake loads have pushed the structure to a specific limit.

This method evaluates the real strength and structure seismic performance. Therefore, after running the pushover analysis, the base shear and displacement curve can be obtained, this curve shows the start point and the maximum point that the structure has reached whether it collapsed after this point or not as shown in Fig 5.

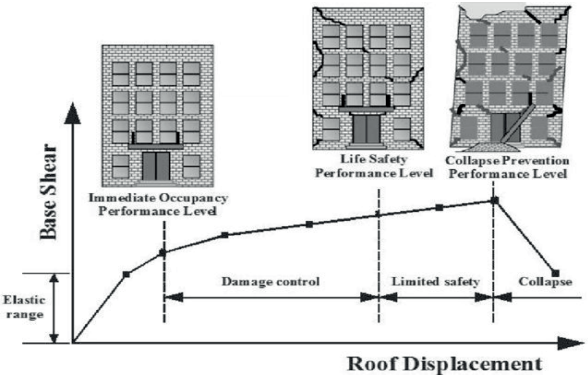


Figure 5. Capacity Curve of Structures with Demonstration of Damage State and Building Performance Level (Abd-Elhamed & Mahmoud, 2016)

The previous figure describes the seismic performance of a building during an earthquake in four steps Operational, Immediate Occupancy (IO), Life Safety (LS), and Collapse Prevention (CP), respectively, and each step has a worse state compared to the previous step.

METHODOLOGY

Several case studies were analyzed according to these three earthquake regulations NCSC-2015, EC 8, and TBEC-2018, targeting to obtain different outcomes for strengthening the comparative study.

In this study, regular and irregular floorplan structures have been selected with specific details. For example, the ground story height is 3.2 m, whereas the remaining stories' heights are 3 m. The beams and columns were modelled as frame elements, whereas solid slabs and shear walls were modelled as shell elements. Additionally, Plastic hinges were added at 10% and 90% of the length of each column and beam, to achieve more accurate results while applying the pushover analysis method and observing plastic hinges occurrence, which is practical to predict the first member to fail.

The modeling of foundations was intentionally omitted from the scope of this study and was simply treated as fixed within the software to streamline and expedite the process, given the large number of buildings being modeled. The primary objective of the study is to compare the outcomes of different codes and determine the most effective one for future studies. Consequently, this assumption was uniformly applied across all selected models. However, it is important to note that the results could be influenced and altered if alternative foundation types were utilized. In a 2015 study by Somwanshi and Pantawane, it was revealed that buildings with fixed bases exhibit no displacement at their base, whereas those with base isolation exhibit discernible displacement. This implies that the application of this assumption to all models could uniformly impact the results of each model.

The ETABS models were executed following a systematic procedure:

1. Material properties were selected.
2. Cross-sections for columns, beams, shear walls, and slabs were added.
3. Models were drawn.
4. Pattern loads including dead load, super dead load, live load, wind load, and earthquake load were incorporated.
5. Loads were applied to the members, excluding earthquake loads.
6. Plastic hinges were defined at the corners.
7. Nonlinear Static (pushover) load cases were addressed as follows:

A. The first load case considered dead load only.

B. The second load case considered super dead load with a scale factor of 1 and live load with a scale factor of 0.25. This case initiated after the completion of the first load case.

C. The third load case considered earthquake acceleration for both x and y directions with a scale factor of -1. Additionally, this case commenced after the second load case, and P-Delta effects were considered.

8. The analysis was executed.

P-Delta effect occurs when horizontal earthquake loads induce drift on structural elements, resulting in an eccentricity of the gravity loads along the vertical column axis. This induced eccentricity amplifies internal moments, consequently influencing the first-order moment (Istiono et al., 2022), as depicted in Figure 6.

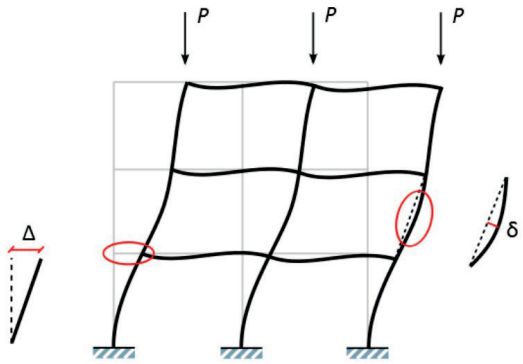


Figure 6. P-Large Delta (P-Δ) & P-Small Delta (P-δ)

In this study, the analyzed models consist of two systems: the Moment Resisting Frame (MRF) system and the combination of MRF with Shear Walls (MRF+SW) system. These systems were assessed with a shear wall span length of 1.5 meters in regular form for low, mid, and high-rise buildings. Additionally, irregular forms were considered solely for high-rise structures. Moreover, to ensure a robust comparison, the member sizes were kept consistent across all structures within each story for all three selected codes. Furthermore, two locations were selected: Yeni Iskele (Long Beach region) and

Nicosia (Gönyeli region). These locations exhibit distinct soil characteristics, as detailed in Tables 2, 3, and 4. Ground surveys aimed at earthquake resilience in the country reveal that the Long Beach region's coastal area has the lowest bearing capacity and is susceptible to liquefaction (Selcukhan & Ekinci, 2023). This region is characterized by soft alluvial soil, classified as class D in NCSC-2015 and class E in EC8 and TBEC-2018. Conversely, Nicosia city's soil varies, with the north featuring rocky medium soil, the center consisting of soft rock or very dense soil, and the south comprising solidified soil groups (Dindar, 2021). The Göneyli region, located in Nicosia, is characterized by stiff soil, classified as class C across all codes. Despite these differences, both locations were chosen due to their notable population growth and urbanization trends, as depicted in Figure 7.

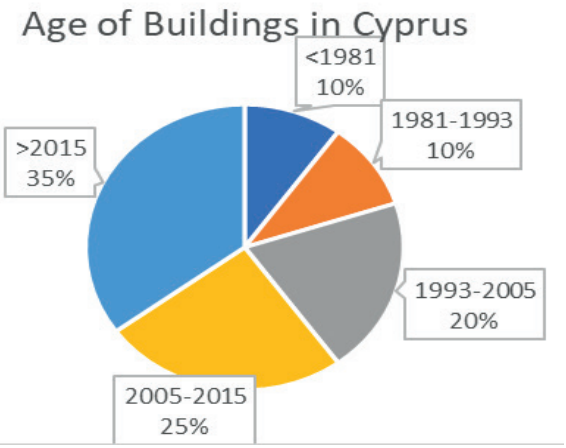


Figure 7. Buildings Age in Northern Cyprus (Earthquake committee meetings of the presidency of TRNC)

A. Regular Structures

These structures should be symmetrical in principle direction and have no significant discontinuity in plan or lateral configurations. In addition, members must continuously run from the highest point to the foundation without interruptions (Yadav & Hazari, 2022). Additionally, the structure can be described as having continuities in both plan and vertical configurations (Naveen et al., 2019). For this study, a regular typical plan was chosen, representing a residential building with three different story configurations: G+3, G+7, and G+11. These configurations have dimensions of 25 meters on the X axis and 25 meters on the Y axis, comprising five bays with a 5-meter bay length in each direction.

- Moment-Resisting Frame (MRF) in regular form as shown in Fig 8 and Fig 9.
- Moment-Resisting Frame with Shear Walls (MRF+SW) in regular form as shown in Fig 10 and Fig 11.

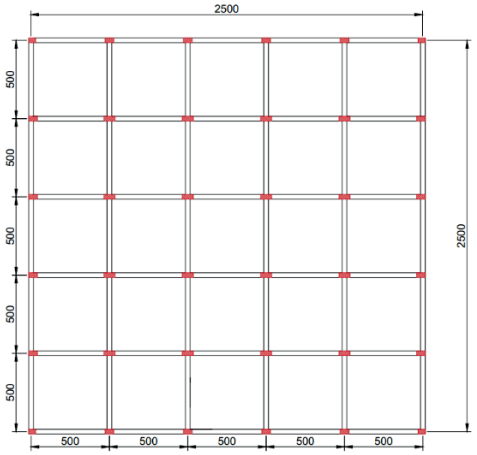
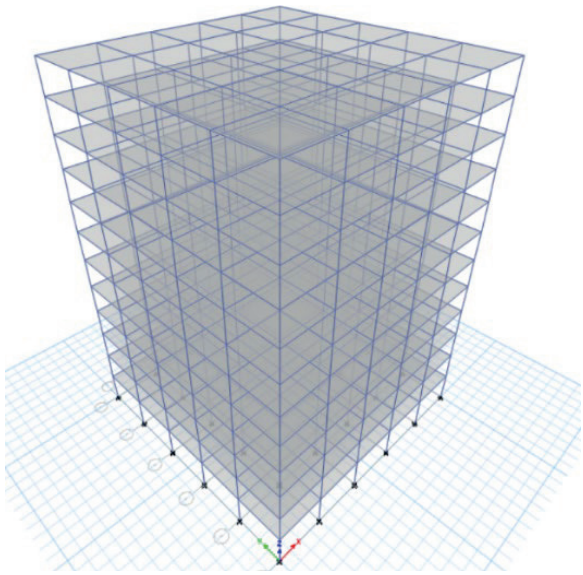
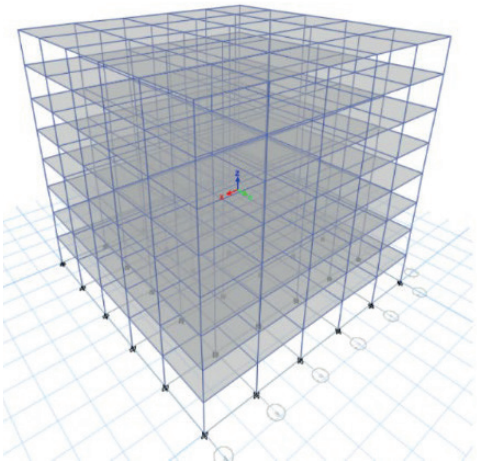


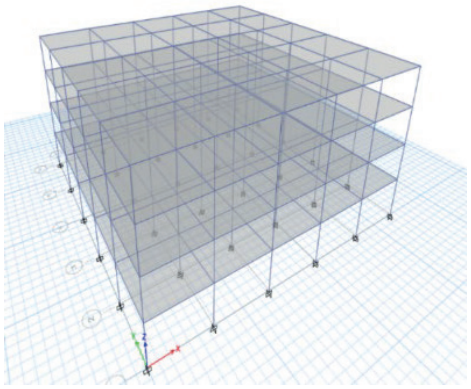
Figure 8. Floor plan for Moment-Resisting Frame (MRF) in Regular Form



a) G+11 stories



b) G+7 stories



c) G+3 stories

Figure 9. The 3D dimensional view for moment resisting frames (MRF) in regular form. a) G+11 Stories, b) G+7 Stories, c) G+3 Stories

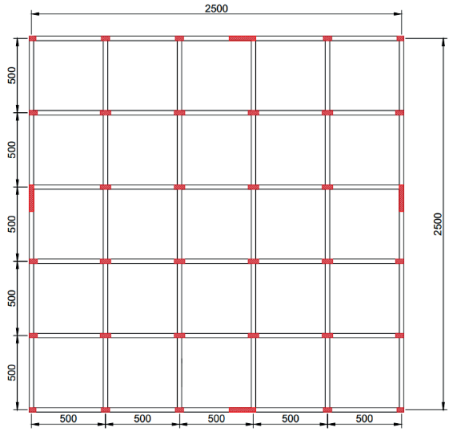
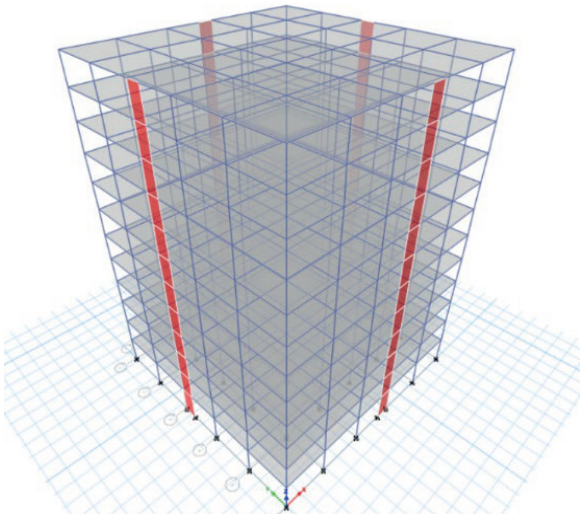
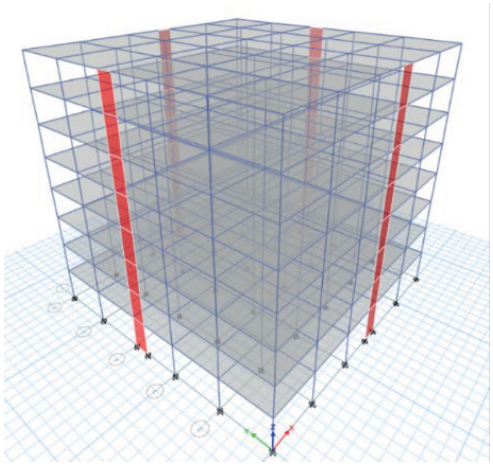


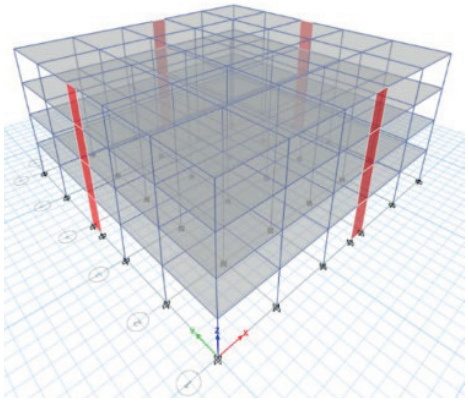
Figure 10. Floor Plan for Moment-Resisting Frame with shear walls (MRF+SW) in Regular Form



a) G+11 stories



b) G+7



c) G+8 stories

Figure 11. The 3D Dimensional View for (MRF+SW) in Regular Form a) G+3 Stories, b) G+7 Stories, c) G+11 Stories

B. Irregular Structures

These structures have a sudden physical discontinuity, either in plan, lateral configuration, or both, as they are kept unsymmetrical in the principal direction. (Yadav & Hazari, 2022). As a consequence, irregularity affects the structure's performance when it's subjected to seismic loads (Naveen et al, 2019). In simpler terms, irregular structures lack symmetry either in the X or Y coordinates, or both. Despite being recognized as weaker compared to regular structures in previous studies, they remain prevalent due to factors such as geographical constraints and other considerations. A residential building with an irregular plan was chosen for this study. It comprises eleven stories (G+11) and has dimensions of 25 meters on both the X and Y axes. The building features discontinuous five bays, each with a length of 5 meters.

- Moment-Resisting Frame (MRF) in irregular form as shown in Fig 12 and Fig 13.

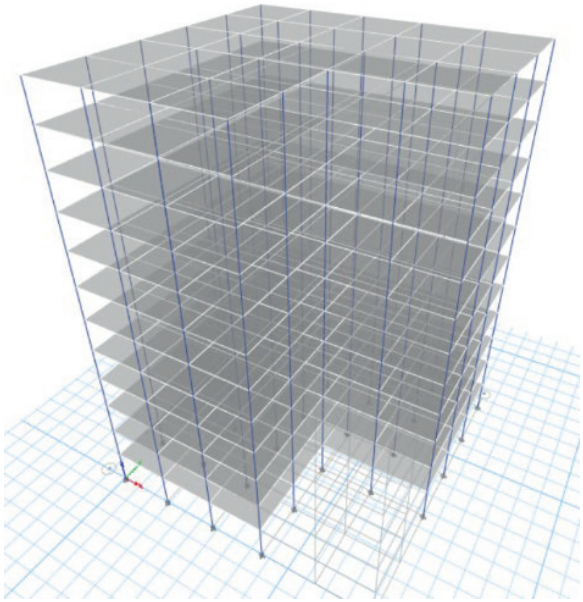


Figure 13. The 3D Dimensional View for (MRF) in Irregular Form

- Moment Resisting Frame with Shear walls (MRF+SW) in irregular form as shown in Fig 14 and Fig 15.

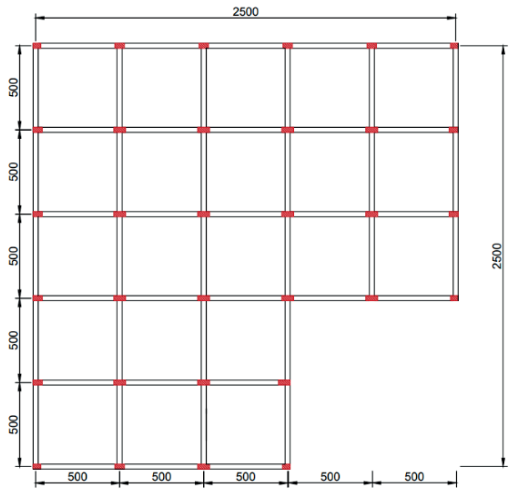


Figure 12. Floor Plan for Moment-Resisting Frame (MRF) in Irregular Form

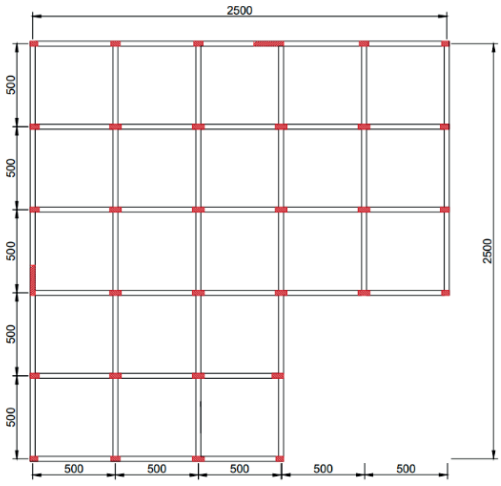


Figure 14. Floor Plan for (MRF+SW) in Irregular Form

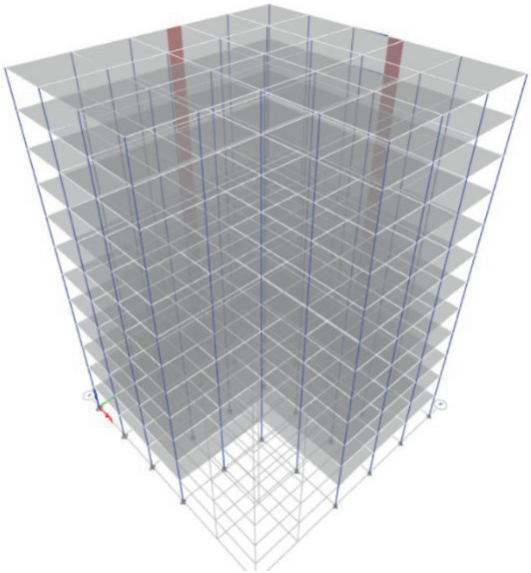


Figure 15. The 3D Dimensional View for (MRF+SW) in Irregular Form

DESIGN CRITERIA

48 models were analyzed by applying the nonlinear static analysis (Pushover Analysis) using ETABSv18 software. Furthermore, the same material properties and loads were applied for all buildings, such as dead load, super dead load, and live load. On the other hand, earthquake loads were selected according to the parameters of each code. The design criteria are shown as follows.

A. Material Properties.

The materials selected for the study were chosen to meet the requirements of all three codes. For instance, the minimum concrete strength specified by NCSC-2015, EC8, and TBEC-2018 is C20, C20/25, and C25, respectively. Additionally, following the 1999 earthquakes, the Turkish Ready Mixed Concrete Association recommended the use of C30 concrete in earthquake-prone areas (Zengin et al., 2023). Therefore, for this study, C30 concrete, which possesses a compressive strength of 30 MPa, was selected, with other concrete parameters determined accordingly based on this strength grade. The codes have different reinforcement steel classes. NCSC-2015 contains three steel classes S220, S420, and S500, while EC8 and TBEC-2018 have different steel classes. However, the only common steel class among the codes is S420. Therefore, this study uses the S420 steel grade. For brick walls, the approach differs as they can be chosen based on the prevalent brick wall type in the region. Hence, an average value was selected for the unit weight of brick walls. The table below displays the chosen parameters for concrete, steel, and brick walls for the study:

Table 1. Material properties of steel, concrete and walls

Parameter	Value
Compressive Strength ($f'c$)	30 MPa
Unit weight of Concrete	$30\ kN/m^3$
Concrete Modulus of Elasticity	25743 MPa
Yield Stress (Fy)	420 MPa
Minimum Tensile Strength (Fu)	520 MPa
Unit weight of Steel	$78.5\ kN/m^3$
Steel Modulus of Elasticity	210000 MPa
Unit weight of Brick walls	$16\ kN/m^3$

B. Section Properties.

Regular and Irregular models were selected for the analyzed structures consisting of 180mm solid slabs, (250mm*500mm) beams, 250mm external clay brick walls, 200mm internal clay brick walls, 250mm shear walls, and columns ranging from (300mm*300mm) to (300mm*800mm) depending on the floor and the position of the column, for example, the columns at the top floor are the smallest, and their size increase gradually to the bottom floor. In addition, the corner columns are the smallest, and the size increases in the external

columns, where the center columns are the biggest.

C. Load Properties.

The selected loads were considered according to the codes and unit weight of the materials as follows: live load (2kN/m2), Super Dead load (2.5 kN/m2), external walls (12 kN/m), internal walls (9.6 kN/m), where dead load and wind load considered from the software. In addition, earthquake loads were taken according to each code as shown in part D.

D. Seismic Properties.

Earthquake properties are considered according to the requirements of each code, and the selected locations that mentioned in this study.

The properties are shown in the following tables:

Table 2. NCSC-2015 earthquake regulations for both selected locations in the study

Description		Nicosia (Gönyeli region)	Yeni Iskele (Long beach region)
Seismic Zone		1	1
Peak Ground acceleration (PGA)		0.3	0.3
Soil type		C	D
Behaviour factor (R)	**MRF**	8	8
	MRF+ SW	7	7
Importance factor (I)		1	1

Table 3. EC 8 earthquake regulations for both selected locations in the study

Description		Nicosia (Gönyeli region)	Yeni Iskele (Long beach region)
Seismic Zone		2	2
Peak Ground acceleration (PGA)		0.2	0.2
Soil type		C	E
Soil Factor		1.15	1.4
Importance factor (I)		1	1
Lower limit of the period (TB)		0.2	0.15
Upper limit of the period (TC)		0.6	0.5
The beginning of the constant displacement (TD)		2	2
Behaviour Factor q	**MRF**	5.85	5.85
	MRF +SW	5.4	5.4
Correction Factor		1	1

Table 4. TBEC-2018 earthquake regulations for both selected locations in the study

Description		Nicosia (Gönyeli region)	Yeni Iskele (Long beach region)
Spectral Acceleration for short period (Ss)		0.6795	0.6795
Spectral Acceleration for 1 second (S1)		0.2259	0.2259
Long-Period Transition Period		8	8
Site type		ZC	ZE
Response modification (R)	**MRF**	8	8
	MRF +SW	7	7
System overstrength (D)	**MRF**	3	3
	MRF +SW	2.5	2.5
Importance factor (I)		1	1

RESULTS AND DISCUSSION

In this part, all obtained results from the Non-linear Static Analysis method such as base shear, displacement, and plastic hinges occurrence were presented and explained as graphs and compared according to regular and irregular structures. The results were prepared in order of building type as follows:

1. MRF in Regular Form

The results such as base shear, displacement, and plastic hinges formation for MRF in regular form were obtained according to two soil types, three codes, and three different story structures with different numbers of stories.

A. Base Shear and Displacement.

The pushover curve that shows the base shear forces and displacement for MRF residential buildings in regular form with different number of stories, different codes, and soil classes are shown below in Fig 16 and Fig 17.

Based on the preceding graph charts, both NCSC-2015 and EC8 exhibited marginal increases, not exceeding 5%, in the soft soil class across all the models. In contrast, TBEC-2018 demonstrated an increase in the soft soil class for all models.

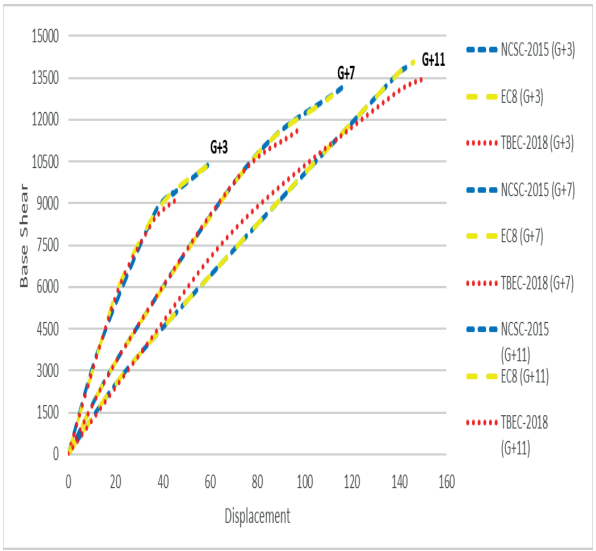


Figure 16. Pushover Curves for MRF structure in regular form, medium soil class

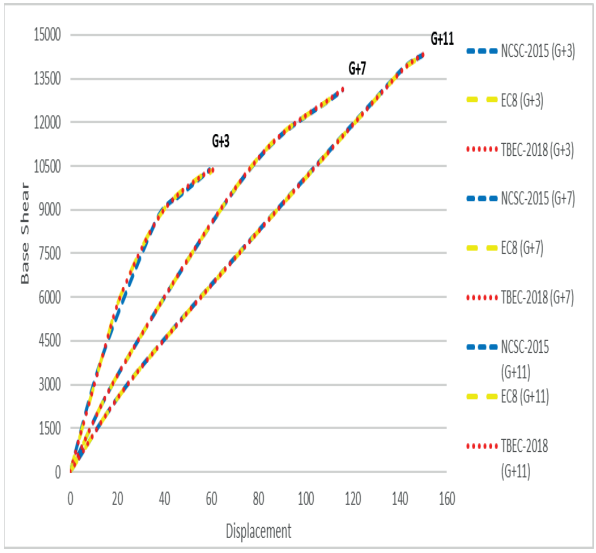


Figure 17. Pushover Curves for MRF structure in regular form, soft soil class

In TBEC-2018, there was a modest 6% increase in base shear for the G+11 model in the soft soil class. However, this increase escalated in the G+7 models, reaching 12% for base shear and 18% for displacement. Moreover, the G+3 models experienced a slight rise in the soft soil class, reaching 14% for base shear and 23% for displacement.

B. Plastic Hinges.

The presence of plastic hinges plays a critical role in determining the structural integrity of buildings during earthquakes. In many instances, plastic hinges were observed in various locations throughout the buildings, with some exceeding the critical plastic (CP) state, particularly in the ground and first stories. As a consequence, all those models in the selected areas are in danger and not lucky enough to stay standing during earthquakes.

C. Summary.

EC8 and NCSC-2015 exhibited only a slight disparity between medium and soft soil classes, whereas TBEC-2018 demonstrated a more significant and realistic discrepancy, with a notable increase in the soft soil class.

The regular MRF models appeared to be vulnerable in earthquake-prone areas, as indicated by the increase in base shear and displacement in soft soil class models.

Moreover, in some instances, these values remained comparable to those in medium soil class models.

Furthermore, the majority of plastic hinge occurrences, including the CP state, were concentrated in the first three stories. Consequently, these models appear to be at substantial risk, as failure in any of these plastic hinges could potentially result in the collapse of the entire structure in practice.

2. MRF+SW In Regular Form

The results such as base shear, displacement, and plastic hinges formation for MRF+SW in regular form were obtained according to two soil types, three codes, and three different story structures with different numbers of stories.

A. Base Shear and Displacement.

The pushover curve that shows the base shear forces and displacement for MRF+SW residential buildings in regular form with different number of stories, different codes, and soil classes are shown below in Fig 18 and Fig 19.

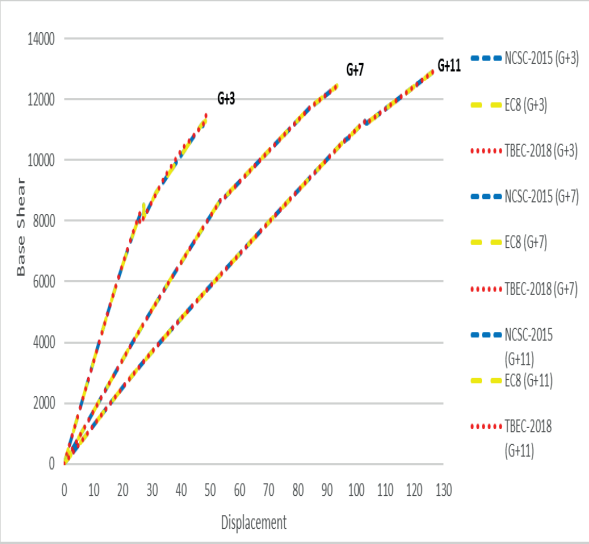


Figure 18. Pushover Curves for MRF+SW structures in regular form, medium soil class

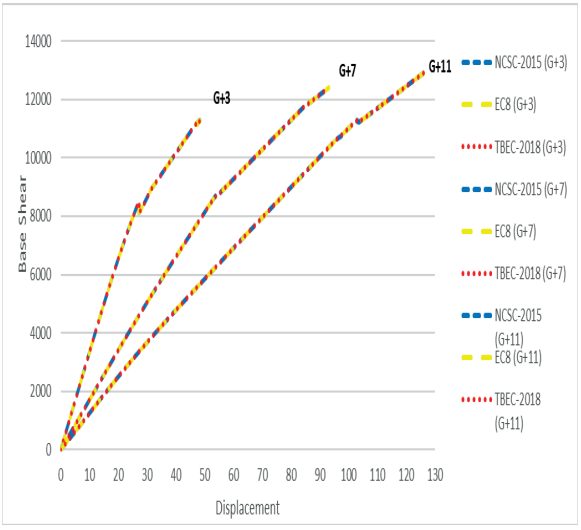


Figure 19. Pushover Curves for MRF+SW structures in regular form, soft soil class

The graph lines indicate that across all cases, there are relatively consistent results between medium and soft soil types. However, while the base shear shows a slight increase from G+3 to G+11, the displacement experiences a significant rise over the same range.

In NCSC-2015 and EC8 models, no notable distinctions were observed between medium and soft soil classes; their performances appeared similar.

Contrastingly, TBEC-2018 exhibited a slight decrease in base shear and displacement by approximately 5% in the soft soil class for G+3 models. Additionally, only one plastic hinge, reaching the critical plastic (CP) state, was identified in the G+3 soft soil class model. Consequently, this model may reach failure sooner than the corresponding medium soil class model, which could explain the observed decrease rather than an increase.

B. Plastic Hinges.

The occurrence of plastic hinges was consistent across all codes, with one plastic hinge reaching the critical plastic (CP) state in all G+3 models on the ground floor. Additionally, some plastic hinges with IO and LS states occurred in all G+7 and G+11 models on both the first and ground floors. Consequently, G+7 and G+11 configurations

appeared to exhibit greater safety in this regard compared to G+3 configurations.

C. Summary.

NCSC-2015 and EC8 depicted no difference between medium and soft soil classes, while TBEC-2018 depicted a slight base shear decrease in the soft soil of G+3. Although the results showed only one difference, MRF+SW models seemed to perform better compared to MRF, especially in G+7 models and above.

3. MRF In Irregular Form

The results, including base shear, displacement, and plastic hinge formation, for irregular MRF configurations were obtained based on two soil types and three seismic design codes, specifically for high-rise buildings.

A. Base Shear and Displacement

The pushover curve that shows the base shear forces and displacement for high-rise MRF residential buildings in irregular form with different codes and different soil classes are shown below in Fig 20.

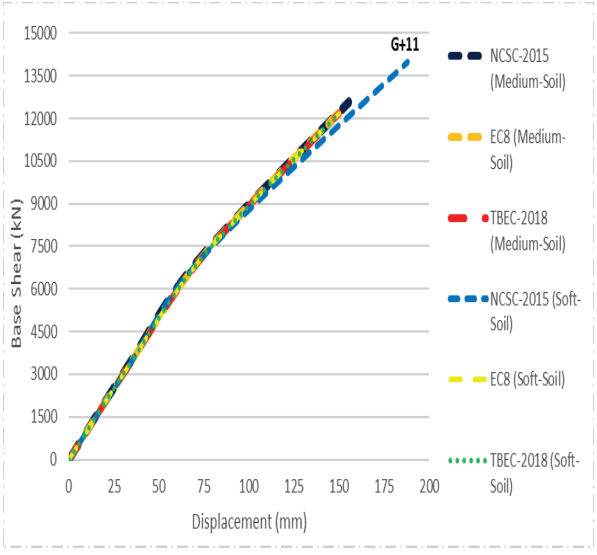


Figure 20. Pushover curves for MRF in an irregular form, medium and soft soil class

The preceding line graph reveals that the peak base shear and displacement were observed in NCSC-2015. However, there was no notable change in the results for EC8 and TBEC-2018. In NCSC-2015, both base shear and displacement increased by 10% and 17%, respectively, in the soft soil class. Consequently, models designed according to NCSC-2015 exhibited greater resilience and endured for a longer period before collapse compared to those designed according to other codes.

B. Plastic Hinges.

Plastic hinges reaching the critical plastic (CP) state were observed in all models. In NCSC-2015, these hinges appeared on the ground, first, and second floors for the soft soil class, while fewer hinges were observed in the medium soil class, appearing only on the ground and first floors.

Conversely, EC8 and TBEC-2018 did not exhibit a distinction between medium and soft soil classes. However, CP state plastic hinges were predominantly located on the ground and first floors.

C. Summary.

The models seemed unsafe in all cases, but in EC8 and TBEC-2018 the consideration of danger occurrence was higher and the collapse seemed to happen earlier than NCSC-2015.

The irregular MRF models appeared very weak and unable to resist earthquake loads.

4. MRF+SW in Irregular Form.

The results such as base shear, displacement, and plastic hinges formation for MRF+SW in irregular form were obtained according to two soil types, and three codes, and for only high-rise buildings.

A. Base Shear and Displacement.

The pushover curve that shows the base shear forces and displacement for high-rise MRF+SW residential buildings in irregular form with different codes and different soil classes are shown below in Fig 21.

The results depicted in this graph showed minimal variation among all models, with differences, if any, not exceeding 1%.

Primarily, the similarity in results can be attributed to the timing and location consistency of critical plastic hinge occurrences.

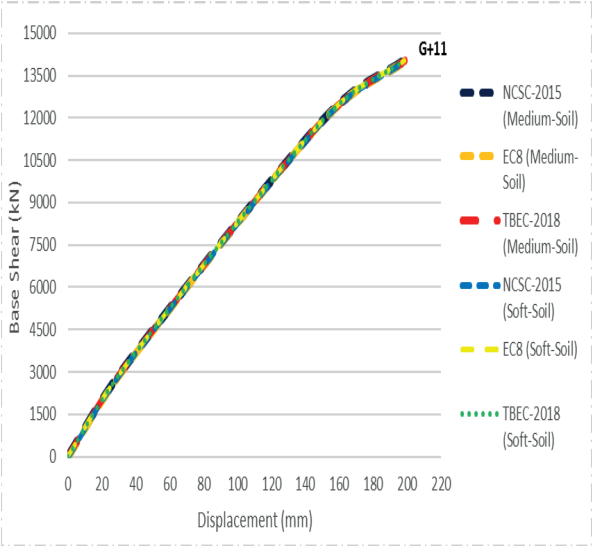


Figure 21. Pushover Curves for MRF+SW structures in an irregular form, medium and soft soil

B. Plastic Hinges.
All models faced plastic hinges occurrence with a CP state in the first three stories. Therefore, these structures appeared weak and couldn't resist the applied earthquake loads.
C. Summary.
The models displayed vulnerability and are unlikely to remain standing under the imposed earthquake conditions. Even though the 1.5 m span length shear walls may provide some resistance, it appeared to be insufficient.
Moreover, the simultaneous occurrence of critical plastic hinges at consistent locations suggests that the codes in this scenario predicted collapse at the same juncture.

CONCLUSION

1. MRF in the regular form:
The base shear and displacement exhibited an increase from G+3 to G+11 buildings. Particularly in TBEC-2018, the transition from medium to soft soil had a more realistic impact on base shear and displacement. However, across all structures, the presence of critical hinges indicated that they were unsafe.
2. MRF+SW in the regular form:
Base shear and displacement increased as the number of stories rose from G+3 to G+11 buildings. The results appeared consistent for both soil classes in all codes, except for TBEC-2018, which showed a slight decrease from medium to soft soil class for G+3 buildings. Overall, all structures seemed to remain stable and capable of withstanding the applied earthquake loads.
3. MRF in the irregular form:
In NCSC-2015, both base shear and displacement increased from medium to soft soil, while TBEC-2018 and EC 8 showed consistent results for both soil classes. However, TBEC-2018 and EC 8 predicted the occurrence of critical hinges earlier than NCSC-2015, suggesting that structures evaluated by NCSC-2015 may withstand more before collapsing. Nevertheless, all structures appeared unsafe due to the presence of critical hinges.
4. MRF+SW in the irregular form:
For all codes, base shear and displacement showed no variation between soil classes, and critical hinges occurred at identical locations. Consequently, all structures were deemed unsafe due to the presence of critical hinges.
5. Primary conclusions:
- The codes stated similar results when:

A. Structures are safe, and no plastic hinges appeared.
B. Structures are unsafe but did not collapse according to the applied seismic loads.

- Shear walls play a critical role in mitigating the impact of earthquake loads.
- Buildings with regular shapes are generally more resilient to earthquakes compared to buildings with irregular shapes.
- The first three stories of a building are typically the most critical, as plastic hinges tend to occur in them predominantly.
- The findings underscore the importance of soil class as a significant factor influencing the results across different seismic design codes.
- It has been observed that the earthquake impact did not significantly change between the old and new regulations. However, this outcome

may vary depending on buildings with diverse geometric characteristics and soil classes.

- NCSC-2015 divides the island into four seismic regions with corresponding peak ground acceleration values, irrespective of local site conditions. In contrast, TBEC-2018 introduces a revised approach by incorporating a seismic hazard map and offering site-specific data based on the building's coordinates.
- TBEC-2018 appears to be more comprehensive and adapted to advanced technologies, considering parameters in a more detailed manner.
- Based on the findings, variations among the codes were not always evident. However, EC 8 and TBEC-2018 tended to be more conservative most of the time.
- The most significant change in TBEC-2018 compared to NCSC-2015 is the implementation of the Earthquake Hazard Map. TBEC-2018 utilizes specific earthquake properties based on coordinates from this map, defining short-period and long-period spectral acceleration for each location. Therefore, it would be beneficial to develop a new map for Cyprus using the updated procedure introduced in TBEC-2018.
- Despite the codes not indicating significant differences in the results, TBEC-2018 appeared to show more logical results and predict the danger earlier as this code also considers more parameters and specific details. Therefore, this study can state that TBEC-2018 is the most appropriate code compared to NCSC-2015 and EC8.

RECOMMENDATIONS

Based on the findings of this study, the following recommendations are proposed for future research:

1. Future studies should consider comparing seismic design codes while also incorporating specific types of foundations within the scope of the study, such as mat foundations or base-isolated foundations.
2. It would be beneficial to conduct additional studies focusing on various types of soil to further explore their impact on structural behavior under earthquake loads.
3. Utilizing 3D models that closely resemble real-world structures is recommended for future studies, despite potential challenges in comparison. Such models provide increased accuracy and realism.
4. Future research endeavors can explore the development of a new earthquake map for Cyprus, similar to the approach adopted in Turkey, with coordinates providing site-specific seismic hazard data.
5. Researchers are encouraged to carefully select a subset of models and analyze them using multiple seismic analysis methods. This approach can yield more robust and accurate results, enhancing the understanding of structural response to seismic events.

REFERENCES

1. **Abd-Elhamed, A., Mahmoud, S.** (2016). Nonlinear static analysis of reinforced concrete framed buildings - A case study on Cairo earthquake. Journal of Engineering Research, Vol 4, No 4.
2. **Abraham, N.M., & SD, A.K.** (2019). Analysis of irregular structures under earthquake loads. Procedia Structural Integrity, 14, 806-819. https://doi.org/10.1016/j.prostr.2019.07.059
3. **Aksoylu, C., Mobark, A., Hakan Arslan, M., & Hakkı Erkan, İ.** (2020). A comparative study on ASCE 7-16, TBEC-2018 and TEC-2007 for reinforced concrete buildings. Revista de la Construcción, 19(2), 282-305.
4. ASCE 7: American Society of Civil Engineers, Minimum Design Loads for Buildings and Other Structures from ASCE 7: Minimum Design Loads for Buildings and Other Structures (resource.org)
5. **Asim, K.M., Moustafa, S.S., Niaz, I.A., Elawadi, E.A., Iqbal, T., & Martínez-**

Álvarez, F. (2020). Seismicity analysis and machine learning models for short-term low magnitude seismic activity predictions in Cyprus. Soil Dynamics and Earthquake Engineering, 130, 105932.

6. **Atmaca, N., Atmaca, A., & KILÇIK, S.** (2019). Comparison of 2018 and 2007 Turkish Earthquake Regulations. The International Journal of Energy and Engineering Sciences, 4(2), 19-25.
7. **Bhatt, C., & Bento, R.** (2014). A 3D pushover methodology for seismic assessment of plan asymmetric buildings. Earthq Spectra Earthq Eng Res Inst, 30(2), 683-703.
8. **Büyüksaraç, A., Işık, E., & Bektaş, Ö.** (2022). A comparative evaluation of earthquake code change on seismic parameter and structural analysis; a case of Turkey. Arabian Journal for Science and Engineering, 47(10), 12301-12321.
9. **Cagnan, Z., & Tanircan, G.B.** (2010). Seismic hazard assessment for Cyprus. Journal of Seismology, 14, 225-246. https://doi.org/10.1007/s10950-009-9163-1
10. Cyprus National Annex, Eurocode 8, Design of structures for earthquake resistance.
11. **Dindar, H., Akgün, M., Atalar, C., & Özdağ, Ö.C.** (2021). The assessment of local site effects and dynamic behaviour in Nicosia, Cyprus. G eofizika, 38(1), 61-80.
12. Earthquake.Zone, (2023), from https://earthquakes.zone/cyprus
13. **Elhadidy, M., Abdalzaher, M.S., & Gaber, H.** (2021). Up-to-date PSHA along the Gulf of Aqaba-Dead Sea transform fault. Soil Dynamics and Earthquake Engineering, 148, 106835. https://doi.org/10.1016/j.soildyn.2021.106835
14. **Evelpidou, N.; Karkani, A.; Polidorou, M.; Saitis, G.; Zerefos, C.; Synolakis, C.; Repapis, C.; Tzouxanioti, M.; Gogou, M.** (2022). Palaeo-Tsunami Events on the Coasts of Cyprus. Geosciences, 12, 58. https://doi.org/10.3390/geosciences12020058
15. **Ferraioli, M.** (2019). Dynamic increase factor for nonlinear static analysis of RC frame buildings against progressive collapse. International Journal of Civil Engineering, 17(3), 281-303.
16. Geological Survey Department- Seismic Zoning Map of Cyprus. Retrieved from Event Map - GSD_Athena (gsd-seismology.org.cy)
17. **Hamed, M.** (2018). Comparative Study of Different Seismic Codes for Reinforced Concrete Buildings in Northern Cyprus, Near East University. International Building Code (2012).
18. **Işık, E.** (2021). A comparative study on the structural performance of an RC building based on updated seismic design codes: Case of Turkey. Challenge, 7, 123-134. https://doi.org/10.20528/cjsmec.2021.03.002
19. **Işık, E., Büyüksaraç, A., Ekinci, Y.L., Aydın, M.C., & Harirchian, E**. (2020). The effect of site-specific design spectrum on earthquake-building parameters: A case study from the Marmara region (NW Turkey). Applied Sciences, 10(20), 7247. https://doi.org/10.3390/app10207247
20. **Ismail, A.** (2014). Non linear static analysis of a retrofitted reinforced concrete building. HBRC Journal, 10(1), 100-107. https://doi.org/10.1016/j.hbrcj.2013.07.002
21. **Istiono, H., Susanti, E., Propika, J., & Ramadhan, A.Y.** (2022). Study comparison P-Delta Effect analysis depends on height variation of the building. Journal of Civil Engineering, Planning and Design, 1(1), 50-59.
22. KKTC Cumhurbaşkanlığı Toplantı (2022)
23. K.T.C. Deprem Bölgelerinde Yapılacak Binalar Hakkında Yönetmelik 2015.
24. **Koçer, M.,Mehmet, U.Z. U.N., & Çöğürcü, M.T.** (2021). Comparison of TSC-2018 and TSC-2007 regulations for Konya in terms of equivalent earthquake load method. Konya Journal of Engineering Sciences, 9(3), 535-550. https://doi.org/10.36306/konjes.866044

25. **Lubkowski, Z.A., & Aluisi, B.** (2012, September). Deriving Ss and S1 parameters from PGA maps. In Proceedings of the 15th World Conference of Earthquake Engineering, Lisbon, Portugal (pp. 24-28).
26. **Moctar, H., Sadeghi, K.** (2023). Strong Column-Weak Beam Concept and Stiffness Factor Study for Moment Resisting Frames. International Journal of Innovative Science and Research Technology.
27. **Mule, N.R., Tupe, D.H., & Gandhe, G.R.** (2020). Analysis and Design of High Rise Building Subjected to Combined Effect of Earthquake and Strong Wind using E-Tab Software. International Research Journal of Engineering and Technology (IRJET), 07 (11), 1114-1119.
28. **Resatoglu, R., & Atiyah, R.S.** (2016). Evaluation of reinforced concrete buildings in Northern Cyprus using TEC2007 and EC8 in respect of cost estimation. Scientific Research and Essays, 11(19), 194-201.
29. **Resatoglu, R., & Hamed, M.** (2019). Comparative study of Different Seismic Codes for Reinforced Concrete Buildings in Northern Cyprus Using Static and Dynamic Methods. Journal of Engineering Science and Technology, 14(3), 1314-1329.
30. **Resatoglu, R., & Jkhsi, S.** (2022). Evaluation of Ductility of Reinforced Concrete Structures with Shear Walls having Different Thicknesses and Different Positions. IIUM Engineering Journal, 23(2), 32-44. https://doi.org/10.31436/iiumej.v23i2.2070
31. **Safkan, I.** (2012). Comparison of Eurocode 8 and Turkish Earthquake Code 2007 for Residential RC Buildings in Cyprus. In Proceedings of the 15th Conference on Earthquake Engineering, Lizbon, Portekiz.
32. SeismicPortal.eu, (2023) from www.seismicportal.eu
33. **Selcukhan, O., & Ekinci, A.** (2021). Liquefaction Potential Determination and Hazard Mapping Based on Standard Penetration Tests in Long Beach and Tuzla Regions of Cyprus. https://doi.org/10.21203/rs.3.rs-1077123/v1
34. **Selcukhan, O., & Ekinci, A.** (2023). Assessment of Liquefaction Hazard and Mapping Based on Standard Penetration Tests in the Long Beach and Tuzla Regions of Cyprus. Infrastructures, 8(6), 99. https://doi.org/10.3390/infrastructures8060099.
35. **Somwanshi, M.A., & Pantawane, R.N.** (2015). Seismic analysis of fixed based and base isolated building structures. International Journal of Multidisciplinary and Current Research, 3, 2321-3124. Türkiye Bina Deprem Yönetmeliği 2018 (TBDY-2018).
36. **Yadav, A., Hazari, D.** (2022). Static Pushover Analysis For Regular And Irregular Structures In All Zones. YMER Journal, 21(5).
37. **Yassin, A., & Sadeghi, K.** (2023). Structure Behaviour under Seismic loads using X-Bracing, Inverted V-Bracing Systems and without Bracing. International Journal of Innovative Science and Research Technology, Connections, 8(1).
38. **Zengin, B., & Aydin, F.** (2023). The Effect of Material Quality on Buildings Moderately and Heavily Damaged by the Kahramanmaraş Earthquakes. Applied Sciences, 13(19), 10668.

СПИСОК ЛИТЕРАТУРЫ

1. **Abd-Elhamed, A., Mahmoud, S.** (2016). Nonlinear static analysis of reinforced concrete framed buildings - A case study on Cairo earthquake. Journal of Engineering Research, Vol 4, No 4.
2. **Abraham, N.M., & SD, A.K.** (2019). Analysis of irregular structures under earthquake loads. Procedia Structural Integrity, 14, 806-819. https://doi.org/10.1016/j.prostr.2019.07.059
3. **Aksoylu, C., Mobark, A., Hakan Arslan, M., & Hakkı Erkan, İ.** (2020). A comparative study on ASCE 7-16, TBEC-2018 and TEC-2007 for reinforced concrete buildings. Revista de la Construcción, 19(2), 282-305.

4. ASCE 7: American Society of Civil Engineers, Minimum Design Loads for Buildings and Other Structures from ASCE 7: Minimum Design Loads for Buildings and Other Structures (resource.org)
5. **Asim, K.M., Moustafa, S.S., Niaz, I.A., Elawadi, E.A., Iqbal, T., & Martínez-Álvarez, F.** (2020). Seismicity analysis and machine learning models for short-term low magnitude seismic activity predictions in Cyprus. Soil Dynamics and Earthquake Engineering, 130, 105932.
6. **Atmaca, N., Atmaca, A., & KILÇIK, S.** (2019). Comparison of 2018 and 2007 Turkish Earthquake Regulations. The International Journal of Energy and Engineering Sciences, 4(2), 19-25.
7. **Bhatt, C., & Bento, R.** (2014). A 3D pushover methodology for seismic assessment of plan asymmetric buildings. Earthq Spectra Earthq Eng Res Inst, 30(2), 683-703.
8. **Büyüksaraç, A., Işık, E., & Bektaş, Ö.** (2022). A comparative evaluation of earthquake code change on seismic parameter and structural analysis; a case of Turkey. Arabian Journal for Science and Engineering, 47(10), 12301-12321.
9. **Cagnan, Z., & Tanircan, G.B.** (2010). Seismic hazard assessment for Cyprus. Journal of Seismology, 14, 225-246. https://doi.org/10.1007/s10950-009-9163-1
10. Cyprus National Annex, Eurocode 8, Design of structures for earthquake resistance.
11. **Dindar, H., Akgün, M., Atalar, C., & Özdağ, Ö.C.** (2021). The assessment of local site effects and dynamic behaviour in Nicosia, Cyprus. G eofizika, 38(1), 61-80.
12. Earthquake.Zone, (2023), from https://earthquakes.zone/cyprus
13. **Elhadidy, M., Abdalzaher, M.S., & Gaber, H.** (2021). Up-to-date PSHA along the Gulf of Aqaba-Dead Sea transform fault. Soil Dynamics and Earthquake Engineering, 148, 106835. https://doi.org/10.1016/j.soildyn.2021.106835
14. **Evelpidou, N.; Karkani, A.; Polidorou, M.; Saitis, G.; Zerefos, C.; Synolakis, C.; Repapis, C.; Tzouxanioti, M.; Gogou, M.** (2022). Palaeo-Tsunami Events on the Coasts of Cyprus. Geosciences, 12, 58. https://doi.org/10.3390/geosciences12020058
15. **Ferraioli, M.** (2019). Dynamic increase factor for nonlinear static analysis of RC frame buildings against progressive collapse. International Journal of Civil Engineering, 17(3), 281-303.
16. Geological Survey Department- Seismic Zoning Map of Cyprus. Retrieved from Event Map - GSD_Athena (gsd-seismology.org.cy)
17. **Hamed, M.** (2018). Comparative Study of Different Seismic Codes for Reinforced Concrete Buildings in Northern Cyprus, Near East University. International Building Code (2012).
18. **Işık, E.** (2021). A comparative study on the structural performance of an RC building based on updated seismic design codes: Case of Turkey. Challenge, 7, 123-134. https://doi.org/10.20528/cjsmec.2021.03.002
19. **Işık, E., Büyüksaraç, A., Ekinci, Y.L., Aydın, M.C., & Harirchian, E**. (2020). The effect of site-specific design spectrum on earthquake-building parameters: A case study from the Marmara region (NW Turkey). Applied Sciences, 10(20), 7247. https://doi.org/10.3390/app10207247
20. **Ismail, A.** (2014). Non linear static analysis of a retrofitted reinforced concrete building. HBRC Journal, 10(1), 100-107. https://doi.org/10.1016/j.hbrcj.2013.07.002
21. **Istiono, H., Susanti, E., Propika, J., & Ramadhan, A.Y.** (2022). Study comparison P-Delta Effect analysis depends on height variation of the building. Journal of Civil Engineering, Planning and Design, 1(1), 50-59.
22. KKTC Cumhurbaşkanlığı Toplantı (2022)
23. K.T.C. Deprem Bölgelerinde Yapılacak Binalar Hakkında Yönetmelik 2015.
24. **Koçer, M.,Mehmet, U.Z. U.N., & Çöğürcü, M.T.** (2021). Comparison of TSC-2018 and TSC-2007 regulations for Konya in terms of equivalent earthquake load method. Konya

Journal of Engineering Sciences, 9(3), 535-550. https://doi.org/10.36306/konjes.866044

25. **Lubkowski, Z.A., & Aluisi, B.** (2012, September). Deriving Ss and S1 parameters from PGA maps. In Proceedings of the 15th World Conference of Earthquake Engineering, Lisbon, Portugal (pp. 24-28).
26. **Moctar, H., Sadeghi, K.** (2023). Strong Column-Weak Beam Concept and Stiffness Factor Study for Moment Resisting Frames. International Journal of Innovative Science and Research Technology.
27. **Mule, N.R., Tupe, D.H., & Gandhe, G.R.** (2020). Analysis and Design of High Rise Building Subjected to Combined Effect of Earthquake and Strong Wind using E-Tab Software. International Research Journal of Engineering and Technology (IRJET), 07 (11), 1114-1119.
28. **Resatoglu, R., & Atiyah, R.S.** (2016). Evaluation of reinforced concrete buildings in Northern Cyprus using TEC2007 and EC8 in respect of cost estimation. Scientific Research and Essays, 11(19), 194-201.
29. **Resatoglu, R., & Hamed, M.** (2019). Comparative study of Different Seismic Codes for Reinforced Concrete Buildings in Northern Cyprus Using Static and Dynamic Methods. Journal of Engineering Science and Technology, 14(3), 1314-1329.
30. **Resatoglu, R., & Jkhsi, S.** (2022). Evaluation of Ductility of Reinforced Concrete Structures with Shear Walls having Different Thicknesses and Different Positions. IIUM Engineering Journal, 23(2), 32-44. https://doi.org/10.31436/iiumej.v23i2.2070
31. **Safkan, I.** (2012). Comparison of Eurocode 8 and Turkish Earthquake Code 2007 for Residential RC Buildings in Cyprus. In Proceedings of the 15th Conference on Earthquake Engineering, Lizbon, Portekiz.
32. SeismicPortal.eu, (2023) from www.seismicportal.eu
33. **Selcukhan, O., & Ekinci, A.** (2021). Liquefaction Potential Determination and Hazard Mapping Based on Standard Penetration Tests in Long Beach and Tuzla Regions of Cyprus. https://doi.org/10.21203/rs.3.rs-1077123/v1
34. **Selcukhan, O., & Ekinci, A.** (2023). Assessment of Liquefaction Hazard and Mapping Based on Standard Penetration Tests in the Long Beach and Tuzla Regions of Cyprus. Infrastructures, 8(6), 99. https://doi.org/10.3390/infrastructures8060099.
35. **Somwanshi, M.A., & Pantawane, R.N.** (2015). Seismic analysis of fixed based and base isolated building structures. International Journal of Multidisciplinary and Current Research, 3, 2321-3124. Türkiye Bina Deprem Yönetmeliği 2018 (TBDY-2018).
36. **Yadav, A., Hazari, D.** (2022). Static Pushover Analysis For Regular And Irregular Structures In All Zones. YMER Journal, 21(5).
37. **Yassin, A., & Sadeghi, K.** (2023). Structure Behaviour under Seismic loads using X-Bracing, Inverted V-Bracing Systems and without Bracing. International Journal of Innovative Science and Research Technology, Connections, 8(1).
38. **Zengin, B., & Aydin, F.** (2023). The Effect of Material Quality on Buildings Moderately and Heavily Damaged by the Kahramanmaraş Earthquakes. Applied Sciences, 13(19), 10668.

Amer Yassin - Master degree, M.Sc Student, Near East University, Faculty of Civil Engineering, Civil Engineering Department. E-mail: ameryaseen099@gmail.com

Амер Яссин - Студент магистратуры. Ближневосточный университет, факультет промышленного и гражданского строительства, кафедра промышленного и гражданского строительства. E-mail: ameryaseen099@gmail.com

Rifat Resatoglu - PhD degree, Assoc. Prof. Dr, Near East University, Faculty of Civil Engineering, Civil Engineering Department. E-mail: rifat.resatoglu@neu.edu.tr

Рифат Резатоглу - доцент, профессор, кандидат наук, Ближневосточный университет, факультет промышленного и гражданского строительства, кафедра промышленного и гражданского строительства. E-mail: rifat.resatoglu@neu.edu.tr

International Journal for Computational Civil and Structural Engineering, 20(3) 145–158(2024)

DOI:10.22337/2587-9618-2024-20-3-145-158

SERVICEABILITY LIMIT STATE PARAMETERS FOR HIGH STRENGTH CONCRETE STRUCTURES

Vladimir I. Kolchunov [1,2], Sergei S. Fedorov [1]

[1] National Research Moscow State University of Civil Engineering (NRU MGSU), Moscow, RUSSIA
[2] Research Institute of Building Physics of RAACS, Moscow, RUSSIA

Abstract. High-strength concrete structures become more and more widespread in construction practice due to certain advantages. At the same time the current Russian and foreign standards for the design of reinforced high-strength concrete structures are not rigorous enough, since it is based on the conceptual provisions for reinforced concrete structures made of ordinary concrete. The article analyzes the basic provisions for calculation of high-strength concrete structures for serviceability limit state and compares it with the available experimental data. The study points out not only significant quantitative discrepancies in design and experimental values of stiffness and crack resistance parameters of such structures, but also indicate inadequacy of physical phenomena laid in the basic design provisions adopted in the current Russian and foreign standards by analogy with the physical nature of deformation of reinforced concrete structures made of ordinary concrete. The paper proposes to adjust the deformation model for calculating the parameters of serviceability limit state for high-strength concrete structures based on the results of experimental investigations.

Keywords: high-strength concrete, reinforced concrete structures, cracks, serviceability limit state, spacing between cracks

ПРОБЛЕМА НОРМИРОВАНИЯ ПАРАМЕТРОВ ПРЕДЕЛЬНЫХ СОСТОЯНИЙ ВТОРОЙ ГРУППЫ ДЛЯ КОНСТРУКЦИЙ ИЗ ВЫСОКОПРОЧНОГО ЖЕЛЕЗОБЕТОНА

Вл.И. Колчунов [1,2], С.С. Федоров [1]

[1] Национальный исследовательский Московский государственный строительный университет (НИУ МГСУ), г. Москва, РОССИЯ
[2] Научно-исследовательский институт строительной физики РААСН, г. Москва, РОССИЯ

Аннотация. Конструкции из высокопрочного железобетона благодаря определенным достоинствам находят все более широкое распространение в строительной практике. В то же время действующие российские и зарубежные нормативные документы по проектированию бетонных железобетонных конструкций из высокопрочных бетонов, построенные на основе концептуальных положений норм проектирования железобетонных конструкций из обычных бетонов являются недостаточно строгими. В статье приведен анализ основных положений расчета конструкций высокопрочного железобетона по предельным состояниям второй группы в сопоставлении с имеющимися опытными данными. Отмечаются не только значительные количественные расхождения в расчетных и опытных значениях параметров жесткости и трещиностойкости конструкций из такого железобетона, но и неадекватность физической природы явлений, заложенных в основные расчетные положения принятые в действующих российских и зарубежных нормах по аналогии с физической природой деформирования железобетонных конструкций из обычных бетонов без соответствующего обоснования. Даны предложения к корректировке деформационной модели для расчета параметров предельных состояний второй группы конструкции из высокопрочного железобетона основанные на результатах экспериментальных исследований.

Ключевые слова: высокопрочный бетон, железобетонные конструкции, трещины, вторая группа предельных состояний, расстояние между трещинами

INTRODUCTION

The main issues in the design of structures made of new types of concrete, including high-strength concrete and fiber-reinforced concrete, are their safety and decrease in metal consumption. For this purpose, it is necessary to develop and improve new design models which correspond to the real operation regime of structures made of such materials under different types of stress state. The absence of effective models accounting for the specifics of deformation and fracture of reinforced high-strength concrete structures leads not only to the design of structures with unreasonable reserves of bearing capacity and, accordingly, material consumption, but also to the decrease of their safety. Imperfection of deformation models included in regulatory documents significantly affects the quality of structural design.

The analysis of basic provisions of the new Russian Building Code SP311.1325800 for the design of high-strength concrete structures according serviceability limit state criteria showed that it offers a methodology for determining the parameters of serviceability limit state using the same theoretical and methodological basis as for ordinary concrete structures. Such an approach is not apricated in the publications available today in Russian [1-4] and foreign literature [5-7], where deformation models and methods for calculation of high-strength concrete structures are proposed on the basis of modern experimental studies of such structures. Thus, tests of high-strength concrete beams [1,2,4,8] show that, as a rule, there is only one main crack in the tensile zone. And failure occurs along this crack. The similar character of cracking is observed in fiber reinforced concrete structures [9,10,11]. If we proceed from the traditional model of deformation of reinforced concrete components with cracks proposed, which was developed for concrete of relatively low strength, then this model assumes the formation of a network of cracks in the tensile zone and, accordingly, the strains of concrete and reinforcement in the areas between the cracks and in the crack are reduced to some mean values through the coefficient proposed by Murashev. However, if one or two cracks are formed in the tensile zone of a high-strength concrete structure, such a physical model does not reflect the physical aspect of the problem under consideration. Here, as shown in [8,12], it is necessary to attract more perfect models of deformation of reinforced concrete components with cracks adequately describing the physical phenomenon under consideration, including new hypotheses and more rigorous relationships of fracture mechanics adapted to high-strength concrete structures.

Another important specific feature established experimentally for deformation of high-strength concrete structures [1,2,10] is a relatively small range of deformation in serviceability stage from the bending moment of crack formation to failure one. If low-strength concrete structures have the range of 0.7-0.8 of the capacity, then this range for high-strength structures does not exceed 0.25-0.4. This imposes serious limitations on the analysis of such structures according to the serviceability limit state and its criteria.

To take into account the mentioned and other peculiarities of deformation of high-strength concrete structures in calculation for the serviceable limit state, a more advanced calculation apparatus should be used. It should allow considering the specificity of the noted and other physical phenomena of deformation and cracking of such material. Here, as mentioned in [12], the calculation relationships for determining the level spacing between cracks and the crack opening width can be used within the framework of the general methodology, taking into account the deformation effect in a single crack [8,9] and more rigorous relationships of the semi-analytical model for determining the stiffness of structures in the zone of normal and inclined cracks [3,5, 12-14].

Thus, the purpose of this study is to substantiate the necessity and efficiency of transition to more rigorous and experimentally confirmed models of deformation of high-strength concrete structures for updating regulatory documents, in particular, Russian Building Code (SP311.1325800) in the part concerning the calculation of such structures for serviceability limit state.

Physical and design models of stiffness and crack resistance of high-strength concrete structures. According to the current Russian Building Code (SP 311.1325800) for the design of high-strength concrete structures, the design of such structures for the serviceability limit state should be carried out using the same requirements as for reinforced concrete structures made of ordinary concrete with some adjustment of the deformation modulus and elastic-plastic moment of resistance of the section, taking into account the increased strength of high-strength concrete. It follows that the physical model of deformation and cracking in the tensile zones of high-strength concrete structure remains the same as for ordinary reinforced concrete. As the data of experimental studies [1,2,4,5, 10] and the results of numerical investigations of high-strength concrete structures [4, 9] show, the knowledge obtained in the last decade about physical phenomena of deformation, crack formation and opening in such structures qualitatively differs from those parameters under loading of ordinary concrete structures. Thus, it has been found that instead of a network of irregular cracks formed during testing of structures made of low-strength concrete, single so-called discrete cracks are formed in structures made of high-strength concrete [2,3,4, 5, 10] (Figure 1a-c). In beams with deformable transverse contour in the most stressed tensile zone, several cracks may appear (Figure 1d-f), but only one of which increases sharply in opening width as the load grows, and fracture happens along this crack.

This cracking process qualitatively changes the Murashev deformation model traditionally used in design. In this model, the key hypothesis is the hypothesis of mean strains (or stresses) in the reinforcement located in the tensile zone. Meanwhile, for high-strength concrete structures, the crack opening process can be described more rigorously by a model in which the strains in concrete and rebars are determined for a block between cracks, if there is a network of irregular cracks, or by a model for a block in the zone of a single crack, if there is a single crack in the structure. In accordance with this model [12, 14], the strains of tensile concrete $\varepsilon_{bt}(x)$ are determined from the equilibrium of the block located between the section with a crack and the section passing at a distance $t_* + x$ from the crack (Figure 2):

$$\varepsilon_{bt}(x)\big|_{x=0,5l_{crc}-t_*} = \varepsilon_{bt,u} . \quad (1)$$

According to this block model, the mutual slip strains of reinforcement and concrete are determined by the formula:

$$\varepsilon_g(x) = \varepsilon_s(x) - \varepsilon_{bt}(x) \quad (2)$$

where $\varepsilon_s(x)$ is the strain in steel rebar; $\varepsilon_{bt}(x)$ is the strain in concrete at the section x.

An important particularity of the physical phenomenon of cracking in reinforced concrete structures is the so-called deformation effect, which is experimentally established at crack opening. In existing Russian [16,17] and foreign [18-20] regulatory documents, the crack opening width is calculated at the level of the rebar axis by the strains of concrete and reinforcement in the area between adjacent cracks and using the triangle profile for crack opening. The calculation model introduces such a parameter as the distance between cracks lm,crc. In this case, the profile of the crack itself changes linearly from the maximum opening at the level of the reinforcing bar with a decrease in the width of the opening as it moves away from it in the direction of the compressed zone (Figure 3a). Based on numerous experimental studies of the crack formation and crack opening in reinforced concrete structures with different geometry and reinforcement parameters, [21, 27], the study provides substantiated results of the analysis of this process and a refined SCC model [21] of the effective crack opening width in slender and deep beams. It considers two types of external cracks in flexural elements subjected to pure bending: primary flexural cracks penetrating most of the tensile zone and reaching the neutral axis, and

local secondary cracks of smaller size located near the tensile reinforcement, respectively. It also differentiates approach to the types of cracks in deep and slender beams (Figure3b). The basic idea of the SCC model proposed in [20] is to predict the mean crack spacing in an RC element from the strain profile of the tensile reinforcement. This model allows predicting the mean spacing between primary $l_{m,crc}$ and secondary $l_{m,crc,s}$ cracks. As observed by the authors of the model, who had analyzed the experimental data, the primary crack width profile in deep beams follows a bilinear shape, while the traditionally accepted model (see Figure3a) uses a linear primary crack width profile. In deep beams, the crack opening width increases linearly between the crack depth levels representing the vertices of the primary (point 1) and secondary (point 2) cracks (see Figure 3b).

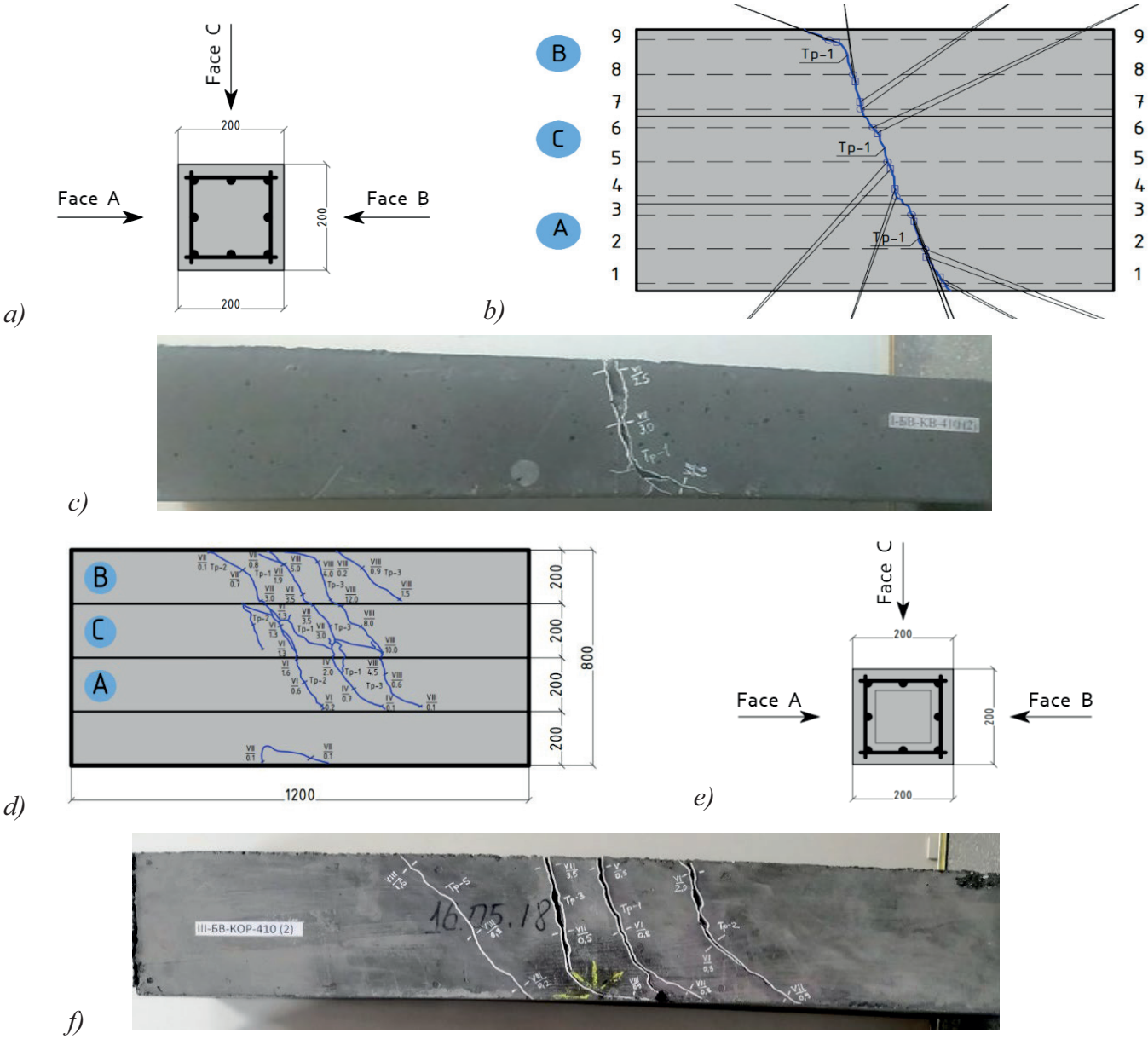


Figure 1. Cross section of a solid beam (a), a pattern of a single crack sweep (b) and a general view of a crack from a side face (c); d,e, f - the same for a box section beam

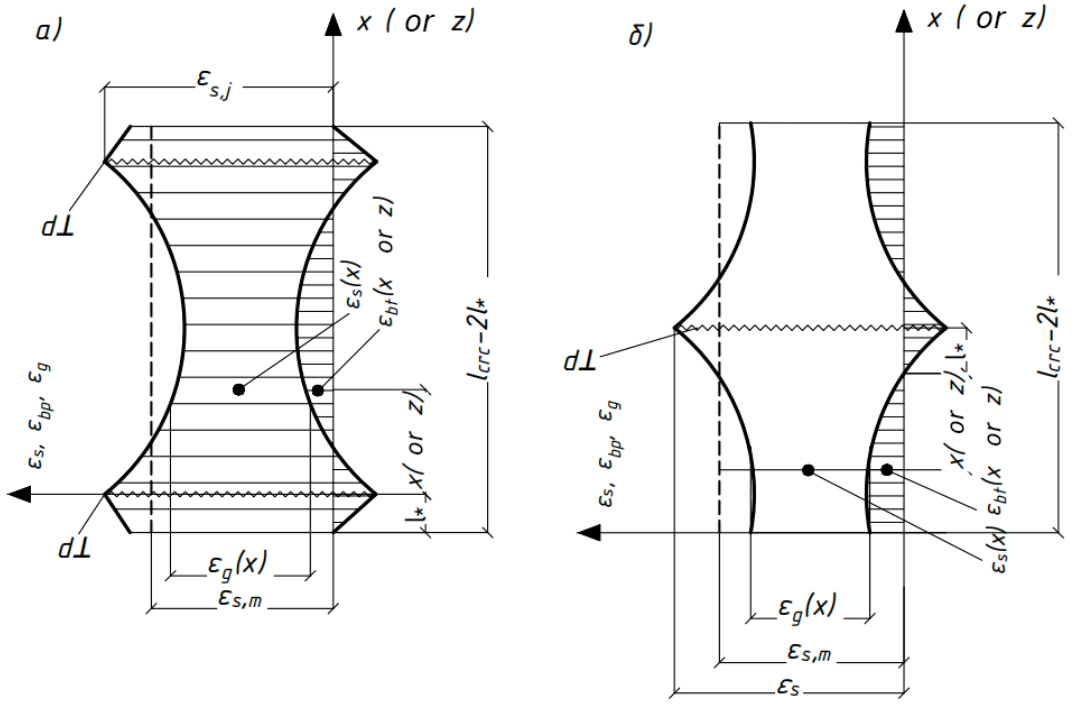


Figure 2. Diagrams of strain in concrete ε_{bt} (x or z), steel rebars ε_s (x or z) and mutual slip strains ε_g (x or z) in the block between adjacent normal or inclined cracks at presence of network of cracks (a) or at appearing of a single crack (b)

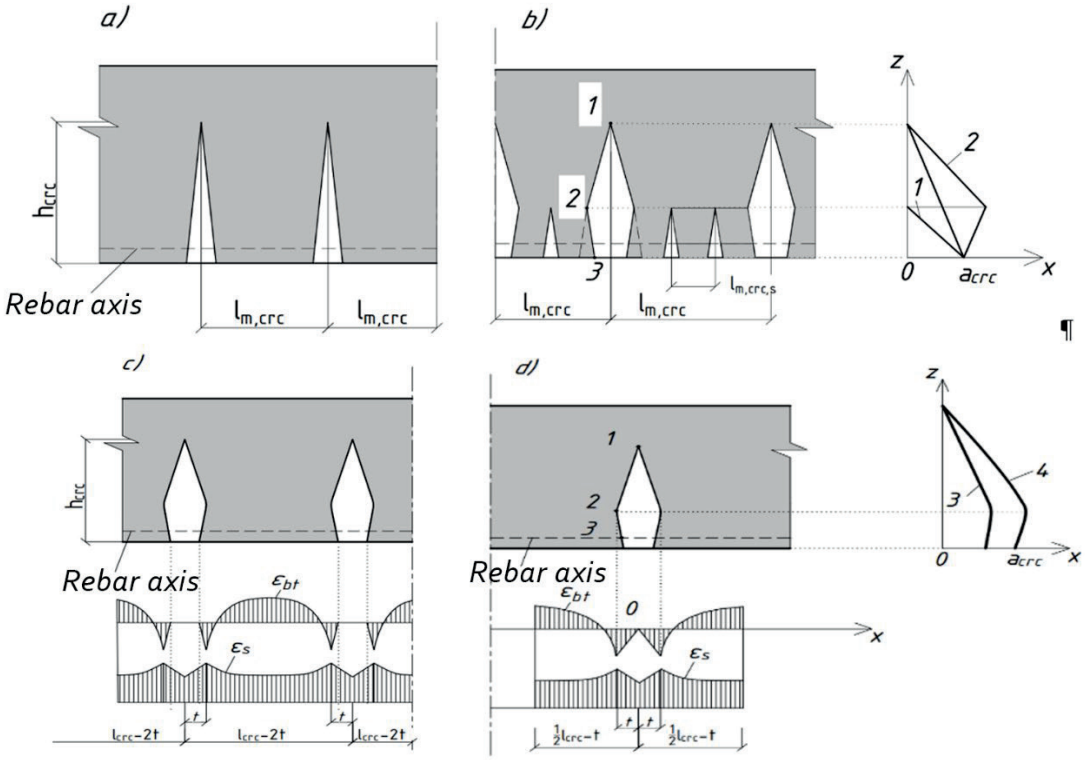


Figure 3. Model of cracks in bending element: a - according to the method [17,18]; b - according to the method [21]; c, d - according to the method [12]

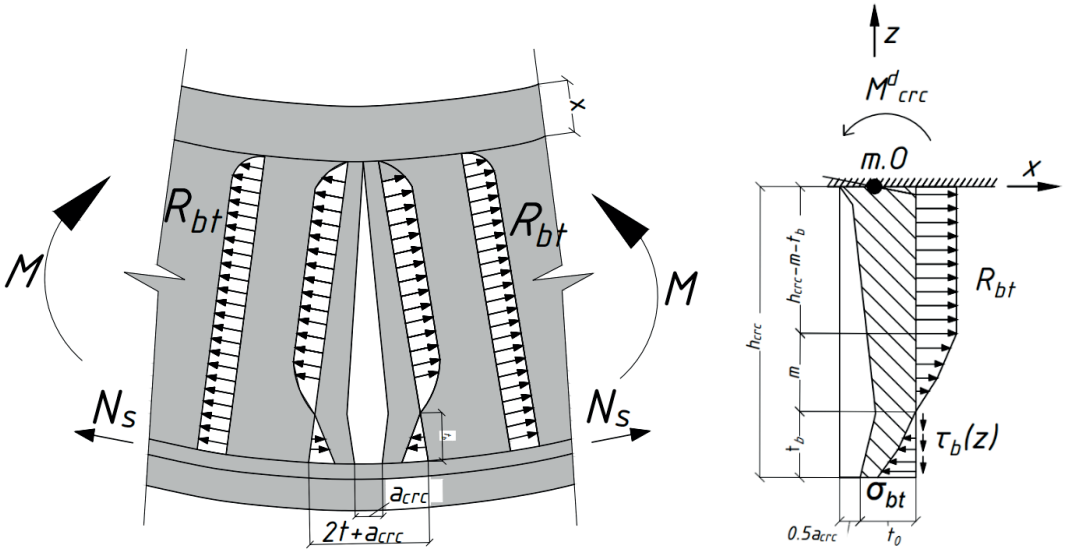
Within this interval, the crack width is determined by the spacing between primary cracks. Further, the crack width growth rate decreases due to the appearance of secondary cracks. For very deep beams, the growth rate may even become negative, i.e., the width decreases and the crack width profile takes the shape of a fish. The SCC crack model is an experimentally based approach with a minimum number of empirical parameters. In addition to the mean strains, a single empirical parameter characterizing the strain profile of the reinforcement is introduced. According to the authors [20] in contrast to the Model Code 2010 [20] and Eurocode 2 [19] methodologies, the proposed calculation model is free from the empirically determined effective deformation region of concrete under tension.

The use of more precise tools in the experimental studies by V.I. Kolchunov [8], I.A. Yakovenko [22], A. I. Demyanov [15] et al of crack opening width in tests of structures made of concrete of different strength and with different types of stress state allowed to identify that the physical nature of the investigated phenomenon of crack opening in reinforced concrete structures has more universal regularities and should not be separated to specific concrete structures. This nature can be described by the model of the so-called deformation effect or the effect of discontinuity in reinforced concrete structure near the steel rebar [12]. The nature of concrete strain patterns obtained in the mentioned studies, as well as in the studies of other researchers [23-26] show that in the zones adjacent to the crack, concrete tensile strains turn into compressive strains. The tangential bond stresses also change sign and the pattern of strains in the rebar in the area between the cracks changes respectively (see Figure 3c). Avalanche-like opening of cracks along the triangular profile which is typical for a concrete element, is restrained by rebars in reinforced concrete elements. This can be considered as a concentrated deformation effect after the continuity violation. Thus, the crack profile is complex and can be described as an ellipse curve, with the maximum opening above the level of the reinforcement bar. As a result, in a two-component system of reinforced concrete matrix with a crack in the vicinity of cracks, a reaction appears at the contact between concrete and reinforcement called the effect of continuity violation or deformation effect.

The theoretical solution of the problem under consideration is developed using clearly structured and interrelated design assumptions that incorporate the mechanics of reinforced concrete and fracture mechanics [12, 15, 22]. The perturbation of the stress-strain state in the vicinity of the crack is found by using the model of the so-called double-cantilever element (DCE), which relates the constants of the concrete strain diagrams to the ductility of this element (Figure 4). The pliability function is derived from the expression of the energy release rate at crack opening

$$\varphi_{bu} = \lim_{\delta A \to 0} \left[\frac{\delta W - \delta V}{\delta A}\right] = \frac{dW}{dA} - \frac{dV}{dA} \quad (3)$$

where δW is the additional work done over the element when the crack propagates by a small distance δA; δV is the additional work done on the element as the crack propagates by a small distanceδA; A is the area of crack surface.



a) *b)*

Figure 4. Model of double-cantilever element (DCE) in reinforced concrete beam: stress-strain state in the vicinity of the crack (a); model of double-cantilever element (b)

Providing the relation between the constants of fracture mechanics and traditional mechanics of reinforced concrete structures, the equivalent experimental characteristic σ_{bt} amenable to standardization is used. As a result, the physical resistance model (PRM) called the double-cantilever element model is universal for single and discrete cracks. Having all the components of the stress state such as stresses in the compressed and tensile concrete along the crack sides (σ_{bt}, R_{bt}), tangential stresses in the contact zone of the tensile reinforcement and concrete (τ_{bt}) (see Fig. 4), it allows modeling theoretically the deformation effect in transverse [25], inclined [26] and spatial [1, 2] cracks in a reinforced concrete element made of concretes of different strengths without introducing additional experimental parameters and without using hypotheses about the mean crack opening width.

It is relevant to note that the idea of block models taking into account shear in concrete above the crack tip in combination with the spacing effect and the nagel effect at the level of the tensile reinforcement axis has been recently proposed in a number of foreign publications, for example, in a rather detailed study [27] on the theory of shear cracks in reinforced concrete beams. This model has some similarity with the idea proposed by the DCE model, but the determination of the parameters of this shear theory is based on the use of static-kinematic equations and has less generality, since it is oriented to the use of an increased number of initial assumptions and experimental constants. Such models are usually applicable to special cases of stress states of concrete structures and types of cracks. At the same time, the physical nature of deformation in these models remains within the framework of traditional approaches: the idea of the mean spacing between cracks is retained, the deformation effect of concrete in the crack is not taken into account, the Bernoulli-Navier hypothesis is used to determine the height of the compressed zone of concrete, etc.

It is easy to see that the introduction of the DCE model into the mechanics of reinforced concrete makes it possible to adequately describe both variants of cracking in the tensile zone (see Figure 3 c, d) and to develop a general design model for solving the problems of stiffness, crack resistance and strength of high-strength concrete structures, considering different types of cracks and experimentally established new

effects of deformation of reinforced concrete with cracks under different types of stress state.
Another argument to justify the expediency of introducing in the design practice more rigorous models in the assessment of serviceability limit states to take into account the specifics of deformation of high-strength concrete structures can be the experimentally obtained curvatures (strains) and deflections of beams made of such material. Thus, analyzing the qualitative character of the experimental diagrams "relative value of the generalized support reaction vs. relative deflection" and "relative value of the generalized support reaction vs. relative angle of rotation" of high-strength concrete beams experiencing bending with torsion [1,2,10] it is possible to note the following (Figure 5). In these structures, up to the level of 0.75-0.80 of the generalized ultimate support reactions, the change in deflections was close to a linear relationship. At the same time, there were no cracks in the beam structures. The range of nonlinear deformation at increase of loads up to exhaustion of bearing capacity was relatively small and amounted to 0.2-0.25 of the failure loads. At the same time, it is known that in beams made of ordinary reinforced concrete the second stage of stress-strain state is the main operational stage for estimation of parameters of serviceability limit state associated with determination of crack opening width and displacements of elements with cracks.

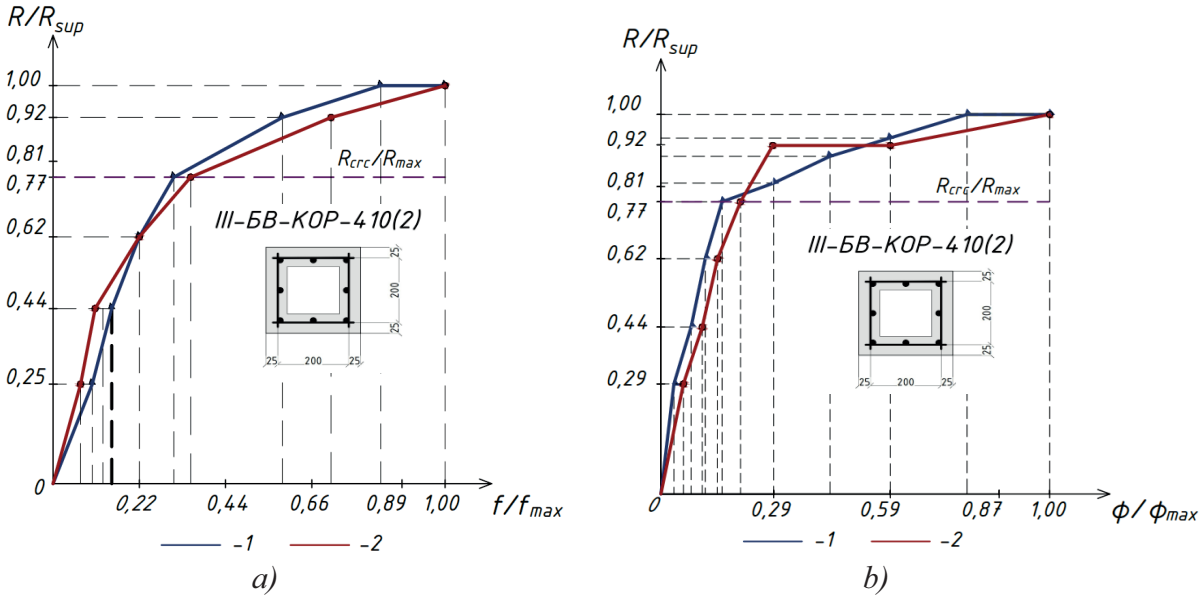


Figure 5. Experimental diagrams "generalized reaction vs. relative deflection" (a) and "generalized reaction vs. angle of rotation" (b) of box section high-strength concrete beam experiencing bending and torsion: 1 - by the first indicator, 2- by the second indicator

Considering the extremely small range of deformation of high-strength concrete structures from the moment of crack initiation to failure and the fact that after crack initiation the intensity of nonlinear displacements and, accordingly, crack opening sharply increases. Thus, the failure of such structures is brittle under the considered stress state and reduced deformability of high-strength concrete [28,29]. Apparently, quantitative criteria of limit states of high-strength concrete structures should be revised in the existing standards.
The same conclusion can be drawn from the analysis of the crack opening pattern in experimental high-strength concrete beams (Figure 6) tested in the research [1]. The quantitative values of the width of opening of a single crack 1 (Tp.1) at different stages of loading (indicated by Roman numerals) show that the crack opening width along the axes of

reinforcement bars (axes 1-9 on the sweep of beam faces A,B,C) has values two or more times smaller than at distances of two or three diameters (shown in brackets) from these axes. For example, the crack opening at stage IV is 0. 2(0.5), at stage VI is 0.8 (1.7), at stage VII is 3.0 (6.2).

This experimentally confirms the presence of deformation effect and bilinear or curvilinear crack profile shown in Figure 3 b,d. The crack profile specified today by Russian and foreign standards does not consider the deformation effect and significantly overestimates the normalized crack opening width for high-strength concrete structures by more than twice. Ignoring the type of cracks (distributed or single) in high-strength concrete structures also significantly affects the calculated values of displacements, and not to the reserve for the stiffness of structures.

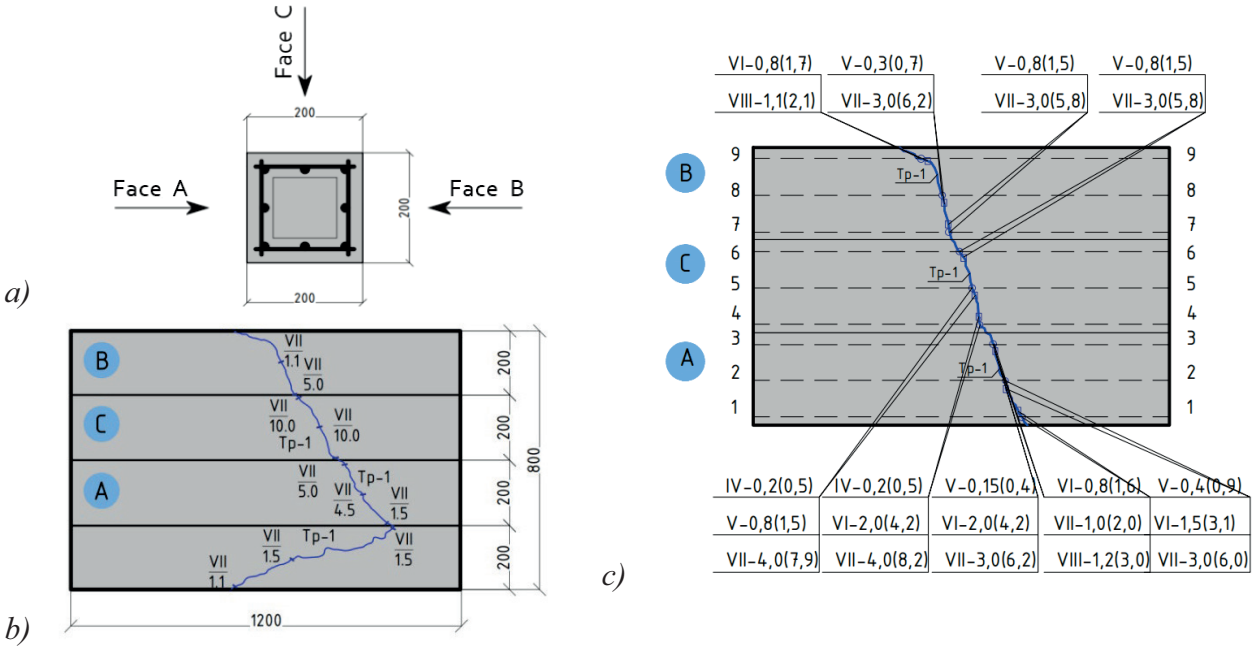


Figure 6. Cross section (a), single crack sweep pattern (b) and crack opening width on the faces of a high-strength concrete beam experiencing bending with torsion

CONCLUSIONS

1. Design models of high-strength concrete structures for serviceability limit state provided in the current Russian and foreign regulatory documents have been developed using conceptual provisions of the design standards for reinforced concrete structures made of ordinary concrete. Thus, they do not strictly enough describe the stress-strain state of structures made of high-strength concrete at the second and third stages of their deformation. They also do not take into account the formation of single cracks in the structures, the presence of the deformation effect in the cracks and changes in the distribution of longitudinal strains in concrete and reinforcement bars in the zone of the crack, the relatively small range of deformation of the section in stage II of stress-strain state.

2. In order to take into account these and other peculiarities of deformation of high-strength concrete structures in the calculation for serviceability limit state, a more advanced calculation apparatus should be used, which allows to account the specifics of deformation and cracking of such material. As shown by the data of experimental studies conducted in recent years with the use of more refined tools, the physical phenomena of deformation, cracking

and crack opening in such structures qualitatively differ from those parameters for structures made of ordinary concrete. Thus, instead of a network of regular cracks formed during testing of low-strength concrete structures, single so-called discrete cracks appear in high-strength concrete structures. This qualitatively changes the deformation model traditionally used in design. The key hypothesis in this model is the hypothesis of strain (stress) averaging in tensile reinforcement. Even the notion of the spacing between cracks used in the design models of serviceability limit state is changed.

3. The physical nature of experimentally determined phenomena of crack opening has more general regularities and is not separated for specific types of structures, specific types of concrete and reinforcement. It can be described by the so-called deformation effect or the effect of violation of the continuity of the concrete matrix in the zone of the reinforcement bar. Theoretical solution of this problem can be constructed using clearly structured and interrelated design assumptions combining the traditional mechanics of reinforced concrete and fracture mechanics. In this case, the perturbation of the stress-strain state in the vicinity of the crack is determined using the model of the so-called double-cantilever element (DCE), relating the constants of concrete strain diagrams to the pliability of this element.

4. In high-strength concrete structures, the strain rate of compressed concrete and reinforcement in the section with the crack increases after the formation of single cracks and, accordingly, the displacements in the structure increase sharply in a relatively short range of load changes. Yielding occurs in the reinforcement bars, i.e., the structure collapses. The operating range of high-strength concrete structures after the formation of single cracks in stage II of stress-strain state is more than twice as short as in beams made of ordinary concrete after the formation of a network of distributed regular cracks.

REFERENCES

1. **Travush V.I., Karpenko N.I., Kolchunov V.I., Kaprielov S.S., Dem'Yanov A.I., Konorev A.V.** The Results of Experimental Studies of Structures Square and Box Sections in Torsion with Bending. Building and Reconstruction. 2018;(6):32-43. (In Russ.)
2. **Travush V.I., Karpenko N.I., Kolchunov V.I., Kaprielov S.S., Demyanov A.I., Konorev A.V**. Main results of experimental research of reinforced concrete structures made of high-strength concrete B100 of circular and circular cross-sections under torsion with bending // Stroitelnaya mechanika of engineering structures and constructions. 2019. No. 1. Pp. 51-61.
3. **Kolchunov V.I., Dem'yanov A.I.** The modeling method of discrete cracks in reinforced concrete under the torsion with bending //Magazine of Civil Engineering. – 2018. – T. 81. – №. 5.
4. **Chiu, CK., Chi, KN. & Ho, BT.** Experimental Investigation on Flexural Crack Control for High-Strength Reinforced-Concrete Beam Members. Int J Concr Struct Mater 12, 41 (2018). https://doi.org/10.1186/s40069-018-0253-8
5. **Chiu, CK., Ueda, T., Chi, KN. et al.** Shear Crack Control for High Strength Reinforced Concrete Beams Considering the Effect of Shear-Span to Depth Ratio of Member. Int J Concr Struct Mater 10, 407–424 (2016). https://doi.org/10.1007/s40069-016-0161-8;
6. **Gennadiy, Murashkin, Vasiliy, Denis and Panfilov.** "An Improved Technique of Calculating Deflections of Flexural Reinforced Concrete Elements Made of Conventional and High-Strength Concrete." Journal of civil engineering and architecture 7 (2013): 125-131
8. **Kolchunov V.I., Demyanov A.I., Yakovenko I.A., Garba M.O..** Reconciliation of experimental data of crack resistance of reinforced concrete structures

to their theoretical values. Nauka ta budyvnitsitstvo. 2018. №1 (15). Pp. 42-49.
9. **Bulkin S.A.** Torsion with Bending of Rectangular Steel Fiber Reinforced Concrete Beam. Building and Reconstruction. 2021;(2):3-13. (In Russ.) https://doi.org/10.33979/2073-7416-2021-94-2-3-15
10. **Travush.V.I. et al.** Results of Experimental Investigations of Complexly Stressed Beams of Round Cross-Section Made of High-Strength Fiber Reinforced Concrete. / V.I. Travush, N.I. Karpenko, V.I. Kolchunov, S.S. Kaprielov, A.I. Demyanov, S.A. Bulkin, V.S. Moskovtseva // Stroitelnaya mekhanika of engineering structures and constructions. 2020. T. 16. no. 4. Pp. 290-297.
11. **Travush V.I., Konin D.V., Krylov A.S.** Strength of reinforced concrete beams of high-performance concrete andfiber reinforced concrete. *Magazine of Civil Engineering*. 2018. No. 1. Pp. 90–100. doi: 10.18720/MCE.77.8.
12. **Kolchunov V.I.** The problem of crack opening in reinforced concrete. Building and Reconstruction. 2024;(1):14-29. (In Russ.) https://doi.org/10.33979/2073-7416-2024-111-1-14-29
13. **Kolchunov V.I., Krylov S.B., Fedorov S.S.** Stiffness of reinforced concrete structures under bending considering shear and axial forces (part 1). Building and Reconstruction. 2023; (6): 25-40. https://doi.org/10.33979/2073-7416-2023-110-6-25-40
14. **Kolchunov V.I., Krylov S.B**. Stiffness of inclined sections of reinforced concrete structures//Industrial and civil engineering .2024. no. 2. Pp.27-32.doi:10.33622/0869-7019.2024/02/27-32.
15. **Kolchunov, V.I., Dem'yanov, A.I.** The modeling method of discrete cracks and rigidity in reinforced concrete. Magazine of Civil Engineering. 2019. 88(4). Pp. 60–69. DOI: 10.18720/MCE.88.6.
16. SP 63.13330.2018 “Concrete and reinforced concrete structures. Basic provisions”. (With change No.1 and Change No.2). Moscow: FGBU “RST”, 2022.
17. SP 311.1325800.2017 “Concrete and reinforced concrete structures of high-strength concrete. Design rules”. (With Modification No.1). Moscow: FGBU “RST”, 2023.
18. ACI Committee 318. (2014). Building Code Requirements for Structural Concrete and Commentary. Farmington Hills, Mich: American Concrete Institute.
19. CEN (Comit´e Europ´een de Normalisation). Eurocode 2: Design of Concrete Structures – Part 1: General Rules and Rules for Buildings, EN 1992-1-1:2004. CEN, Brussels, 2004
20. CEB (Comit´e Euro-International du Beton). CEB-FIP Model Code 2010: Model Code for concrete structures. Ernst & Sohn, Wiley, Berlin, Germany, 2013. 434 p.
21. **Gintaris Kaklauskas, Aleksandr Sokolov, Karolis Sakalauskas** Strain compliance crack model for RC beams: primary versus secondary cracks. Engineering Structures. 2023. 281. 115770
22. **Iakovenko I., Kolchunov Vl.** (2017). The development of fracture mechanics hypotheses applicable to the calculation of reinforced concrete structures for the second group of limit states. Journal of Applied Engineering Science, vol. 15(2017)3, article 455, pp. 366–375, doi:10.5937/jaes15-14662
23. **Adischev, V.V.** Determination of the crack formation moment as a fuzzy value from experimental data / V.V. Adischev, D.S. Shmatkov // Izvestia of higher educational institutions. Construction. - 2012. - no. 5. - Pp. 3-13.
24. **Bashirov, H.Z.** K Determination of the parameters of stress-strain state of reinforced concrete composite structures in the zone of normal cracks / H.Z. Bashirov // Academia. Architecture and Construction. - 2013.-no.2.-Pp. 125-128.

25. **Pimochkin, V.N.** Methodology of determination of the basic parameter of reinforced concrete (ts/g) at taking into account the effect of concrete continuity violation and relative mutual displacements of reinforcement and concrete in bending reinforced concrete structures [Text] I VN Pimochkin, V.I. Kolchunov // Izvestiya OrelGTU Series “Construction Transport” - Orel Izd-voor OrelGTU, 2007 - no.3 - Pp 46-52.
26. **Kolchunov V.I., Al-Hashimi O., Protchenko M.V.** Stiffness of reinforced concrete structures under bending with transverse and longitudinal forces. Building and Reconstruction. 2021;(6):5-19. (In Russ.) https://doi.org/10.33979/2073-7416-2021-98-6-5-19
27. **Classen, Martin.** (2020). Shear Crack Propagation Theory (SCPT) -The mechanical solution to the riddle of shear in RC members without shear reinforcement. Engineering Structures. 210. 110207. 10.1016/j.engstruct.2020.110207.
28. **Karpenko N.I., Moiseenko G.A.** Properties of high-strength steel-fiber concrete with minimum effective fiber content under loading of different duration///Structural mechanics of engineering structures and constructions,2022,T.18, no. 6. Pp.503-5014. DOI 10.22363/1815-5235-2022-18-6-503-514
29. **Stepanov M., Moiseenko G**. Deformation Diagrams of Fine-Grained High-Strength Concrete and High-Strength Steel-Fibro Concrete Under Compression. Building and Reconstruction. 2019;(3):11-21. (In Russ.) https://doi.org/10.33979/2073-7416-2019-83-3-11-21

СПИСОК ИСТОЧНИКОВ

1. **Травуш В.И., Карпенко Н.И., Колчунов Вл.И., Каприелов С.С., Демьянов А.И., Конорев А.В.** Результаты экспериментальных исследований конструкций квадратного и коробчатого сечений из высокопрочного бетона при кручении с изгибом // Строительство и реконструкция. 2018. №6. С. 32–43.
2. **Травуш В.И., Карпенко Н.И., Колчунов Вл.И., Каприелов С.С., Демьянов А.И., Конорев А.В.** Основные результаты экспериментальных исследований железобетонных конструкций из высокопрочного бетона В100 круглого и кольцевого сечений при кручении с изгибом // Строительная механика инженерных конструкций и сооружений. 2019. №1. С. 51–61.
3. **Kolchunov V.I., Dem'yanov A.I.** The modeling method of discrete cracks in reinforced concrete under the torsion with bending //Magazine of Civil Engineering. – 2018. – Т. 81. – №. 5.
4. **Chiu, CK., Chi, KN. & Ho, BT**. Experimental Investigation on Flexural Crack Control for High-Strength Reinforced-Concrete Beam Members. Int J Concr Struct Mater 12, 41 (2018). https://doi.org/10.1186/s40069-018-0253-8
5. **Chiu, CK., Ueda, T., Chi, KN. et al.** Shear Crack Control for High Strength Reinforced Concrete Beams Considering the Effect of Shear-Span to Depth Ratio of Member. Int J Concr Struct Mater 10, 407–424 (2016). https://doi.org/10.1007/s40069-016-0161-8;
6. **Gennadiy, Murashkin, Vasiliy, Denis and Panfilov.** “An Improved Technique of Calculating Deflections of Flexural Reinforced Concrete Elements Made of Conventional and High-Strength Concrete.” Journal of civil engineering and architecture 7 (2013): 125-131.
8. **Колчунов В.И., Демьянов А.И., Яковенко И.А., Гарба М.О.** Приведение в соответствие опытных данных трещиностойкости железобетонных конструкций их теоретическим значениям. Наука та будівництво. 2018. №1 (15). С. 42–49.

9. **Булкин А.С.** Кручение с изгибом сталефиброжелезобетонной балки прямоугольного сечения // Строительство и реконструкция. 2021. № 2. С. 3-13.
10. **Травуш В.И. и др.** Результаты экспериментальных исследований сложнонапряженных балок круглого поперечного сечения из высокопрочного фиброжелезобетона. / В.И. Травуш, Н.И. Карпенко, Вл.И. Колчунов, С.С. Каприелов, А.И. Демьянов, С.А. Булкин, В.С. Московцева // Строительная механика инженерных конструкций и сооружений. 2020. Т. 16. № 4. С. 290-297.
11. **Travush V.I., Konin D.V., Krylov A.S.** Strength of reinforced concrete beams of high-performance concrete andfiber reinforced concrete. *Magazine of Civil Engineering*. 2018. No. 1. Pp. 90–100. doi: 10.18720/MCE.77.8.
12. **Колчунов В.И.** Проблема раскрытия трещин в железобетоне. *Строительство и реконструкция*. 2024;(1):14-29. https://doi.org/10.33979/2073-7416-2024-111-1-14-29
13. **Колчунов В.И., Крылов С.Б., Федоров С.С.** Жесткость железобетонных конструкций при изгибе с учётом поперечной и продольной сил (часть 1). *Строительство и реконструкция*. 2023;(6):25-40. https://doi.org/10.33979/2073-7416-2023-110-6-25-40.
14. **Колчунов В.И., Крылов С.Б.** Жесткость наклонных сечений железобетонных конструкций//Промышленное и гражданское строительство. 2024. №2. С.27-32.doi:10.33622/0869-7019.2024/02/27-32.
15. **Kolchunov, V.I., Dem'yanov, A.I.** The modeling method of discrete cracks and rigidity in reinforced concrete. Magazine of Civil Engineering. 2019. 88(4). Pp. 60–69. DOI: 10.18720/MCE.88.6.
16. СП 63.13330.2018 «Бетонные и железобетонные конструкции. Основные положения». (С Изм.№1 и Изм.№2). М.: ФГБУ "РСТ", 2022.
17. СП 311.1325800.2017 «Бетонные и железобетонные конструкции из высокопрочных бетонов . Праила проектирования». (С Изм.№1). М.: ФГБУ "РСТ", 2023.
18. ACI Committee 318. (2014). Building Code Requirements for Structural Concrete and Commentary. Farmington Hills, Mich: American Concrete Institute.
19. CEN (Comit´e Europ´een de Normalisation). Eurocode 2: Design of Concrete Structures – Part 1: General Rules and Rules for Buildings, EN 1992-1-1:2004. CEN, Brussels, 2004
20. CEB (Comit´e Euro-International du Beton). CEB-FIP Model Code 2010: Model Code for concrete structures. Ernst & Sohn, Wiley, Berlin, Germany, 2013. 434 p.
21. **Gintaris Kaklauskas, Aleksandr Sokolov, Karolis Sakalauskas** Strain compliance crack model for RC beams: primary versus secondary cracks. Engineering Structures. 2023. 281. 115770
22. **Iakovenko I., Kolchunov Vl.** (2017). The development of fracture mechanics hypotheses applicable to the calculation of reinforced concrete structures for the second group of limit states. Journal of Applied Engineering Science, vol. 15(2017)3, article 455, pp. 366–375, doi:10.5937/jaes15-14662
23. **Адищев, В.В.** Определение момента образования трещины как нечеткой величины по экспериментальным данным / В.В. Адищев, Д.С. Шматков // Известия высших учебных заведений. Строительство. – 2012. – № 5. – С. 3–13.
24. **Баширов, Х.З.** К определению параметров напрязкеннодеформированного состояния железобетонных составных конструкций в зоне нормальных трещин / Х.З. Баширов // Academia. Архитектура и строительство. - 2013. - №2. - С. 125-128.
25. **Пимочкин, В.Н**. Методика определения основного параметра железобетона*(ц/г)*

при учете эффекта нарушения сплошности бетона и относительныхвзаимных смещений арматуры и бетона в изгибаемых железобетонных конструкциях[Текст] *I ВН Пимочкин,* В.И. Колчунов // Известия ОрелГТУ Серия"Строительство Транспорт" - Орел Изд-во ОрелГТУ, 2007 - №3 - С 46-52.

26. **Колчунов В.И., Аль-Хашими О., Протченко М.В.** Жесткость железобетонных конструкций при изгибе поперечной и продольной силами. *Строительство и реконструкция*. 2021;(6):5-19. https://doi.org/10.33979/2073-7416-2021-98-6-5-19
27. **Classen, Martin.** (2020). Shear Crack Propagation Theory (SCPT) -The mechanical solution to the riddle of shear in RC members without shear reinforcement. Engineering Structures. 210. 110207. 10.1016/j.engstruct.2020.110207.
28. **Карпенко Н.И., Моисеенко Г.А.** Своиства высокопрочного сталефибробетона с минимальным эффективным содержанием фибры при нагружении различной длительности//Строительная механикаинженерных конструкций и сооружений, 2022, Т.18,»6С.503-5014. DOI 10.22363/1815-5235-2022-18-6-503-514
29. **Степанов М.В., Моисеенко Г.А.** Диаграммы деформирования мелкозернистого высокопрочного бетона и сталефибробетона при сжатии // Строительство и реконструкция. 2019. № 3 (83). С. 11–21. http://doi.org/10.33979/2073-7416-2019-83-3-11-21

Vladimir Ivanovich Kolchunov - National Research Moscow State University of Civil Engineering (NRU MGSU), Moscow, Russia, Corresponding Member of RAACS, Doctor of Technical Sciences, Professor, Professor of the Department of Engineering Graphics and Computer Technologies. Research Institute of Building Physics of the Russian Academy of Architecture and Construction Sciences (127238, Russia, Moscow, Lokomotivny proezd, 21, NIISF RAASN). E-mail: vlik52@mail.ru, ph. +7-910-317-93-55.

Колчунов Владимир Иванович - Федеральное государственное бюджетное образовательное учреждение высшего образования "Национальный исследовательский Московский государственный строительный университет" (НИУ МГСУ), Москва, Россия, член-корреспондент РААСН, доктор технических наук, профессор, профессор кафедры инженерной графики и компьютерных технологий. Научно-исследовательский институт строительной физики Российской академии архитектуры и строительных наук (127238, Россия, Москва, Локомотивный проезд, 21, НИИСФ РААСН). E-mail: vlik52@mail.ru, тел. +7-910-317-93-55

Sergei Sergeevich Fedorov - National Research Moscow State University of Civil Engineering (NRU MGSU), Moscow, Russia, Associate Professor, Candidate of Technical Sciences, Head of the Department of Engineering Graphics and Computer Technologies, E-mail: ssfedorov-niip@yandex.ru. ph. +79038760368

Федоров Сергей Сергеевич - Федеральное государственное бюджетное образовательное учреждение высшего образования "Национальный исследовательский Московский государственный строительный университет" (НИУ МГСУ), Москва, Россия, доц., к.т.н., зав. кафедрой инженерной графики и компъютерных технологий, E-mail: ssfedorov-niip@yandex.ru. тел. +79038760368

DOI:10.22337/2587-9618-2024-20-3-159-166

THE MOISTURE REGIME OF ENCLOSING STRUCTURES IN DIFFERENT CONSTRUCTION AREAS

Kirill P. Zubarev

National Research Moscow State University of Civil Engineering, Moscow, RUSSIA
Research Institute of Building Physics of Russian Academy of Architecture and Construction Sciences, Moscow, RUSSIA
RUDN University, Moscow, RUSSIA

Abstract: Heat and mass transfer mathematical model is formulated. Solution of the moisture transfer equation was obtained by discrete-continuum approach, which gives an opportunity to obtain the new analytical solution. Algorithm for calculating the moisture regime according to the proposed mathematical model is given. Enclosing structure with aerated concrete base and expanded polystyrene insulation is chosen for moisture regime calculation. Moisture behaviour calculation is done in three construction areas (dry, normal, wet) for four different moisture regimes of building room (dry, normal, moist, wet). Calculation results were summarized in a table which engineers can use in their practical work.

Keywords: moisture regime, mathematical model, discrete-continuum approach, moisture potential, vapor permeability, sorption isotherm, enclosing structure

ВЛАЖНОСТНЫЙ РЕЖИМ ОГРАЖДАЮЩИХ КОНСТРУКЦИЙ В РАЗЛИЧНЫХ РАЙОНАХ СТРОИТЕЛЬСТВА

К.П. Зубарев

Национальный исследовательский Московский государственный строительный университет, г. Москва, РОССИЯ
Научно-исследовательский институт строительной физики Российской академии архитектуры и строительных наук, г. Москва, РОССИЯ
Российский университет дружбы народов, г. Москва, РОССИЯ

Абстракт: Сформулирована математическая модель тепловлагопереноса. Получено решение нестационарного уравнения влагопереноса с помощью дискретно-континуального подхода, что дало возможность вывести новую аналитическую формулу. Приведен алгоритм расчета нестационарного влажностного режима по предложенной математической модели. Для расчета влажностного режима выбрана ограждающая конструкция с основанием из газобетона и утеплителем из пенополистирола. Проведен расчет влажностного режима в трех зонах влажности (сухая, нормальная, влажная) для четырех различных влажностных режимов помещения здания (сухой, нормальный, влажный, мокрый). Результаты расчетов сведены в таблицу, которую возможно использовать в практической инженерной работе.

Ключевые слова: влажностный режим, математическая модель, дискретно-континуальный подход, потенциал влажности, паропроницаемость, изотерма сорбции, ограждающая конструкция.

1. INTRODUCTION

Modern technology development improves some technique directions of our life. There are some innovations, which are introduced in building industry [1,2]. Although these innovations make modern level of live better than previously, the demand for calculation methods becomes higher because humanity works with complicated systems like passive and smart houses [3-5].

1.1. The complexity of the research of moisture transfer processes

One of the most complicated directions in building is the moisture transfer. This problem became crucial 100 years ago, when multilayer inclosing structures were included in building industry. Earlier there were no problems with the moisture transfer of building walls because all water vapour which penetrates inside inner surfaces of single-layer enclosing structures comes out through outer surfaces of enclosing

structures. However, if we talk about a multilayer inclosing structure, water vapour can diffuse through separate layers with different speed, so we can observe moisture accumulation on the border between the layers [6,7].
This problem is complemented by the fact that moisture consists of vapor and liquid components. Each component can move by different private gradients of transfer potentials: partial pressure gradient of water vapor, capillary pressure gradient of liquid moisture, temperature gradient, gradient of air filtration, etc. The moisture field constantly interacts with temperature distribution, which complicates the problem, so scientists usually tell about combined heat and moisture transfer [7].
The moisture transfer research gives opportunities to reduce the heat losses by building heat shield, increase the energy efficiency of the building including houses with insulation layers and gives additional comfort and safety to human [8]. Moreover, the moisture transfer research is investigated in different types of the HVAC (Heating, Ventilation, Air Conditioning) Systems.

1.2. Separate accounting of moisture transfer mechanisms and moisture potential

The first unsteady-state mathematical model was proposed by K.F. Fokin. This model takes into account moisture transfer under vapour gradient partial pressure only, so the solution of the moisture transfer equation exists in sorption zone [9].
However, this method has fundamental weakness. Water vapor partial pressure cannot be more than saturated water vapor pressure, so this equation has indeterminacy for calculations. K.F. Fokin developed another equation to solve this problem. The second Fokin's model takes into account water vapor and liquid moisture movements and they can be calculated in sorption zone and ultrasorption zone contemporaneously, but this model has another complicated problem, which requires working with the two separate moisture transfer potentials: capillary pressure gradient of liquid moisture and partial pressure gradient of water vapor [9].
Another approach to the moisture regime calculation is using the moisture potential. Instead of calculating the separate transfer potentials, the moisture potential allows to solve the problem with single transfer potentials [9].

1.3. Ways of calculating moisture value of building materials

Modern engineers use averaged data of moisture value which are included in different standards, but it will be possible to improve energy efficiency and energy saving if we predict exactly the value of building material moisture at the moment of maximum moisture accumulation.
There are some approaches to obtain the moisture value of building materials.
One of them is determining moisture value by field studies or laboratory experiments [10,11], but this way is too difficult and expensive.
Another path is prediction of moisture value of building material by mathematical model, which uses computer and numerical method [10,11]. In this case, we need to have a lot of experimental data and high qualification of engineers.
We can calculate steady-state moisture transfer equation and obtain moisture behaviour. Although we will receive required values, the accuracy of this approach will be not high.

2. THE PROBLEM

The aims of this paper are development of the new analytical formula for calculation the moisture behaviour using discrete-continuous approach.

3. MATERIALS AND METHODS

The moisture potential F was taken as the basis of the development of the mathematical model.

3.1. The mathematical model which is based on the moisture potential F

Let's formulate heat and mass transfer mathematical model:

$$\begin{cases} \frac{\partial^2 t}{\partial x^2} = 0 \ - \text{ heat transfer equation} \\ \frac{\partial F(w,t)}{\partial \tau} = \kappa_{F0} \cdot E_t(t) \cdot \frac{\partial^2 F(w,t)}{\partial x^2} \ - \text{ moisture transfer equation} \\ E_t(t) = 1{,}84 \cdot 10^{11} \cdot \exp(-\frac{5330}{273+t}) \ - \text{ depends } E_t(t) \text{ on } t \\ 0 \le x \le l, \ \tau > 0 \ - \text{ space-time domain} \\ -\lambda \frac{\partial t}{\partial x}\Big|_{x=0} = \alpha_{ext}\left(t_{ext} - t_1\right) \ - \text{ boundary condition} \\ \lambda \frac{\partial t}{\partial x}\Big|_{x=l} = \alpha_{in}\left(t_{in} - t_N\right) \ - \text{ boundary condition} \\ -\mu \frac{\partial F}{\partial x}\Big|_{x=0} = \frac{1}{R_{m.ext}}\left(F_{ext} - F_1\right) \ - \text{ boundary condition} \\ \mu \frac{\partial F}{\partial x}\Big|_{x=l} = \frac{1}{R_{m.in}}\left(F_{in} - F_N\right) \ - \text{ boundary condition} \\ F(x,0) = f(x), \ 0 \le x \le l \ - \text{ initial condition} \end{cases} \quad (1)$$

3.2. Discrete-continuous approach for the moisture regime calculating

Discrete-continuous approach was used to solve the moisture transfer equation [12] in the system (1).

The system of equations (1) was presented in the form of a matrix equation which has an analytical solution.

As a result, the new analytical expression was obtained:

$$\overline{F} = p \cdot \left(\left(E_t \cdot A\right)^{-2} \cdot e^{E_t \cdot A \cdot \tau} - \tau \cdot \left(E_t \cdot A\right)^{-1} - \left(E_t \cdot A\right)^{-2} \right) \cdot \cdot \overline{L} + \left(E_t \cdot A\right)^{-1} \left(e^{E_t \cdot A \cdot \tau} - E\right) \cdot \overline{B} + e^{E_t \cdot A \cdot \tau} \cdot \overline{F}_0. \quad (2)$$

3.3. Algorithm for calculating the moisture regime according to the proposed mathematical model

The algorithm for calculating the unsteady-state moisture regime of enclosing structures using the discrete-continuous method is proposed:

1) The building enclosing structure is divided into sections along the *x* coordinate.

2) The initial distribution of the moisture potential over all sections of the building enclosing structure and the initial moment of time are specified.

3) Calculation of the distribution of moisture potential at the end of the month for a multilayer building enclosing structure is obtained by the formula (2).

4) The moisture regime of the building enclosing structure is determined at the end of the month using the moisture potential scales of the building enclosing structure materials according to the obtained moisture potential distributions.

5) The temperature field of the enclosing structure changes in accordance with the climatic conditions of the next month outside the enclosure.

6) The initial distribution of the moisture potential at the beginning of the next month is determined using the moisture potential scales according to the moisture regime of the building enclosing structure at the end of the previous month.

7) The calculation is repeated in clauses 3-6 for the required period.

In previous papers it was shown that formula (2) has higher accuracy than the analytical expression and this approach simplifies the solution of unsteady-state moisture transfer equation by the finite difference method using an explicit difference scheme [13].

4. RESULTS AND DISCUSSION

Moisture behaviour calculations in different construction areas for the enclosing structure with aerated concrete base and expanded polystyrene insulation are made.

4.1. Research of moisture behaviour in different construction areas

Three construction areas exist in Russia: dry, normal, wet.

We chose 18 cities (six cities in each construction area) for the moisture regime calculation (Table 1).

Table 1. Cities for the moisture regime calculation

No.	Dry construction area	Normal construction area	Wet construction area
1	2	3	4
1	Krasnodar	Moscow	Petropavlovsk-Kamchatsky
2	Samara	Kaliningrad	Ayan
3	Omsk	Nizhny Novgorod	Vladivostok
4	Novosibirsk	Tomsk	Murmansk
5	Irkutsk	Khabarovsk	Yuzhno-Kurilsk
6	Volgograd	Perm	Arkhangelsk

In each construction area there can be four types of moisture regime of building room: dry, normal, moist, wet.

Temperature and relative humidity were chosen for each moisture regime of building room for the moisture behaviour calculation (Table 2).

Table 2. Temperature and relative humidity for each moisture regime of building room

No.	Type of moisture regime of building room	Temperature and relative humidity inside a room
1	2	3
1	Dry	t_{in} = 22 °C; φ_{in} = 50 %
2	Normal	t_{in} = 22 °C; φ_{in} = 60 %
3	Moist	t_{in} = 22 °C; φ_{in} = 75 %
4	Wet	t_{in} = 22 °C; φ_{in} = 90 %

4.2. Research of moisture behaviour in different construction areas

Moisture behaviour calculations in different construction areas for the enclosing structure with aerated concrete base and expanded polystyrene insulation are made.

The moisture regime calculation of enclosing structure with aerated concrete base and expanded polystyrene insulation is presented for cities of dry construction area (Krasnodar, Samara, Omsk, Novosibirsk, Irkutsk, Volgograd) for different moisture regimes of building room (Fig. 1).

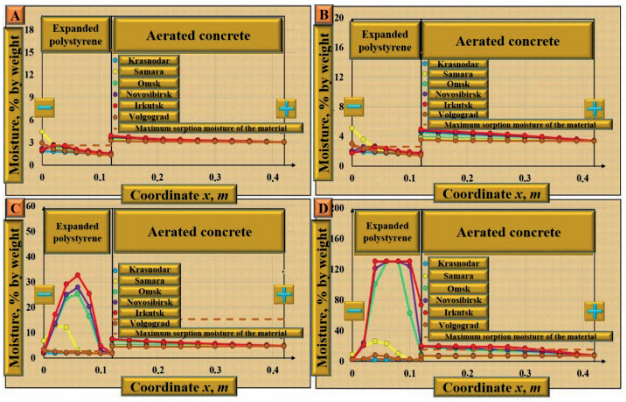


Figure 1. The moisture regime calculation of enclosing structure with aerated concrete base and expanded polystyrene insulation for cities of dry construction area (Krasnodar, Samara, Omsk, Novosibirsk, Irkutsk, Volgograd) for different moisture regimes of building room: A is dry; B is normal; C is moist; D is wet

The moisture regime calculation of enclosing structure with aerated concrete base and expanded polystyrene insulation is presented for cities of normal construction area (Moscow, Kaliningrad, Nizhny Novgorod, Tomsk, Khabarovsk, Permian) for different moisture regimes of building room (Fig. 2).

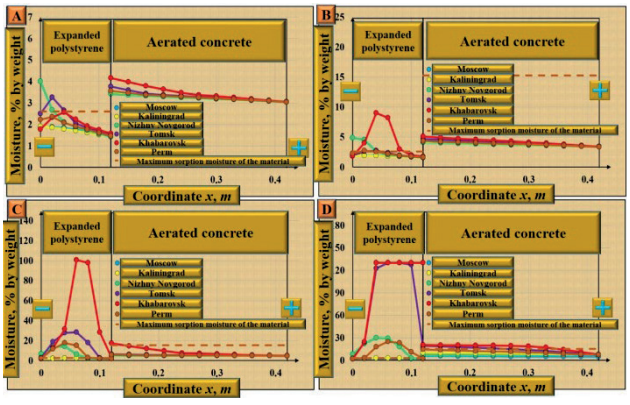


Figure 2. The moisture regime calculation of enclosing structure with aerated concrete base and expanded polystyrene insulation for cities of normal construction area (Moscow, Kaliningrad, Nizhny Novgorod, Tomsk, Khabarovsk, Perm) for different moisture regimes of building room: A is dry; B is normal; C is moist; D is wet

The moisture regime calculation of enclosing structure with aerated concrete base and expanded polystyrene insulation is presented for cities of wet construction area (Petropavlovsk-Kamchatsky, Ayan, Vladivostok, Murmansk, Yuzhno-Kurilsk, Arkhangelsk) for different moisture regimes of building room (Fig. 3).

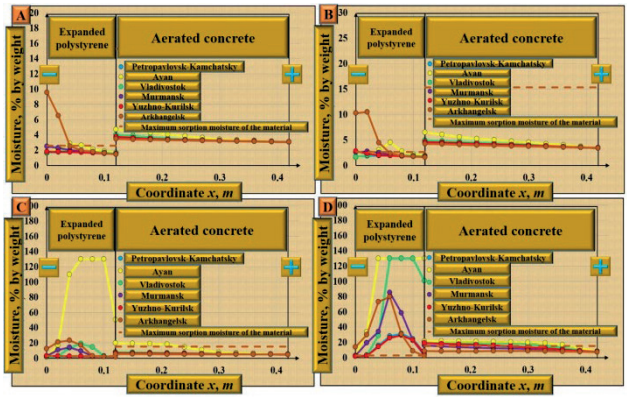


Figure 3. The moisture regime calculation of enclosing structure with aerated concrete base and expanded polystyrene insulation for cities of normal construction area (Petropavlovsk-Kamchatsky, Ayan, Vladivostok, Murmansk, Yuzhno-Kurilsk, Arkhangelsk) for different moisture regimes of building room: A is dry; B is normal; C is moist; D is wet

The results of moisture regime calculation are combined in the table. The maximum calculation values are presented in each gap (Table 3).

Table 3. The obtained moisture values in different construction area for different moisture regimes of building room

Moisture behavior of the building room	Material moisture content determined according to the unsteady-state moisture behavior calculation in various moisture areas, mass percent (1 - insulation layer; 2 – base layer)					
	Dry		Normal		Wet	
	1	2	1	2	1	2
Dry	2.2	3.8	2.2	3.5	3.6	3.7
Normal	2.6	4.2	4.3	4.3	4.7	4.8
Moist	16.1	5.9	39.4	8.7	81.2	11.1
Wet	88.0	16.0	96.7	17.1	97.9	18.3

Obtained values are possible to use in an engineering method to calculate the exact value of the thermal conductivity coefficient and these values exist in all areas of Russia.

4.3. Comparison of the obtained results with results of other authors

If we take into account moisture values which are presented in the regulatory standard Set of Rules 50.13330.2012 "Thermal protection of buildings", we will compare proposed results with modern view of construction industry.

For the enclosing structure with aerated concrete base and expanded polystyrene insulation moisture values, according to the standard, can be written as (Table 4).

Table 4. The moisture values in different construction areas for different moisture regimes of building room determined according to the Set of Rules 50.13330.2012 "Thermal protection of buildings"

Moisture behavior of the building room	Material moisture content determined according to Set of Rules 50.13330.2012 «Thermal protection of buildings» in various moisture areas, mass percent (1 - insulation layer; 2 – base layer)					
	Dry		Normal		Wet	
	1	2	1	2	1	2
Dry	2.0	8.0	2.0	8.0	10.0	12.0
Normal	2.0	8.0	10.0	12.0	10.0	12.0
Moist	10.0	12.0	10.0	12.0	10.0	12.0
Wet	10.0	12.0	10.0	12.0	10.0	12.0

As we can see, the obtained moisture values determined according to the unsteady-state moisture behavior calculation can differ from moisture values determined according to the Set of Rules 50.13330.2012 "Thermal protection of buildings". The use of proposed method improves the accuracy of moisture calculation and can achieve energy saving because in dry and normal construction area moisture content is less than in regulatory standard.

4.4. Comparison of the obtained results with results of other authors

In current paper we predict moisture content and it gives opportunities not to do field studies [10,11] in each construction area.

The accuracy of moisture regime calculation by proposed method is higher than the accuracy by steady-state method [6]. Moreover, we do not need to use numerical method, which simplifies calculations [12].
This article proposes Table. 3, which we can use without additional calculation and it is better than to determine unsteady-state moisture behaviour in each instance.

5. CONCLUSIONS

The new effective method for calculating unsteady-state moisture regime has been developed. Proposed method allows to calculate moisture transfer by analytical expression with higher accuracy than steady-state method, but without using numerical method.
The moisture behaviour calculations in different construction areas for the enclosing structure with aerated concrete base and expanded polystyrene insulation are given. This approach allows to obtain the table with moisture value data. Engineers can use obtained data when they calculate heat conductivity coefficients of building materials of inclosing structures. This article allows to clarify the moisture values in the regulatory standard.

REFERENCES

1. **Bespalov V., Kotlyarova E.** Improving the environmental assessment of objects in the system of construction engineering. // E3S Web of Conferences. 2020, Vol. 164, L 01009.
2. **Bespalov V., Kotlyarova E., Adamyan R.** Scientific and methodological principles of forming an assessment of the level of environmental safety of construction projects in urban areas. // E3S Web of Conferences, 2020, Vol. 193, No. 02007.
3. **Statsenko E.A., Musorina T.A., Ostrovaia A.F., Olshevskiy V., Antuskov A.L.** Moisture transport in the ventilated channel with heating by coil. // Magazine of Civil Engineering, 2017, No. 2(70), pp. 11-17.
4. **Musorina T., Olshevskyi V., Ostrovaia A., Statsenko E.** Experimental assessment of moisture transfer in the vertical ventilated channel. // MATEC Web of Conferences, 2016, No. 02002.
5. **Gumerova E., Gamayunova O., Meshcheryakova T.** Energy efficiency upgrading of enclosing structures of mass housing of the Soviet Union. // Advances in Intelligent Systems and Computing, 2017, Vol. 692, pp. 432-439.
6. **Vavrovic, B.** Importance of envelope construction renewal in panel apartment buildings in terms of basic thermal properties. // Advanced Materials Research, Vol. 855, 2014, pp. 97-101.
7. **Galbraith G.H., Guo G.H., McLean R.C.** The effect of temperature on the moisture permeability of building materials. // Building research and information, Vol. 28 Iss. 4, 2000 – pp. 245-259.
8. **Hoseini A., Bahrami A.** Effects of humidity on thermal performance of aerogel insulation blankets. // Journal of building engineering, Vol. 13, 2017, pp. 107-115.
9. **Arfvidsson, J., Claesson J.** Isothermal moisture flow in building materials: modelling, measurements and calculations based on Kirchhoff's potential. // Building and environment. Vol. 35, Iss. 6, 2000, pp. 519-536.
10. **Petrov A., Ivantsov A.** Design and calculation of the internal roof drain system structure in terms of thermal protection and moisture condensation. // IOP Conference Series: Materials Science and Engineering, 2020, Vol. 890, № 022141.
11. **Petrov A.S., Kupriyanov V.N.** About operational factor influence on vapor permeability of heat-insulating materials. // International Journal of Pharmacy and Technology, 2016, Vol. 8(1), pp. 11248-11256.
12. **Sidorov V.N. Matskevich S.M.** Discrete-analytical solution of the unsteady-state

heat conduction transfer problem based on the finite element method. // IDT 2016 - Proceedings of the International Conference on Information and Digital Technologies 2016. 2016, pp. 241-244.
13. **Zubarev K.P.** Using discrete-continuous approach for the solution of unsteady-state moisture transfer equation for multilayer building walls. // International Journal for Computational Civil and Structural Engineering, 2021, Vol. 17, No. 2, pp. 50-57.

СПИСОК ЛИТЕРАТУРЫ

1. **Bespalov V., Kotlyarova E.** Improving the environmental assessment of objects in the system of construction engineering. // E3S Web of Conferences. 2020, Vol. 164, L 01009.
2. **Bespalov V., Kotlyarova E., Adamyan R.** Scientific and methodological principles of forming an assessment of the level of environmental safety of construction projects in urban areas. // E3S Web of Conferences, 2020, Vol. 193, No. 02007.
3. **Statsenko E.A., Musorina T.A., Ostrovaia A.F., Olshevskiy V., Antuskov A.L.** Moisture transport in the ventilated channel with heating by coil. // Magazine of Civil Engineering, 2017, No. 2(70), pp. 11-17.
4. **Musorina T., Olshevskyi V., Ostrovaia A., Statsenko E.** Experimental assessment of moisture transfer in the vertical ventilated channel. // MATEC Web of Conferences, 2016, No. 02002.
5. **Gumerova E., Gamayunova O., Meshcheryakova T.** Energy efficiency upgrading of enclosing structures of mass housing of the Soviet Union. // Advances in Intelligent Systems and Computing, 2017, Vol. 692, pp. 432-439.
6. **Vavrovic, B.** Importance of envelope construction renewal in panel apartment buildings in terms of basic thermal properties. // Advanced Materials Research, Vol. 855, 2014, pp. 97-101.
7. **Galbraith G.H., Guo G.H., McLean R.C.** The effect of temperature on the moisture permeability of building materials. // Building research and information, Vol. 28 Iss. 4, 2000 – pp. 245-259.
8. **Hoseini A., Bahrami A.** Effects of humidity on thermal performance of aerogel insulation blankets. // Journal of building engineering, Vol. 13, 2017, pp. 107-115.
9. **Arfvidsson, J., Claesson J.** Isothermal moisture flow in building materials: modelling, measurements and calculations based on Kirchhoff's potential. // Building and environment. Vol. 35, Iss. 6, 2000, pp. 519-536.
10. **Petrov A., Ivantsov A.** Design and calculation of the internal roof drain system structure in terms of thermal protection and moisture condensation. // IOP Conference Series: Materials Science and Engineering, 2020, Vol. 890, № 022141.
11. **Petrov A.S., Kupriyanov V.N.** About operational factor influence on vapor permeability of heat-insulating materials. // International Journal of Pharmacy and Technology, 2016, Vol. 8(1), pp. 11248-11256.
12. **Sidorov V.N. Matskevich S.M.** Discrete-analytical solution of the unsteady-state heat conduction transfer problem based on the finite element method. // IDT 2016 - Proceedings of the International Conference on Information and Digital Technologies 2016. 2016, – pp. 241-244.
13. **Zubarev K.P.** Using discrete-continuous approach for the solution of unsteady-state moisture transfer equation for multilayer building walls. // International Journal for Computational Civil and Structural Engineering, 2021, Vol. 17, No. 2, pp. 50-57.

Zubarev Kirill Pavlovich, Ph.D. (Candidate of Engineering Sciences), Associate Professor, Associate Professor at the Department of General and Applied Physics of the Moscow State University of Civil Engineering, 129337, Moscow, Yaroslavskoe shosse, 26; Lecturer at the Department of Heat and Gas Supply and Ventilation of the Moscow State University of Civil Engineering, 129337, Moscow, Yaroslavskoe shosse, 26; Senior Researcher at the Laboratory of Building Thermal Physics of the Research Institute of Building Physics of Russian Academy of Architecture and Construction Sciences, 127238, Moscow, Lokomotivny proezd, 21; Associate Professor at the Department of Civil Engineering, Academy of Engineering, the Peoples' Friendship University of Russia (RUDN University) 117198, Moscow, st. Miklukho-Maclaya, 6; Leading Researcher at the Scientific Center of Engineering and Construction Technologies, Academy of Engineering, the Peoples' Friendship University of Russia (RUDN University) 117198, Moscow, st. Miklukho-Maclaya, 6; Tel. +7 (905) 706-77-63. e-mail.: zubarevkirill93@mail.ru

Зубарев Кирилл Павлович, кандидат технических наук, доцент, доцент кафедры общей и прикладной физики Национального исследовательского Московского государственного строительного университета 129337, г. Москва, Ярославское шоссе, 26; преподаватель кафедры теплогазоснабжения и вентиляции Национального исследовательского Московского государственного строительного университета 129337, г. Москва, Ярославское шоссе, 26; старший научный сотрудник лаборатории строительной теплофизики Научно-исследовательского института строительной физики Российской академии архитектуры и строительных наук 127238, г. Москва, Локомотивный проезд, 21; доцент департамента строительства инженерной академии Российского университета дружбы народов 117198, г. Москва, ул. Миклухо-Маклая, 6; ведущий научный сотрудник научного центра техники и технологий строительства Российского университета дружбы народов 117198, г. Москва, ул. Миклухо-Маклая, 6; тел. +7 (905) 706-77-63. e-mail.: zubarevkirill93@mail.ru

International Journal for Computational Civil and Structural Engineering, 20(3) 167–179(2024)

DOI:10.22337/2587-9618-2024-20-3-167-179

NONLOCAL IN TIME MODEL OF THE LONGITUDINAL VIBRATIONS OF THE HIGH-DAMPING STEEL ROD ELEMENT

Sergey I. Zhavoronok [1,2], Elena. S. Badina [1,2,3]

[1] Institute of Applied Mechanics of Russian Academy of Sciences, Moscow, RUSSIA
[2] Moscow State University of Civil Engineering, Moscow, RUSSIA
[3] Russian University of Transport (MIIT), Moscow, RUSSIA

Abstract: The paper is devoted to the modeling of longitudinal vibrations of a 01Yu5T damping steel rod, taking into account the typical features of the material damping. A brief review of the various damping alloys is given, as well as a brief review of the models of frequency-independent and amplitude-dependent internal friction, theoretically applicable to describe the damping capacity of steel 01Y5T. Considered rod is represented in the article as a one-degree-of-freedom system. The model of its longitudinal vibrations, accounting for the internal friction, is based on the principals of nonlocal mechanics: the impact of the previous history of deformation on the current state of the system is taken into account. The IV order Runge-Kutta method was used to solve the equation of motion. The impact of the nonlocal scale parameter on the material damping in terms of the considered model is shown on the basis of the simulation of the rod free oscillation. The calibration of the nonlocal in time model of rod vibrations based on experimental data was performed using the least squares method. The results of the forced vibrations modeling under the stochastic load for an element made of 01Y5T steel, taking into account amplitude-dependent damping, are presented in comparison with the results obtained for a steel with a constant level of internal friction.

Keywords: high-damping alloys, damping steel, rod vibrations, material damping, amplitude-dependent damping, nonlocal mechanics

НЕЛОКАЛЬНАЯ ВО ВРЕМЕНИ МОДЕЛЬ ПРОДОЛЬНЫХ КОЛЕБАНИЙ СТЕРЖНЕВОГО ЭЛЕМЕНТА, ВЫПОЛНЕННОГО ИЗ СТАЛИ СО СВЕРХВЫСОКИМ ДЕМПФИРОВАНИЕМ

С.И. Жаворонок [1,2], Е.С. Бадьина [1,2,3]

[1] Институт прикладной механики Российской академии наук, г. Москва, РОССИЯ
[2] Национальный исследовательский Московский государственный строительный университет, г. Москва, РОССИЯ
[3] Российский университет транспорта (МИИТ), г. Москва, РОССИЯ

Аннотация: Статья посвящена моделированию продольных колебаний стержня, выполненного из демпфирующей стали 01Yu5T, с учётом характерных свойств внутреннего демпфирования материала. Приведен краткий обзор различных демпфирующих сплавов, а также краткий обзор моделей частотно-независимого и амплитудно-зависимого внутреннего трения, теоретически применимых для описания демпфирующей способности стали 01Ю5Т. Рассматриваемый стержень представлен в статье, как система с одной степенью свободы. Модель для описания его продольных колебаний с учётом внутреннего трения построена на основании положений нелокальной механики: учтено влияние предыдущей истории деформирования на состояние системы в настоящий момент. Для решения уравнения движения использован метод Рунге-Кутта IV порядка. На примере свободных колебаний стержня показано влияние изменения масштабного параметра нелокальной модели на результаты расчета. Калибровка нелокальной во времени модели колебаний стержня выполнена на основании экспериментальных данных методом наименьших квадратов. Приведены результаты моделирования вынужденных колебаний под действием нагрузки, представленной как случайный стационарный процесс, для элемента из стали 01Ю5Т с учетом амплитудно-зависимого демпфирования, в сравнении с результатами, полученными для стали с постоянным уровнем внутреннего трения.

Ключевые слова: сплавы высокого демпфирования, демпфирующая сталь, колебания стержней, внутреннее трение, амплитудно-зависимое демпфирование, нелокальная механика

INTRODUCTION

The protection of the engineering structures against vibrations remains a topical problem due to high level of noise from transport, industrial, and construction facilities. Another key problem of civil engineering consists in the protection of buildings, bridges, and other structures against impact loads including seismic ones. A possible way of solution of such problems consists in the use of specific structural materials with high damping properties. Commonly, one could use layers of polymer materials to decrease the vibration impact on the structure; it should be noted that most polymers have low moduli and strength.

Another promising approach consists in the use of high damping metallic alloys to design functional structural elements [1-4]. Magnesium based alloys show high level of damping properties: 5 times that of iron and 12 times that of aluminum [1]. Moreover, their low mass density makes them useful for various lightweight structures; a good corrosion resistance is also one of the features of Mg-based alloys. At the same time the tensile strength of Mg alloys remains relatively low, thus, they cannot be used in bearing structural elements.

Shape memory alloys, or SMAs, (Copper alloys, Titanium Nickelide, etc.) show also very high damping capacity [2, 5-11]. SMAs of Ti-Ni system having two stable phase constitutions, the low-modulus face-centered martensite stable at lower temperatures and high-modulus volume-centered austenite stable at higher temperatures, provide two possible mechanisms of damping, the martensite inelasticity and pseudoelasticity [5, 9]. The first one consists in structural transitions between twinned and untwinned martensite induced by stress impacts [11, 12]; such strains irreversible in the martensite state could be removed after the temperature-induced martensite-to-austenite phase transform. The second mechanism so-called also "superelasticity" due to high reversible strains consists in the phase transform from austenite into martensite when the stress intensity rises and vice versa when it drops with large hysteretic loops [6, 7, 11]. The maximum damping capacity of TiNi alloy is about 40%; at the same time, it depends strongly on the amplitude. Since the maximum could be reached at strain amplitude level of 10^{-5} and higher, the TiNi damping element is inefficient for low-amplitude vibration suppression but is promising in seismic protection devices [5-7]. On the other hand, the pseudoelastic deforming of SMA damping elements results in the possibility of its shape restauration after unloading; indeed, "…in base isolation of buildings, the superelasticity creates the property of self-centering; the base isolation device acting alone can restore the building to its original position" [6]. Despite these facts the application the high cost of SMAs makes they industrial use in most cases almost impossible, moreover the mechanical behavior of SMAs is very complex, especially in case of thin-walled structures that could buckle under extremely low stresses [13-16].

Iron based high damping alloys have high mechanical strength and also lower cost as compared with shape memory alloys [3]. Fe-Cr alloys were developed and studied e.g. in [17-19]. The researchers were looking for the ways to increase the damping capacity of the material. It is noted in [19] that since the Fe-Cr alloys are ferromagnetic, their high damping capacity is correlated to the magneto-mechanical hysteresis loss. In this regard the iron-based alloys differ from magnesium alloys, where the main cause of increased damping level is dislocation [1].

In [3] the major experimental research of the irons alloyed with rare earth elements is presented. It is shown that the energy loss in the magneto-mechanical hysteresis damping is proportional to the "saturated magnetostriction" [3] and the level of internal stress, i.e. the level of damping in the ferromagnetic alloys depends on the stress rate. The approximation of those correlations for different types of alloys is also provided in the paper.

Steel 01Yu5T [20] that consists 5% of aluminum also has high damping properties due

to magnetostriction. The experimental studies of the material have shown that its damping capacity depends on the stress intensity and does not depend on vibration frequency and temperature. The maximum damping capacity of 37% is reached at the 12 MPa stress level. The steel 01Yu5T is strong enough to be used for making of bearing elements and it is way more cost efficient in comparison to the other iron based alloys, especially to the ones that contains rare earth elements.

To unlock the full potential of the high damping steel it is necessary to design structural elements so they work in the stress range where the damping capacity is the highest. The design process requires special damping model, which can describe the behavior of the magnetostriction material. Obviously, this models have to be frequency independent and dependent on stress attitude at the same time.

The frequency independence of internal friction was found out experimentally in the beginning of XX century [21]. The results of that study contradicted to the theory of viscous damping [22] and since then many attempts have been taken by different researchers to develop the uncontroversial mathematical model of the internal damping that does not depend on vibration frequency, but depends on the level of stress.

One of the most well-known frequency independent damping models is the complex stiffness model derived by E.S. Sorokin [23]. This model provides good alignment with an experiment. However, it might be challenging to use it for the analysis of the complicated engineering systems with big amount of degrees of freedom [24].

An interesting concept of the internal damping is proposed in [25]. In this paper a viscous "geometric" damping term is introduced to the equilibrium equation considering an internal shear force to be proportional to the time rate of change of the slope. Even though this model is frequency independent, it has no correlation with the level of stress in the structure, at least in the form proposed in [25].

In [24] three nonlinear models of the frequency independent damping are studied: the hysteretic model, the modified hysteretic model and the quasi-hysteretic model. It is shown on the example of the single-degree-of-freedom system that for the high level of damping properties first two models give significantly different results from the ones for the complex stiffness model and the equivalent viscous damping model. Oppositely, the quasi hysteretic model is holding close to the complex stiffness model and the equivalent viscous damping model for the wide range of damping levels. Such a stability of the quasi hysteretic model is explained by the fact that it deals with the mean values of displacements and velocities, i.e. considers the previous time history of the vibration process.

The model of frequency independent internal damping with the use of the Rzhanitsyn rod approximation is presented in [26]. On each iteration of the vibration process simulation the stress values are determined in every element of the rod structure and according to that the damping constants determined experimentally are entered into the model. This model allows to take into account the dependence of the material damping on the stress level. It is also noted that the history of the rod loading is taken into account.

In [27] the experimentally determined damping constants are implemented in the FEA computational scheme to build up the stress level dependent damping model. It is concluded in the paper that the damping characteristics are integral, i.e. they can be represented as a summation of the instant changing during the vibration process values of damping coefficients. As well as in [26] it is mentioned that such method of damping consideration makes the computational model complex and increases the computing time.

Damping models based on the principals of nonlocal mechanics are flexible enough to be used for the dynamic problems where the classic models do not provide adequate results [28, 29]. Nonlocal in time damping model [30] allows

considering the influence of the previous time history of the vibration process on the damping forces in current moment. Moreover, it can be easily incorporated to the FEA algorithm and therefore applied for the modeling of relatively complicated engineering systems. However, the damping described by this model is frequency dependent. Thus it cannot be used for modeling of the dynamics of elements made of the high-damping steel. In [31] the previous history of dynamic deformation of the bending element is considered to affect the elastic forces in the structure. In [32] it is shown with the series of numerical experiments that the model is applicable to simulate frequency independence of damping properties. In addition, the flexibility of the model can be used for modelling of the stress level dependent damping.

MODELLING OF A SINGLE-DEGREE-OF-FREEDOM SYSTEM FREE VIBRATIONS

Consider free oscillation of a rod of constant cross-section area A, referred to the frame $Oxyz$ ($0 \le x \le l$), clamped at a point $x = 0$, with a point mass m at $x = l$. Let the rod material be homogeneous with mass density ρ and Young modulus E, and let us assume $m \gg \rho A l$, therefore the inertial forces in longitudinally deforming rod could be neglected (Figure 1a). Since the stress-strain state of the rod is homogeneous the oscillation of the considered structure could be approximated by the discrete spring-mass system with the stiffness of spring equal to $\frac{EA}{l}$ and the single degree of freedom $y(t) = u(x,t)\big|_{x=l}$, i.e. the longitudinal translation of the mass m (Fig. 1b).

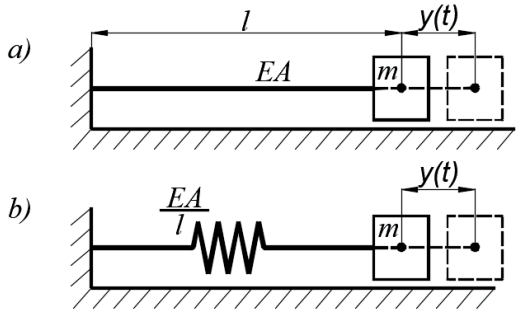


Figure 1 – a) Considered rod with a point mass, subjected to the longitudinal oscillations; b) the spring-mass system equivalent to the considered rod.

Let us assume the damping be viscous; the oscillation of such systems could be defined by the dynamic equation (1) [33]:

$$\ddot{y}(t) + 2n\dot{y}(t) + \omega_0^2 y(t) = 0 \qquad (1)$$

where dots define time derivative, $n = \xi\omega_0$ is the external damping factor, the eigenfrequency ω_0 is determined as follows:

$$\omega_0 = \sqrt{\frac{r_{11}}{m}}, \quad r_{11} = l^{-1}EA \qquad (2)$$

where r_{11} denotes the reaction of the beam on the unit end point translation $y \equiv 1$.

The nonlocal damping model is based on the hypothesis of dependence of the elastic reaction force at the time t as well on the instantaneous deformed state defined here as $y(t)$ on the deforming history, i.e. on the state of the system at any previous time instant denoted hereinafter as t_1. Let us note that the interference between two different states of the system corresponding to t_1 and t vanishes with growing time range $|t - t_1|$ [34, 31]; such effect could be described by the integral operator with the kernel $R(t - t_1)$ normalized as follows:

$$\int_0^t R(t-\tau)\,d\tau = 1 \tag{3}$$

For instance, the kernel $R(t-t_1)$ could be based on the normalized error function (4) [35]:

$$R(t-\tau) = \frac{2\eta}{\sqrt{\pi}} \cdot e^{-\eta^2(t-\tau)^2}. \tag{4}$$

Here η denotes the scale parameter that corresponds to the time nonlocality level of the model. Lower η values result in higher nonlocal effects (Fig. 2).

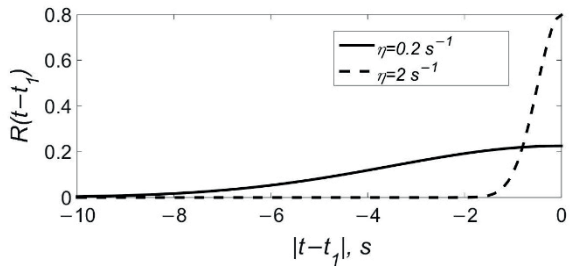


Figure 2 – Kernels $R(t-t_1)$ based on the normalized error function for the different values of the scale parameter η

On the other hand the model reduces to the classical local one when $\eta \to \infty$ and $R(t-t_1) \to \delta(t-t_1)$ where δ is the Dirac delta.

The dynamic equation (1) accounting for nonlocal behavior defined by (3) could be written as follows:

$$\ddot{y}(t) + 2n\dot{y}(t) + \\ +\omega_0^2 \int_0^t R(t-t_1)y(t_1)dt_1 = 0. \tag{5}$$

Let us introduce the following dimensionless variables:

$$\xi(t) = \frac{y(t)}{l}, \tau = t\omega_0, \ \ \tau_1 = t_1\omega_0 \tag{6}$$

As a result, we obtain the dimensionless dynamic equation (7):

$$\ddot{\xi}(\tau) + \frac{2n\dot{\xi}(\tau)}{\omega_0} + \frac{1}{\omega_0}\int_0^\tau \frac{2\eta}{\sqrt{\pi}} e^{-\frac{\eta^2}{\omega_0^2}(\tau-\tau_1)^2} \xi(\tau)d\tau_1 = 0. \tag{7}$$

This equation could be solved numerically using the fourth-order Runge-Kutta algorithm [36].

DETERMINING OF THE SCALE PARAMETER BASED ON THE EXPERIMENTAL DATA

Since the dissipation properties of the investigated 01Yu5T steel depend strictly on the stress amplitude the model calibration should be implemented using the test data [32] and the solution for the damped oscillations of the system (7) excited by the unit initial translation of the mass m.

The impact of the value of the scale parameter η on the oscillations is shown on the Fig. 3:

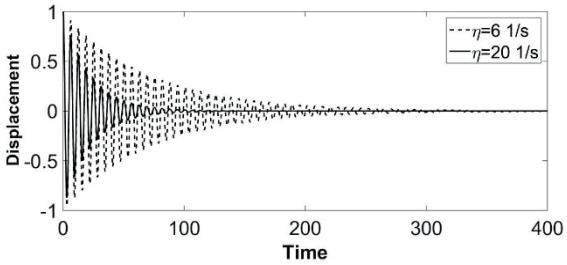


Figure 3 – The impact of the value of the scale parameter η on the oscillations of the rod

It could be seen that the damping in the nonlocal system rises with increasing scale factor η.

To take into account the amplitude dependence of the damping the scale factor η should be computed for a set of different stress amplitudes using the corresponding values of the absorption factor ψ obtained

experimentally. The appropriate test data for the 01Yu5T steel [20] is presented on the Figure 4.

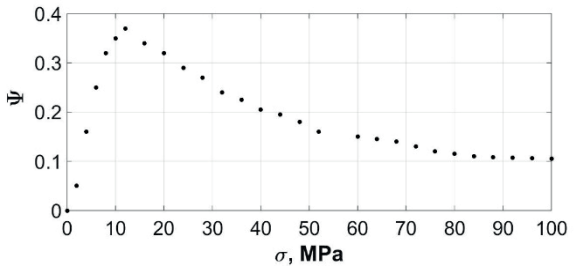


Figure. 4 – Values of the absorption factor ψ for the different stress amplitudes obtained experimentally.

The dependence of the scale parameter η on the active stress amplitude was obtained for the discrete set of points σ^K, $K = 0,1\ldots N$ corresponding to the test data shown on the Fig. 4 by the least square method (Fig. 5). The set of computer simulations was implemented to identify the values of η which provide damping (fig. 3) with the absorption factors ψ matching with the considered σ^K.

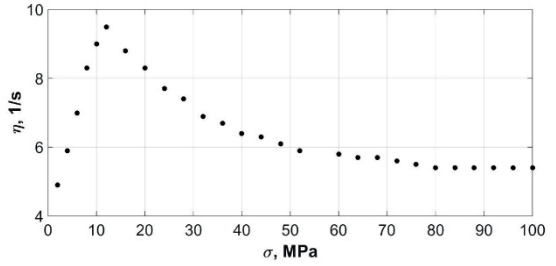


Figure 5 – Values of the scale parameter η for the different stress amplitudes obtained by the least square method

The scale parameter η in the numerical implementation of the proposed nonlocal model could be determined using the simplest linear interpolation:

$$\eta(\sigma)\big|_{\sigma^{K-1}\le\sigma<\sigma^K} \approx \frac{\eta^K-\eta^{K-1}}{\sigma^K-\sigma^{K-1}}\sigma+\eta^K. \qquad (8)$$

Here the normal stress $\sigma(t)$ in the oscillating rod is defined using the formula:

$$\sigma(t) = \frac{Ey(t)}{l} \qquad (9)$$

The integral operator with vanishing memory defined by (4) accounts the stress amplitude history at least near the current time instant. Thus, the nonlocal model presented above allows one to obtain the stress-dependent damping property of a material that could be applied to simulate the dynamics of the 01Yu5T steel structure.

SINGLE-DEGREE-OF-FREEDOM SYSTEM VIBRATIONS UNDER THE STOCHASTIC LOAD

Noise and industrial vibrations generally are stochastic. As soon as the high-damping steel 01Yu5T is expected to be used for protection from those impacts, the oscillations of the rod were simulated under the stochastic load. The equation of motion in this case is:

$$\ddot{\xi}(\tau)+\frac{2n\dot{\xi}(\tau)}{\omega_0}+\frac{1}{\omega_0}\int_0^\tau \frac{2\eta}{\sqrt{\pi}} e^{-\frac{\eta^2}{\omega_0^2}(\tau-\tau_1)^2}\xi(\tau)d\tau_1 = \Phi(\tau), \qquad (10)$$

where $\Phi = \frac{F(\tau)}{m}$ and F is the dynamic load, modelled as the stochastic stationary process.
The characteristics of a stochastic stationary process do not change over time, so it can be considered as indefinitely long and any point in time can be chosen as the starting point.
In order for the stationary process to proceed uniformly, we require compliance with certain conditions [38]. First, the expected value must be constant (11).

$$m_x(t) = m_x = const \qquad (11)$$

The second condition is the condition of constant variance (12).

$$D_x(t) = D_x = const \tag{12}$$

The third condition concerns the correlation function of a stationary process. If the stochastic process is stationary, then the correlation moment $K_x(t, t+\tau)$ should depend only on the length of the time interval τ, and not on where exactly this interval is taken on the time axis (13).

$$K_x(t, t+\tau) = k_x(\tau) \tag{13}$$

In this paper, the method of canonical expansion is used to model a stationary process [38]. In this case a random time function is represented as a sum of elementary random functions:

$$q(t) = \sum_{k=0}^{n} (U_k \cos\omega_k t + V_k \cos\omega_k t) \tag{14}$$

Here $\omega_k \in (0;\pi)$, U_k, V_k are uncorrelated random variables distributed normally, with mathematical expectations equal to zero and the variances which are the same for each pair of random variables with the same indices *k*. To calculate these variances we select an interval on the ω_k-axis with a total length of *2L* so that the origin is in the middle of this interval. At $|\omega| > L$ the spectral density can be considered equal to zero. We divide the entire selected segment into equal sections of length $\Delta\omega$. Then the variance of the random variables U_k, V_k is calculated as:

$$D_k = 2S(\omega_k) \cdot \Delta\omega \tag{15}$$

where $S(\omega_k)$ is spectral density of a stationary random function $q(t)$. Since there is a relationship between the spectral density and the correlation function of a random process (16, 17), the spectral decomposition of the random load function is determined by the correlation function [39].

$$S(\omega_k) = \frac{1}{2\pi} \int_{-\infty}^{\infty} e^{-i\omega t} K_x(\tau) d\tau, \tag{16}$$

$$K_x(\tau) = \int_{-\infty}^{\infty} e^{-i\omega t} S(\omega_k) d\tau, \tag{17}$$

The correlation function for the load, which is a Gaussian process, is defined by the expression:

$$K(\tau) = \sigma^2 e^{-\delta|\tau_1 - \tau_2|} \left[\cos\theta(\tau) + \frac{\delta}{\theta}\sin\theta(\tau)\right] \tag{18}$$

Here σ is the standard deviation of the stationary process, θ is the frequency of the implicit periodicity of the stationary process, δ is a correlation scale parameter of a random function.

With the correlation function (18), the spectral density of a stationary process has the form:

$$S(\omega) = \frac{2\sigma^2 \cdot \delta(\delta^2 + \theta^2)}{\pi[(\omega^2 - \theta^2 - \delta^2)^2 + 4\delta^2 \cdot \omega^2]} \tag{19}$$

Figure 6 shows one implementation of a random stationary loading. In the considered numerical example the characteristics of spectral density are θ =0.25 and δ = 0.05.

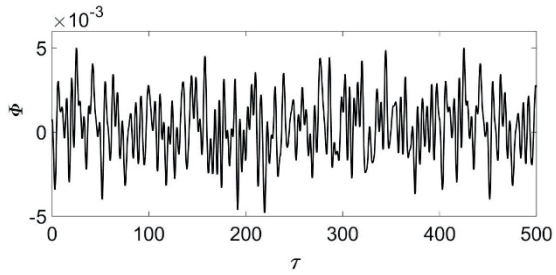


Figure 6 – One implementation of a random stationary loading

The stresses and corresponding scale parameters were determined as it was described in the previous section (8,9). Those values for several time increments of the oscillations under the stochastic load (fig.6) are provided in table 1.

Table 1. Scale parameters η determined for several increments of the oscillation process

τ	σ, MPa	$\eta, 1/s$
15.75	-19.71	8.34
15.8	-13.22	9.29
15.85	-6.80	7.52
15.9	-0.46	4.90
15.95	5.81	6.90
16	12.00	9.50
16.05	18.08	8.54
16.1	24.06	7.70
16.15	29.93	7.16
16.2	35.68	6.72
16.25	41.31	6.37

The results obtained for the 01Yu5T steel with the use of stress-dependent nonlocal model are shown on fig.7 in comparison to the oscillations of the same rod made of the steel St3 which has low and amplitude independent absorption factor $\psi = 0.05$.

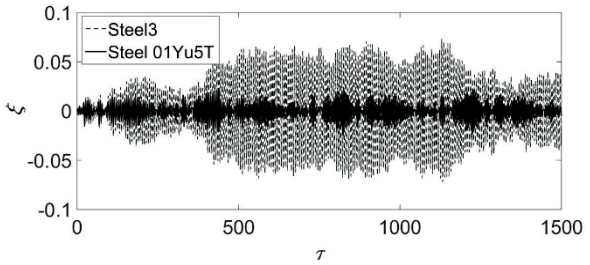


Figure 7 – Comparison of the oscillations of the one-degree-of-freedom element made of 01Yu5T steel and St3

It can be seen from the figure 7 that in comparison to the St3 01Yu5T steel demonstrates stable decrease of the oscillations amplitude.

CONCLUSION

Due to its relatively low cost and high tensile strength high-damping steel 01Yu5T can be effectively applied for vibration protection, particularly as a material for the bearing structural elements.

Modelling of the dynamic behavior of elements made of 01Yu5T steel requires special approaches to simulate its stress dependent damping properties. The application of a non-local approach in describing of the damping properties of a material, depending on the stress level, allows to build a numerical model that is more flexible in comparison to the classic local one.

For now, the stress-dependent nonlocal damping model is derived for the simplest case of longitudinal vibrations, when the stress level is uniform over the entire length of the element and its entire cross-section. To simulate the dynamics of the elements subjected to bending it is necessary to adequately describe the influence of stress distribution on the damping properties.

ACKNOWLEDGEMENT

This research is supported by Russian Science Foundation (Project # 24-19-00845)

REFERENCES

1. **Wang J., Zou Y., Dang C., Wan Z., Wang J., Pan F**. Research Progress and the Prospect of Damping Magnesium Alloys. Materials, 2024, 17(6), 1285.
2. **Ivanić I., Kožuh S., Grgurić T.H., Vrsalović L., Gojić M.** The Effect of Heat Treatment on Damping Capacity and Mechanical Properties of CuAlNi Shape Memory Alloy. Materials (Basel), 2022, 15(5), 1825.
3. **Sun M., Wang X., Fang Q., Balagurov A., Bobrikov I., Wen W., Golovin I.S**. High Damping in FE-GA-LA Alloys:

Phenomenological Model for Magneto-Mechanical Hysteresis Damping and Experiment. Journal of Materials Science and Technology, 2021, V. 72, pp. 69-80.
4. **Ritchie I.G., Pan Z.L.** High-damping metals and alloys. Metallurgical Transactions A, 1991, V. 22, pp. 607–616.
5. **Van Humbeeck J., Kustov S.** Active and passive damping of noise and vibrations through shape memory alloys: applications and mechanisms. IOP Smart Materials and Structures, 2005, V. 14, pp. S171-S185.
6. **Witting P., Corzarelli F.A.** Shape memory structural dampers: material properties, design and seismic testing. Technical Report NCEER-92-0013.
7. **Fang Ch., Yam M.C.H.** Emerging superelastic SMA core damping elements for seismic application. Frontiers in Built Environment, 2023, V. 8, 953273.
8. **Saedi S., Acar E., Raji H., Saghaian S.E., Mirsayar M.** Energy damping in shape memory alloys: A Review. Journal of Alloys and Compounds, 2023, V. 956, 170286.
9. **Helbert G., Volkov A., Evard M., Dieng L., Chirani S.A.** On the understanding of damping capacity in SMA: from the material thermomechanical behaviour to the structure response. Journal of Intelligent Material Systems and Structures, 2021, V. 32, No. 11, pp. 1167-1184.
10. **Liu M., Li H., Song G., Ou J.** Investigation of vibration mitigation of stay cables incorporated with superelastic shape memory alloy dampers. IOP Smart Materials and Structures, 2007, V. 16, pp. 2203-2213.
11. **Movchan A.A., Kazarina S.A.** Materials with shape memory as an object of solid mechanics: experimental studies, determining relations, setting boundary value problems. Physical Mesomechanics, 2012, vol. 15, No. 1, pp. 105-116 (in Russian).
12. **Movchan A.A., Kazarina S.A., Mashikhin A.E., Mishustin I.V., Saganov E.B., Safronov P.A.** Boundary value problems for shape memory alloys. Scientific notes of Kazan University. Series: Physical and Mathematical Sciences, 2015, T. 157(3), C. 97–110 (in Russian).
13. **Movchan A.A., Silchenko L.G., Kazarina S.A., Zhavoronok S.I., Silchenko T.L.** Stability of titanium nickelide rods loaded in the mode of martensite inelasticity. Journal of Machinery Manufacture and Reliability, 2012, V. 41, pp. 245–251.
14. **Movchan A.A., Dumanscii S.A.** Solution of the double-coupled problem of buckling of a shape memory alloy rod due to the direct thermoelastic phase transformation. Journal of the Applied Mechanics and Technical Physics, 2018, V. 59, No. 4, pp. 716–723.
15. **Dumanskii S.A., Movchan A.A.** Loss of stability of a rod from a shape-memory alloy caused by reverse martensitic transformation. Mechanics of Solids, 2019, V. 54, No. 6, Pp. 929–940.
16. **Nushtaev D.V., Zhavoronok S.I.** Abnormal Buckling of Thin-Walled Bodies with Shape Memory Effects Under Thermally Induced Phase Transitions. Advanced Structured Materials, 2019, V. 110, pp. 493-524.
17. **Mituo K., Takashi F., Hideo Sh., Masatoshi N., Hiroshi A.** High Damping Fe-Cr-Al Alloy. United States Patent # 89312, 1979.
18. **Igata N., Aoyama H., Kanja Y., Habara Y**. High Damping Fe-Cr-Mn Alloy. Journal de Physique IV Proceedings, 1996, 06 (C8), pp.C8-791-C8-794.
19. **Pulino-Sagradi D., Sagradi M., Karimi A., Martin J.L.** Damping capacity of Fe-Cr-X high-damping alloys and its dependence on magnetic domain structure. Scripta Materialia, 1998, 39(2), pp. 131-138.
20. **Chudakov I.B., Alexandrova N.M., Makushev S.Yu.** Features of consumer properties of new high-damping steels. Steel, 2014, № 8, c. 92-95 (in Russian).
21. **Rowett F.E.** Elastic Hysteresis in Steel. Proceedings of The Royal Society A: Mathematical, Physical and Engineering Sciences, 1914, V. 89, pp. 528-543.

22. **Voigt W.** Lehrbuch der Kristallphysik (mit Ausschluß der Kristalloptik), Stuttgart-New York: B.G. Teubner Verlagsgesellschaft, 1966, Johnson Reprint Corporation.
23. **Sorokin E.S.** On the theory of internal friction during vibrations of elastic systems. Gosstroyizdat, Moscow, 1960 (in Russian).
24. **Muravskii G.** On frequency independent damping. Journal of Sound and Vibration, 2004, 274(3-5) pp.653-668.
25. **Lesieutre G.A.** Frequency-Independent Modal Damping for Flexural Structures via a Viscous "Geometric" Damping Model. Journal of Guidance, Control, and Dynamics. 2010, 33(60), pp. 1931-1935.
26. **Zylev V.B., Platnov P.O.** Consideration of damping in a continuous medium using rod approximation according to A.R. Rzhanitsyn. Mechanics of engineering constructions and structures, 2023, т. 19, № 2, с. 149-161 (in Russian).
27. **Kazakova O.I., Smolin I.Yu., Bezmozgiy I.M.** Analysis of amplitude-dependent damping and the possibility of their application in the numerical calculations. Bulletin of Tomsk State University. Mathematics and Mechanics. 2018, № 54, с. 66-78 (in Russian).
28. **Potapov V.D.** On the stability of a rod under deterministic and stochastic loading with allowance for nonlocal elasticity and nonlocal material damping. Journal of Machinery Manufacture and Reliability, 2015, 44, pp. 6–13.
29. **Shepitko E.S., Sidorov V.N.** Defining of Nonlocal Damping Model Parameters Based on Composite Beam Dynamic Behaviour Numerical Simulation Results. IOP Conference Series: Materials Science and Engineering, 2019, 675(1), 012056
30. **Sidorov V.N., Badina E.S., Detina E.P.** Modified Newmark method for the dynamic analysis of composite structural elements considering damping with memory. Mechanics of Composite Materials and Structures, 2022, V. 28, No. 1, pp. 98-111 (in Russian).
31. **Sidorov V.N., Badina E.S., Tsarev R.O.** Dynamic Model of Beam Deformation with Consider Nonlocal in Time Elastic Properties of the Material. International Journal for Computational Civil and Structural Engineering, 2022, 18(4), pp. 124–131.
32. **Sidorov V.N., Badina E.S., Tsarev R.O.** Calibration of the Nonlocal Dynamic Deformation Model of a Flexural Beam Based on Numerical Experiment Results. International Journal for Computational Civil and Structural Engineering, 2024, 20(2), 132–140.
33. **Alexandrov A.V., Potapov V.D., Zylev V.B.** Structural mechanics. Dynamics and stability of elastic systems: a textbook for universities. Edited by A.V. Alexandrov. Higher School, 2008, 384 p. (in Russian).
34. **Potapov V.D.** Stability of a compressed nonlocally viscoelastic rod lying on an elastic base. Proceedings of the Russian Academy of Sciences. Mechanics of Solids, 2016, No. 1, pp. 90-96 (in Russian).
35. **Lei Y., Friswell, M.I., Adhikari S.A.** Galerkin method for distributed systems with non-local damping. International Journal of Solids and Structures, 2006, V. 43, pp. 3381 - 3400.
36. **Kalitkin N.N.** Numerical Methods. BHV-St. Petersburg, 2011, 592 c (in Russian).
37. **Panovko Ya.G.** Internal friction during vibrations of elastic systems. State Publishing House of Physical and Mathematical Literature, 1960, 193 p (in Russian).
38. **Wentzel E.C.** Probability theory. Higher School, 1999, 576 p (in Russian).
39. **Sveshnikov A.A.** Applied methods of the theory of random functions. Science, 1968, 464 p. (in Russian).

СПИСОК ЛИТЕРАТУРЫ

1. **Wang J., Zou Y., Dang C., Wan Z., Wang J., Pan F**. Research Progress and the

Prospect of Damping Magnesium Alloys. Materials, 2024, 17(6), 1285.
2. **Ivanić I., Kožuh S., Grgurić T.H., Vrsalović L., Gojić M.** The Effect of Heat Treatment on Damping Capacity and Mechanical Properties of CuAlNi Shape Memory Alloy. Materials (Basel), 2022, 15(5), 1825.
3. **Sun M., Wang X., Fang Q., Balagurov A., Bobrikov I., Wen W., Golovin I.S**. High Damping in FE-GA-LA Alloys: Phenomenological Model for Magneto-Mechanical Hysteresis Damping and Experiment. Journal of Materials Science and Technology, 2021, V. 72, pp. 69-80.
4. **Ritchie I.G., Pan Z.L.** High-damping metals and alloys. Metallurgical Transactions A, 1991, V. 22, pp. 607–616.
5. **Van Humbeeck J., Kustov S.** Active and passive damping of noise and vibrations through shape memory alloys: applications and mechanisms. IOP Smart Materials and Structures, 2005, V. 14, pp. S171-S185.
6. **Witting P., Corzarelli F.A.** Shape memory structural dampers: material properties, design and seismic testing. Technical Report NCEER-92-0013.
7. **Fang Ch., Yam M.C.H.** Emerging superelastic SMA core damping elements for seismic application. Frontiers in Built Environment, 2023, V. 8, 953273.
8. **Saedi S., Acar E., Raji H., Saghaian S.E., Mirsayar M.** Energy damping in shape memory alloys: A Review. Journal of Alloys and Compounds, 2023, V. 956, 170286.
9. **Helbert G., Volkov A., Evard M., Dieng L., Chirani S.A.** On the understanding of damping capacity in SMA: from the material thermomechanical behaviour to the structure response. Journal of Intelligent Material Systems and Structures, 2021, V. 32, No. 11, pp. 1167-1184.
10. **Liu M., Li H., Song G., Ou J.** Investigation of vibration mitigation of stay cables incorporated with superelastic shape memory alloy dampers. IOP Smart Materials and Structures, 2007, V. 16, pp. 2203-2213.
11. **Мовчан А.А., Казарина С.А.** Материалы с памятью формы как объект механики деформируемого твёрдого тела: экспериментальные исследования, определяющие соотношения, постановки краевых задач. Физическая мезомеханика, 2012, Т. 15, № 1, с. 105-116.
12. **Мовчан А.А., Казарина С.А., Машихин А.Е., Мишустин И.В., Саганов Е.Б., Сафронов П.А.** Краевые задачи для сплавов с памятью формы. Учёные записки Казанского университета. Серия: Физико-математические науки, 2015, Т. 157(3), С. 97–110.
13. **Movchan A.A., Silchenko L.G., Kazarina S.A., Zhavoronok S.I., Silchenko T.L.** Stability of titanium nickelide rods loaded in the mode of martensite inelasticity. Journal of Machinery Manufacture and Reliability, 2012, V. 41, pp. 245–251.
14. **Movchan A.A., Dumanscii S.A.** Solution of the double-coupled problem of buckling of a shape memory alloy rod due to the direct thermoelastic phase transformation. Journal of the Applied Mechanics and Technical Physics, 2018, V. 59, No. 4, pp. 716–723.
15. **Dumanskii S.A., Movchan A.A.** Loss of stability of a rod from a shape-memory alloy caused by reverse martensitic transformation. Mechanics of Solids, 2019, V. 54, No. 6, Pp. 929–940.
16. **Nushtaev D.V., Zhavoronok S.I.** Abnormal Buckling of Thin-Walled Bodies with Shape Memory Effects Under Thermally Induced Phase Transitions. Advanced Structured Materials, 2019, V. 110, pp. 493-524.
17. **Mituo K., Takashi F., Hideo Sh., Masatoshi N., Hiroshi A.** High Damping Fe-Cr-Al Alloy. United States Patent No. 89312, 1979.
18. **Igata N., Aoyama H., Kanja Y., Habara Y**. High Damping Fe-Cr-Mn Alloy. Journal

de Physique IV Proceedings, 1996, 06 (C8), pp.C8-791-C8-794.
19. **Pulino-Sagradi D., Sagradi M., Karimi A., Martin J.L.** Damping capacity of Fe-Cr-X high-damping alloys and its dependence on magnetic domain structure. Scripta Materialia, 1998, 39(2), pp. 131-138.
20. **Чудаков И.Б., Александрова Н.М., Макушев С.Ю**. Особенности потребительских свойств новых высокодемпфирующих сталей. Сталь, 2014, № 8, с. 92-95.
21. **Rowett F. E.** Elastic Hysteresis in Steel. Proceedings of The Royal Society A: Mathematical, Physical and Engineering Sciences, 1914, V. 89, pp. 528-543.
22. **Voigt W.** Lehrbuch der Kristallphysik (mit Ausschluß der Kristalloptik), Stuttgart-New York: B.G. Teubner Verlagsgesellschaft, 1966, Johnson Reprint Corporation.
23. **Сорокин Е.С.** К теории внутреннего трения при колебаниях упругих систем. Госстройиздат, Москва, 1960.
24. **Muravskii G.** On frequency independent damping. Journal of Sound and Vibration, 2004, 274(3-5) pp.653-668.
25. **Lesieutre G.A.** Frequency-Independent Modal Damping for Flexural Structures via a Viscous “Geometric” Damping Model. Journal of Guidance, Control, and Dynamics. 2010, 33(60), pp. 1931-1935.
26. **Зылев В.Б., Платнов П.О.** Учет демпфирования в сплошной среде с использованием стержневой аппроксимации по А.Р. Ржаницыну. Строительная механика инженерных конструкций и сооружений, 2023, т. 19, № 2, с. 149-161.
27. **Казакова О.И., Смолин И.Ю., Безмозгий И.М.** Анализ амплитудно-зависимых демпфирований и возможности их применения при расчете численными методами. Вестник Томского государственного университета. Математика и механика. 2018, № 54, с. 66-78.
28. **Potapov V.D.** On the stability of a rod under deterministic and stochastic loading with allowance for nonlocal elasticity and nonlocal material damping. Journal of Machinery Manufacture and Reliability, 2015, 44, pp. 6–13.
29. **Shepitko E.S., Sidorov V.N.** Defining of Nonlocal Damping Model Parameters Based on Composite Beam Dynamic Behaviour Numerical Simulation Results. IOP Conference Series: Materials Science and Engineering, 2019, 675(1), 012056
30. **Сидоров В.Н., Детина Е.П., Бадьина Е.С.** Модифицированный метод Ньюмарка при динамическом расчете композитных элементов с учётом демпфирования с памятью. Механика композиционных материалов и конструкций, 2022, т. 28, №1. с. 98-111.
31. **Sidorov V.N., Badina E.S., Tsarev R.O.** Dynamic Model of Beam Deformation with Consider Nonlocal in Time Elastic Properties of the Material. International Journal for Computational Civil and Structural Engineering, 2022, 18(4), pp. 124–131.
32. **Sidorov V.N., Badina E.S., Tsarev R.O.** Calibration of the Nonlocal Dynamic Deformation Model of a Flexural Beam Based on Numerical Experiment Results. International Journal for Computational Civil and Structural Engineering, 2024, 20(2), 132–140.
33. **Александров А.В., Потапов В.Д., Зылев В.Б.** Строительная механика. Динамика и устойчивость упругих систем: учебное пособие для вузов. Под ред. А.В. Александрова. Высшая школа, 2008, 384 с.
34. **Потапов В.Д.** Устойчивость сжатого нелокально вязкоупругого стержня, лежащего на упругом основании. Известия Российской академии наук. Механика твердого тела, 2016, № 1, С. 90-96.
35. **Lei Y., Friswell, M. I., Adhikari S. A.** Galerkin method for distributed systems with non-local damping. International

Journal of Solids and Structures, 2006, V. 43, pp. 3381 - 3400.
36. **Калиткин Н.Н.** Численные методы. БХВ-Петербург, 2011, 592 с.
37. **Пановко Я. Г.** Внутреннее трение при колебаниях упругих систем. Государственное издательство физико-математической литературы, 1960, 193 с.
38. **Вентцель Е.С.** Теория вероятностей. Высшая школа, 1999, 576 с.
39. **Свешников А.А.** Прикладные методы теории случайных функций. Наука, 1968, 464 с.

Sergey I. Zhavoronok, Associate Professor, Ph.D., Leading Researcher of the Department of Smart and Composite Materials and Systems of the Institute of Applied Mechanics of Russian Academy of Sciences, Associate Professor of the Department of Computer Science and Applied Mathematics, National Research University Moscow State University of Civil Engineering, 125040, Moscow, Leningradskii prospect, 7, phone: +7495946-1806, e-mail: zhavoronok@iam.ras.ru.

Elena S. Badina, Associate Professor, Ph.D, Senior Researcher at the Department of Mechanics of Structured and Heterogeneous Environment of the Institute of Applied Mechanics of the Russian Academy of Sciences; Associate Professor of the Department of Computer Science and Applied Mathematics, National Research University Moscow State University of Civil Engineering, Associate Professor of «Computer Aided Design» Department, Institute of Railway Track, Construction and Structures, Russian University of Transport (MIIT), 125040, Moscow, Leningradskii prospect, 7, phone: +7495946-1806, e-mail: shepitko-es@mail.ru.

Жаворонок Сергей Игоревич, доцент, кандидат физико-математических наук, ведущий научный сотрудник отдела механики адаптивных и композиционных материалов и систем Института прикладной механики Российской академии наук, доцент кафедры информатики и прикладной математики Национального исследовательского Московского государственного строительного университета, 125040, Москва, Ленинградский проспект, 7, телефон: +7495946-1806, e-mail: zhavoronok@iam.ras.ru.

Бадьина Елена Сергеевна, доцент, кандидат технических наук, старший научный сотрудник отдела механики структурированной и гетерогенной среды Института прикладной механики Российской академии наук, доцент кафедры информатики и прикладной математики Национального исследовательского Московского государственного строительного университета, доцент кафедры «Системы автоматизированного проектирования» Института пути, строительства и сооружений Российского университета транспорта (МИИТа), 125040, Москва, Ленинградский проспект, 7, телефон: +7495946-1806, e-mail: shepitko-es@mail.ru.

International Journal for Computational Civil and Structural Engineering, 20(3) 180–185(2024)

DOI:10.22337/2587-9618-2024-20-3-180-185

DEVELOPMENT OF COMPUTATIONAL SCHEMES OF GROUP TARGET CONSTRAINTS FOR SOME ELASTIC SYSTEMS PART 1: THEORETICAL FOUNDATIONS

Leonid S. Lyakhovich [1, 2], Pavel A. Akimov [2], Zaur R. Galyautdinov [1], Andrey S. Plyaskin [1]

[1] Tomsk State University of Architecture and Civil Engineering, Tomsk, RUSSIA
[2] National Research Moscow State University of Civil Engineering, Moscow, RUSSIA

Abstract: For some elastic systems with a finite number of degrees of freedom of masses, in which the directions of mass movement are parallel, methods have been developed for creating additional constraints, the introduction of each of which purposefully increases the value of only one natural frequency to a given value, while not changing any of the other natural frequencies and not one of the natural modes (forms of natural oscillations). If it is necessary to increase the values of several natural frequencies in a targeted manner, then this requirement can be implemented by creating an appropriate number of separate targeted constraints. The computational scheme of each of the individual targeted constraints should include racks installed at the nodes of mass application and directed along the trajectory of their movement. In some cases, individual targeted constraints can be independently installed on the original (initial) system. In most cases, on the basis of individual targeted constraints, a computational scheme of a united group targeted constraint is developed, which increases all the intended frequencies to the set values, without changing any of the other natural frequencies and not one of the natural modes. The distinctive paper is devoted to a method for forming a matrix of additional stiffness, which corresponds to a group targeted constraint. The requirements for those targeted constraints, on the basis of which a group targeted constraint is formed, are formulated. An algorithm for the development of group targeted constraint is proposed with allowance for the formulated requirements.

Keywords: natural frequency, natural mode, targeted constraint, group targeted constraint, |additional stiffness coefficients

О ФОРМИРОВАНИИ РАСЧЕТНЫХ СХЕМ ГРУППОВЫХ ПРИЦЕЛЬНЫХ СВЯЗЕЙ ДЛЯ НЕКОТОРЫХ УПРУГИХ СИСТЕМ ЧАСТЬ 1: ТЕОРЕТИЧЕСКИЕ ОСНОВЫ ПОДХОДА

Л.С. Ляхович [1, 2], П.А. Акимов [2], З.Р. Галяутдинов [1], А.С. Пляскин [1]

[1] Томский государственный архитектурно-строительный университет, г. Томск, РОССИЯ
[2] Национальный исследовательский Московский государственный строительный университет, г. Москва, РОССИЯ

Аннотация: Для некоторых упругих систем с конечным числом степеней свободы масс, у которых направления движения масс параллельны, разработаны методы создания дополнительных связей, введение каждой из которых прицельно увеличивает величину только одной собственной частоты до заданного значения, не изменяет при этом ни одну из остальных собственных частот и не одну из форм собственных колебаний. Если необходимо прицельно увеличить величины нескольких собственных частот, то это требование можно реализовать созданием соответствующего количества отдельных прицельных связей. Расчётная схема каждой из отдельных прицельных связей должна включать стойки, установленные в узлах приложения масс и направленные по траектории их движения. В некоторых случаях отдельные прицельные связи могут автономно устанавливаться на исходной системе. В большинстве случаев на основе отдельных прицельных связей формируется расчётная схема единой групповой прицельной

связи, которая увеличивает все намеченные частоты до заданных значений, не изменяя при этом ни одну из остальных собственных частот и не одну из форм собственных колебаний. В данной статье рассмотрен способ формирования матрицы дополнительных жесткостей, которой соответствует групповая прицельная связь. Сформулированы требования к тем отдельным прицельным связям, на основе которых формируется групповая прицельная связь. Предложен алгоритм формирования групповых прицельных связей с учётом сформулированных требований

Ключевые слова: частота собственных колебаний, форма собственных колебаний, отдельная прицельная связь, групповая прицельная связь, коэффициенты дополнительных жесткостей

INTRODUCTION

In [1-7, 11-15] for elastic systems with a finite number of degrees of freedom [8-10, 16, 17] of masses, in which the directions of mass motion are parallel, theoretical approaches were formulated and methods for development of computational schemes of targeted constraints were proposed. Each of them increases the value of only one natural frequency (frequency of natural oscillations) to a given value, without changing any of the other natural frequencies or any of the natural modes (modes of natural oscillations). If the operating conditions require freeing a certain interval of the spectrum of natural frequencies from several of them, then this requirement can be implemented by creating an appropriate number of individual targeted constraints. Each of these individual targeted constraints includes the main racks, installed in the nodes of mass application and directed along the trajectory of their motion. In some cases, individual targeted constraints can be autonomously installed autonomously on the original system.

The distinctive paper is a continuation of [4, 5, 13-15]. It is devoted to a method of development of computational scheme of a united group targeted constraint based on individual targeted constraint, which increases all the intended frequencies to specified values, without changing any of the remaining natural frequencies or any of the natural modes.

Since the development of a group targeted constraint is based on the synthesis of individual targeted constraints, it is necessary to ensure the adequacy of the parameters of each individual targeted constraint with its component in the group targeted constraint.

The rods of the belts of individual targeted constraint retain their independence and parameters in the group targeted constraint. The main racks installed in the nodes of mass application and directed along the trajectory of their movement are combined. In order for the parameters of the main racks of individual targeted constraint to be adequate to their parameters in the group targeted constraint, it is necessary within development of individual targeted constraints, to design the stiffness of the sections of the rods of the racks of these constraints so that they depend only on the number of the rack and do not depend on the numbers of individual targeted constraints.

Let $E[i,k]\cdot F_{st}[i,k]$ be the rigidity of the section of the i-th rack in k-th targeted constraint. Thus, $E[i,k]\cdot F_{st}[i,k]$ should depend only on i and not depend on k.

ALGORITHM OF DEVELOPMENT OF COMPUTATIONA SCHEME OF THE GROUP TARGETED CONSTRAINT

The first step.

Individual targeted constraints are developed. Each of them increases one of the intended natural frequencies to a given value. In this case, all actions [4, 5, 13-15] are performed, in which the values of the lengths of all the main racks will be of the same sign. Besides, rigidity of the sections $E[i,k]\cdot F_{st}[i,k]$ should depend only on i and not depend on k.

The second step.

All individual targeted constraints are placed in the nodes of the plate.

The third step.
In areas where several racks are combined, only one is left.
The fourth step.
Hinges are introduced at the intersections of the rods.
When implementing the first step of the algorithm, the frequency spectrum of natural oscillations of the original system with n degrees of freedom

$$\omega[1],\ \omega[2],\ ...,\ \omega[q],..,$$
$$\omega[q+j],\ \omega[q+(j+1)],\ ...,\ \omega[n]$$

is considered, in which it is required to specifically free the frequency interval

$$\omega[q],\ ...,\ \omega[q+j]$$

from i frequencies, increasing their values, respectively, to values

$$\omega[s],\ ...,\ \omega[s+j],$$

each of which is greater than $\omega[q+j]$.
When implementing the second step of the algorithm individual targeted constraints are placed in the nodes of the plate. In this case, on the lower sections of the constraint, the racks are combined and, of these, on each of these sections, only one is left.
Within developments of individual targeted constraints, the stiffnesses of the sections of the rods of the racks were set so that they would coincide with each other in each node. It is this circumstance that ensures the adequacy of the parameters of the main racks of individual targeted constraints to their parameters in the group constraint.

REFERENCES

1. **Akimov P.A, Lyahovich L.S.** Pricel'noe regulirovanie spektra chastot sobstvennyh kolebanij uprugih plastin s konechnym chislom stepenej svobody mass putem vvedenija dopolnitel'nyh obobshhennyh svjazej i obobshhennyh kinematicheskih ustrojstv [Precision control for eigen-frequency of elastic plates with finite number of mass degrees of freedom by using additional generalized connections and kinematic devices]. // Vestnik Tomskogo gosudarstvennogo arkhitekturno-stroitel'nogo universiteta. Journal of Construction and Architecture, 2021, Vol. 23, No. 4, pp. 57-67 (In Russian).
2. **Giterman D.M., Lyakhovich L.S., Nudelman Ya.L.** Algoritm sozdanija rezonansno-bezopasnyh zon pri pomoshhi nalozhenija dopolnitel'nyh svjazej [Algorithm for creating resonance-safe zones by imposing additional connections]. // Dynamics and Strength of Machines, 1984, Issue 39, pp. 63-69 (in Russian).
3. **Lyahovich L.S.** Osobye svojstva optimal'nyh sistem i osnovnye napravlenija ih realizacii v metodah rascheta sooruzhenij [Special properties of optimal systems and the main directions of their implementation in the methods of structural analysis]. Tomsk, TGASU, 2009. – 372 pages (In Russian).
4. **Lyakhovich L.S., Akimov P.A.** About Development of Computational Schemes of Some Additional Constraints for Elastic Systems. Part 1: Theoretical Foundations [O formirovanii raschetnyh shem nekotoryh dopolnitel'nyh svjazej dlja uprugih sistem. Chast' 1: Teoreticheskie osnovy podhoda]. // Promyshlennoe i Grazhdanskoe Stroitelstvo, 2022, No. 9, pp. 4-10 (in Russian).
5. **Lyakhovich L.S., Akimov P.A., Mescheulov N.V.** About Development of Computational Schemes of Some Additional Constraints for Elastic Systems. Part 2: Samples of Analysis [O formirovanii raschetnyh shem nekotoryh dopolnitel'nyh svjazej dlja uprugih sistem. Chast' 2: Primery raschetov]. // Promyshlennoe i Grazhdanskoe Stroitelstvo, 2022, No. 9, pp. 4-10 (in Russian).
6. **Lyahovich L.S., Maletkin O.Ju.** O pricel'nom regulirovanii sobstvennyh

chastot uprugih system [On targeted control of natural frequencies of elastic systems]. // Izvestija vuzov. Stroitel'stvo i arhitektura, 1990, No. 1, pp. 113-117 (In Russian).

7. **Nudelman Ya.L., Lyakhovich L.S., Gitterman D.M.** O naibolee podatlivyh svjazjah naibol'shej zhestkosti. [On the most flexible connections of the greatest rigidity]. // Voprosy prikladnoj Mehaniki i Matematiki. Tomsk: TSU Publishing House, 1981, pp. 113-126 (in Russian).
8. **Chau-Dinh T., Tran-Chi N., Nguyen V.-H., Nguyen T.-K.** Geometrically nonlinear analysis of plates and shells by a cell-based smoothed CS-MITC18+ flat shell element with drilling degrees of freedom. // Thin-Walled Structures, 2024, Volume 203, 112254.
9. **De Angelis M., Basili M., Pietrosanti D.** On the optimal design and placement of Tuned-Mass-Damper-Inerter for Multi-Degree-Of-Freedom structures. // Structures, 2023, Volume 56, 104781.
10. **Jiang Y., Zhang W., Zhang Y.F., Lu S.F.** Nonlinear vibration of four-degrees of freedom for piezoelectric functionally graded graphene-reinforced laminated composite cantilever rectangular plate with PPF control strategy. // Thin-Walled Structures, 2023, Volume 188, 110830.
11. **Lyakhovich L.S., Akimov P.A.** Aimed control of the frequency spectrum of eigenvibrations of elastic plates with a finite number of degrees of freedom of masses by superimposing additional constraints. // International Journal for Computational Civil and Structural Engineering, 2021, Volume 17, Issue 2, pp. 76-82.
12. **Lyakhovich L.S., Akimov P.A.** Aimed control of the frequency spectrum of eigenvibrations of elastic plates with a finite number of degrees of freedom by introducing additional generalized kinematic devices. // International Journal for Computational Civil and Structural Engineering, 2021, Volume 17, Issue 3, pp. 14-20.
13. **Lyakhovich L.S., Akimov P.A.** Formation of Computational Schemes of Additional Targeted Constraints That Regulate The Frequency Spectrum of Natural Oscillations of Elastic Systems With a Finite Number of Degrees of Mass Freedom, the Directions of Movement of Which are Parallel, But Do Not Lie in the Same Plane. Part 1: Theoretical Foundations. // International Journal for Computational Civil and Structural Engineering, 2022, Volume 18, Issue 2, pp. 183-193.
14. **Lyakhovich L.S., Akimov P.A.** Formation of Computational Schemes of Additional Targeted Constraints That Regulate The Frequency Spectrum of Natural Oscillations of Elastic Systems With a Finite Number of Degrees of Mass Freedom, the Directions of Movement of Which are Parallel, But Do Not Lie in the Same Plane. Part 2: The First Sample of Analysis. // International Journal for Computational Civil and Structural Engineering, 2022, Volume 18, Issue 3, pp. 137-146.
15. **Lyakhovich L.S., Akimov P.A., Mescheulov N.V.** Formation of computational schemes of additional targeted constraints that regulate the frequency spectrum of natural oscillations of elastic systems with a finite number of degrees of mass freedom, the directions of movement of which are parallel, but do not lie in the same plane. Part 3. The second sample of analysis and conclusion. // International Journal for Computational Civil and Structural Engineering, 2022, Volume 18, Issue 4, pp. 71-81.
16. **Zhu Yu, Ma T., Ma Y., Yin Y., Fang Z.** Research on intelligent compaction stiffness index and its application based on three-degree-of-freedom elastic-plastic dynamical model. // Construction and Building Materials, 2023, Volume 409, 133978.
17. **Zurru M.** A three-degree of freedom approach for the unilateral contact problem of plane cable trusses with tension-only harnesses. // Structures, 2020, Volume 25, pp. 274-284.

СПИСОК ЛИТЕРАТУРЫ

1. **Акимов П.А., Ляхович Л.С.** Прицельное регулирование спектра частот собственных колебаний упругих пластин с конечным числом степеней свободы масс путем введения дополнительных обобщенных связей и обобщенных кинематических устройств. // Вестник Томского государственного архитектурно-строительного университета, 2021, том 23, № 4, с. 57-67.
2. **Гитерман Д.М., Ляхович Л.С., Нудельман Я.Л.** Алгоритм создания резонансно-безопасных зон при помощи наложения дополнительных связей. // Динамика и прочность машин, 1984, выпуск 39, с. 63-69.
3. **Ляхович Л.С.** Особые свойства оптимальных систем и основные направления их реализации в методах расчета сооружений. Монография. – Томск: Издательство ТГАСУ, 2009. - 372 с.
4. **Ляхович Л.С., Акимов П.А.** О формировании расчетных схем некоторых дополнительных связей для упругих систем. Часть 1. Теоретические основы подхода. // Промышленное и гражданское строительство, 202, №9, с. 4-10.
5. **Ляхович Л.С., Акимов П.А., Мешеулов Н.В.** О формировании расчетных схем некоторых дополнительных связей для упругих систем. Часть 2. Примеры расчёта. // Промышленное и гражданское строительство, 2022, №9, с. 11-19.
6. **Ляхович Л.С., Малеткин О.Ю.** О прицельном регулировании собственных частот упругих систем. // Известия вузов. Строительство и архитектура, 1990, № 1, с. 113-117.
7. **Нудельман Я.Л., Ляхович Л.С., Гитерман Д.М.** О наиболее податливых связях наибольшей жесткости. // Вопросы прикладной Механики и математики. - Томск: Издательство ТГУ, 1981, с. 113-126.
8. **Chau-Dinh T., Tran-Chi N., Nguyen V.-H., Nguyen T.-K.** Geometrically nonlinear analysis of plates and shells by a cell-based smoothed CS-MITC18+ flat shell element with drilling degrees of freedom. // Thin-Walled Structures, 2024, Volume 203, 112254.
9. **De Angelis M., Basili M., Pietrosanti D.** On the optimal design and placement of Tuned-Mass-Damper-Inerter for Multi-Degree-Of-Freedom structures. // Structures, 2023, Volume 56, 104781.
10. **Jiang Y., Zhang W., Zhang Y.F., Lu S.F.** Nonlinear vibration of four-degrees of freedom for piezoelectric functionally graded graphene-reinforced laminated composite cantilever rectangular plate with PPF control strategy. // Thin-Walled Structures, 2023, Volume 188, 110830.
11. **Lyakhovich L.S., Akimov P.A.** Aimed control of the frequency spectrum of eigenvibrations of elastic plates with a finite number of degrees of freedom of masses by superimposing additional constraints. // International Journal for Computational Civil and Structural Engineering, 2021, Volume 17, Issue 2, pp. 76-82.
12. **Lyakhovich L.S., Akimov P.A.** Aimed control of the frequency spectrum of eigenvibrations of elastic plates with a finite number of degrees of freedom by introducing additional generalized kinematic devices. // International Journal for Computational Civil and Structural Engineering, 2021, Volume 17, Issue 3, pp. 14-20.
13. **Lyakhovich L.S., Akimov P.A.** Formation of Computational Schemes of Additional Targeted Constraints That Regulate The Frequency Spectrum of Natural Oscillations of Elastic Systems With a Finite Number of Degrees of Mass Freedom, the Directions of Movement of Which are Parallel, But Do Not Lie in the Same Plane. Part 1: Theoretical Foundations. // International Journal for Computational Civil and Structural Engineering, 2022, Volume 18, Issue 2, pp. 183-193.
14. **Lyakhovich L.S., Akimov P.A.** Formation of Computational Schemes of Additional Targeted Constraints That Regulate The

Frequency Spectrum of Natural Oscillations of Elastic Systems With a Finite Number of Degrees of Mass Freedom, the Directions of Movement of Which are Parallel, But Do Not Lie in the Same Plane. Part 2: The First Sample of Analysis. // International Journal for Computational Civil and Structural Engineering, 2022, Volume 18, Issue 3, pp. 137-146.

15. **Lyakhovich L.S., Akimov P.A., Mescheulov N.V.** Formation of computational schemes of additional targeted constraints that regulate the frequency spectrum of natural oscillations of elastic systems with a finite number of degrees of mass freedom, the directions of movement of which are parallel, but do not lie in the same plane. Part 3. The second sample of analysis and conclusion. // International Journal for Computational Civil and Structural Engineering, 2022, Volume 18, Issue 4, pp. 71-81.
16. **Zhu Yu, Ma T., Ma Y., Yin Y., Fang Z.** Research on intelligent compaction stiffness index and its application based on three-degree-of-freedom elastic-plastic dynamical model. // Construction and Building Materials, 2023, Volume 409, 133978.
17. **Zurru M.** A three-degree of freedom approach for the unilateral contact problem of plane cable trusses with tension-only harnesses. // Structures, 2020, Volume 25, pp. 274-284.

Leonid S. Lyakhovich, Full Member of the Russian Academy of Architecture and Construction Sciences, Professor, DSc, Professor of Department of Structural Mechanics, Tomsk State University of Architecture and Building; 2, Solyanaya St., 2, Tomsk, 634003, Russia; Professor of Department of Applied Mathematics and Computer Science, National Research Moscow State University of Civil Engineering; 26, Yaroslavskoe Shosse, Moscow, 129337, Russia; E-mail: lls@tsuab.ru.

Pavel A. Akimov, Full Member of the Russian Academy of Architecture and Construction Sciences, Professor, Dr.Sc.; Rector, Professor of Department of Applied Mathematics and Computer Science of National Research Moscow State University of Civil Engineering; 26, Yaroslavskoe Shosse, Moscow, 129337, Russia; phone: +7(495) 651-81-85; Fax: +7(499) 183-44-38; E-mail: AkimovPA@mgsu.ru, rector@mgsu.ru, pavel.akimov@gmail.com.

Zaur R. Galyautdinov, Associate Professor, DSc, Professor of Department of Reinforced Concrete and Stone Structures, Tomsk State University of Architecture and Building; 2, Solyanaya St., 2, Tomsk, 634003, Russia;
E-mail: gazr@yandex.ru.

Andrey S. Plyaskin, Associate Professor, Ph.D., Head of Department of Metal and Wooden Structures, Tomsk State University of Architecture and Building; 2, Solyanaya St., 2, Tomsk, 634003, Russia;
E-mail: plyaskinandrei@mail.ru.

Ляхович Леонид Семенович, академик РААСН, профессор, доктор технических наук, профессор кафедры строительной механики, Томский государственный архитектурно-строительный университет; 634003, Россия, г. Томск, Соляная пл. 2; профессор кафедры информатики и прикладной математики, Национальный исследовательский Московский государственный строительный университет; 129337, Россия, г. Москва, Ярославское шоссе, дом 26; E-mail: lls@tsuab.ru.

Акимов Павел Алексеевич, академик РААСН, профессор, доктор технических наук; ректор, профессор кафедры информатики и прикладной математики Национального исследовательского Московского государственного строительного университета; 129337, Россия, г. Москва, Ярославское шоссе, дом 26; телефон: +7(495) 651-81-85; факс: +7(499) 183-44-38; Email: AkimovPA@mgsu.ru, rector@mgsu.ru, pavel.akimov@gmail.com.

Галяутдинов Заур Рашидович, доцент, доктор технических наук, доцент кафедры железобетонных и каменных конструкций, Томский государственный архитектурно-строительный университет; 634003, Россия, г. Томск, Соляная пл. 2; E-mail: gazr@yandex.ru.

Пляскин Андрей Сергеевич, доцент, кандидат технических наук, заведующий кафедрой металлических и деревянных конструкций, Томский государственный архитектурно-строительный университет; 634003, Россия, г. Томск, Соляная пл. 2; E-mail: plyaskinandrei@mail.ru.

International Journal for Computational Civil and Structural Engineering, 20(3) 186–197(2024)

DOI:10.22337/2587-9618-2024-20-3-186-197

DEVELOPMENT OF COMPUTATIONAL SCHEMES OF GROUP TARGET CONSTRAINTS FOR SOME ELASTIC SYSTEMS PART 2: SAMPLES OF ANALYSIS

Leonid S. Lyakhovich [1, 2], Pavel A. Akimov [2], Zaur R. Galyautdinov [1], Andrey S. Plyaskin [1]

[1] Tomsk State University of Architecture and Civil Engineering, Tomsk, RUSSIA
[2] National Research Moscow State University of Civil Engineering, Moscow, RUSSIA

Abstract: For some elastic systems with a finite number of degrees of freedom of masses, in which the directions of mass movement are parallel, methods have been developed for creating additional constraints, the introduction of each of which purposefully increases the value of only one natural frequency to a given value, while not changing any of the other natural frequencies and not one of the natural modes (forms of natural oscillations). If it is necessary to increase the values of several natural frequencies in a targeted manner, then this requirement can be implemented by creating an appropriate number of separate targeted constraints. The computational scheme of each of the individual targeted constraints should include racks installed at the nodes of mass application and directed along the trajectory of their movement. In some cases, individual targeted constraints can be independently installed on the original (initial) system. In most cases, on the basis of individual targeted constraints, a computational scheme of a united group targeted constraint is developed, which increases all the intended frequencies to the set values, without changing any of the other natural frequencies and not one of the natural modes. The distinctive paper is devoted verification of the proposed algorithm for the development of group targeted constraint on SCAD and "Lira Software" products.

Keywords: natural frequency, natural mode, targeted constraint, group targeted constraint, |additional stiffness coefficients, algorithm

О ФОРМИРОВАНИИ РАСЧЕТНЫХ СХЕМ ГРУППОВЫХ ПРИЦЕЛЬНЫХ СВЯЗЕЙ ДЛЯ НЕКОТОРЫХ УПРУГИХ СИСТЕМ ЧАСТЬ 2: ПРИМЕРЫ РАСЧЕТОВ

Л.С. Ляхович [1, 2], П.А. Акимов [2], З.Р. Галяутдинов [1], А.С. Пляскин [1]

[1] Томский государственный архитектурно-строительный университет, г. Томск, РОССИЯ
[2] Национальный исследовательский Московский государственный строительный университет, г. Москва, РОССИЯ

Аннотация: Для некоторых упругих систем с конечным числом степеней свободы масс, у которых направления движения масс параллельны, разработаны методы создания дополнительных связей, введение каждой из которых прицельно увеличивает величину только одной собственной частоты до заданного значения, не изменяет при этом ни одну из остальных собственных частот и не одну из форм собственных колебаний. Если необходимо прицельно увеличить величины нескольких собственных частот, то это требование можно реализовать созданием соответствующего количества отдельных прицельных связей. Расчётная схема каждой из отдельных прицельных связей должна включать стойки, установленные в узлах приложения масс и направленные по траектории их движения. В некоторых случаях отдельные прицельные связи могут автономно устанавливаться на исходной системе. В большинстве случаев на основе отдельных прицельных связей формируется расчётная схема единой групповой прицельной связи, которая увеличивает все намеченные частоты до заданных значений, не изменяя при этом ни одну из остальных собственных частот и не одну из форм собственных колебаний. В данной статье рассмотрен способ формирования матрицы дополнительных жесткостей, которой соответствует групповая при-

цельная связь. Сформулированы требования к тем отдельным прицельным связям, на основе которых формируется групповая прицельная связь. Рассматривается верификация алгоритма формирования групповых прицельных связей с учётом сформулированных требований на основе решения тестовых задач с использованием программных продуктов “SCAD” и “Лира”.

Ключевые слова: частота собственных колебаний, форма собственных колебаний, отдельная прицельная связь, групповая прицельная связь, коэффициенты дополнительных жесткостей

Let us demonstrate the implementation of the algorithm using examples from [4, 5, 18-20]. Figure 1*a* shows the original (initial) system.

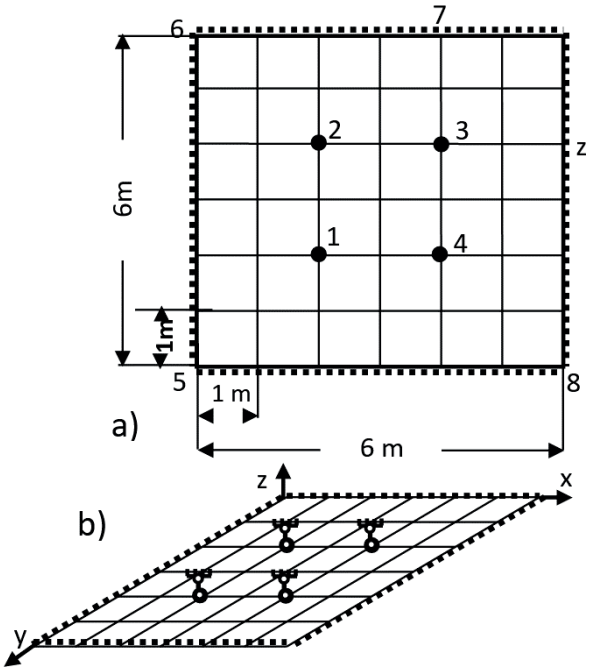


Figure 1. Considering problem

The plate is hinged along the contour. The plate thickness is equal to 0.12 *m*. The modulus of elasticity of the plate material is equal to E = 24000000000 N/m^2 Poisson's ratio is equal to $\nu_0 = 0.2$.

Let the mass of the plate be extremely small (0.00000001 kg/m^3).

The masses

$$m[1] = 1000\,kg,\quad m[2] = 1100\,kg,$$
$$m[3] = 1150\,kg,\quad m[4] = 1200\,kg$$

are located at the nodes of the plate. Figure 1*b* shows the basic system of the displacement method [1-3, 6, 7, 16, 17].

The coefficients of the equations of the displacement method and the values of the nodal masses form the matrices $A = \|r[i,k]\|$ and $M = \|m[i]\|$.

The values of the coefficients of the displacement method equations are given in Table 1.

The roots of the equation

$$\left|A - \omega^2 M\right| = 0 \qquad (2)$$

determine the frequency spectrum of the natural oscillations of the system. The natural frequencies and natural modes (forms of the natural oscillations) of the plate are presented in Table 2.

It is required to increase the third natural frequency to 220 sec^{-1} and the fourth to 230 sec^{-1} by introducing targeted constraints.

Thus, for further implementation of the first action of the algorithm for the example under consideration, it is necessary to create two separate targeted constraints, one of which will increase the third natural frequency to 220 sec^{-1}, and the other the fourth to 230 sec^{-1}.

In [4, 5, 18-20] it is shown that the development of targeted generalized constraint is based on the formation of a matrix of additional stiffness coefficients

$$A_0 = \|a_0[i,k]\|_{i,k=1}^{n} \qquad (2)$$

and the procedure for their determination is given.

The values of the coefficients of the additional stiffness matrix, increasing the third natural frequency to 220 sec^{-1}, are presented in Table 3.

The roots of equation (3) determine the spectrum of frequencies and modes of natural oscillations of the system, reinforced by a targeted

constraint, increasing the third natural frequency to 220 sec^{-1}

$$\left|(A + A_0) - \omega^2 M\right| = 0\,. \qquad (3)$$

Table 1. The values of the coefficients of the displacement method equations.

i, k	1	2	3	4
1	22758257.28	-9604812.96	585308.28	-9604812.96
2	-9604812.96	22758257.28	-9604812.96	585308.28
3	585308.28	-9604812.96	22758257.28	-9604812.96
4	-9604812.96	585308.28	-9604812.96	22758257.28

Table 2. The natural frequencies and natural modes of the plate.

ω	60,932	138,865	143,624	196,414
1	0.4905	0.0001	0.7047	-0.5934
2	0.4966	-0.7075	0.0945	0.5167
3	0.5058	-0.0711	-0.7029	-0.4387
4	0.5069	0.7032	0.0190	0.4341

Table 3. The values of the coefficients of the additional stiffness matrix, increasing the third natural frequency to 220 sec^{-1}.

i, k	1	2	3	4
1	12829437.77	1892709.01	-14715733.27	414235.72
2	1892709.01	279228.71	-2170991.55	61111.62
3	-14715733.27	-2170991.55	16879368.34	-475140.26
4	414235.72	61111.62	-475140.26	13374.81

Table 4. The natural frequencies and natural modes of the plate.

ω	60,932	138,865	196,414	220
1	0.4905	0.0001	-0.5934	-0.5934
2	0.4966	-0.7075	0.5167	0.5167
3	0.5058	-0.0711	-0.4387	-0.4387
4	0.5069	0.7032	0.4341	0.4341

The frequencies and coordinates of the natural modes are presented in Table 4.

Within development of computational scheme of this targeted constraint, the length of the first rack was taken to be equal to $l_{st}[1] = 0.4\ m$, and the cross-sectional area of the rack rods is equal to $F_{st} = 0.004\ m^2$, corresponding diameter is equal to $D_{st} = 0.07136496\ m$. The cross-sectional areas of the belt rods were taken to be the same, and their value was determined in the process of development of constraint [4, 5, 18-20].

Parameters of cross-sectional area of the belt rods are equal to $F_p = 0.00684\ m^2$, $D_p = 0.0933\ m$.

We have the following lengths of racks of the constraint:

$$l_{st}[1] = 0.4\,m,\ \ l_{st}[2] = 0.09782\,m,$$
$$l_{st}[3] = -0.26064\,m,\ \ l_{st}[4] = 0.05770\,m.$$

The modulus of elasticity of the material of the rods of constraint is equal to

$$E_{sp} = 206000000000\ N/m^2\ .$$

The lengths of the racks turned out to be of different signs. Therefore, the rods of the belts connecting the tops of racks 2 – 3 and 3 - 4 must pass "through" the plate. Structurally, such a scheme requires an ideally free "passage" of part of the rods of the targeted constraint "through" the original system, which is almost impossible to implement.
The general appearance of this targeted constraint is shown in Figure 2.

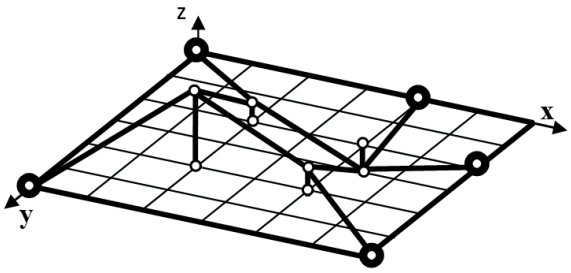


Figure 2. The general appearance of targeted constraint

In these cases, the targeted constraint should be shifted in the direction of mass movement in a positive or negative direction by an amount at which the values of all the lengths of the main racks will be of the same sign.
When choosing the shift values, it is necessary to take into account the operating conditions and design requirements within development of a group targeted constraint.
In this example, the value of the shift of constraint is equal to 0.3 *m*. Accordingly, the length of the first rack will now be equal to 0.7 *m*, and the cross-sectional areas of the racks are equal to $F_{st} = 0.004\ m^2$.
After the shift, the lengths of the racks changed:

$$l_{st}[1] = 0.7\,m,\ \ l_{st}[2] = 0.39782\,m,$$
$$l_{st}[3] = 0.03945\,m,\ \ l_{st}[4] = 0.35770\,m.$$

The general appearance of this modified targeted constraint is shown in Figure 3.
A separate targeted constraint, increasing the fourth natural frequency to 230 sec^{-1}, is developed similarly to the previous constraint. The values of the coefficients of the additional stiffness matrix are presented in Table 5.
The length of the first rack is set at 0.4 *m*, and the cross-sectional areas of the racks are taken as $F_{st} = 0.004\ m^2$, that is, the same as when creating the previous targeted constraint.

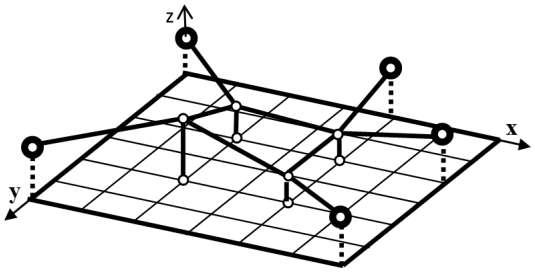


Figure 3. The general appearance of modified targeted constraint

The cross-sectional areas of the belt rods are taken to be the same, and their value was determined in the process of development of the constraint [4, 5, 18-20]. The frequencies and coordinates of the natural modes are presented in Table 6.
Parameters of the sections of the belt rods are equal to $F_p = 0.000697\ m^2$, $D_p = 0.02988\ m$.
The lengths of the racks of this constraint are equal to

$$l_{st}[1] = 0.4\,m,\ \ l_{st}[2] = -0.43643\,m,$$
$$l_{st}[3] = 0.22436\,m,\ \ l_{st}[4] = -0.38251\,m.$$

The lengths of the racks here also turned out to be of different signs. The general appearance of this targeted constraint is shown in Figure 4.

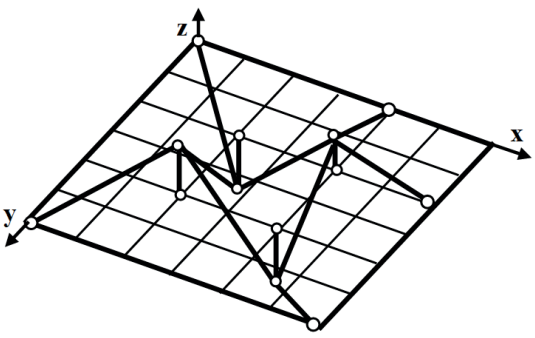


Figure 4. The general appearance of targeted constraint.

Therefore, the targeted constraint should be shifted in the direction of the mass movement in a positive or negative direction by an amount at which the values of all the lengths of the main racks will be of the same sign.

Table 5. The values of the coefficients of the additional stiffness matrix, increasing the fourth natural frequency to 230 sec^{-1}.

i, k	1	2	3	4
1	4613401.93	-4418412.37	3922001.78	-4049185.23
2	-4418412.37	4231664.23	-3756234.88	3878042.80
3	3922001.78	-3756234.88	3334220.22	-3442342.97
4	-4049185.23	3878042.80	-3442342.97	3553971.95

Table 6. The natural frequencies and natural modes of the plate.

ω	60,932	138,865	196,414	230
1	0.4905	0.0001	0.7047	-0.5934
2	0.4966	-0.7075	0.0945	0.5167
3	0.5058	-0.0711	-0.7029	-0.4387
4	0.5069	0.7032	0.0190	0.4341

Table 5. The values of the coefficients of the group matrix of additional stiffness.

i, k	1	2	3	4
1	4613401.93	-4418412.37	3922001.78	-4049185.23
2	-4418412.37	4231664.23	-3756234.88	3878042.80
3	3922001.78	-3756234.88	3334220.22	-3442342.97
4	-4049185.23	3878042.80	-3442342.97	3553971.95

The general appearance of this modified targeted constraint is shown in Figure 5.

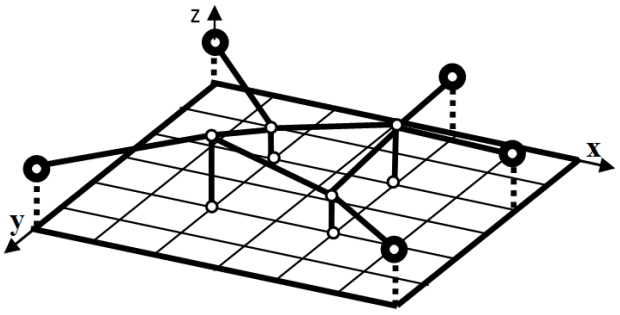


Figure 5. The general appearance of modified targeted constraint.

Let us assume that in accordance with the design requirements the belt rods do not intersect in the computational scheme of the group targeted constraint. Therefore, in the considering case, the value of the constraint shift is adopted at 0.85 m. Thus, we have

$$l_{st}[1] = 1.25\,m, \quad l_{st}[2] = 0.4136\,m,$$
$$l_{st}[3] = 1.0744\,m, \quad l_{st}[4] = 0.4674\,m.$$

The general appearance of this targeted constraint is shown in Figure 5.

After forming all the individual targeted constraints, which are required for solution of the problem, it is possible to form a group matrix of additional stiffness coefficients. In order to do this, it is sufficient to sum up the coefficients of the additional stiffness matrices of individual targeted constraints.

In the considering sample the corresponding coefficients of Tables 3 and 5 are summed up. The coefficients of the group matrix of additional stiffness are given in Table 7.

If we denote the group matrix of additional stiffness, then the roots of the equation

$$\left|(A+\overline{A}_0)-\omega^2 M\right|=0 \qquad (4)$$

determine the spectrum of frequencies and forms of natural oscillations of the system, enhanced by group targeted constraint, increasing the third frequency of natural oscillations to 220 sec^{-1}, and the fourth to 230 sec^{-1}. The natural frequencies and coordinates of the natural modes are presented in Table 8.

Table 8. The natural frequencies and natural modes of the plate

ω	60,932	138,865	220	230
1	0.4905	0.0001	0.7047	-0.5934
2	0.4966	-0.7075	0.0945	0.5167
3	0.5058	-0.0711	-0.7029	-0.4387
4	0.5069	0.7032	0.0190	0.4341

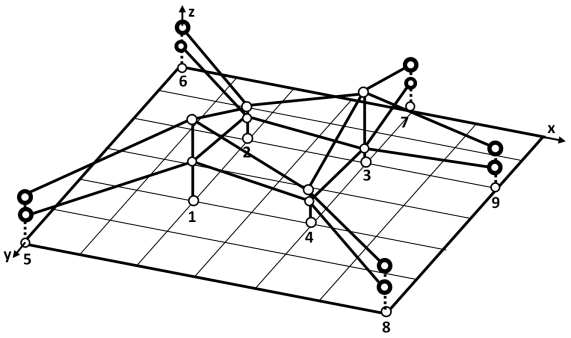


Figure 6. The general appearance of the group targeted constraint

By implementing the second, the third and the fourth steps of the above algorithm, we form a group targeted constraint. The general appearance of this constraint is shown in Figure 6.
The plan view of this constraint and the numbering of the nodes are shown in Figure 7.
The z coordinates of the nodes of the group targeted constraint are given in Table 9.
When implementing the second step of the algorithm of development of a group targeted constraint, individual targeted constraints are placed in the nodes of the plate. In this case, on the lower sections of the constraint, the racks are combined and, of these, on each of these sections, only one is left.
Within development of individual targeted constraints the stiffnesses of the sections of the rods of the racks were set so that they would coincide with each other in each node.

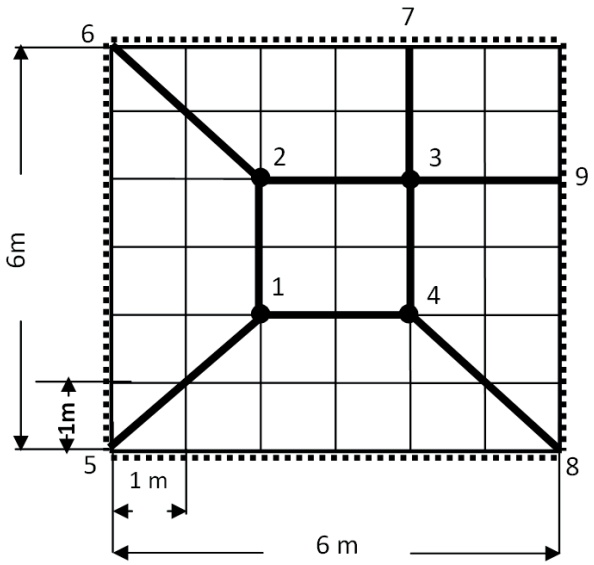


Figure 7. The plan view of the targeted constraint and the numbering of the nodes

Table 10. The natural frequencies and natural modes of the plate

ω	60,341	137,618	142,334	194,681
1	0.4903	0.0012	0.7213	-0.5747
2	0.4968	-0.7042	0.0805	0.5212
3	0.5056	0.0721	-0.6879	-0.4586
4	0.5071	0.7063	0.0072	0.4333

Table 11. The natural frequencies and natural modes of the plate

ω	60,341	137,618	219,151	227,946
1	0.4903	0.0012	0.7213	-0.5747
2	0.4968	-0.7042	0.0805	0.5212
3	0.5056	0.0721	-0.6879	-0.4586
4	0.5071	0.7063	0.0072	0.4333

Table 9. The z coordinates of the nodes of the group targeted constraint

Number of node	Coordinates z	
	top	bottom
1	1.25	0.7
2	0.4136	0.3978
3	1.0744	0.03944
4	0.4764	0.3577
5	0.85	0.3
6	0.85	0.3
7	0.85	0.3
8	0.85	0.3
9	0.85	0.3

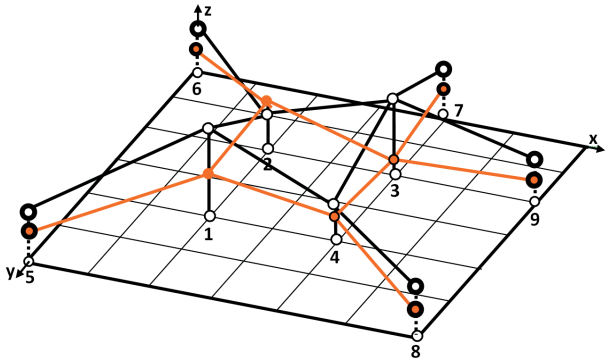


Figure 8. The general appearance of the group targeted constraint

It is this circumstance that ensures the adequacy of the parameters of the main racks of individual targeted constraints to their parameters in the group constraint.

Let us test this group targeted constraint with the use of "SCAD" and "Lira" software products [8-15]. First, we will determine the natural frequencies and coordinates of the natural modes of the original plate. The test results presented in Table 10 are quite close (differences of about one percent) to the results given in Table 2, which confirms the reliability of the initial data. The natural frequencies and coordinates of the natural modes presented in Table 8 were obtained as the roots of equation (4) based on the use of a group matrix of additional stiffness coefficients $\bar{A}_0$ before development the computational scheme of the group targeted constraint.

The natural frequencies and coordinates of the natural modes of computational scheme of the group targeted constraint obtained by the test are presented in Table 11. These results were obtained by testing the computational scheme of the group targeted constraint. Comparison of the results given in Tables 10 and 11 shows that only those frequencies have changed that the group constraint was targeted at, while the coordinates of the natural modes and other natural frequencies have remained the same. These test results confirm the "targeting" of the group constraint with sufficient accuracy.

The closeness of the results given in Tables 8 and 11 confirms the reliability of the proposed approach.

Let us consider the case when the operating conditions require that the lengths of the individual targeted constraints be greater than 0.08 m. The individual targeted constraint racks that increase the fourth natural frequency meet this condition. Among the individual targeted constraint racks that increase the third natural frequency we have

$$l_{st}[3] = 0.03945\,m < 0.08\,m\,.$$

It doesn't meet the stated condition. Therefore, the shift of this initially created targeted constraint link must be increased, for example, from 0.3 m to 0.36 m. Thus, we have the following modified parameters:

$$l_{st}[1] = 0.76\,m,\quad l_{st}[2] = 0.4578\,m,$$
$$l_{st}[3] = 0.0994\,m,\quad l_{st}[4] = 0.4177\,m.$$

The development of the group targeted constraint in this case is implemented in the same way as in the previous one, but taking into account the changes in the parameters of an individual targeted constraint, increasing the third natural frequency. The z coordinates of the nodes of the group targeted constraint are given in Table 12. The general view of this group targeted constraint is shown in Figure 8.

In this group constraint, some of the rods of the belts intersect (in spans "1 – 2", "2 – 6", "2 – 3"). The nodes in which the rods intersect are structurally feasible, but their specificity is not discussed in this paper.

A test check of the computational scheme of this group constraint confirmed its targeting.

So, this paper considers a verification of method of forming a matrix of additional stiffness, which corresponds to a group targeted constraint. Requirements are formulated for those individual targeted constraints, on the basis of which the group targeted constraint is formed.

Table 12. The z coordinates of the nodes of the group targeted constraint

Number of node	Coordinates z	
	black	red
1	1.25	0.76
2	0.4136	0.4578
3	1.0744	0.0994
4	0.4764	0.4177
5	0.85	0.36
6	0.85	0.36
7	0.85	0.36
8	0.85	0.36
9	0.85	0.36

An algorithm for development of group targeted constraint is proposed with allowance for formulated requirements. The proposed algorithm was tested with the use of "SCAD" and "Lira" software products [8-15].

REFERENCES

1. **Akimov P.A, Lyahovich L.S.** Pricel'noe regulirovanie spektra chastot sobstvennyh kolebanij uprugih plastin s konechnym chislom stepenej svobody mass putem vvedenija dopolnitel'nyh obobshhennyh svjazej i obobshhennyh kinematicheskih ustrojstv [Precision control for eigen-frequency of elastic plates with finite number of mass degrees of freedom by using additional generalized connections and kinematic devices]. // Vestnik Tomskogo gosudarstvennogo arkhitekturno-stroitel'nogo universiteta. Journal of Construction and Architecture, 2021, Vol. 23, No. 4, pp. 57-67 (In Russian).
2. **Giterman D.M., Lyakhovich L.S., Nudelman Ya.L.** Algoritm sozdanija rezonansno-bezopasnyh zon pri pomoshhi nalozhenija dopolnitel'nyh svjazej [Algorithm for creating resonance-safe zones by imposing additional connections]. // Dynamics and Strength of Machines, 1984, Issue 39, pp. 63-69 (in Russian).
3. **Lyahovich L.S.** Osobye svojstva optimal'nyh sistem i osnovnye napravlenija ih realizacii v metodah rascheta sooruzhenij [Special properties of optimal systems and the main directions of their implementation in the methods of structural analysis]. Tomsk, TGASU, 2009. – 372 pages (In Russian).
4. **Lyakhovich L.S., Akimov P.A.** About Development of Computational Schemes of Some Additional Constraints for Elastic Systems. Part 1: Theoretical Foundations [O formirovanii raschetnyh shem nekotoryh dopolnitel'nyh svjazej dlja uprugih sistem. Chast' 1: Teoreticheskie osnovy podhoda]. // Promyshlennoe i Grazhdanskoe Stroitelstvo, 2022, No. 9, pp. 4-10 (in Russian).
5. **Lyakhovich L.S., Akimov P.A., Mescheulov N.V.** About Development of Computational Schemes of Some Additional Constraints for Elastic Systems. Part 2: Samples of Analysis [O formirovanii raschetnyh

shem nekotoryh dopolnitel'nyh svjazej dlja uprugih sistem. Chast' 2: Primery raschetov]. // Promyshlennoe i Grazhdanskoe Stroitelstvo, 2022, No. 9, pp. 4-10 (in Russian).

6. **Lyahovich L.S., Maletkin O.Ju.** O pricel'nom regulirovanii sobstvennyh chastot uprugih system [On targeted control of natural frequencies of elastic systems]. // Izvestija vuzov. Stroitel'stvo i arhitektura, 1990, No. 1, pp. 113-117 (In Russian).
7. **Nudelman Ya.L., Lyakhovich L.S., Gitterman D.M.** O naibolee podatlivyh svjazjah naibol'shej zhestkosti. [On the most flexible connections of the greatest rigidity]. // Voprosy prikladnoj Mehaniki i Matematiki. Tomsk: TSU Publishing House, 1981, pp. 113-126 (in Russian).
8. **Fialko S.** Parallel finite element solver for multi-core computers with shared memory. // Computers & Mathematics with Applications, 2021, Vol. 94, pp. 1-14.
9. **Fialko S.** Parallel finite element solver PARFES for the structural analysis in NUMA architecture. // Advances in Engineering Software, 2022, Vol. 174, 103290 pp. 1-12.
10. **Fialko S.** Time history analysis of buildings and structures design models in SCAD software on multicore computers. // ECMS 2024: proceedings of the 38th ECMS International Conference on Modelling and Simulation, June 4th-June 7th, 2024 Cracow, Poland / Grzonka Daniel [etc] (red.), Communications of the ECMS, 2024, Vol. 38, No. 1, Caserta, ECMS, pp. 187-193.
11. **Fialko S.Yu.** Block Subspace Iteration Method for Structural Analysis on Multicore Computers. // Proceedings of the of the 17th Conference on Computer Science and Intelligence Systems, 2022, Vol. 30, pp. 457-465.
12. **Fialko S.Yu., Kabantsev O.V., Perelmuter A.V.** Elasto-plastic progressive collapse analysis based on the integration of the equations of motion. // Magazine of Civil Engineering, 2021, No. 102 (2), pp. 1-10.
13. **Karpilovskyi V., Kriksunov E., Perelmuter A., Yurchenko V.** Analysis and design of structural steel joints and connection: software implementation. // International Journal for Computational Civil and Structural Engineering, 2021, Volume 17, Issue 2, pp. 58-66.
14. **Karpilovskyi V.S.** Finite Elements for the Analysis of Reissner-Mindlin Plates With Joint Interpolation of Displacements and Rotations (JIDP). // International Journal for Computational Civil and Structural Engineering, 2021, Volume 17, Issue 3, pp. 49-63.
15. **Karpilovskyi V.S.** Finite Elements of the Plane Problem of the Theory of Elasticity with Drilling Degrees of Freedom. // International Journal for Computational Civil and Structural Engineering, 2020, Volume 16, Issue 1, pp. 48-72.
16. **Lyakhovich L.S., Akimov P.A.** Aimed control of the frequency spectrum of eigenvibrations of elastic plates with a finite number of degrees of freedom of masses by superimposing additional constraints. // International Journal for Computational Civil and Structural Engineering, 2021, Volume 17, Issue 2, pp. 76-82.
17. **Lyakhovich L.S., Akimov P.A.** Aimed control of the frequency spectrum of eigenvibrations of elastic plates with a finite number of degrees of freedom by introducing additional generalized kinematic devices. // International Journal for Computational Civil and Structural Engineering, 2021, Volume 17, Issue 3, pp. 14-20.
18. **Lyakhovich L.S., Akimov P.A.** Formation of Computational Schemes of Additional Targeted Constraints That Regulate The Frequency Spectrum of Natural Oscillations of Elastic Systems With a Finite Number of Degrees of Mass Freedom, the Directions of Movement of Which are Parallel, But Do Not Lie in the Same Plane. Part 1: Theoretical Foundations. // International Journal for Computational Civil and Structural Engineering, 2022, Volume 18, Issue 2, pp. 183-193.

19. **Lyakhovich L.S., Akimov P.A.** Formation of Computational Schemes of Additional Targeted Constraints That Regulate The Frequency Spectrum of Natural Oscillations of Elastic Systems With a Finite Number of Degrees of Mass Freedom, the Directions of Movement of Which are Parallel, But Do Not Lie in the Same Plane. Part 2: The First Sample of Analysis. // International Journal for Computational Civil and Structural Engineering, 2022, Volume 18, Issue 3, pp. 137-146.
20. **Lyakhovich L.S., Akimov P.A., Mescheulov N.V.** Formation of computational schemes of additional targeted constraints that regulate the frequency spectrum of natural oscillations of elastic systems with a finite number of degrees of mass freedom, the directions of movement of which are parallel, but do not lie in the same plane. Part 3. The second sample of analysis and conclusion. // International Journal for Computational Civil and Structural Engineering, 2022, Volume 18, Issue 4, pp. 71-81.

СПИСОК ЛИТЕРАТУРЫ

1. **Акимов П.А., Ляхович Л.С.** Прицельное регулирование спектра частот собственных колебаний упругих пластин с конечным числом степеней свободы масс путем введения дополнительных обобщенных связей и обобщенных кинематических устройств. // Вестник Томского государственного архитектурно-строительного университета, 2021, том 23, № 4, с. 57-67.
2. **Гитерман Д.М., Ляхович Л.С., Нудельман Я.Л.** Алгоритм создания резонансно-безопасных зон при помощи наложения дополнительных связей. // Динамика и прочность машин, 1984, выпуск 39, с. 63-69.
3. **Ляхович Л.С.** Особые свойства оптимальных систем и основные направления их реализации в методах расчета сооружений. Монография. – Томск: Издательство ТГАСУ, 2009. - 372 с.
4. **Ляхович Л.С., Акимов П.А.** О формировании расчетных схем некоторых дополнительных связей для упругих систем. Часть 1. Теоретические основы подхода. // Промышленное и гражданское строительство, 202, №9, с. 4-10.
5. **Ляхович Л.С., Акимов П.А., Мешеулов Н.В.** О формировании расчетных схем некоторых дополнительных связей для упругих систем. Часть 2. Примеры расчёта. // Промышленное и гражданское строительство, 2022, №9, с. 11-19.
6. **Ляхович Л.С., Малеткин О.Ю.** О прицельном регулировании собственных частот упругих систем. // Известия вузов. Строительство и архитектура, 1990, № 1, с. 113-117.
7. **Нудельман Я.Л., Ляхович Л.С., Гитерман Д.М.** О наиболее податливых связях наибольшей жесткости. // Вопросы прикладной Механики и математики. - Томск: Издательство ТГУ, 1981, с. 113-126.
8. **Fialko S.** Parallel finite element solver for multi-core computers with shared memory. // Computers & Mathematics with Applications, 2021, Vol. 94, pp. 1-14.
9. **Fialko S.** Parallel finite element solver PARFES for the structural analysis in NUMA architecture. // Advances in Engineering Software, 2022, Vol. 174, 103290 pp. 1-12.
10. **Fialko S.** Time history analysis of buildings and structures design models in SCAD software on multicore computers. // ECMS 2024: proceedings of the 38th ECMS International Conference on Modelling and Simulation, June 4th-June 7th, 2024 Cracow, Poland / Grzonka Daniel [etc] (red.), Communications of the ECMS, 2024, Vol. 38, No. 1, Caserta, ECMS, pp. 187-193.
11. **Fialko S.Yu.** Block Subspace Iteration Method for Structural Analysis on Multicore Computers. // Proceedings of the of the 17th

Conference on Computer Science and Intelligence Systems, 2022, Vol. 30, pp. 457-465.
12. **Fialko S.Yu., Kabantsev O.V., Perelmuter A.V.** Elasto-plastic progressive collapse analysis based on the integration of the equations of motion. // Magazine of Civil Engineering, 2021, No. 102 (2), pp. 1-10.
13. **Karpilovskyi V., Kriksunov E., Perelmuter A., Yurchenko V.** Analysis and design of structural steel joints and connection: software implementation. // International Journal for Computational Civil and Structural Engineering, 2021, Volume 17, Issue 2, pp. 58-66.
14. **Karpilovskyi V.S.** Finite Elements for the Analysis of Reissner-Mindlin Plates With Joint Interpolation of Displacements and Rotations (JIDP). // International Journal for Computational Civil and Structural Engineering, 2021, Volume 17, Issue 3, pp. 49-63.
15. **Karpilovskyi V.S.** Finite Elements of the Plane Problem of the Theory of Elasticity with Drilling Degrees of Freedom. // International Journal for Computational Civil and Structural Engineering, 2020, Volume 16, Issue 1, pp. 48-72.
16. **Lyakhovich L.S., Akimov P.A.** Aimed control of the frequency spectrum of eigenvibrations of elastic plates with a finite number of degrees of freedom of masses by superimposing additional constraints. // International Journal for Computational Civil and Structural Engineering, 2021, Volume 17, Issue 2, pp. 76-82.
17. **Lyakhovich L.S., Akimov P.A.** Aimed control of the frequency spectrum of eigenvibrations of elastic plates with a finite number of degrees of freedom by introducing additional generalized kinematic devices. // International Journal for Computational Civil and Structural Engineering, 2021, Volume 17, Issue 3, pp. 14-20.
18. **Lyakhovich L.S., Akimov P.A.** Formation of Computational Schemes of Additional Targeted Constraints That Regulate The Frequency Spectrum of Natural Oscillations of Elastic Systems With a Finite Number of Degrees of Mass Freedom, the Directions of Movement of Which are Parallel, But Do Not Lie in the Same Plane. Part 1: Theoretical Foundations. // International Journal for Computational Civil and Structural Engineering, 2022, Volume 18, Issue 2, pp. 183-193.
19. **Lyakhovich L.S., Akimov P.A.** Formation of Computational Schemes of Additional Targeted Constraints That Regulate The Frequency Spectrum of Natural Oscillations of Elastic Systems With a Finite Number of Degrees of Mass Freedom, the Directions of Movement of Which are Parallel, But Do Not Lie in the Same Plane. Part 2: The First Sample of Analysis. // International Journal for Computational Civil and Structural Engineering, 2022, Volume 18, Issue 3, pp. 137-146.
20. **Lyakhovich L.S., Akimov P.A., Mescheulov N.V.** Formation of computational schemes of additional targeted constraints that regulate the frequency spectrum of natural oscillations of elastic systems with a finite number of degrees of mass freedom, the directions of movement of which are parallel, but do not lie in the same plane. Part 3. The second sample of analysis and conclusion. // International Journal for Computational Civil and Structural Engineering, 2022, Volume 18, Issue 4, pp. 71-81.

Leonid S. Lyakhovich, Full Member of the Russian Academy of Architecture and Construction Sciences, Professor, DSc, Professor of Department of Structural Mechanics, Tomsk State University of Architecture and Building; 2, Solyanaya St., 2, Tomsk, 634003, Russia; Professor of Department of Applied Mathematics and Computer Science, National Research Moscow State University of Civil Engineering; 26, Yaroslavskoe Shosse, Moscow, 129337, Russia; E-mail: lls@tsuab.ru.

Ляхович Леонид Семенович, академик РААСН, профессор, доктор технических наук, профессор кафедры строительной механики, Томский государственный архитектурно-строительный университет; 634003, Россия, г. Томск, Соляная пл. 2; профессор кафедры информатики и прикладной математики, Национальный исследовательский Московский государственный строительный университет; 129337, Россия, г. Москва, Ярославское шоссе, дом 26; E-mail: lls@tsuab.ru.

Pavel A. Akimov, Full Member of the Russian Academy of Architecture and Construction Sciences, Professor, Dr.Sc.; Rector, Professor of Department of Applied Mathematics and Computer Science of National Research Moscow State University of Civil Engineering; 26, Yaroslavskoe Shosse, Moscow, 129337, Russia; phone: +7(495) 651-81-85; Fax: +7(499) 183-44-38; E-mail: AkimovPA@mgsu.ru, rector@mgsu.ru, pavel.akimov@gmail.com.

Zaur R. Galyautdinov, Associate Professor, DSc, Professor of Department of Reinforced Concrete and Stone Structures, Tomsk State University of Architecture and Building; 2, Solyanaya St., 2, Tomsk, 634003, Russia;
E-mail: gazr@yandex.ru.

Andrey S. Plyaskin, Associate Professor, Ph.D., Head of Department of Metal and Wooden Structures, Tomsk State University of Architecture and Building; 2, Solyanaya St., 2, Tomsk, 634003, Russia;
E-mail: plyaskinandrei@mail.ru.

Акимов Павел Алексеевич, академик РААСН, профессор, доктор технических наук; ректор, профессор кафедры информатики и прикладной математики Национального исследовательского Московского государственного строительного университета; 129337, Россия, г. Москва, Ярославское шоссе, дом 26; телефон: +7(495) 651-81-85; факс: +7(499) 183-44-38; Email: AkimovPA@mgsu.ru, rector@mgsu.ru, pavel.akimov@gmail.com.

Галяутдинов Заур Рашидович, доцент, доктор технических наук, доцент кафедры железобетонных и каменных конструкций, Томский государственный архитектурно-строительный университет; 634003, Россия, г. Томск, Соляная пл. 2; E-mail: gazr@yandex.ru.

Пляскин Андрей Сергеевич, доцент, кандидат технических наук, заведующий кафедрой металлических и деревянных конструкций, Томский государственный архитектурно-строительный университет; 634003, Россия, г. Томск, Соляная пл. 2; E-mail: plyaskinandrei@mail.ru.

International Journal for Computational Civil and Structural Engineering, 20(3) 198–205(2024)

DOI:10.22337/2587-9618-2024-20-3-198-205

CONSIDERATION OF THE SEISMIC IMPACT'S WAVE NATURE IN THE DESIGN JUSTIFICATION OF HIGH-RISE BUILDINGS' SEISMIC RESISTANCE

Dmitry S. Dmitriev, Pavel I. Novikov, Sergey O. Petryashev, Alexandr I. Nagibovich

National Research Moscow State University of Civil Engineering, Moscow, RUSSIA

Abstract: This paper presents the seismic resistance calculation results for a high-rise building that considers the wave nature of the impact, its heterogeneity and irregularity in the structural plan, performed in SCAD Office. The analysis of normative requirements to consider the wave action and existing calculation methodologies is carried out. Recommendations are given on possible consideration of the seismic impact's irregularity using the direct dynamic method to solve the MDE-level seismic impact on the structures.

Keywords: seismic impact's wave nature, rotational components of seismic motion, linear-spectral method, direct dynamic method, SCAD Office, seismic resistance

УЧЕТ ВОЛНОВОГО ХАРАКТЕРА СЕЙСМИЧЕСКОГО ВОЗДЕЙСТВИЯ ПРИ РАСЧЕТНОМ ОБОСНОВАНИИ СЕЙСМОСТОЙКОСТИ ВЫСОТНЫХ ЗДАНИЙ

Д.С. Дмитриев, П.И. Новиков, С.О. Петряшев, А.И. Нагибович

Национальный исследовательский Московский государственный строительный университет, г. Москва, РОССИЯ

Аннотация: В настоящей статье представлены результаты расчета на сейсмостойкость высотного здания с учетом волнового характера воздействия и его неоднородности и неравномерности в плане сооружения, в программном комплексе SCAD Office. Проведен анализ нормативных требований в части учета волнового воздействия и существующих методик расчета. Даны рекомендации по возможному учету неравномерности сейсмического воздействия при расчете сооружений прямым динамическим методом на сейсмическое воздействие уровня МРЗ (КЗ).

Ключевые слова: Волновой характер сейсмического воздействия, ротационные составляющие сейсмического движения, линейно-спектральный метод, прямой динамический метод, ПК SCAD Office, сейсмостойкость

1. INTRODUCTION

Paragraph 6.1.4 of SP 14.13330.2018 [1] demands for the buildings with reinforced concrete framing that, if the design seismicity of the construction site is or above 7-8 points, the distances between aseismic joints should not exceed 80 m. If this condition cannot be satisfied, *analysis of structures should consider the seismic impact's wave nature, its inhomogeneity and irregularity in the structural plan according to the established methodologies*. This requirement first appeared in Amendment 1 to SP 14.13330.2018 and simply stated the need consider the seismic impact's wave nature without describing any approaches to carry out such calculations or referring to any methodologies.

To date, there are still no consistent approaches or methodologies accepted by the engineering community for earthquake-resistant buildings and structures analysis that consider wave-like spatial and temporal seismic effects that can be applied in engineering design practice, as well as adopted methodological recommendations to SP 14.13330.2018.

A number of works by Yu. P. Nazarov on the application of the linear-spectral method to solve these issues [2, 3, 4, 5, 6] formed the basis of the manual [7]. It presents:
– an engineering methodology for determining the prevailing wavelengths and selecting a computational model of seismic ground motion;
– a methodology for calculation of rotational components for the integral dilatational-rotational model of seismic ground motion;
– a modified linear-spectral method for calculation of earthquake-resistant buildings and structures for the integral dilatation-rotation model of seismic ground motion.
In the EU seismic standards [8] there is also a requirement to take into account rotational components of seismic ground motion for high-rise structures in regions with high seismicity, but it is only applicable for such structures (towers, masts, chimneys, etc.) which utilise the obsolete cantilever dynamic model.
It should be noted that all the described methodologies are applicable to the analysis of buildings using the linear-spectral theory. The most widespread software packages in the Russian construction industry (SCAD Office, LIRA-SAPR, LIRA 10) currently lack convenient tools for their application in the calculation practice. Which, in fact, makes it practically impossible to deviate from the normative requirements in terms of distances between aseismic joints.
SP 14.13330.2018 demands that analysis of buildings for seismic effects of control earthquake-level (CE), or, per custom, maximum design earthquake-level (MDE), should be performed using the direct dynamic method. In practice, rather complicatedly implemented approaches are used for the design justification of structures' seismic resistance in terms of wave action [9]. Few works consider the seismic impact's wave nature in the direct dynamic method excluding the foundation. It's primarily due to the complexity of the impact's character at the "foundation-structure" boundary, which should account for the velocity of the seismic wave propagation, depending on the type of soil [10].

This paper describes a simplified method to consider the seismic impact's wave nature in the analysis of a building using the direct dynamic method in SCAD Office. This approach can be used in addition to the aforementioned methodologies when calculating the seismic resistance of high-rise buildings.

2. PROBLEM STATEMENT

The building considered in this article is a 99-meter-tall multifunctional hotel complex with *XY*-dimensions of 104×87 m and an underground 3-storey car parking (*Figure 1*).
The frame-wall structural system with a load-bearing core is adopted in this project. The foundation is a continuous monolithic 1.8-meter-thick slab on a natural bed. The frame is formed by a system of vertical elements (columns, pylons, walls and a load-bearing core, which consists of stairwells and lift shafts) and horizontal floor slabs. All joints of the frame elements (walls, diaphragms, columns, beams, floor slabs) are connected using fixed supports, which ensures the continuity of the frame elements' systems. Spatial rigidity is ensured by the joint work of load-bearing structures of slabs, reinforced concrete columns, pylons and the vertical load-bearing core, which are all connected to the foundation slab using fixed supports.
All vertical structures are made of B40 concrete, all horizontal load-bearing structures are made of B30 concrete.
Seismicity of the construction site, according to the geophysical surveys, is 8 points. The soils belong to the II (second) category of seismic properties. A three-component accelerogram was presented for the initial impact (as per the geophysical surveys), which was multiplied by the coefficients K_0 =1.3, K_1 =1.0 and K_ψ =1.0 before being used in the calculation. Due to the fact that in SCAD Office's direct dynamic method the seismic impact is specified in the form of displacements [11], the corresponding seismograms were obtained from the initial accelerograms.
For dynamic calculations, a finite-element (FE) model was developed in SCAD Office. The

structures of the building (reinforced concrete foundation slab, floor slabs, walls, cover disc) were modelled by shell 44 FE. The beam elements (columns) were modelled by a spatial beam FE, which implements the Timoshenko beam theory. The elements are connected using fixed supports. Computational dimensionality of the model is 822 295 nodes (4 588 118 degrees of freedom) and 894 287 FE.

As part of the considered building's seismic resistance design justification, calculations for the seismic impact of a design earthquake-level (DE) or, per custom, a project earthquake-level (PE), were carried out using the linear-spectral method with the response spectra obtained from synthesised three-component accelerograms (with 5% damping). From this calculation's results, the reinforcement of elements was chosen, and the seismic impact of the MDE-level was calculated using the direct dynamic method. The implementation of a simplified method to consider the impact's wave nature in SCAD is presented below. A comparison of the results of the platform scheme (when the same impact is applied to all nodes of the foundation simultaneously) and the designed wave scheme is also presented.

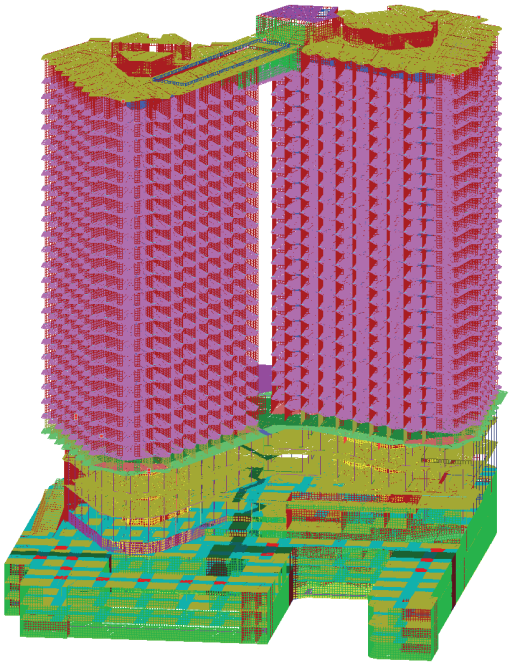


Figure 1. General view of the calculation model of a high-rise building

3. METHODOLOGY FOR THE SEISMIC IMPACT WAVE NATURE'S CONSIDERATION

1) The calculation of dynamic stress-strain state of load-bearing structures under special combinations of loads and influences (MDE-level) is considered. The dynamic calculation of an impact represented by accelerograms of ground vibrations at the base of the structure is done by numerical integration of the motion equations.

2) The dynamic characteristics of the foundation obtained from geophysical survey data are used.

3) The wave-induced seismic loading is represented by a discrete set of loads, which are represented as "bands" in the structural plan. The width of these bands is determined by the geophysical survey data regarding the transverse wave velocity in the foundation bed. In this case:

– transverse wave velocity $V = 760$ m/s;

– integration step: $h_{st} = 0.01$ s;

– strip width: $\Delta l = V \times h_{st} = 760 \times 0.01 = 7.6$ m (*Figure 4*).

4) Loads for the horizontal and vertical components of the seismic load are specified separately as single displacements along the global axes of the model. The displacements are applied to the nodes of one-way tie elements (type 352, *Figure 2*). Horizontal displacements are applied to the top tie node, and vertical displacements to the bottom tie node. It is possible to correct the direction of horizontal loads using cosine guides.

5) The impact's wave nature is considered by applying the load to different bands with a time offset, which corresponds to the chosen integration step (so they are included in the oscillation process one by one).

The integration step (at known wave propagation velocity) determines the width of the band to which the seismic load is applied.

6) Each band should be assigned both a horizontal and a vertical seismic load component.

7) In order to account for the most dangerous direction of seismic action, the bands should be oriented perpendicular to the direction of the first mode of the system in the structural plan.

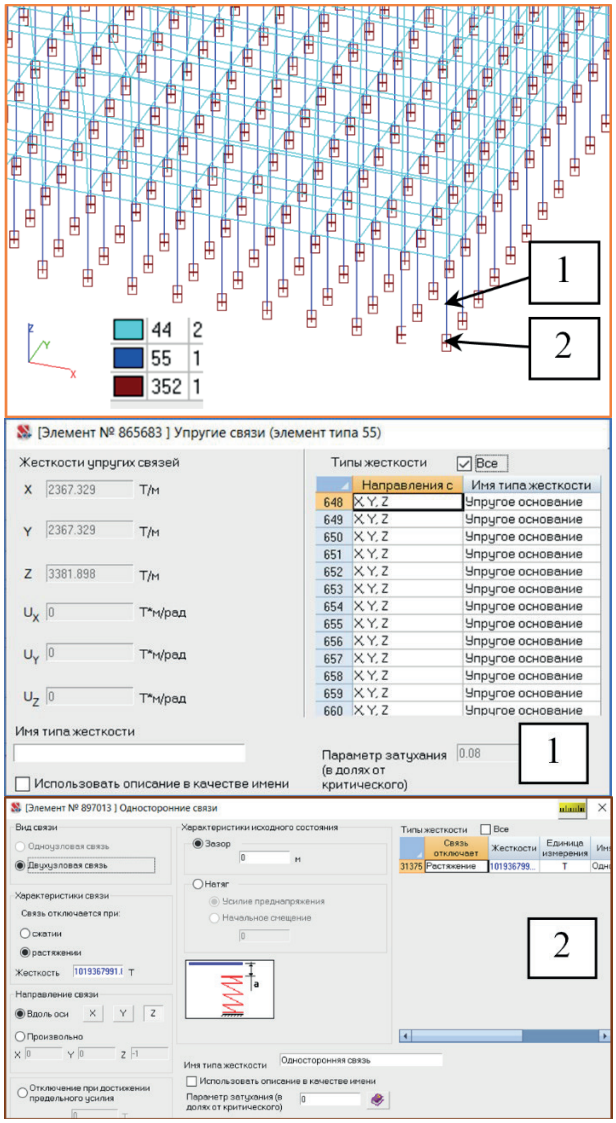


Figure 2. Structure and parameters of a dynamic elastic foundation

The three-component seismogram used is shown in *Figure 3* (seismogram along *Z* axis is given in green, *X*-axis in red and *Y*-axis in blue).



Figure 3. Three-component seismogram. Time step 0.01 s. Range 0-20 s

The most dangerous direction of horizontal seismic impact, determined from the analysis of the eigenfrequencies and modes, is shown in the *Figure 4*. The time offset of the bands is 0.01 s (corresponding to the integration step). Investigation of influence of the integration step (and, consequently, the width of the "bands") on the final dynamic response of the building has not been carried out in this study, but is planned for the future. The direction of the first mode of the system is shown in purple.

Thus, the *Y* component is selected for the horizontal component and the *Z* component for the vertical component.

4. RESULTS

Following the results of the performed dynamic calculations for two schemes (wave and platform), considering the physical nonlinearity, the displacements at the nodes with maximum amplitudes in the nonlinear analysis (486700, 466484, 223778, 486540, 487389), as well as the transient changes of internal forces for a number of finite elements (FE 830115, FE 819373) are compared (*Figure 5*).

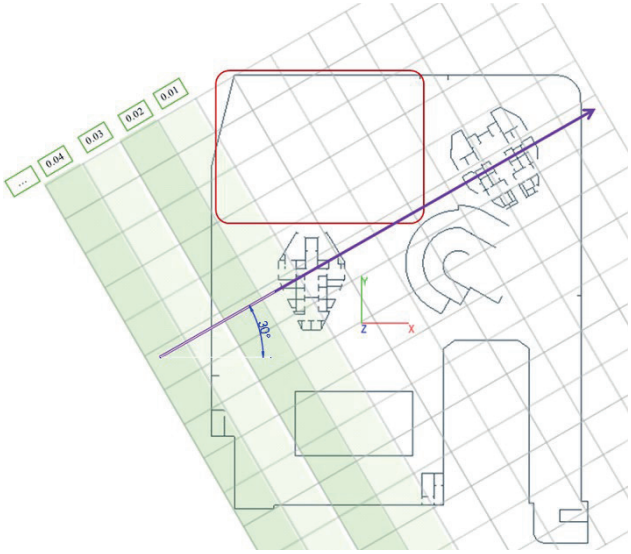


Figure 4. Configuration of the "bands" (t = 7.6 s) and their orientation in plan

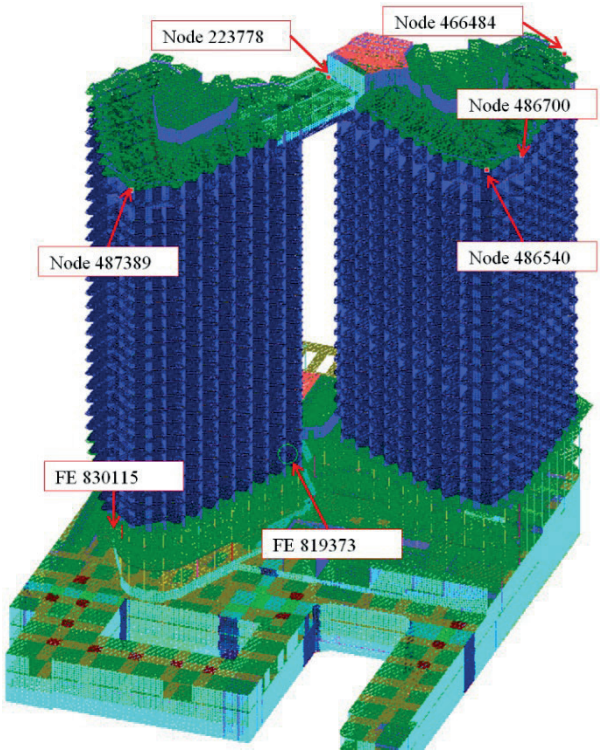


Figure 5. Locations of nodes/elements for the post-processing

Figure 6 shows a plot of the linear horizontal displacements of node 466484 for the two schemes, and *Table 1* summarises the results for all nodes and shows the relative differences in values.

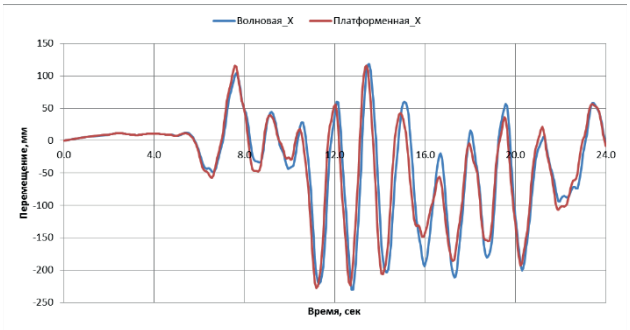


Figure 6. Nonlinear analysis. Comparison of absolute displacements UX for the platform and wave scheme for the node 466484

Table 1. Comparison of peak displacements in the selected nodes

Node No.	Min/max	Platform scheme. Displacements, mm			"Wave" scheme. Displacements, mm			Relative difference, %		
		UX	UY	UZ	UX	UY	UZ	UX	UY	UZ
486700	min	-367.3	-345.6	-49.9	-338.6	-337.2	-51.4	7.81	2.43	-3.01
	max	211.8	173.1	46.3	223.9	185.3	47.9	-5.71	-7.05	-3.46
466484	min	-227.5	-300.2	-46.5	-230.1	-290.6	-46.1	-1.14	3.20	0.86
	max	115.7	152.5	58.2	117.8	164	57.7	-1.82	-7.54	0.86
223778	min	-207.9	-206.8	-61.3	-215.6	-223.1	-57.9	-3.70	-7.88	5.55
	max	145.7	86.8	63.8	157.5	100.3	68.6	-8.10	-15.55	-7.52
486540	min	-425.6	-311.6	-58.5	-398.6	-302.3	-59.6	6.34	2.98	-1.88
	max	241.6	156.9	31.4	256.38	168.7	32.6	-6.12	-7.52	-3.82
487389	min	-385	-181.4	-67	-386.6	-206.4	-68	-0.42	-13.78	-1.49
	max	215.7	51.1	35.1	209.2	75.6	35.4	3.01	-47.95	-0.85

+	The platform scheme values are bigger than the wave scheme values.
-	The wave scheme values are bigger than the platform scheme values.

The forces in element 819373 (beam 60*80 at +11.700) for the platform scheme are shown in *Figure 7* and *Figure 8*. The normal stresses in the beam section at the moment of time (12.86 s) are given in *Figure 9*.

The forces in same element 819373 for the "wave" scheme are shown in *Figure 10* and *Figure 11*. The normal stresses in the beam section at the moment of time (12.98 s) are given in *Figure 12*.

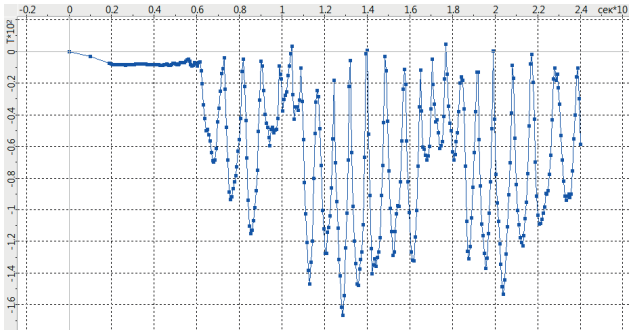


Figure 7. FE 819373. Longitudinal force.
N_{min}= -166.8 m (t = 12.86 s),
N_{max}= 4.68 m (t = 17.7 s)

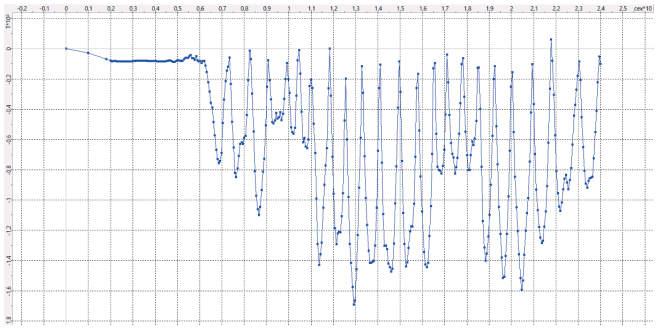


Figure 10. FE 819373. Longitudinal force.
N_{min}= -169.11 m (t = 12.92 s),
N_{max}= 6.22 m (t = 21.78 s)

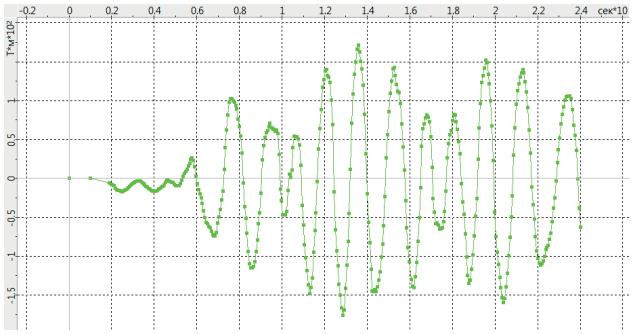


Figure 8. FE 819373. Bending moment.
My_{min}= -176.40 m (t = 12.86 s),
My_{max}= 171.65 m (t = 13.58 s)

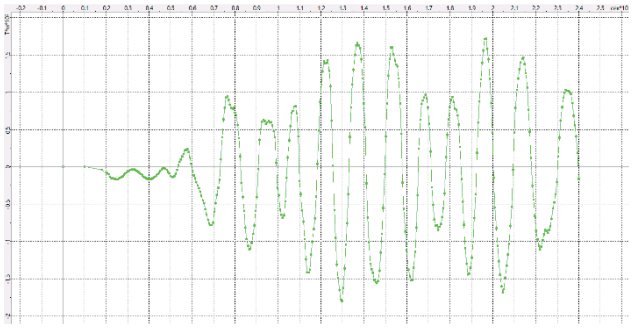
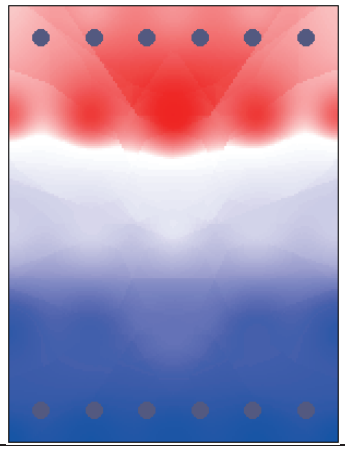
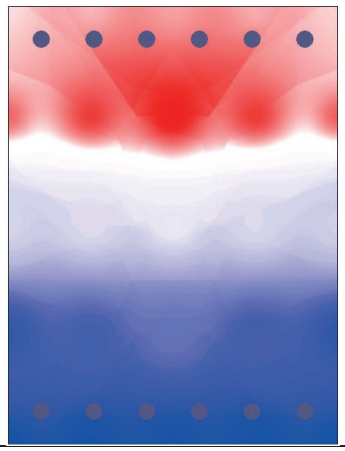


Figure 11. FE 819373. Bending moment.
My_{min}= -179.77 m (t = 12.98 s),
My_{max}= 171.69 m (t = 19.68 s)



	Concrete compression. Min -1307.66 t/m^2
	Concrete tension. Max 54.43 t/m^2

Figure 9. Normal stresses in the beam section, (t=12.85 s)



	Concrete compression. Min -1322.63 t/m^2
	Concrete tension. Max 52.46 t/m^2

Figure 12. Normal stresses in the beam section, (t=12.98 s)

5. CONCLUSIONS

The following conclusions can be drawn from the presented results of the comparative analysis:
1) Qualitatively, structural displacements are generally similar for both the platform and the wave scheme;
2) With the described methodology to apply the impact's wave nature, a slight delay of the displacement peaks can be seen in comparison with the platform scheme. It reaches 0.15 s in displacements for different parts of the model;
3) For individual local peak displacements, the difference reaches up to 18.1%, but for absolute maximum displacements on the roof the difference does not exceed 10%.
Taking into account the available ground conditions (wave propagation velocity) and the foundation dimensions (104×87 m), the influence of the wave action on the stress-strain state of the building is insignificant. In the development of this work, it is planned to carry out design studies using the described approach on a structure with more extensive foundation dimensions.
Also, in the considered example, the seismic wave propagation velocity according to geophysical survey data is 760 m/s, and it is recommended [1] to consider the wave nature at smaller phase velocities' values of $V < 400$ m/s.
The methodology for consideration of the seismic impact's wave nature in the analysis of high-rise buildings using the direct dynamic method can be applied with the methodologies that utilise the linear-spectral theory.
In light of the current architectural evolution of modern buildings and structures, and in the presence of the paragraph's 6.1.4 of SP 14.13330.2018 [11] requirements, it is extremely necessary to develop engineering methods to consider the seismic impact's wave nature, as well as to introduce them into the software used in the industry.

ACKNOWLEDGEMENTS

The research was funded by the National Research Moscow State University of Civil Engineering (grant for fundamental and applied scientific research, project No. 31-392/130).

REFERENCES

1. **SP 14.13330.2018** Svod pravil. Stroitelstvo v seysmicheskikh rayonakh. Izm. №3. (in Russian)
2. **Nazarov Yu.P.** Raschetnyye modeli seysmicheskikh vozdeystviy. – M.: Nauka. 2012. 414 p. (in Russian)
3. **Nazarov Yu.P., Poznyak E.V., Filimonov A.V.** Analiz vida volnovoy modeli i polucheniye raschetnykh parametrov seysmicheskogo vozdeystviya dlya vysotnogo zdaniya // Promyshlennoye i grazhdanskoye stroitelstvo. – 2014. – №5. – Pp. 40-45. (in Russian)
4. **Nazarov Yu.P.** Raschetnyye parametry volnovykh poley seysmicheskikh dvizheniy grunta. - M.: Nauka. 2015. 401 p. (in Russian)
5. **Nazarov Yu.P.. Poznyak E.V.** Otsenka rotatsionnykh komponent seysmicheskogo dvizheniya grunta // Osnovaniya. fundamenty i mekhanika gruntov. – 2015. – №6. – Pp. 22-26. (in Russian)
6. **Nazarov Yu.P.. Poznyak E.V.** Sovremennaya kontseptsiya integralnoy modeli seysmicheskogo dvizheniya grunta v stroitelnykh raschetakh na seysmostoykost //Promyshlennoye i grazhdanskoye stroitelstvo. – 2016. – № 9. – Pp. 74-80. (in Russian)
7. **Posobiye** po inzhenernym podkhodam i metodam raschetov zdaniy i sooruzheniy s uchetom volnovogo kharaktera seysmicheskogo vozdeystviya. Proyekt. 2020. (in Russian)
8. **EN 1998-6:2005 Eurocode 8:** Design of structures for earthquake resistance — Part 6: Towers. masts and chimneys.
9. **Sinelshchikov A.V., Panasenko N.N.** Obosnovaniye seysmostoykosti zdaniy i sooruzheniy s uchetom volnovykh svoystv seysmicheskogo vozdeystviya //Vestnik Belgorodskogo gosudarstvennogo tekhnologicheskogo universiteta im. VG Shu-

khova. – 2018. – №. 10. – Pp. 52-63. (in Russian)
10. **Korchinskiy I.L., Grill A.A.** Raschet visyachikh pokrytiy na dinamicheskiye vozdeystviya (zemletryaseniya. veter). – M.: Stroyizdat. 1978. 220 p. (in Russian)
11. **SCAD Office.** Version 23. SCAD++ software, 2022.

СПИСОК ЛИТЕРАТУРЫ

1. **СП 14.13330.2018** Свод правил. Строительство в сейсмических районах. Изм. №3.
2. **Назаров Ю.П.** Расчетные модели сейсмических воздействий. - М.: Наука, 2012, 414 с.
3. **Назаров Ю.П., Позняк Е.В., Филимонов А.В.** Анализ вида волновой модели и получение расчетных параметров сейсмического воздействия для высотного здания // Промышленное и гражданское строительство. – 2014. – №5. – С.40-45.
4. **Назаров Ю.П.** Расчетные параметры волновых полей сейсмических движений грунта. - М.: Наука, 2015, 401с.
5. **Назаров Ю.П., Позняк Е.В.** Оценка ротационных компонент сейсмического движения грунта. Основания, фундаменты и механика грунтов // 2015. – №6. – С. 22-26.
6. **Назаров Ю.П., Позняк Е.В.** Современная концепция интегральной модели сейсмического движения грунта в строительных расчетах на сейсмостойкость//Промышленное и гражданское строительство. 2016. № 9. С. 74-80.
7. **Пособие** по инженерным подходам и методам расчетов зданий и сооружений с учетом волнового характера сейсмического воздействия. Проект. 2020 год.
8. **EN 1998-6:2005 Eurocode 8:** Design of structures for earthquake resistance — Part 6: Towers, masts and chimneys.
9. **Синельщиков А. В., Панасенко Н. Н.** Обоснование сейсмостойкости зданий и сооружений с учётом волновых свойств сейсмического воздействия //Вестник Белгородского государственного технологического университета им. ВГ Шухова. – 2018. – №. 10. – С. 52-63.
10. **Корчинский И.Л., Грилль А.А.** Расчёт висячих покрытий на динамические воздействия (землетрясения, ветер). М.: Стройиздат, 1978. 220 с.
11. **SCAD Office**. Версия 23 Вычислительный комплекс SCAD++. 2022 год.

Dmitry S. Dmitriev - CSc, engineer of A.B. Zolotov REC SM of the National Research Moscow State University of Civil Engineering; 129337, Russia, Moscow, Yaroslavskoe shosse, 26. E-mail: dmitriev.d.s@yandex.ru

Pavel I. Novikov - CSc, Senior Research Fellow of A.B. Zolotov REC SM of the National Research Moscow State University of Civil Engineering; 129337, Russia, Moscow, Yaroslavskoe shosse, 26. E-mail: novikov.mgsu@gmail.com

Sergey O. Petrashev - Junior Research Fellow of A.B. Zolotov REC SM of the National Research Moscow State University of Civil Engineering; 129337, Russia, Moscow, Yaroslavskoe shosse, 26. E-mail: petsero@mail.ru

Alexandr I. Nagibovich - CSc, Director at A.B. Zolotov REC SM of the National Research Moscow State University of Civil Engineering; 129337, Russia, Moscow, Yaroslavskoe shosse, 26. E-mail: nagibovich@yandex.ru

Дмитриев Дмитрий Сергеевич – к.т.н, инженер НОЦ КМ им. А.Б. Золотова Национального исследовательского Московского государственного строительного университета; 129337, Россия, г. Москва, Ярославское шоссе, д. 26. E-mail: dmitriev.d.s@yandex.ru

Новиков Павел Игоревич - к.т.н, старший научный сотрудник НОЦ КМ им. А.Б. Золотова Национального исследовательского Московского государственного строительного университета; 129337, Россия, г. Москва, Ярославское шоссе, д. 26. E-mail: novikov.mgsu@gmail.com

Петряшев Сергей Олегович – младший научный сотрудник НОЦ КМ им. А.Б. Золотова Национального исследовательского Московского государственного строительного университета; 129337, Россия, г. Москва, Ярославское шоссе, д. 26. E-mail: petsero@mail.ru

Нагибович Александр Игоревич – к.т.н, директор НОЦ КМ им. А.Б. Золотова Национального исследовательского Московского государственного строительного университета; 129337, Россия, г. Москва, Ярославское шоссе, д. 26. E-mail: nagibovich@yandex.ru

International Journal for Computational Civil and Structural Engineering, 20(3) 206–217(2024)

DOI:10.22337/2587-9618-2024-20-3-206-217

DEVELOPMENT OF METHODS FOR DESIGNING PILE FOUNDATIONS FOR MULTI-STOREY CIVIL BUILDINGS CONSTRUCTED ON MACROPOROUS SUBSIDENCE SOILS

Maxim B. Marinichev [1], Nadezhda S. Nikitina [2], Anatoly I. Polishchuk [1]

[1] I.T. Trubilin Kuban State Agrarian University, Krasnodar, RUSSIA
[2] Moscow State University of Civil Engineering, Moscow, RUSSIA

Abstract: The study considers the methods (separate stages) of designing pile foundations made of driven reinforced concrete piles on macroporous subsidence soils of the second type of subsidence using multi-storey buildings as an example. The paper provides a brief description of the buildings under consideration, analyzes the soil conditions of construction, including data on physical, deformation, strength, subsidence characteristics of soils and methods of their determination. Using the calculation, it establishes the type of soil conditions in terms of subsidence, describes the method of selecting the type of piles and their length in macroporous subsidence soils. The data of experimental studies of bearing capacity of driven piles in macroporous subsidence soils, justification of the method of numerical studies of pile performance and theoretical evaluation of their bearing capacity are given.

Keywords: Driven piles, foundations, design, ground conditions of construction, soil properties, bearing capacity of piles, subsidence type of ground conditions, results of experimental and numerical studies

РАЗВИТИЕ МЕТОДОВ ПРОЕКТИРОВАНИЯ СВАЙНЫХ ФУНДАМЕНТОВ НА МАКРОПОРИСТЫХ ПРОСАДОЧНЫХ ГРУНТАХ ДЛЯ МНОГОЭТАЖНЫХ ГРАЖДАНСКИХ ЗДАНИЙ

М.Б. Мариничев [1], Н.С. Никитина [2], А.И. Полищук [1]

[1] Кубанский государственный аграрный университет имени И.Т. Трубилина, г. Краснодар, РОССИЯ
[2] Московский государственный строительный университет, г. Москва, РОССИЯ

Аннотация: На примере многоэтажных зданий рассматриваются методы (отдельные этапы) проектирования свайных фундаментов из забивных железобетонных свай на макропористых просадочных грунтах второго типа по просадочности. Дается краткая характеристика рассматриваемых зданий, анализируются грунтовые условия строительства, включая данные о физических, деформационных, прочностных, просадочных характеристиках грунтов и методы их определения. Расчетом устанавливается тип грунтовых условий по просадочности, излагается метод выбора типа свай и их длины в макропористых просадочных грунтах. Приводятся данные экспериментальных исследований несущей способности забивных свай в макропористых просадочных грунтах, обоснование метода численных исследований работы свай и теоретической оценки их несущей способности.

Ключевые слова: Сваи забивные, фундаменты, проектирование, грунтовые условия строительства, характеристики грунтов, несущая способность свай, тип грунтовых условий по просадочности, результаты экспериментальных и численных исследований

INTRODUCTION

The authors of this study conduct research on substantiation of soil conditions and development of pile foundation design solutions for construction of civil multi-storey residential buildings constructed on macroporous subsidence soils [1, 2, 3]. Such soils are widespread in Russia and other countries. They are found in the southern, south-eastern and south-western

regions of our country (Krasnodar Krai, Republic of Adygea, Volgograd Oblast, Stavropol Krai, Chechen Republic, Republic of Crimea, Zabaikalye, etc.). Therefore, they are often called as regional soils. The conditions of construction on such soils are referred to regional (or special). The article considers the methods (main stages) of pile foundation design on construction sites composed of macroporous subsidence soils using the example of civil buildings in Grozny with load-bearing walls and frame buildings [4, 5].

SOIL CONDITIONS OF A TYPICAL CONSTRUCTION SITE

The construction site is located in the Chechen Republic. The relief of the site is relatively flat, with absolute elevations of 285.5-286.5 m and a slight slope to the southwest. To find out the lithologic structure of the site 47 boreholes were drilled to a depth of 4 to 25 m and 5 pits up to 3.5 m deep were excavated. The engineering-geological section of the experimental site is represented by the following soils (engineering-geological elements):

1. Soil-vegetation layer, thickness 0.2-0.4 m.
2. Below there is a layer of low-moisture, macroporous subsidence loam, from semi-hard to hard consistency, yellow-brown color with inclusions of gypsum and carbonate salts (EGE-1). The thickness of this layer varies from 9.6 to 11.8 m.
3. At a depth of about 10.7 m from the surface there is a 1.9-2.5 m thick layer of buried soil (EGE-2) represented by hard, semi-hard, subsidence loam, dark brown in color with abundant inclusion of salts.
4. Below, at a depth of about 11.5 - 14.3 m, there is a layer of low-moisture, macroporous loam of tight plastic, yellow-brown color, with inclusion of carbonate salts. The thickness of this layer varies from 6.9 - 7.7 m (EGE-3).
5. At a depth of 18.4 - 22.0 m from the surface there is a fine gravel with sandy fill (EGE-4). There is not groundwater up to a depth of 25 m.

PHYSICAL, DEFORMATION, STRENGTH AND SUBSIDENCE PROPERTIES OF SOILS

Since the foundations of civil buildings are supposed to be constructed on macroporous subsidence soils, the study of their properties at the design stage is envisaged on soils with different moisture content (natural and pre-moistened). To determine the physical, strength, deformation and subsidence properties of the base under consideration, soils were taken mainly in the form of monoliths and separate samples, specimens at the entire depth (72 monoliths) in accordance with the requirements of GOST 12071-2000 [6]. Soils (monoliths, samples) were taken from the base of natural composition (low-moisture) and after its preliminary soaking (wet). Hereinafter in the text the term *"low-moisture soils"* means macroporous base of natural composition at its natural moisture content ($Sr \leq 0.5$). *"Wet soils"* means macroporous base after its preliminary wetting ($0.5 \leq Sr \leq 0.8$).

For the proposed construction of civil multi-storey buildings, macroporous soils were soaked gradually for 25-30 days. For this purpose, a pilot site was prepared previously, where a pit with the plan size of 20 x 20 m and depth of 0.4 - 0.5 m was made (Grozny). The surface of the excavation before soaking was filled with fine crushed stone (fraction 3-10 mm) to a thickness of 7-10 cm. Along the perimeter of the pit, as well as along its area, wells with diameter up to 120 mm were made to a depth of 14-15 m, which were also backfilled with fine crushed stone. Wells on the area of the excavation were arranged on a grid of 4x4 meters. Water was supplied to the experimental site with a hose under low pressure. The flow rate was fixed by a water meter connected to the water supply system on the territory of the experimental site. The minimum volume of poured water was determined by calculation. Soaking was controlled visually and instrumentally by taking samples and soil samples from different depths and determining its weight moisture [7, 8, etc.].

The study of *physical properties* of soils was carried out according to the current regulatory documents and recommendations (GOST 5180-2015,

A.I. Polishchuk, M.B. Marinichev, 2023, etc.) [9, 10]. Analysis of the results of studies of properties of macroporous subsidence soils of the experimental site revealed that up to the depth of 15 m the change in their density and moisture content within each engineering-geological element (EGE-1, EGE-2) is insignificant, which does not exceed 3-5%. Consequently, the soil base can be considered practically homogeneous and the mean values of the considered physical characteristics for each engineering-geological element can be used for forecast calculations (Table 1).

Table 1 shows that the upper layer of low-moisture loam of natural composition (EGE-1) belongs to the hard consistency state ($I_L \leq 0$), and the same layer of loam additionally moistened (wet) is characterized as soft-plastic (I_L = 0.66). After additional moistening (soaking) of the soil, complete filling of its pores with water did not occur. This is confirmed by the value of water saturation coefficient S_r = 0.72, which is less than S_r < 0.8...1.0. The characteristic of porosity coefficient e of low-moisture and wet soil indicates its macroporous (loose) state, which is confirmed by the values e = 0.90 - 0.94, which are close to the value e = 1.0.

Table 1. Physical properties of loess subsidence soils of the experimental site

Base soils, engineering geological elements (EGE)	Layer thickness, m	Density ρ, g/cm³	Skeleton density ρ_d, g/cm³	Natural moisture W, %	Density of particles ρ_s, g/cm³	Porosity factor e,	Water saturation factor S_r,.	Moisture at the liquidity limit W_l, %	Moisture at the plastic limit W_p, %	Plasticity index J_p,%	Liquidity index J_L,
Hummocky loam, macroporous EGE-1	10,4	1,59 / 1,79	1,41 / 1,44	12,5 / 23,6	2,73	0,94 / 0,90	0,36 / 0,720	0,94 / 0,90	17,7	9,0	< 0 / 0,66
Dark brown loam (interlayer), EGE-2	1,9-2,5	1,70 / 1,81	1,49 / 1,48	14,2 / 22,0	2,72	0,82 / 0,83	0,47 / 0,72	27,1	16,9	10,2	< 0 / 0,51
Yellow-brown loam, EGE-3	6,9-7,7	1,75	1,45	21,0	2,71	0,87	0,65	27,0	17,0	10,0	0,4
Shallow gravel, EGE-4	More than 5,0	-	-	-	2,68	0,65	-	-	-	-	-

Note. In the numerator - properties of low-moisture natural moisture soils, in the denominator - pre-moistened wet soils.

Deformation properties of macroporous subsidence soils (EGE-1, EGE-2, etc.) were determined in laboratory conditions using compression devices in accordance with the requirements of regulatory documents and standards: GOST 12248.4-2020, SP 22.13330.2016, GOST 23161-2012. [11-13]. Stages of loading on the soil samples were accepted in the range of 20 - 40 kPa until complete stabilization of settlements. Settlement increment not exceeding 0.01 mm / day was adopted as a stabilization criterion. The maximum pressure on the soil samples in the experiments did not exceed 250 - 350 kPa.

Comparison of the values of total deformation modulus of subsidence soils within the depth up to 13-15 m shows that their values within each engineering-geological element differ insignificantly. The deviation at the same pressure interval varies

within 8-10%. In total, about 30 compression tests for low-moisture and wet macroporous subsidence soils were analyzed (Table 2). The analysis of the obtained results indicates that the values of the properties of the total deformation modulus of soils significantly depend on the moisture content, porosity, the magnitude of the applied pressure and structural strength of soils [14].

Table 2. Data on the results of compression tests of loess subsidence soils

Engineering-geological elements	Sample pressure interval, kPa	Values of total deformation modulus *E* of loess soils, MPa	
		low-moisture	wet
EGE-1	100…140	7,1	1,6
	140…200	11,4	1,0
	200…250	14,2	1,3
EGE -2	100…140	7,7	11,1
	140…200	12,4	10,9
	200…250	15,4	14,0
EGE -3	100…140	7,8	-
	140…200	12,5	-
	200…250	15,6	-
EGE -4	-	25	-

Strength properties of soils φ and c were determined by the single-plane shear test according to GOST 12248.1-2020. In the experiments the scheme of rapid shear under conditions of incomplete consolidation without preliminary compaction of soil samples was used. Under this shear scheme the values of strength properties are the lowest compared to other test methods (M.Y. Abelev, 1979, 1983, 2023; V.F. Sidorchuk et al., 1980; G.G. Boldyrev 1985-1993). It was found that the specific cohesion characteristics for low-moisture soils are about three times greater than for moist soils. The characteristic of the angle of internal friction changes insignificantly. For low-moisture soils, the characteristic of the angle of internal friction is 1-2 degrees higher than that of moist soils (Table 3) [15, 16, etc.].

Table 3. Data on the results of laboratory tests of strength properties of macroporous subsidence soils

Engineering-geological elements	Strength properties of soils *c* and *φ*	Values of strength properties of loess subsidence soils *c*, kPa; *φ*, deg.	
		low-moisture	wet
EGE-1	*c*	42	10
	φ	24	22
EGE -2	*c*	38	14
	φ	23	21
EGE -3	*c*	25	-
	φ	22	-
EGE -4	*c*	-	-
	φ	-	-

Table 4. Results of studies of relative subsidence Ɛsl under pressure on soil samples

BASE soil	Design thickness of EGE, m	Elementary layer thickness h_i, m	Distance of sampling from the ground surface, m	Relative subsidence $\mathcal{E}_{sl}$, at pressure *p*, kPa						Initial subsidence pressure P_s, kPa
				20	60	100	140	200	250	
Hard, hummocky, macroporous loam EGE-1	10,4	2,7	-2,7	0,000	0,013	0,027	0,034	0,052	0,056	65
		2,7	-5,4	0,000	0,011	0,024	0,030	0,046	0,050	65
		2,7	-8,1	0,000	0,010	0,021	0,027	0,040	0,045	-
		2,6	-10,7	0,000	-	-	0,025	-	0,042	-
Hard, semi-hard, dark brown loam EGE-2	2,2	0,7	-11,4	0,000	0,010	0,013	0,017	0,021	0,023	-
		0,7	-12,1	0,000	0,011	0,012	0,015	0,019	0,021	-
		0,8	-12,9	0,000	0,011	0,012	-	0,015	0,013	-
tight plastic loam, yellowish brown EGE-3	7,3	1,8	-14,7	-	-	0,008	0,010	0,010	0,010	-
		1,8	-16,5	0,000	0,000	0,000	0,000	0,012	0,000	-
		1,8	-18,3	-	-	-	-	-	-	-
		1,9	-20,2	-	-	-	-	-	-	-

The subsidence properties such as relative subsidence ε_{sl} and initial subsidence pressure p_{sl} were determined in laboratory conditions in accordance with the requirements of GOST 23161-2012 [12]. The values of relative subsidence were established by the "two curves" method which implies testing twin specimens in compression devices taking into account the pressure from own weight of the soil and the pressure transmitted by the foundation sole at the considered depth. The values of the initial subsidence pressure parameter p_{sl}, according to the requirements of regulatory documents, were assumed to be equal to the pressure on the soil sample, at which the relative subsidence ε_{sl} was $\varepsilon_{sl} = 0.01$ (Table 4) [4, 17].

ESTIMATION OF SOIL CONDITIONS TYPE IN TERMS OF SUBSIDENCE

To evaluate the type of ground conditions in terms of subsidence of the construction site under consideration, we plot the stress variation from the soil self-weight σ_{zg} along the depth of the subsidence stratum, taking into account its engineering-geological structure (Fig. 1).

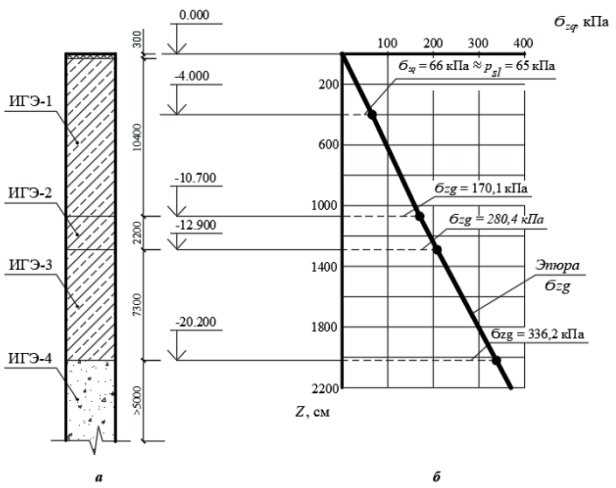


Figure 1. Schematic diagram for determining the type of ground conditions by subsidence for macroporous soils: a - geological column; b - stress distribution diagram from own weight of the soil σ_{zq}

For this purpose, we previously calculate [4]:

Z = 2.7 m, σ_{zg} = 15. 9 x 2.7 = 42.92 kPa;
Z = 5.4 m, σ_{zg} = 15. 9 x 5.4 = 85.86 kPa;
Z = 8.1 m, σ_{zg} = 15. 9 x 8.1 = 128.79 kPa;
Z = 10.7 m, σ_{zg} = 15. 9 x 10.7 = 170.13 kPa;
Z = 11.4 m, σ_{zg} = 170.13+(17.0 x 0.7) = 182.03 kPa;
Z = 12.1 m, σ_{zg} = 182.93+(17.0 x 0.7) = 194.83 kPa;
Z = 12.9 m, σ_{zg} = 194.83+(17.0 x 0.8) = 208.43 kPa;
Z = 14.7 m, σ_{zg} = 208.43+(17.5 x 1.8) = 239.93 kPa;
Z = 16.5 m, σ_{zg} = 239.93+(17.5 x 1.8) = 271.43 kPa;
Z = 18.3 m, σ_{zg} = 271.43+(17.5 x 1.8) = 302.93 kPa;
Z = 20.2 m, σ_{zg} = 302.93+(17.5 x 1.9) = 336.18 kPa

Using the graph (Fig. 1), we can find the depth where the condition $\sigma_{zg} \approx p_{sl}$ is fulfilled, i.e., σ_{zg} is the stress from own weight of the soil; p_{sl} is the initial subsidence pressure. This condition is fulfilled at the depth z = 4 m, where σ_{zg} = 66 kPa ≈ p_{sl} = 65 kPa as shown Fig. 1 and Table 4.
To determine the subsidence from own weight of soil S_{sl}, we conventionally divide the subsidence stratum into layers 2.7-2.8 m thick for EGE-1 and 0.7-0.8 m thick for EGE-2. In this case, the subsidence S_{sl} within the subsidence strata is calculated starting from the depth z = 4 m, where the stress from own weight of the soil σ_{zg} is equal to the initial subsidence pressure p_{sl} (σ_{zg} = 66 kPa ≈ p_{sl} = 65 kPa). For the soil strata of tight plastic loam (EGE-3), lying below EGE-2, the breakdown into separate layers is not performed, as the considered thickness of tight plastic loam (EGE-3) practically does not possess subsidence properties and has permissible limits of relative subsidence ε_{sl}. Using the data of Table 4 we plot the dependence of relative subsidence ε_{sl} on the applied external pressure p on the soil (Fig. 2): $\varepsilon_{sl} = f(p)$. All initial data for calculations are summarized in Table 5

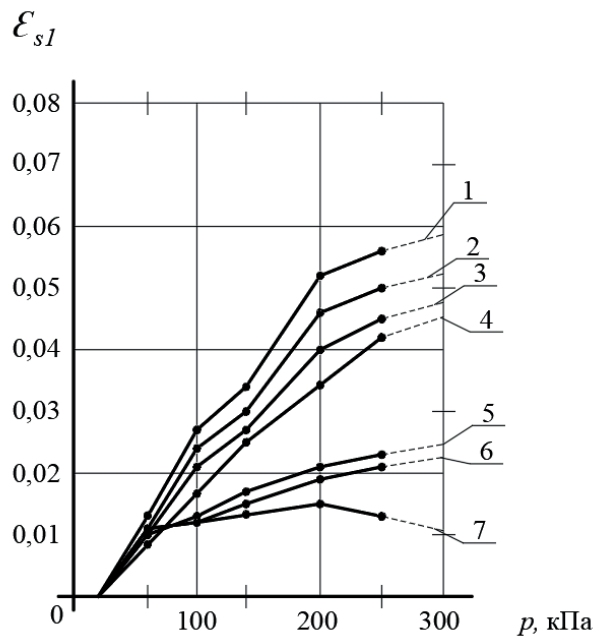


Figure 2. Relative ground subsidence $\mathcal{E}_{sl}$ depending on the external applied pressure p: 1...4 - respectively, for EGE-1 soil at -2.7, -5.4, -8.1 and -10.7 m from the ground surface; 5...7 - respectively, for EGE-2 soil at 11.4, 12.1 and 12.9 m from the ground surface.

Table 5. Relative subsidence $\mathcal{E}_{sl}$, at acting stress caused by own weight of the soil σ_{zq}

Soils	Distance to the bottom of the layer under consideration from the ground surface, m	Stresses σ_{zq} at the base elevation of the layer under consideration, kPa	Relative subsidence ε_{sl} at acting stress σ_{zq}
EGE-1	-2,7	42,9	0,012
	-5,4	85,8	0,020
	-8,1	128,8	0,025
	-10,7	170,1	0,030
EGE -2	-11,4	182,0	0,020
	-12,1	194,8	0,017
	-12,9	208,4	0,014

The expected soil subsidence from the action of its own weight S_{sl} (cm) within the subsidence strata is determined from the condition (Krutov V.I. et al., 2013; Polishchuk A.I., Marinichev M.B., 2023):

$S_{sl} = \sum \varepsilon_{sl,i}\, h_i\, K_{sl,i}$ = 0.02 x 270 x 1 + 0.025 x 270 x 1 + 0.03 x 260 x 1 + 0.02 x 70 x 1 + 0.017 x 70 x 1 + 0.014 x 80 x 1 = 5.4 + 6.75 + 7.8 + 1.4 + 1.19 + 1.12 = 23.7 cm,

where, n is the number of layers into which the subsidence stratum is divided;

$\varepsilon_{sl,i}$ is relative subsidence, determined for each ith layer of the subsidence stratum at the acting stress ($\sigma_{zg} + \sigma_{zr}$);

h_i is the thickness of the considered ith layer of soil, m;

$K_{sl,i}$ is the coefficient of operating conditions of the base.

Thus, it is established that, there are layers of macroporous soil (loam) with total thickness z = 12,9 - 4,0 = 8,9 meters within the depth where the condition $\sigma_{zg} > p_{sl}$ fulfills. The subsidence of the considered soil thickness caused by the action of its own weight is more than 5 cm (S_{sl} = 23.7 cm). Consequently, the ground conditions of the site under consideration belong to the ***second type of subsidence***.

JUSTIFICATION OF PILE TYPE AND LENGTH

For the buildings to be constructed on pile foundations, we accept ***prefabricated reinforced concrete prismatic piles*** with a cross-section of 300 x 300 mm, which are sunk into the ground ready-made from the bottom of the excavation [2, 4, 18]. This is because of the developed material and technical resources in the construction area (Chechen Republic), where driven reinforced concrete piles will be produced in the required volume. Since the base of the construction site under consideration is composed of macroporous hard loams, the piles should be driven into such soils by means of leader holes, the cross-sectional area of which should be 15-20% smaller than the cross-sectional area of prismatic piles. It is recommended that the depth of the leader wells is approximately 10.5-11.0 m from the surface of the foundation. Within this depth lies the EGE-1 (upper from the base surface). The bearing layer for factory-made prismatic piles is recommended to be hard, semi-hard, dark brown loam, which is part

of EGE-2. The depth of immersion of the lower end of prismatic piles into the bearing layer should be at least 1.0 m in accordance with Table 1.

EXPERIMENTAL AND NUMERICAL DATA ON BEARING CAPACITY OF DRIVEN REINFORCED CONCRETE PILES IN SUBSIDENCE SOILS

The bearing capacity of the considered driven reinforced concrete piles was determined **experimentally** based on the results of **field tests** by static push-in load. Static tests of full-scale piles were carried out in macroporous subsidence soils of natural composition (**low-moisture**) and on pre-wetted (**wet**) soils in accordance with the requirements of Russian standards (GOST 30672-2019, GOST 5686-2020, SP.24.13330.2021, etc.) [19, 20, 21]. In the experiments, driven reinforced concrete prismatic piles of 10 m length and 30x30 cm cross-section were used. The load on the natural piles was transferred by a hydraulic jack with a manual pumping station providing the required operating pressure. The displacements of the test piles were measured by deflection meters.

According to SP 22.13330.2016 (c. 7.3. 5) [13], the bearing capacity of the pile (partial value of the ultimate resistance) Fu under push-in load was assumed to be the load under the influence of which the tested pile received a settlement $S=\xi S_{u,mt}$. ξ is a factor equal to 0.2 if the pile was tested at a conditional stabilization equal to 0.1 mm in 1 hour, if sandy soils and clay soils of solid consistency were under its lower end. $S_{u,mt}$ is the limit value of the mean foundation settlement of the designed building, which is set according to the instructions of the design organization. In the considered case, the value of $S_{u,mt}$ was accepted equal to 12 cm (SP 22.13330.2016). Based on the above formula, the settlement S corresponding to the bearing capacity (ultimate resistance) of the pile Fu at natural moisture content was S = 0.2 x 12 = 2.4 cm (24 mm). The experimental results are presented in the form of graphs showing the dependences of pile settlements on external load (presented below).

To evaluate the performance of prefabricated reinforced concrete piles in macroporous subsidence soils of the second type, the authors simultaneously carried out numerical studies using the Midas FEA NX software. At the same time, the influence of soaking of the foundation soils (e.g., emergency soaking) on the bearing capacity and settlement of piles, as well as on the development of non-uniform deformations of pile foundations was revealed.

To simulate the loading ("performance") of soils in the base, the model of hardening soil at small deformations (HS small) was used [22]. This model accounts for the relation of soil stiffness and strength to stress and strain, as well as its over consolidation during load history. This allows for more accurate modeling of its nonlinear deformation under loads. The discussed model provides a correct description of cyclic loading and pore pressure development under undrained conditions, which is important for complex engineering problems. A linear-elastic model with its stiffness characteristics was used for the pile material. Soaking of the subsidence soil was taken into account in the modeling by lowering its strength and deformation characteristics (Figs. 3, 4).

The investigation results of driven reinforced concrete piles' performance in low-moisture and wet subsidence soils are presented in Fig. 5. It is established that in low-moisture and wet (soaking wet) loess soils, the pile settlements recorded during field tests are much smaller compared to the settlements obtained by numerical modeling.

For example, the pile settlement is 4.5 mm under an external load of 140 tf for low-moisture soils, while the pile settlement obtained by numerical modeling under the same load of 140 tf is much larger and amounts to 15.0 mm. In wet subsidence soils, the same trend is also observed. With an external load of 100 tf, the pile settlement is 5.5 mm, while in the case of numerical modeling, the pile settlement at the same load in wet soil is 12.5 mm.

According to the results of field static tests, a load

of 100 tf was taken as the bearing capacity of the pile in wet (soaking wet) macroporous soils. The pattern of the resulting graph indicates that the actual bearing capacity of the pile was not established due to the limitation of the maximum load in the test system used. At the same time, a value of 145 tf was found to be the bearing capacity of the pile according to the results of numerical modeling (at 24 mm settlement) as shown in Fig. 5.

Due to the idealized conditions of numerical simulation, as well as the discreteness of the problem to be solved, compiled for a single pile, the relationship between settlement and external load after the first iteration, as a rule, has a divergence from the natural plot and does not allow to accept initial stiffnesses for modeling a larger-sized pile group. The applied principle of iterative refinement of strength and shear properties at the pile-soil contact continues until the shape of the load-displacement branches approximates the experimental data. Perfect convergence is achieved with great difficulty, since the full-scale plot incorporates and displays a set of nonlinear processes. The description of these processes is not possible with simplified models that imply an inseparable connection between the pile and the soil during loading [25].

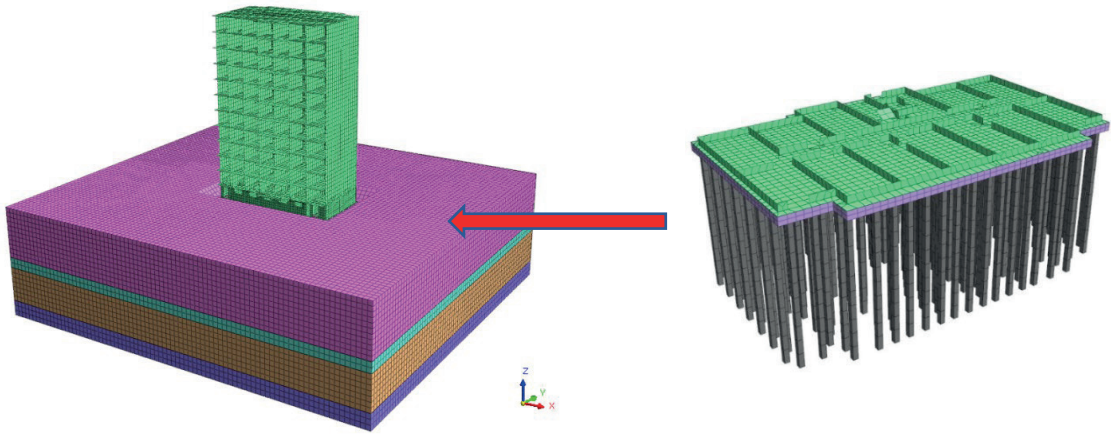


Figure 3. Basement-foundation-structure system with separation of the considered pile foundation (right)

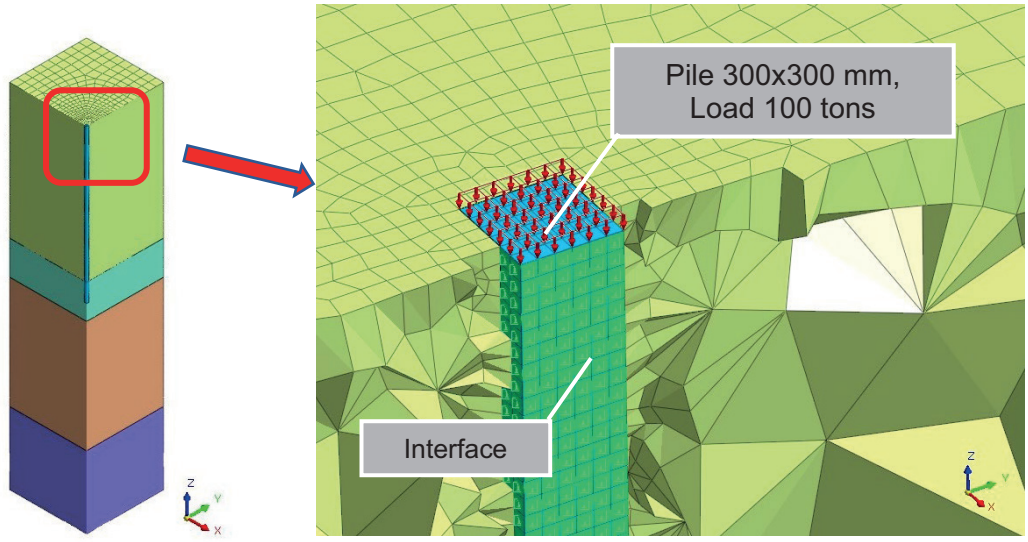


Figure 4. Calculation model of a 30x30 cm pile 10 m in length consisting of solid elements in the given engineering-geological conditions

Fig. 5 shows plots of pile settlement-load dependence for iteratively refined interface properties. Ultimately, a certain convergence of the results was achieved, which allows the synthesized graph to be applied in finite element analysis of the whole system. At the same time, it accounts for the varying properties of the base soils in the manifestation of subsidence properties for loess subsidence soils of the second type of subsidence.

As a result, after the calculations with regard to the verified stiffnesses, the deformations of the system are obtained. They show a high convergence with the results of geotechnical monitoring and can be used for predicting the settlement of single piles on loess macroporous subsidence soils of the second type of subsidence, considering their possible soaking.

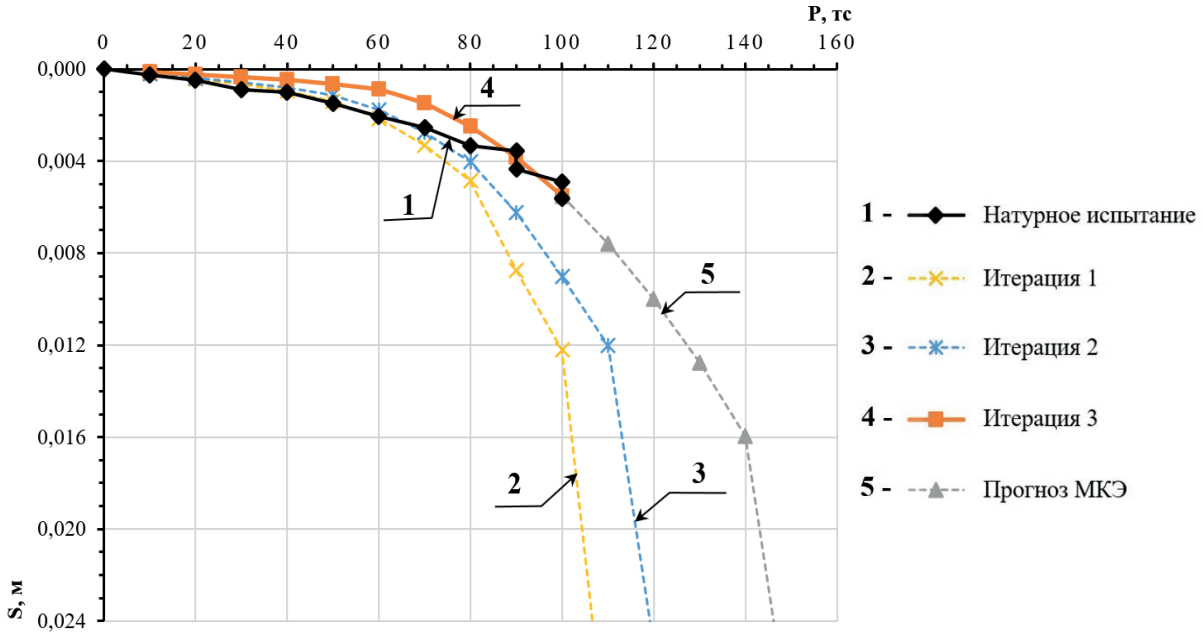


Figure 5. Sequential approximation of the calculated load-settlement diagram to the actual dependence obtained from field tests of a single 30x30 cm pile 10 m length at a construction site made of wet macroporous soils

Thus, the correct analysis of ground conditions of the planned construction, the rules for selecting the structural solution of piles for multistorey civil buildings, as well as the peculiarities of finite element analysis allow us to justify the main stages of designing pile foundations on macroporous subsidence soils of the second type of subsidence, considering the possible soaking of the compressible thickness of the base.

REFERENCES

1. **Krutov V.I., Kovalev A.S., Kovalev V.A.** Design and construction of bases and foundations on subsidence soils. - Moscow: ASV Publishing House, 2013. - 544 p.
2. Geotechnical Engineering Handbook. Bases, foundations and underground structures: 3rd edition, supplemented and revised / Under the general editorship of **V.A. Ilyichev and R.A. Mangushev.** - Moscow: Publishing house ASV, 2023. - 1084 p.
3. **Abelev Y.M., Abelev M.Y.** Fundamentals of design and construction on subsidence macroporous soils. 3rd ed. revision and supplement. - Moscow: Stroyizdat, 1979. - 271 p.
4. **Polischuk A.I., Marinichev M.B.** Bases and foundations, underground structures; ed. by A.I. Polischuk. 3rd ed. revision and add. - M.: Publishing house ASV, 2023. - 558 p.

5. **Polishchuk A.I.** Analysis of ground conditions of construction in the design of buildings: Scientific and practical manual. -Moscow: Publishing house ASV, 2016. - 104 p.
6. **GOST 12071-2000.** Sampling, packing, transportation and keeping of samples. – Moscow: 2001.
7. **Mangushev R.A., Usmanov R.A.** Bases and Foundations. Solution of practical problems: Textbook. -2nd ed. ster. SPb.: Publishing "Lan", 2018. - 172 p.
8. **Mangushev R.A., Osokin A.I., Usmanov R.A.** Arrangement and reconstruction of bases and foundations on structurally unstable soils / Edited by R.A. Mangushev: Monograph. -Saint Peterburg: Publishing "Lan", 2018. - 460 p.
9. **GOST 5180-2015.** Soils. Laboratory methods for determination of physical characteristics. – Moscow: 2016.
10. **Ilyichev V.A., Mangushev R.A.** Geotechnical Engineering Handbook. Bases, foundations and underground structures. -Moscow: ASV Publishing House, 2014. - 728 p.
11. **GOST 12248.4-2000.** Soils. Determination of deformation parameters by compression testing. – Moscow: 2003.
12. **GOST 23161-2012.** Soils. Method of laboratory determination of subsiding characteristics. – Moscow: 2013.
13. **SP 22.13330.2016.** Soil bases of buildings and structures. Updated version of SNiP 2.02.01-83*. – Moscow: 2017.
14. **GOST 20522-2012.** Soils. Statistical treatment of the test results. – Moscow: 2012.
15. **GOST 12248-2020.** Soils. Determination of strength parameters by shear strength testing. – Moscow: 2020.
16. **Abelev M.Yu.** Peculiarities of construction on loess subsidence soaking soils. - Moscow: Publishing house ASV, 2023. -144 p.
17. Fundamentals of calculation and design of foundations for multi-storey, high-rise and unique buildings: scientific and practical manual / **M.B. Marinichev, O.Y. Yeschenko, V.A. Demchenko, I.G. Tkachev.** - Krasnodar: KubGAU, 2022. - 224 p.
18. **Mangushev R.A., Osokin A.I., Konyushkov V.V., Diakonov I.P., Lanko S.V.** Design of foundations and underground structures (textbook and practical manual). Edited by Corr. of RAACS, Dr. of Technical Sciences, Professor R.A. Mangushev. -Moscow: ASV Publishing House, 2021. - 632 p.
19. **GOST 30672-2019.** Soils. Field testing. General requirements. – Moscow: 2019.
20. **GOST 5686-2020.** Soils. Field test methods by piles. –Moscow: 2020.
21. **SP 24.13330.2021.** Pile foundations. Updated version of SNiP 2.02.03.85. – Moscow: 2021.
22. **Marinichev M.B.** Foundations of multistorey and high-rise buildings in special conditions of the South of Russia : Cand. Doctor of technical sciences : 2.1.2 / M.B. Marinichev ; KubGAU (Krasnodar). - Saint-Petersburg : SPBGASU, 2023. - 355 p.
23. **Marinichev M.B.** Compensation of uneven compressibility of the base by the foundation stiffness (at the ground conditions of Krasnodar city and region): Avtoref. dissertation cand. techn. sciences - Volgograd, 2004. - 24 p.
24. **Marinichev M.B.** Implementation of nonstandard design solutions in high-rise construction using modern drilling technologies. Polythematic network electronic scientific journal of Kuban State Agrarian University. - 2009. - no. 54. - Pp. 1-8.
25. **Marinichev, M.B.** Research of bored hanging piles in the foundations of multistory and high-rise buildings: Monograph / M.B. Marinichev. - Krasnodar : KubGAU : Prosveschenie-Yug, 2022. - 155 p. ISBN 978-5-93491-917-8.

СПИСОК ЛИТЕРАТУРЫ

1. **Крутов В.И., Ковалев А.С., Ковалев В.А.** Проектирование и устройство оснований и фундаментов на просадочных грунтах. – М.: Изд-во АСВ, 2013. – 544 с.

2. Справочник геотехника. Основания, фундаменты и подземные сооружения: 3-е издание, дополненное и переработанное / Под общей ред. **В.А. Ильичева и Р.А. Мангушева.** – М.: Изд-во АСВ, 2023. – 1084 с.
3. **Абелев Ю.М., Абелев М.Ю.** Основы проектирования и строительства на просадочных макропористых грунтах. 3-е изд. перераб. и доп. – М.: Стройиздат, 1979. – 271 с.
4. **Полищук А.И., Мариничев М.Б.** Основания и фундаменты, подземные сооружения; под. ред. А.И. Полищука. 3-е изд. перераб. и доп. – М.: Изд-во АСВ, 2023. – 558 С.
5. **Полищук А.И.** Анализ грунтовых условий строительства при проектировании зданий: Научно-практическое пособие. – М.: Изд-во АСВ, 2016. – 104 с.
6. **ГОСТ 12071-2000.** Грунты. Отбор, упаковка, транспортирование и хранение оборудования. – М.: 2001.
7. **Мангушев Р.А., Усманов Р.А.** Основания и фундаменты. Решение практических задач: Учебное пособие. -2-е изд. стер. СПб.: Изд-во «Лань», 2018. – 172 с.
8. **Мангушев Р.А., Осокин А.И., Усманов Р.А.** Устройство и реконструкция оснований и фундаментов на структурно-неустойчивых грунтах / Под ред. Р.А. Мангушева: Монография. –СПб.: Изд-во «Лань», 2018. – 460 с.
9. **ГОСТ 5180-2015.** Грунты. Методы лабораторного определения физических характеристик. – М.: 2016.
10. **Ильичев В.А., Мангушев Р.А.** Справочник геотехника. Основания, фундаменты и подземные сооружения. –М.: Изд-во АСВ, 2014. – 728 с.
11. **ГОСТ 12248.4-2000.** Грунты. Определение характеристик деформируемости методом компрессионного сжатия. – М.: 2003.
12. **ГОСТ 23161-2012.** Межгосударственный стандарт. Метод лабораторного определения характеристик просадочности. – М.: 2013.
13. **СП 22.13330.2016.** Основания зданий и сооружений. Актуализированная редакция СНиП 2.02.01-83*. – М.: 2017.
14. **ГОСТ 20522-2012.** Грунты. Методы статистической обработки результатов испытаний. – М.: 2012.
15. **ГОСТ 12248-2020.** Грунты. Определение характеристик прочности методом одноплоскостного среза. – М.: 2020.
16. **Абелев М.Ю.** Особенности строительства на лессовых просадочных при замачивании грунтах. – М.: Изд-во АСВ, 2023. –144 с.
17. Основы расчета и конструирования фундаментов многоэтажных, высотных и уникальных зданий: научно-практическое пособие / **М.Б. Мариничев, О.Ю. Ещенко, В.А. Демченко, И.Г. Ткачев.** – Краснодар: КубГАУ, 2022. – 224 с.
18. **Мангушев Р.А., Осокин А.И., Конюшков В.В., Дьяконов И.П., Ланько С.В.** Проектирований оснований фундаментов и подземных сооружений (учебное и практическое пособие). Под ред. чл. корр. РААСН, д-ра техн. наук, профессора Р.А. Мангушева. –М.: Изд-во АСВ, 2021. – 632 с.
19. **ГОСТ 30672-2019.** Межгосударственный стандарт. Грунты. Полевые испытания. Общие требования. – М.: 2019.
20. **ГОСТ 5686-2020.** Грунты. Методы полевых испытаний сваями. –М.: 2020.
21. **СП 24.13330.2021.** Свайные фундаменты. Актуализированная редакция СНиП 2.02.03.85. – М.: 2021.
22. **Мариничев М. Б.** Фундаменты многоэтажных и высотных зданий в особых условиях Юга России : дис. … докт. техн. наук : 2.1.2 / М.Б. Мариничев ; КубГАУ (Краснодар). – Санкт-Петербург : СПБГАСУ, 2023. – 355 с.
23. **Мариничев М.Б.** Компенсация неравномерной сжимаемости основания жесткостью фундамента (на примере грунто-

вых условий г. Краснодара и края): Автореф. диссертации канд. техн. наук – Волгоград, 2004. – 24 с.
24. **Мариничев М.Б.** Реализация нестандартных конструктивных решений в высотном строительстве на основе использования современных буровых технологий. Политематический сетевой электронный научный журнал Кубанского государственного аграрного университета. – 2009. – № 54. – С. 1–8.
25. **Мариничев М.Б.** Исследование работы буровых висячих свай в составе фундаментов многоэтажных и высотных зданий: Монография / М. Б. Мариничев. – Краснодар : КубГАУ : Просвещение - Юг, 2022. – 155 с. ISBN 978-5-93491-917-8.

Maxim Borisovich Marinichev, Doctor of Technical Sciences, Professor, I.T. Trubilin Kuban State Agrarian University (KubSAU), Address: 13 Kalinina Street, Krasnodar, 350044, Russia, e-mail: marinichev@list.ru

Максим Борисович Мариничев, д-р техн. наук, профессор кафедры «Основания и фундаменты», Кубанский государственный аграрный университет имени И.Т. Трубилина (КубГАУ), Адрес: д. 13, улица им. Калинина, г. Краснодар 350044, Россия, e-mail: marinichev@list.ru

Anatoly Ivanovich Polishchuk, Doctor of Technical Sciences, Professor, I.T. Trubilin Kuban State Agrarian University (KubSAU), Address: 13 Kalinina Street, Krasnodar, 350044, Russia, e-mail: ofpai@mail.ru

Анатолий Иванович Полищук, д-р техн. наук, профессор кафедры «Основания и фундаменты», Кубанский государственный аграрный университет имени И.Т. Трубилина (КубГАУ), Адрес: д. 13, улица им. Калинина, г. Краснодар 350044, Россия, e-mail: ofpai@mail.ru

Nadezhda Sergeevna Nikitina, Candidate of Technical Sciences, Professor, Moscow State University of Civil Engineering (NRU MGSU), Address: 26, Yaroslavskoye Highway, Moscow, 129337, Russia, e-mail: NikitinaNS@mgsu.ru

Надежда Сергеевна Никитина, канд. техн. наук, профессор кафедры «Механика грунтов и геотехника», Московский государственный строительный университет (НИУ МГСУ), Адрес: д. 26, Ярославское ш., г. Москва, 129337, Россия, e-mail: NikitinaNS@mgsu.ru